Novel techniques to study cardiopulmonary physiology in a preclinical, saline-lavage model of the acute respiratory distress syndrome.

Douglas C Crockett

Wadham College

douglas.crockett@ndcn.ox.ac.uk

A thesis presented for the degree of

Doctor of Philosophy



Nuffield Department of Clinical Neurosciences

University of Oxford

United Kingdom

Michaelmas Term 2019

For Mum & Dad.

Acknowledgements

Thank you to my supervisors, Professor Andrew Farmery and Dr Federico Formenti. You have provided unwavering support from the beginning of this DPhil. Your doors have always been open for teaching, general guidance and inspiration. Thank you for shepherding me with such generous and kind supervision.

Thank you also to Professors Clive Hahn and Angela Vincent for their guidance and encouragement throughout. I am grateful to my fellow PhD student Minh Cong Tran whose ability to bring an engineering perspective to any physiological question has been inspiring. Thank you Minh for the regular welfare checks and support during the last few months of writing. Thanks also to the rest of the Farmery Group: Dr Phi Anh Phan, Dr Richard Bruce and Hanne McPeak.

To Dr Helen Highan, Rosie Warren, Alan Inglis, Russel Sinclair, Charlie McDermott, Wendy Washbourn and the rest of the faculty at the Oxford centre for Simulation, Teaching and Research (OxSTaR): thank you for giving me a teaching stipend and more importantly for providing friendship and support.

Many thanks are also due to the Breathe Oxford Group: Prof. Kyle Pattinson, Dr Sarah Finnegan, Dr Carolin Sievers, Miss Lucy Marlow, Dr Martyn Ezra & Dr Alex Luettich. Their comaraderie, humour and sage advice has been invaluable.

I am grateful too for the productive collaborations that I have been a part of during the course of this degree. To Dr John Cronin and Dr João Batista-Borges of King's College London, thank you. Till det fantastiska teamet på Hedenstierna

Laboratorium vid Uppsala Universitet: Professor Anders Larsson, Professor Göran Hedenstierna, Agneta Roneus, Dr Kerstin Ahlgren, Mariette Andersson, Maria Swälas, Dr Liselotte Pihl och Monica Segelsjö - tack så mycket! Jag tyckte verkligen om att arbeta i ert labb, lära känna er, lära mig om Sverige (och vetenskap) och, icke att förglömma, fika tillsammans! Thank you to the University of Bristol Biomedical Research Centre's Dr Delphine Holopherne-Doran, Dr Cristian Dancker, Dr Will McFadzean & Krissy Britchford. It was great to work back in Langford again, especially with such a nice team.

Thank you to the clinical Nuffield Division of Anaesthetics at the John Radcliffe Hospital, Oxford. Particular thanks to Dr Amy Swinson who supported getting me on to the clinical rota and to Dr Ruth Webster who has provided immense support throughout.

Most importantly, thank you to my family and friends. I owe a world of gratitude to Dr David Menassa, who has been there from the beginning. He has provided reassuring motivation, support and a sympathetic ear. To my family: Mum, Dad, James, Anne, Hilary, Karl, Rachel, Arthur and Philip thank you for everything you've done to get me to this point.

Abstract

The acute respiratory distress syndrome (ARDS) affects 24.4% of all patients requiring mechanical ventilation and has an associated mortality of up to 46%. The complex pathophysiology of the cardiopulmonary system is difficult to study, particularly in the critically ill patient. Pre-clinical models of ARDS afford the possibility to investigate this complex physiology, which allows increased understanding of that physiology and the potential to develop tools which could be translated to clinical practice. This thesis presents experimental studies of two novel techniques to study cardiopulmonary physiology in a mechanically ventilated porcine saline-lavage model of ARDS.

Using fluorescence quenching real-time measurement of P_aO_2 and dynamic computed tomography (CT), the cyclical recruitment/derecruitment of atelectasis (CA) is demonstrated and the previously accepted hypothesis that CA is the main determinant of cyclical oscillations in P_aO_2 is challenged. Real-time changes in P_aO_2 over the course of breath-hold manoeuvres are used to estimate the effective lung volume (ELV). P_aO_2 measured ELV is compared against ELV measured using whole lung CT scans. The P_aO_2 model follows the expected linear relationship with CT volumes and is able to track changes in lung volume with good concordance.

The Inspired Sinewave Technique (IST) is a non-invasive technique which can provide measurements of ELV and cardiac output ($\dot{Q}$). IST's measurements of ELV compare well to those made with SF_6 washout and CT. IST's ability to track PEEP-induced changes in ELV shows excellent concordance with both SF_6 and CT. Comparing IST's measurements of $\dot{Q}$ against those made with intermittent pulmonary artery thermodilution (PATD), IST tracks changes in $\dot{Q}$ well in the uninjured animal model. Agreement between $\dot{Q}$ measurements taken with IST and PATD show less agreement in the injured animal model.

The presented results support translational research into both real-time P_aO_2 measurement and IST. Both techniques have the potential to provide bedside monitoring of important physiologcial parameters in mechanically ventilated patients.

Contents

Acknowledgements iii

Abstract iv

List of Tables xii

List of Figures xiv

List of Abbreviations xvii

1 Introduction 1

1.1 Introduction . . . 2

1.2 Delivering O_2 to tissues . . . 2

1.3 The Acute Respiratory Distress Syndrome (ARDS) . . . 3

1.3.1 Interventions to reduce mortality in ARDS . . . 4

1.3.2 The baby lung in ARDS . . . 5

1.4 Ventilator Induced Lung Injury (VILI), stress and strain . . . 6

1.4.1 Dynamic strain in ARDS . . . 7

1.5 The rationale for measuring lung volume in mechanically ventilated patients with ARDS . . . 11

1.6 Established methods of measuring lung volume . . . 12

1.6.1 Whole body plethysmography . . . 12

1.6.2 Gas-based techniques . . . 13

1.6.3 Imaging-based methods to measure lung volume . . . 17

1.7 The rationale for measuring cardiac output . . . 18

1.8 Research aims . . . 20

1.9 Thesis outline 20

2 Methods **22**

2.1 Introduction 23

2.2 Experimental logistics and timing 23

2.3 The use of an animal model 25

2.3.1 Considerations for the use of animals as experimental subjects. 25

2.3.2 Choice of animal model 25

2.3.3 Anaesthesia and surgical instrumentation 26

2.4 Real time, *in vivo* P_aO_2 measurement using fibre optic photonic sensors 28

2.5 Computed Tomography (CT) image analysis 31

2.5.1 Masking of CT images 32

2.6 The Inspired Sinewave Technique 33

2.6.1 Development of IST 33

2.6.2 The contemporary Inspired Sinewave Technique 36

2.7 Multiple breath sulphur hexafluoride (SF_6) washout 42

2.7.1 Process of measuring FRC with SF_6 multiple breath washout . 43

2.7.2 Comparing lung volumes measured with different techniques. . 45

2.7.3 Statistics 45

3 Investigating the relationship between respiratory oscillations in P_aO_2 and cyclical recruitment/derecruitment of atelectasis **46**

3.1 Introduction 48

3.1.1 Detection of respiratory O_2 oscillations in arterial blood. . . . 48

3.1.2 Causes of respiratory P_aO_2 oscillations. 49

3.1.3 The relationship between pulmonary shunt, cyclical recruitment/derecruitment of atelectasis and respiratory P_aO_2 oscillations. 50

3.1.4 The importance of cyclical recruitment/derecruitment of atelectasis (CA). . . . 52
3.1.5 Clinical importance of respiratory P_aO_2 oscillations. . . . 54
3.1.6 Aims and hypotheses. . . . 55
3.2 Methods . . . 56
3.2.1 Ethical approval . . . 56
3.2.2 Animal preparation . . . 56
3.2.3 Lung injury . . . 56
3.2.4 Data collection and processing . . . 57
3.2.5 Study protocol . . . 57
3.2.6 CT image acquisition . . . 60
3.2.7 CT image analysis . . . 60
3.2.8 Statistical analysis . . . 60
3.3 Results . . . 62
3.3.1 Single slice dCT and P_aO_2 during tidal ventilation. . . . 62
3.3.2 Whole lung CT and P_aO_2 during breath-hold manoeuvres . . 67
3.4 Discussion . . . 75
3.4.1 The relationship between respiratory P_aO_2 oscillations and cyclical atelectasis. . . . 75
3.4.2 The relationship P_aO_2 and fractional lung collapse during breath-hold manoeuvres. . . . 77
3.4.3 Limitations . . . 78
3.4.4 Conclusions . . . 79

4 Measuring lung volumes using real-time changes in P_aO_2: Comparison with Computed Tomography 80
4.1 Introduction . . . 82
4.1.1 Inverting the P_aO_2 rate of decline model to predict lung volume. 84
4.2 Methods . . . 86
4.2.1 Ethical approval . . . 86

4.2.2 Data selection . . . 86
4.2.3 Animal preparation . . . 86
4.2.4 Lung injury . . . 87
4.2.5 CT image acquisition, analysis and calculation of ELV_{O_2} . . . 90
4.2.6 Continuous measurement of P_aO_2 and calculation of ELV_{O_2} . . . 90
4.2.7 Statistical Analyses . . . 91
4.3 Results . . . 92
4.3.1 Repeatability of ELV_{O_2} measurements . . . 96
4.3.2 Correlation between ELV_{O_2} and ELV_{CT} . . . 96
4.3.3 Agreement between ELV_{O_2} and ELV_{CT} . . . 96
4.3.4 Correlation between ΔELV_{O_2} and ΔELV_{CT} . . . 98
4.3.5 Agreement between ΔELV_{O_2} and ΔELV_{CT} . . . 98
4.4 Discussion . . . 101
4.4.1 Limitations of the presented study . . . 102
4.4.2 Further development of the ELV_{O_2} method . . . 103
4.4.3 Conclusions . . . 103

5 Measuring lung volumes with the Inspired Sinewave Technique: Comparison with Computed Tomography and SF_6 105

5.1 Introduction . . . 107
5.2 Methods . . . 109
5.2.1 Ethical approval . . . 109
5.2.2 Animal Preparation . . . 109
5.2.3 Data Collection and processing . . . 112
5.2.4 The Inspired Sinewave Technique (IST) . . . 112
5.2.5 SF_6 Washin-Washout . . . 112
5.2.6 CT Image Acquisition and Analysis . . . 113
5.2.7 Lung Injury . . . 113
5.2.8 Study Protocol . . . 113
5.2.9 Statistical Analyses . . . 116

5.3 Results . . . 118
5.3.1 Repeatability of ELV_{IST} measurements. . . . 121
5.3.2 Correlation between ELV_{IST}, ELV_{SF6} and ELV_{CT}. . . . 121
5.3.3 Agreement between ELV_{IST}, ELV_{SF6} and ELV_{CT}. . . . 121
5.3.4 Correlation between ΔELV_{IST}, ΔELV_{SF6} and ΔELV_{CT}. . . . 124
5.3.5 Agreement between ΔELV_{IST}, ΔELV_{SF6} and ΔELV_{CT}. . . . 124
5.4 Discussion . . . 127
5.4.1 Strengths and limitations of the study . . . 128
5.4.2 Future directions for development of IST in the context of measuring lung volume. . . . 128
5.4.3 Conclusions . . . 129

6 Measuring cardiac output with the Inspired Sinewave Technique: Validation against intermittent thermodilution 130

6.1 Introduction . . . 132
6.2 Methods . . . 134
6.2.1 Ethical approval. . . . 134
6.2.2 Animal preparation and instrumentation. . . . 134
6.2.3 The Inspired Sinewave Technique. . . . 135
6.2.4 Data collection and processing. . . . 137
6.2.5 Pre-injury experimental protocol. . . . 137
6.2.6 Lung injury. . . . 137
6.2.7 Post-injury experimental protocol. . . . 138
6.2.8 Statistical analyses. . . . 138
6.3 Results . . . 139
6.3.1 Relationship between measurements of $\dot{Q}_{IST}$ and $\dot{Q}_T$ in the uninjured lung. . . . 139
6.3.2 Relationship between measurements of $\dot{Q}_{IST}$ and $\dot{Q}_T$ in the injured lung. . . . 143
6.3.3 The effect of shunt fraction on $\dot{Q}_{IST}$. . . . 143

6.3.4 Relationship between measurements of $\Delta\dot{Q}_{IST}$ and $\Delta\dot{Q}_T$ in the uninjured lung. . . . 145
6.3.5 Relationship between measurements of $\Delta\dot{Q}_{IST}$ and $\Delta\dot{Q}_T$ in the injured lung. . . . 145
6.4 Discussion . . . 148
6.4.1 Limitations. . . . 150
6.4.2 Conclusions. . . . 151

7 General discussion and conclusions **152**
7.1 General discussion . . . 153
7.2 Strengths and limitations of the P_aO_2 probes . . . 154
7.3 Strengths and limitations of IST . . . 155
7.4 Experimental limitations . . . 156
7.4.1 The use of an animal model of ARDS . . . 156
7.4.2 CT image analysis . . . 157
7.4.3 Does the single slice imaged in dCT represent the rest of the lung? . . . 157
7.4.4 The timing of the "start" of a breath hold. . . . 157
7.5 Future directions . . . 158
7.5.1 Translating new technologies into human medicine . . . 158
7.5.2 Investigating the role of pulmonary perfusion in understanding P_aO_2 oscillations . . . 158
7.5.3 Investigating the phenomenon of paradoxical changes in P_aO_2 159
7.5.4 Testing IST's measurements of deadspace . . . 159
7.6 Conclusions . . . 160

References **161**

Appendix A Published papers **179**

Appendix B Full protocol for the validation of IST measurements of lung volume 221

Appendix C Protocol for validation of IST measurements of cardiac output 236

List of Tables

3.1 Comparison of previous *in vivo* studies examining respiratory oscillations in arterial oxygenation. 51

3.2 Baseline characteristics and post-injury blood gas data for each animal. 57

3.3 Sequence of breath-hold manoeuvres in each animal. 59

3.4 Mean P_aO_2, amplitude of respiratory P_aO_2 oscillations and mean airway pressure during different ventilatory conditions. 65

3.5 Number of breath-hold manoeuvres carried out per animal 67

3.6 Mean fractional mass of collapsed lung measured by CT at the start and the end of breath-hold manoeuvres. 69

3.7 Results of two-way ANOVA with Tukey's multiple comparison test on the difference between the change in P_aO_2 during different breath-hold manoeuvres in different animals. 72

3.8 Dynamic CT studies examining fractional lung collapse in porcine lung-injury models. 76

4.1 Summary baseline characteristics pre- and post- lung injury. 87

4.2 Baseline characteristics of uninjured animals. 88

4.3 Baseline characteristics of ARDS model animals. 89

4.4 Descriptive statistics for comparisons of absolute lung volume (ELV) and changes in lung volume (ΔELV) made in both the uninjured lung and the ARDS model. 94

4.5 Descriptive statistics for comparisons of absolute lung volume (ELV) and changes in lung volume (ΔELV) made in both the uninjured lung and the ARDS model at each PEEP level. 95

5.1 Comparison of baseline characteristics pre- and post- lung injury. . . 110
5.2 Baseline characteristics for each individual animal pre- and post- lung injury. 111
5.3 Descriptive statistics for comparisons of absolute lung volume (ELV) and changes in lung volume (ΔELV) made in both the uninjured lung and the ARDS model at each PEEP level. 120

6.1 The features of an ideal haemodynamic monitor. 133
6.2 Baseline characteristics of individual animals pre- and post- lung injury. 136
6.3 How IST satisfies the criteria for an ideal haemodynamic monitor. . . 149

List of Figures

1.1 Scaling tidal volume to respiratory system compliance reduces mortality in ARDS. 9

2.1 Summary experimental timeline. 24
2.2 Schematic of invasive line placement for each animal. 27
2.3 Illustration of the process of light transmission at the end of the fibre-optic P_aO_2 probe. 29
2.4 Example fibreoptic P_aO_2 probe. 30
2.5 Reconstitution of single slice CT images into a completely segmented scan of the entire lung. 32
2.6 Schematic representation of IST. 36
2.7 Example output from the inspired sinewave technique. 37
2.8 Schematic diagram showing the tidal ventilation, three compartment lung model on which the inspired sinewave technique is based. 38

3.1 Example recordings of P_aO_2 and airway pressure during tidal ventilation under different conditions. 63
3.2 Changes in compartmental mass over the course of a single breath. . 64
3.3 Mean respiratory P_aO_2 oscillation amplitude during tidal ventilation under different ventilatory conditions. 66
3.4 Example P_aO_2 and airway pressure traces for breath-hold manoeuvres. 68
3.5 Changes in fractional lung collapse and P_aO_2 during breath-hold manoeuvres. 70
3.6 Mean P_aO_2 and airway pressure traces during breath-hold manoeuvres. 73
3.7 P_aO_2 traces during breath-hold manoeuvres for each animal. 74

4.1 Mean absolute ELV measurements using ELV_{O_2} and ELV_{CT} at each PEEP level. . . . 92
4.2 Median ELV measurement using ELV_{O_2} and ELV_{CT} at each PEEP level. . . . 93
4.3 Linear regression and Bland-Altman plots for ELV_{O_2} vs ELV_{CT}. . . . 97
4.4 Four-quadrant and Bland-Altman plots for changes in volume (ΔELV_{O_2} and ΔELV_{CT}). . . . 99
4.5 Polar plot analysis of measured changes in ELV (ΔELV). . . . 100

5.1 Timeline of experimental protocol: validation of IST to measure lung volume. . . . 115
5.2 Mean ELV measurement using ELV_{IST}, ELV_{SF6} and ELV_{CT} at each PEEP level. . . . 119
5.3 Scatter and Bland-Altman plots for changes in volume (ELV_{IST}, ELV_{SF6} and ELV_{CT}). . . . 122
5.4 Conventional Bland-Altman plots for changes in volume (ELV_{IST}, ELV_{SF6} and ELV_{CT}). . . . 123
5.5 Scatter and Bland-Altman plots for changes in volume (ΔELV_{IST}, ΔELV_{SF6} and ΔELV_{CT}). . . . 125
5.6 Polar plot analysis of measured changes in ELV (ΔELV). . . . 126

6.1 Pre-injury: Absolute measurements of cardiac output measured with $\dot{Q}_{IST}$ and $\dot{Q}_T$ in each animal over the period of the protocol. . . . 140
6.2 Post-injury: Absolute measurements of cardiac output measured with $\dot{Q}_{IST}$ and $\dot{Q}_T$ in each animal over the period of the protocol. . . . 141
6.3 Scatter and Bland-Altman plots comparing paired measurements of $\dot{Q}_{IST}$ and $\dot{Q}_T$ pre- and post- lung injury. . . . 142
6.4 The effect of shunt fraction on $\dot{Q}_{IST}$. . . . 144
6.5 Four-quadrant and Bland-Altman plots comparing paired measurements of $\Delta\dot{Q}_{IST}$ and $\Delta\dot{Q}_T$ pre- and post- lung injury. . . . 146

6.6 Polar plots comparing $\Delta\dot{Q}_{IST}$ and $\Delta\dot{Q}_T$ in uninjured and injured lung. 147

List of Abbreviations

$\Delta\mathbf{ELV}_{CT}$ Change in ELV measured by CT

$\Delta\mathbf{ELV}_{IST}$ Change in effective lung volume measured by the inspired sinewave technique

$\Delta\mathbf{ELV}_{O_2}$ Change in ELV measured by real-time change in P_aO_2

$\Delta\mathbf{ELV}_{SF6}$ Change in effective lung volume measured by SF_6 washin-washout

$\Delta\mathbf{P}$ Driving pressure

$\Delta\dot{Q}_T$ Change in cardiac output measured by pulmonary artery thermodilution

$\Delta\dot{Q}_{IST}$ Change in cardiac output measured by IST

$\dot{Q}_T$ Cardiac output measured by pulmonary artery thermodilution

$\dot{Q}_{IST}$ Cardiac output measured by IST

$\dot{D}_{O_2}$ Oxygen delivery

$\dot{Q}$ Cardiac output

$\dot{Q}_P$ Pulmonary bloow flow

$\dot{Q}_S/\dot{Q}_T$ Pulmonary shunt fraction

$\dot{V}_{O_2}$ Oxygen consumption

AART Alveolar amplitude response technique

ARDS Acute Respiratory Distress Syndrome

C_aO_2 Arterial oxygen content

C_{RS} Respiratory system compliance

CA Cyclical Atelectasis

CT Computed tomography

DBP Diastolic Blood Pressure

dCT Dynamic computed tomography

E_TCO_2 End-tidal CO_2

ECG Electrocardiography

EIT Electrical Impedance Tomography

ELV Effective Lung Volume

ELV_{CT} Effective lung volume measured by CT

ELV_{IST} Effective lung volume measured by the inspired sinewave technique

ELV_{O_2} Effective lung volume measured by changes in real-time P_aO_2

ELV_{SF6} Effective lung volume measured by SF_6 washin-washout

F_IO_2 Fraction of inspired oxygen

FQ Fluorescence quenching

FQ-Pt Platinum based fluorescence quenching

FQ-Ru Ruthenium based fluorescence quenching

FRC Functional residual capacity

GA General anaesthesia

GDT Goal-directed therapy

HME Heat moisture exchange filter

HU Hounsfield Units

I:E Inspiratory : expiratory ratio

IST Inspired sinewave technique

IV Intravenous

IVM Intra-Vital Microscopy

LUNGSAFE Large Observational Study to Understand the Global Impact of Severe Acute Respiratory Failure

MBNW Multiple breath N_2 washout

mMBNW Modified multiple breath N_2 washout

MP Mechanical Power

MV Mechanical ventilation

NC3Rs National Centre for Replacement, Refinement and Reduction of Animals in Research

O_2 Oxygen

ODM Oesophageal Doppler monitor

OSCAR Oscillation in ARDS

P_aO_2 Arterial partial oxygen pressure

P_{AW} Airway pressure

$\mathbf{P}_{PLAT}$ Plateau pressure

PAC Pulmonary artery catheter

PADP Pulmonary Artery Diastolic Pressure

PASP Pulmonary Artery Systolic Pressure

PATD Pulmonary Artery Thermodilution

PCV Pressure Controlled Ventilation

PEEP Positive end-expiratory pressure

PFR PaO_2:F_IO_2 ratio

PMMA Polymethylmethacrylate

$\mathbf{R}_{AW}$ Airways resistance

RR Respiratory rate

$\mathbf{S}_a\mathbf{O}_2$ Arterial oxyhaemoglobin saturation

$\mathbf{S}_p\mathbf{O}_2$ Peripheral oxyhaemoglobin saturation

SBP Systolic Blood Pressure

SNR Signal:Noise Ratio

TPTD Transpulmonary Thermodilution

$\mathbf{V}_A$ Volume of the alveolar comparment

$\mathbf{V}_D$ Volume of the dead-space compartment

$\mathbf{V}_T$ Tidal volume

$\mathbf{V}_T$10 End-inspiratory breath-hold manoeuvre with 10 ml kg^{-1} V_T

$\mathbf{V}_T$20 End-inspiratory breath-hold manoeuvre with 20 ml kg^{-1} V_T

VCV Volume controlled ventilation

Ve End-expiratory breath-hold manoeuvre

VILI Ventilator-Induced Lung Injury

CHAPTER 1

Introduction

1.1 Introduction

This thesis examines two novel techniques to study cardiopulmonary physiology in a preclinical, saline-lavage model of the acute respiratory distress syndrome (ARDS). The techniques studied are those of real-time partial pressure of arterial O_2 (P_aO_2) measurement using intra-arterial fibreoptic probes and the inspired sinewave technique (IST). This introductory chapter sets out the importance of mechanical ventilation (MV), the problems associated with MV in ARDS and how those problems are quantified in current clinical practice.

1.2 Delivering O_2 to tissues

Global oxygen (O_2) delivery ($\dot{D}_{O_2}$) is the product of cardiac output ($\dot{Q}$) and arterial O_2 content (C_aO_2). $\dot{D}_{O_2}$ is the amount of O_2 delivered to the tissues per unit time. Once O_2 is delivered to the tissue capillary its final pathway is diffusion from the capillary through interstitial and intracellular spaces to the mitochondrial cytochromes. This diffusion is driven by the PO_2 gradient between the capillary and the mitochondria. $\dot{D}_{O_2}$ maintains the head of pressure at the level of the capillary. From this point, O_2 flux to the mitochondria is limited by the resistance to diffusion and the ability of the mitochondria to consume O_2 and therefore maintain a low PO_2 (Farmery et al. 2001). The stepwise fall in PO_2 from the alveoli to the mitochondria is often referred to as the O_2 cascade. In some states of critical illness the metabolic consumption of O_2 ($\dot{V}_{O_2}$) increases, becoming dependent on $\dot{D}_{O_2}$. It is in this situation that clinicians utilise rescue techniques to support physiology and maintain $\dot{D}_{O_2}$ above its critical level, until the underlying pathology has been treated/corrected. MV is the cornerstone of the artificial physiological support provided in critical care.

In the last century MV has advanced from bulky negative pressure chambers towards microprocessor controlled, closed-loop smart-ventilators capable of responding to physiological variables and changing ventilation automatically (Ingelstedt et al. 1972; Kacmarek 2011). The main driver of ventilator development occurred in the

1930-1950's with the epidemic of poliomyelitis coinciding with mechanical engineering advances during the Second World War. It is at this time that reports from medical facilities ventilating large numbers of polio cases in *"iron lungs"* emerged of the damage MV itself can inflict (Avignon et al. 1956). The contemporary term for the injury which MV causes is ventilator-induced lung injury (VILI) (Slutsky et al. 2013). VILI encompasses the multifarious pathology found in injured lungs (including pathological inflammation, alveolar hyaline membrane formation, pulmonary vascular abnormalities and pulmonary oedema) and its underlying causes are divided into three groups:

- Damage caused by the application of excessive volume, *volutrauma* (Dreyfuss et al. 1995)
- Damage caused by application of excessive pressure, *barotrauma* (Kumar et al. 1973)
- Damage caused by the cyclical opening and closing of lung units, *atelectrauma* (Sugiura et al. 1994)

1.3 The Acute Respiratory Distress Syndrome (ARDS)

One condition which mandates mechanical ventilation in order to buy time for resolution of the underlying pathology is the acute respiratory distress syndrome (ARDS). Ashbaugh et al. (1967) first described ARDS in 1967 as a syndrome characterised by:

> "severe dyspnoea, tachypnoea, cyanosis that is refractory to oxygen therapy, loss of lung compliance and diffuse alveolar infiltration seen on chest X-Ray." (Ashbaugh et al. 1967)

ARDS is defined by an acute deterioration in oxygenation (PaO_2:F_IO_2 ratio (PFR) $<$ 300 mmHg) with bilateral opacities on chest radiography that cannot be explained by cardiac phenomena (Ranieri et al. 2012). A recent international investigation of the epidemiology of patients in intensive care with acute hypoxaemic

respiratory failure, the LUNGSAFE study (Bellani et al. 2016), found 67.2% met the criteria for ARDS which represented 10.4% of all admissions and 23.4% of all patients requiring MV. Mortality from severe ARDS, in this study, was consistent with others and remains up to 46% (Bellani et al. 2016; Ranieri et al. 2012). Whilst there was no analysis of the cause of mortality in the LUNG SAFE study, other authors have demonstrated that $< 20\%$ of deaths in patients with ARDS are a direct consequence of hypoxaemia (Stapleton et al. 2005).

1.3.1 Interventions to reduce mortality in ARDS

The most recent UK guidelines on the management of ARDS (Griffiths et al. 2019) consists of a comprehensive analysis of the quality and impact of data available on therapeutic interventions in ARDS. Of the ten interventions studied, the authors concluded the following had evidence to suggest a reduction in mortality:

- Protective ventilation:
  - Low tidal volume (V_T) ventilation (< 6 ml kg^{-1} ideal body weight)
  - Plateau pressure (P_{PLAT}) < 30 cmH_2O
- High positive end-expiratory pressure (PEEP) strategies for patients with moderate/severe ARDS
- Prone positioning for ≥ 12 hrs per day for patients with moderate/severe ARDS
- Paralysis with cisatracurium for 48 hrs
- Conservative fluid management strategy

Of these five, protective ventilation and the use of PEEP can be "set" on a mechanical ventilator. The impact of low tidal volume ventilation and limited plateau pressures on ARDS mortality was the outcome of one of the first multi-centre randomised controlled trials conducted in critical care. In the 2000 ARMA trial, the ARDSNet consortium showed that ventilation of patients with a protective ventilation strategy constituting V_T 6 - 8 ml kg^{-1} (based on ideal body weight) and P_{PLAT} < 30 cm H_2O had survival benefits over conventional ventilatory strategies (Acute

Respiratory Distress Syndrome Network et al. 2000). A similar strategy was also shown to result in less barotrauma (Amato et al. 1998).

The application of PEEP as an intervention to improve survival from ARDS has been investigated in numerous multi-centre trials with mixed results. PEEP has been demonstrated to improve lung recruitment and P_aO_2 in mechanically ventilated patients with lung injury (Richard et al. 2003). In three large trials (LOVs, ALVEOLI, ExPRESS trials) higher levels of PEEP did not convey survival benefit (Meade et al. 2008; The National Heart Lung and Blood Institute ARDS Clinical Trials Network 2004; Mercat et al. 2008) whilst a retrospective secondary analysis of the 2008 LOVS trial demonstrated increased oxygenation in response to PEEP was associated with improved survival (Goligher et al. 2014). More recently, higher PEEP levels titrated to optimal respiratory system compliance (C_{RS}) increased mortality in patients with moderate - severe ARDS (Cavalcanti 2017). These trials suggest that there is an optimum level of PEEP and taken with the heterogeneity of the ARDS population it follows that each individual's optimum ventilator setting, in terms of PEEP, may be unique to them and dynamic across the course of the disease.

1.3.2 The baby lung in ARDS

First coined in the 1980's, the phrase "baby lung" refers the reduced volume of lung which remains "open" (or aerated) at end-expiration in patients with ARDS (Gattinoni et al. 1986a; Gattinoni et al. 2005). The risk of VILI varies considerably in patients with ARDS receiving the same low tidal volume ventilation strategy (Gattinoni et al. 2005; Acute Respiratory Distress Syndrome Network et al. 2000; Chiumello et al. 2008a). Regional overdistension from high V_T relative to baby-lung size causes alveolar epithelial and capillary endothelial damage, basement membrane detachment, oedema formation and systemic inflammation (Fu et al. 1992). The variability of the size of the baby lung within the ARDS population means that the generic ventilator strategies cause different stresses and strains in different patients. Despite the widespread adoption of the recommended lung protective ventilation strategy with low V_T based on the patient's predicted body weight, patients with ARDS still develop VILI (Grieco et al. 2017). This may be because of the effect of the MV settings on the underlying small aerated lung.

Indeed, one of the original arguments for using and studying low V_T in ARDS was that the V_T should be scaled to the size of the baby lung. As discussed above, this strategy was demonstrated to improve mortality rates in ARDS (Acute Respiratory Distress Syndrome Network et al. 2000). However, the ability to quantify the volume of the baby lung in both research and clinical practice remains limited by the absence of a simple bedside technique (Beitler et al. 2016).

1.4 Ventilator Induced Lung Injury (VILI), stress and strain

Gattinoni's early description of the relationship between lung "stress" and "strain" explains the concepts well (Gattinoni et al. 1987). The authors define "stress" as the tension within the pulmonary parenchyma which is equal and opposite to the force applied to the lung by the ventilator. The applied pressure is not the airway pressure (P_{AW}), but the difference between the airway pressure and the pressure at the pleural surface *i.e.* the transpulmonary pressure. The pulmonary parenchymal tension associated with elongation of the fibres from their resting state is the "strain". The relationship between global lung stress and strain is given by a version of Hooke's law (Gattinoni et al. 2003):

$$Stress = k \times Strain \tag{1.1}$$

where k is the specific lung elastance.

The earlier classification of the causes of lung injury (volutrauma, barotrauma and atelectrauma) can be explained within the context of stress and strain. Stress, which is the force per unit area, is represented in the respiratory system as transpulmonary pressure and excess of which can cause barotrauma (Chiumello et al. 2008a). Lung stress inferred from measured airway pressure alone is a problematic concept for several reasons. Firstly, the distribution of the applied P_{AW} causes non-uniform expansion of lung parenchyma within the thorax. Secondly, when there are alveoli which do not communicate with the conducting airways (such as in ARDS), the stress of these alveoli cannot be inferred from P_{AW}. Thirdly, in the ARDS lung there

exist heterogeneous stress concentrations (so-called stress-risers) between a network of interdependent parenchymal regions, which have the effect of multiplying stresses at these nexuses (Hubmayr et al. 2018).

Strain describes the effect the imposed change in volume has on the underlying aerated lung. The change in volume has both static and dynamic components which contribute to either static or dynamic strain. Static strain represents the change in lung volume at end-expiration with applied PEEP compared to the lung size with zero PEEP (FRC). Dynamic strain represents the change in volume during an imposed breath and is equivalent to the effect of the V_T on available FRC (Chiumello et al. 2008a). Thus the concept of strain accounts for the potentially traumatic effects of the imposed volume (leading to volutrauma) and of opening and closing of lung units during tidal ventilation (leading to atelectrauma) (Gattinoni et al. 2005; Gattinoni et al. 2016a).

In summary,

$$\text{Dynamic strain} = \frac{\Delta V}{V_{FRC}} = \frac{C_{RS} \times \Delta P}{V_{FRC}} \tag{1.2}$$

$$\text{Static strain} = \frac{V_{EXP}}{V_{FRC}} \tag{1.3}$$

where:
ΔV = the change in volume during the breath (V_T),
V_{FRC} = the functional (aerated) volume of the lung at the end of expiration with zero PEEP,
C_{RS} = the respiratory system complicance,
ΔP = the driving pressure or the difference between P_{PLAT} and PEEP,
V_{EXP} = the volume of the lung at the end of expiration (with PEEP).

1.4.1 Dynamic strain in ARDS

Both volutrauma and atelectrauma in ARDS are thought to be manifestations of the effect inappropriate strain on the baby lung. The effect of the interventions of protective ventilation and PEEP can be accounted for by the consideration of

the components of dynamic strain, which are shown in equation 1.2. Low V_T and limiting P_{PLAT} reduce ΔP, whilst the application of PEEP contributes to the optimisation of C_{RS}. ΔP has been demonstrated as the ventilator parameter which best stratifies the risk of mortality in ARDS (Amato et al. 2015). Figure 1.1 demonstrates this finding. Other authors have suggested that this effect may be explained because ΔP is a surrogate for dynamic strain (Guérin et al. 2016). It is possible that the finding of reduced mortality with lower ΔP reflects a change in lung mechanics following a change in ventilator setting and thus targeting a specific threshold of ΔP may not in itself reduce mortality (Guérin et al. 2016).

The effect of specifically titrating ventilation to limit ΔP in ARDS has yet to be tested prospectively. However, *in silico* simulation investigating the association between ΔP and VILI demonstrated that dynamic strain, tidal recruitment and "mechanical power" were strongly positively correlated with the mortality risk associated with changes in ΔP reported by Amato et al. (2015) (Das et al. 2019).

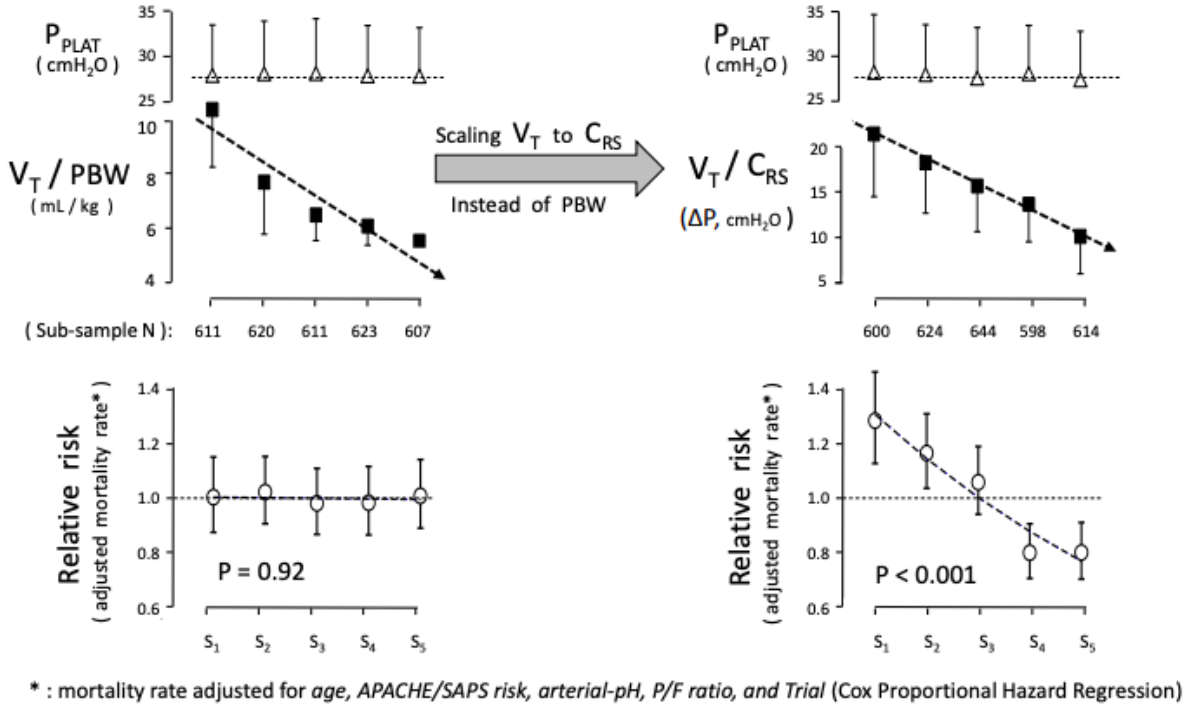


Figure 1.1: Scaling tidal volume to respiratory system compliance reduces mortality in ARDS. *Reproduced with permission from Amato et al. (2015). Copyright Massachusetts Medical Society. In the left column the authors resampled their cohort into quintiles according to V_T and in the right column according to ΔP. In each resampling (left and right columns), the plateau pressures are similar across the ranges of V_T and ΔP. There is no effect on the risk of mortality as V_T scaled to body weight reduces (bottom panel of the left column), however relative risk of mortality decreases when V_T is scaled to respiratory system compliance (bottom panel of the right column). Amato et al. (2015) emphasise in their figure that the mathematical relationship "$\Delta P = V_T/C_{RS}$" represents V_T normalised to respiratory system compliance.*

Atelectrauma is associated with repeated opening and closing of alveoli during ventilation (cyclical atelectasis (CA) and has been identified as a cause of lung injury in animal models (Sugiura et al. 1994; Muscedere et al. 1994; Slutsky 1999). The pressures required to tidally recruit areas of atelectasis are predicted to be much greater than the applied P_{AW} (Mead et al. 1970). CA's contribution to VILI is thought to underlie the survival benefits associated with and "open lung" ventilation strategy (Amato et al. 1995; Briel et al. 2010). It was on this basis that the putative benefits of high frequency oscillatory ventilation in ARDS were considered. A technique which is based around the application of a constant mean pressure to keep airways open. However, the Oscillation in ARDS (OSCAR) study group's 2013 trial showed no improvement in mortality when compared to conventional ventilation (Young et al. 2013) in patients with ARDS. This has lead to further discussion of the balance between CA and over-distension (Dreyfuss et al. 2015).

Gattinoni et al. (2016b) proposed that the ventilator-related causes of lung injury could be unified into a single variable, which they called the mechanical power (MP):

$$MP = RR \times \left\{ {V_T}^2 \left[\frac{1}{2}.EL_{RS} + RR.R_{AW}.\frac{1 + I:E}{60 \times I:E} \right] + V_T.PEEP \right\} \qquad (1.4)$$

where:
RR = the respiratory rate,
V_T = the tidal volume,
EL_{RS} = the elastance of the respiratory system,
I:E = the inspiratory : expiratory ratio and
R_{AW} = the airways resistance
The authors proceeded to test the impact of MP in an animal model to demonstrate that VILI could be induced in healthy lungs when MP exceeded a certain threshold (12.1 J min^{-1}). MP provides a global description of the energy exerted by MV on the lung which is available to receive it.

1.5 The rationale for measuring lung volume in mechanically ventilated patients with ARDS

As discussed, patients with ARDS are at particular risk of VILI owing to their smaller aerated lung volume ("baby lung"). Mortality in ARDS can be reduced by ventilating patients with 6 – 8 ml kg^{-1} tidal volume (V_T) (Acute Respiratory Distress Syndrome Network et al. 2000; Gattinoni et al. 2005; Gattinoni et al. 2016a), optimising PEEP and potentially, limiting ΔP (Amato et al. 2015; Gattinoni et al. 2016b). The concept of dynamic strain can account for the effects of these three mechanisms and depends on the size of the baby lung (Chiumello et al. 2008b; Hubmayr et al. 2018). There would, therefore, be potential benefit in measuring the underlying effective lung volume (ELV) at the bedside of the mechanically ventilated ARDS patient. This would allow:

1. personalised titration of V_T to the underlying aerated lung volume, with limitation of lung stress caused by ΔP
2. personalised optimisation of PEEP to limit both cyclical atelectasis and overdistension (Gattinoni et al. 2017)

Measurements of functional lung volume are not easily made in intubated and ventilated critical care patients (Hedenstierna 1993). In the spontaneously ventilating patient, volume assessment requires cooperation (the ability to obey commands and undertake specific expiratory & inspiratory manoeuvres) and bulky equipment (Criée et al. 2011). These prerequisites exclude mechanically ventilated patients in whom formal assessment of effective lung volume could be used to target specific therapeutic interventions (Rylander et al. 2004; Gattinoni et al. 2005; Chiumello et al. 2008a; Gattinoni et al. 2016a).

1.6 Established methods of measuring lung volume

The term "lung volume" can refer to any of the static lung volumes measured by conventional spirometry. Unless otherwise stated, reference to measurement of lung volume in this thesis refers to the volume of aerated lung at the end of expiration, either FRC (when there is no extrinsic PEEP applied) or end-expiratory lung volume (when PEEP has been applied). The following section summarises the current conventional methods of lung volume measurement in mechanically ventilated patients, which fall into three main categories:

1. Plethysmography
2. Gas-based techniques
3. Imaging techniques

1.6.1 Whole body plethysmography

The "gold-standard" method to quantify FRC is whole body plethysmography (Goldman et al. 2005). The technique requires the patient be enclosed in a rigid-walled chamber which is closed with an air-tight seal. The patient breathes through a tube connected to the atmosphere which has a pressure transducer and flowmeter with a shutter valve.

Plethysmography exploits Boyle's law which states that for a given mass of gas in a closed system, the absolute pressure is inversely proportional to the volume that it occupies ($P \propto \frac{1}{V}$). Thus, for a patient in a sealed box, when the airway shutter valve is closed, the thoracic gas volume changes with inspiratory and expiratory effort and the pressure changes at the mouth (which are assumed to be equivalent to those at the alveoli) are used to deduce the volume of gas within the thorax. The volume of gas measured is that of the total gas within the thoracic cage, regardless of whether or not is that gas is freely communicating with or trapped behind obstructed airways. This may represent an overestimation of the functional volume of gas in lung and has been interpreted as a systematic overinterpretation of FRC in patients with obstructive lung disease (O'Donnell et al. 2010).

Whole-body plethysmography is not practical in the context of mechanically ventilated adults patients. Its use is precluded by the size/bulk of the equipment required (Criée et al. 2011), its expense and the reliance on the patient to undertake respiratory manoeuvres (Newth et al. 1997).

1.6.2 Gas-based techniques

1.6.2.1 Helium Dilution

The He dilution method relies on a known volume of gas containing a known fraction of He equilibrating with the gas in the lung. He dilution requires rebreathing of gas within a closed system until both the reservoir and the lung are in equilibrium, in terms of He concentration. When the concentration of He is the same in all parts of the system, the final concentration of He within the reservoir is measured and the total volume of distribution of the He calculated. The rebreathing of gas demands removal of CO_2 and its replacement with O_2. The absorption of He into the body and shift ot N_2 from the body compartment to the lung compartment are ignored.

The conventional He dilution method was adapted by Heldt et al. (1978) for measurement of FRC in ventilated patients. He dilution shows good repeatability of measurements in ventilated patients (Di Marco et al. 2007) with good correlation to measurements of FRC taken with CT (Chiumello et al. 2008b) and an underestimation compared to both CT and plethysmography (Schaanning et al. 1973; Chiumello et al. 2008b). However, the adapted system has several limitations. The additional equipment adds both increased compliance and resistance to the breathing circuit and if the consumption of O_2 is not balanced with its supply measurement errors are introduced. Like other gas-based techniques, He dilution measures the volume of the gas in continuity with the airway. One advantage of the He dilution method is that low concentrations of He (3%) can be used in O_2, meaning measurements are possible in patients requiring high F_IO_2.

1.6.2.2 Multiple-breath Nitrogen washout (MBNW)

The N_2 washout method relies on the patient breathing 100% O_2 from the start of an inspiration and collection of the expired gases to the point where the N_2 has been "washed-out" of the respiratory system. The total volume of N_2 washed out (less the amount produced by the body) can then be used, in combination with the fractional concentrations of N_2 from the beginning and end of the procedure, to calculate FRC. This is the original "closed-circuit" method. Inaccuracies introduced during measuring the volume of the expiratory bag or final N_2 concentration introduced significant bias in the calculation of FRC (Newth et al. 1997) and the period of 7 mins for washout was inadequate for patients with obstructive airways disease, where a period of up to 15 mins was required for washout collection (DuBois et al. 1956; Emmanuel et al. 1961).

The use of MBNW became simpler with the advent of rapid gas analysers and improved computing ability. These allowed for instantaneous calculation of N_2 volume by integration of the concentration of tracer gas multiplied by the flow measured at that time. MBNW has been applied at the bedside of the ventilated patient requiring a second ventilator. Using one ventilator for inspiration of 100% O_2 a second ventilator measures the volume of N_2 in the expiratory gases. The two-ventilator MBNW method has shown to be both accurate and reproducible during mechanical ventilation (Sivan et al. 1990), however it has several limitations that limit its use. Serial measurements to track changes in FRC over the course of minutes are not possible and the technique requires bulky equipment at the bedside (an extra ventilator). Additionally, because large changes in F_IO_2 are required to create a significant perturbation in N_2, MBNW can only be used for patients breathing $< 70\%$ O_2. Olegård et al. (2005) attempted to circumvent this problem by using smaller changes in O_2 (as described below in Section 1.6.2.3).

Brewer et al. (2011) assessed the feasibility of a modified MBNW (mMBNW) method, which used rapid gas analysis to calculate the fractional concentration of N_2 by measuring and subtracting the fractional concentrations of O_2 and CO_2 from the expired airway gases. The authors demonstrated the mMBNW technique had good agreement with plethysmography (in awake volunteers) but relatively poor repeatability of measurements (coefficient of repeatability 12.7%) in the mechanically ventilated cohort. The change in viscosity of exhaled N_2 affects the accuracy of gas

flow measurements and the use of side stream gas analysers introduces a lag between gas measurements which must be taken into account. Currently, the limitations of MBNW outweigh its benefits and it is not a commonly deployed monitor of FRC in the critically ill patient.

1.6.2.3 O_2 washin-washout

As early as 1982, O_2-based methods of quantifying FRC in during mechanical ventilation were reported (Mitchell et al. 1982). The advantages of using O_2 as a tracer gas, are that it does not require any further cylinders or equipment, is already in use and its analysers are readily available. Fretschner et al. (1993) adapted the technique for use in ventilated patients and further development was undertaken to produce two commercially available systems. At that time, the standard methods of measuring FRC in ventilated patients were based on dilution of inert gases (He or SF_6) or MBNW. Tracer gas dilution required special, costly equipment and MBNW required a large change in F_IO_2 to create a a large enough change in N_2 to measure FRC. This was not possible in unwell patients requiring a high F_IO_2.

Stenqvist and colleagues presented a solution to this problem using only a limited change in F_IO_2 (10 %) and measuring end-tidal concentrations of O_2 and CO_2 (Olegård et al. 2005). Their method forms the basis of the commercially available GE Engström Carestation FRC Inview^{TM}, which has been compared to CT imaging in fully mechanically ventilated adults (Chiumello et al. 2008b) and against an FRC model in a paediatric population (Olegard et al. 2010). In the adult population the technique had a mean bias of + 94 ml compared to CT and in children a bias of + 2 ml compared to the model.

Parallel development of a similar method based on Fretschner et al. (1993)'s work was undertaken to produce the LUFU^{TM} system by Dräger Medical (Weismann et al. 2006; Heinze et al. 2007; Maisch et al. 2007; Patroniti et al. 2008). One source of error with O_2 washin-washout had been the long lag time between measurements of gas flow and measurements of O_2 concentration taken with a sidestream gas analyser. This limitation of Fretschner's method was covercome *in vitro* by utilising more rapid gas sensors (Weismann et al. 2006). Heinze et al. (2007) and Maisch et al. (2007) compared Weismann's adapted system against He dilution and

plethysmography in spontaneously ventilating patients demonstrating comparable accuracy with acceptable repeatability (mean bias compared to He-dilution - 200 ml and compared to plethysmography +100 ml). These results were replicated in mechanically ventilated patients (Patroniti et al. 2008).

Whilst both systems demonstrate good results in fully controlled mechanical ventilation, there are specific limitations that must be taken into account when considering assisted mechanical ventilation (Weismann et al. 2006). During assisted ventilation, the difference between inspired and expired volumes can be altered breath-by-breath by intermittently large tidal volumes which persist until the end of the breath.

1.6.2.4 Sulphur hexafluoride (SF_6) washout

Originally described by Jonmarker et al. (1985) and developed by Larsson et al. (1987) this is an inert tracer gas multiple-breath washout method of measuring end-expiratory lung volume. Although not widely adopted clinically because of the availability of equipment, it provides accurate and repeatable measurements and has been tested in ventilated model lungs, anaesthetised adults and infants (Jonmarker et al. 1985; Larsson et al. 1987; Vilstrup et al. 1992; Schulze et al. 1994; Schibler et al. 2002). It is used as one of the techniques against which IST is compared in Chapter 5 and full details of the SF_6 method of FRC measurement are discussed in Section 2.7.

1.6.2.5 The Inspired Sinewave Technique

The name "Inspired Sinewave Technique" (IST) describes a method based on forcing sinusoids of a tracer gas into inspired airway gases to recover estimates of an alveolar compartment taking part in gas exchange (V_A), a dead-space volume (V_D) and a blood flow to the alveolar compartment ($\dot{Q}_P$). It is based on work by Zwart et al., (Zwart et al. 1976; Zwart et al. 1978) with major contributions to its development coming from Hahn and colleagues. IST is one of the techniques experimentally investigated in this thesis. The method is described fully in Section 2.6.

1.6.2.6 Laser gas absorption spectroscopy

Molecular flow sensing (MFS) using highly precise in-airway laser gas analysis assesses the composition of respiratory gases (Ciaffoni et al. 2016). Using the technology Mountain et al. (2018) modelled 125 units of gas exchange within the lung aiming to develop a novel method to non-invasively assess lung inhomogeneity. The applied model produces estimates of total alveolar volume and deadspace. MFS has not yet been specifically tested in its ability to measure lung volume and remains a research tool, however it is thought to be a promising technique for the early detection of lung damage and monitoring disease progression (Petousi et al. 2019).

1.6.3 Imaging-based methods to measure lung volume

Plain chest radiography, CT and magnetic resonance imaging (MRI) have all been used to quantify absolute lung volumes (Clausen 1997). The advent of modern 3D imaging has superceded the use of plain radiographs. CT and MRI allow measurement of lung volume, make estimates of tissue and air volumes and of volumes of different densities. The 2005 ERS/ATS task force statement on the standardisation of lung volume measurement does not recommend one method over another (Wanger et al. 2005).

The use of CT imaging to gain further insight into the ARDS lung was largely driven by Gattinoni (Bone 1993; Gattinoni et al. 1986a; Gattinoni et al. 1986b). Using quantitative assessment of the x-ray density of lung tissue imaged by CT, the analysis is based on the correlation between x-ray attenuation for a given voxel and the physical density of the volume of lung within that voxel (Gattinoni et al. 2001). The attenuation of the x-rays is expressed in Hounsfield units (HU). The HU attenuation scale assigns complete xray absorption a value of + 1000 HU, no absorption - 1000 units and water a value of 0 HU.

Comparing CT to He dilution and FRC Inview^{TM}, CT underestimated end-expiratory lung volume by 94 ml compared to FRC Inview^{TM} and overestimated by 136 ml compared to He dilution in mechanically ventilated patients (Chiumello et al. 2008b). In non-ventilated patients, there is no significant difference between

lung volume measured by CT, He dilution and body plethysmography (O'Donnell et al. 2010).

1.7 The rationale for measuring cardiac output

Oxygen consumption ($\dot{V}_{O_2}$) may increase in the unwell patient or those undergoing major surgery. Older et al. (1988) demonstrated post-operative increases in $\dot{V}_{O_2}$ by 44% from pre-operative baseline measurements. Under normal circumstances $\dot{D}_{O_2}$ is sufficient to meet the requirements of $\dot{V}_{O_2}$. The increased $\dot{V}_{O_2}$ caused by major surgery or critical illness when combined with intravascular volume depletion can lead to organ dysfunction. Optimisation of $\dot{Q}$ and therefore $\dot{D}_{O_2}$ is the basis of goal-directed therapy (GDT) (Older et al. 1993; Lobo et al. 2011). GDT describes the administration of fluid and vasoactive drugs to peri-operative or critically unwell patients to optimise specific, measured cardiovascular variables, such as caridac output (Dunn et al. 2016).

The ability to quantify and therefore target a specific value of $\dot{Q}$ gained clinical interest in the 1960's as a modified cardiac catheter was used to quantify $\dot{Q}$ using thermodilution (Branthwaite et al. 1968). A balloon-tip was then added to facilitate flotation (Swan et al. 1970) and the pulmonary artery catheter (PAC) was subsequently widely adopted as a diagnostic and therapeutic tool to guide the care of critically unwell patients (Marik 2013b). Use of the PAC subsequently declined as an observational study of 5732 intensive care patients showed a 24 % increase in mortality in patients receiving a PAC within the first 24 hours of their intensive care admission (Connors et al. 1996). Following this study, the PAC-man randomised controlled trial failed to show the benefit of PAC guided therapy in intensive care patients (Harvey et al. 2005) and since that time use of the PAC has mainly been confined to specialist cardiac centres (Marik 2013b).

Despite the evidence against the use of the PAC, interest in targeting therapy to optimise $\dot{Q}$ has continued. The appeal of the early findings of Shoemaker et al. maintained interest in the filed. Shoemaker demonstrated that survivors of high-risk surgery had significantly increased cardiac index and $\dot{D}_{O_2}$ than people who did not survive (Shoemaker et al. 1973). The authors then proceeded to prospectively trial

GDT using PAC measurements and showed improvements in the number of post-operative deaths (Shoemaker et al. 1988). These potential benefits of optimising $\dot{D}_{O_2}$ by targeting specific goals, combined with the risks of the PAC has lead to the development of minimally and non-invasive CO monitoring devices. The most commonly used of these are the oesophageal Doppler monitor (ODM) and peripheral pulse contour analysis (calibrated with with Li or thermodilution).

The use of the CardioQ-ODM device is recommended by the UK's National Institute for Heath and Clinical Excellence (NICE) to guide intraoperative fluid therapy in high risk patients (https://www.nice.org.uk/guidance/mtg3). Mythen et al. (1995) used ODM guided GDT to demonstrate improved gastric mucosal perfusion in the GDT group, which was associated with reduced post-operative complications and post-operative intensive care days. Similarly, Li-dilution CO monitoring (LiDCO^{TM}) was shown to reduce post-operative complications and the length of hospital stay in a 2005 RCT (Pearse et al. 2005).

More recently, a UK multicentre RCT compared outcomes in high-risk surgical patients receiving either usual care or LiDCO guided GDT. Although the trial itself did not demonstrate reduction in complications or mortality in the intervention group, the authors included their data in a meta-analysis which did indicate a reduced complication rate (Pearse et al. 2014). A 2012 Cochrane meta-analysis examined the effect of perioperative goal-direct therapy on post-operative outcome (Grocott et al. 2012). Analysing 31 studies with a total of 5,292 participants, the authors found no difference in mortality, however there were reductions in renal failure, respiratory failure and wound infections were reduced when global blood flow was increased. Additionally, there was a reduction in the length of stay in critical care and the authors highlight that there was no suggestion of harm from using GDT to optimise blood flow.

Considering the intuitive physiological benefits of $\dot{Q}$-based optimisation of $\dot{D}_{O_2}$, the supportive evidence and the lack of harm from minimally-invasive GDT, it seems clear that striving to identify a method of continuous $\dot{Q}$ monitoring may be beneficial to the mechanically ventilated patient.

One of the experimental methods examined in this thesis, the Inspired Sinewave Technique (IST), could potentially provide such monitoring.

1.8 Research aims

Considering the complex relationships between cardiopulmonary variables in the mechanically ventilated patient, the main aim of this thesis was to investigate the use of two novel techniques that may be capable of measuring these variables at the bedside, without patient cooperation and with operator independent results. Using real-time P_aO_2 measurements and IST, this thesis aimed to answer the following questions using a porcine model of mechanical ventilation with a saline-lavage model of ARDS:

1. Whether, and to what extent, CA is present in mechanically ventilated lungs with a saline-lavage model of ARDS and how CA may be involved in the dynamic determination of arterial oxygenation?
2. Can changes in P_aO_2 measured in real-time be used to model the volume of the lung?
3. How well do IST's measurements of lung volume agree with standard techniques?
4. How well do IST's measurements of $\dot{Q}$ agree with standard techniques?

1.9 Thesis outline

To achieve the aims above, the thesis presents background information on the context and rationale for making measurements in patients subjected to mechanical ventilation and then presents the experiments used to examine each of the aims. The chapters are structured as follows:

- The Methods chapter provides details of protocols and techniques common to the subsequent sets of experiments. In addition this chapter provides further details on the two main experimental methods used:
  - Real-time measurement of P_aO_2 using fibre-optic probes
  - The inspired sinewave technique

- Chapter 3 presents the experimental investigation into the relationship between respiratory oscillations in P_aO_2 and cyclical recruitment/derecruitment of atelectasis measured by single-slice dynamic computed tomography.
- Chapter 4 presents experiments designed to test the hypothesis that the same technology applied in Chapter 3 can be used to make measurements of lung volume.
- Chapter 5 proceeds to test measurements of lung volume made with an alternative method, the Inspired Sinewave Technique. IST is compared against the reference techniques of SF_6-washout and CT.
- Chapter 6 extends the interrogation of IST to assess its measurements of CO compared against intermittent PAC thermodilution.
- The final chapter (General discussion and conclusions) summarises and concludes the work presented. It provides some possible future directions the research could take and considers some limitations of the work.

CHAPTER 2

Methods

2.1 Introduction

This chapter provides details of the experimental procedures and data processing which are common to the experimental work carried out in the subsequent experimental chapters.

2.2 Experimental logistics and timing

Experiments for the work detailed in Chapters 3, 4 and 5 were carried out at the Hedenstierna Laboratory, Uppsala University, Sweden. These protocols, although different, all followed similar timings. The specifics of each protocol are detailed in the relevant chapters. The generic experimental timeline for these experiments is shown in Figure 2.1.

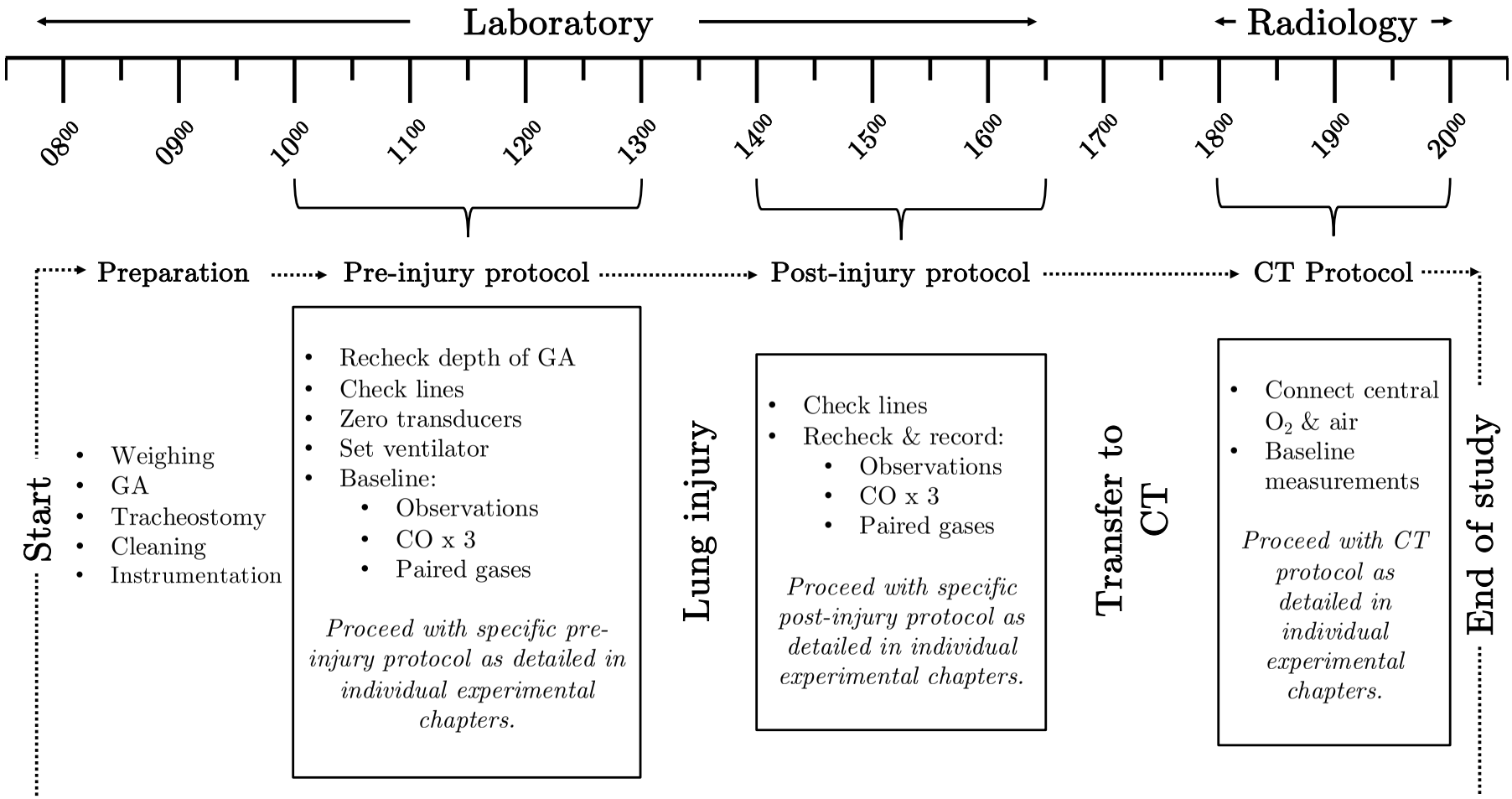


Figure 2.1: Summary experimental timeline. *Animals arrived at c0745, as shown in the timeline. Animal preparation was usually complete by 1000. The CT scanner is available from 1730, and is located a 20 min walk from the laboratory. Not included in this figure is the pre-experimental time for preparation of drugs, syringe labelling and double checking equipment. Likewise, at the end of the protocol, time was taken to clean equipment, backup data and prepare for the next experiment. GA = general anaesthesia, CO = thermodilution cardiac output measurements, paired gases = simultaneous arterial and mixed venous blood gas sampling.*

2.3 The use of an animal model

2.3.1 Considerations for the use of animals as experimental subjects.

The use of animals as experimental subjects is preferably avoided on welfare grounds and because the results have limitations in their direct translation to human medicine. However, testing the hypotheses investigated in this thesis required iatrogenic injury and repeated exposure to ionising radiation. Using human subjects would be unethical. I have endeavoured to answer questions about critical illness and the hypotheses under investigation include the use of non-CE marked equipment. Thus, the use of animal models was necessary. In line with Home Office recommendations, the National Centre for Replacement, Refinement and Reduction of Animals in Research (NC3Rs) guidance, basic principles of animal welfare (Flecknell 2002) and my personal commitment as a member of the Royal College of Veterinary Surgeons the welfare of the subjects was a priority throughout. A minimum number of animals were used to test each of the hypotheses in the experimental chapters and all protocols were subject to the relevant ethical approval, as specified in each chapter.

2.3.2 Choice of animal model

Pigs were chosen as the species of investigation for a number of physiological and pragmatic reasons. On investigation of the cardiorespiratory system, a number of factors were taken into account:

- **Pigs are well established model for translational cardiopulmonary research (Swindle et al. 2012).** In some of the previous studies of both IST and the intravascular PaO_2 probe dogs were used a model (Williams et al. 1994a; Williams et al. 1994b; Hahn 1996; Williams et al. 2000). However, dogs, unlike pigs and humans have extensive collateral ventilation (Domino et al. 1998). In the context of experimental recovery of measured lung volumes and real-time P_aO_2 measurements, the effects of collateral ventilation may well

cause changes in airway pressure and have effects on $\dot{V}/\dot{Q}$ matching which would not best represent the situation in human patients.

- **Resource availability and logistics.** In considering what species to use for an experimental model, consideration must be given to what species have previously been used and where the experiments are to be conducted.

2.3.3 Anaesthesia and surgical instrumentation

Animals were pre-medicated with intramuscular xylazine 2 mg kg^{-1}, ketamine 20 mg kg^{-1} and midazolam 0.5 mg kg^{-1} and underwent induction of anaesthesia with intravenous (IV) propofol titrated to effect (1- 3 mg kg^{-1}). The trachea was intubated via surgical tracheostomy and mechanical ventilation subsequently commenced. During preparation and before commencement of the study protocol, animals were ventilated with volume-controlled ventilation (VCV) at 20 - 25 breaths per minute (to maintain E_TCO_2 4.5 – 6 kPa), with a V_T of 10 ml kg^{-1}, PEEP of 5 cmH_2O and an inspiratory:expiratory ratio (I:E) of 1:2. The ventilator tubing and endotracheal tube were checked for leaks by analysis of the spirometry data. Anaesthesia was maintained with continuous intravenous ketamine 32 mg kg^{-1} hr^{-1}, fentanyl 4 μg kg^{-1} hr^{-1} and midazolam 0.16 mg kg^{-1} hr^{-1}. General anaesthesia was confirmed by absence of spontaneous movements and by lack of reaction to painful stimulation between the front hooves. After confirmation of general anaesthesia, muscle relaxation was achieved with an initial bolus of rocuronium 0.2 mg kg^{-1} followed by 0.1 mg kg^{-1} boluses when spontaneous ventilatory efforts were detected from the airway gas and pressure traces. The adequacy of anaesthesia was determined during the periods of muscle relaxation by absence of cardiovascular signs of sympathetic stimulation (increases in heart rate or arterial blood pressure). Maintenance fluids were administered IV in the form of isotonic electrolyte solution (Ringerfundin; B. Braun Melsungen AG, Melsungen, Germany) at a rate of 10 ml kg^{-1} hr^{-1} during the instrumental phase and 7 ml kg^{-1} hr^{-1} for the rest of the protocol. Figure 2.2 provides a schematic of invasive line placement common to each set of experiments.

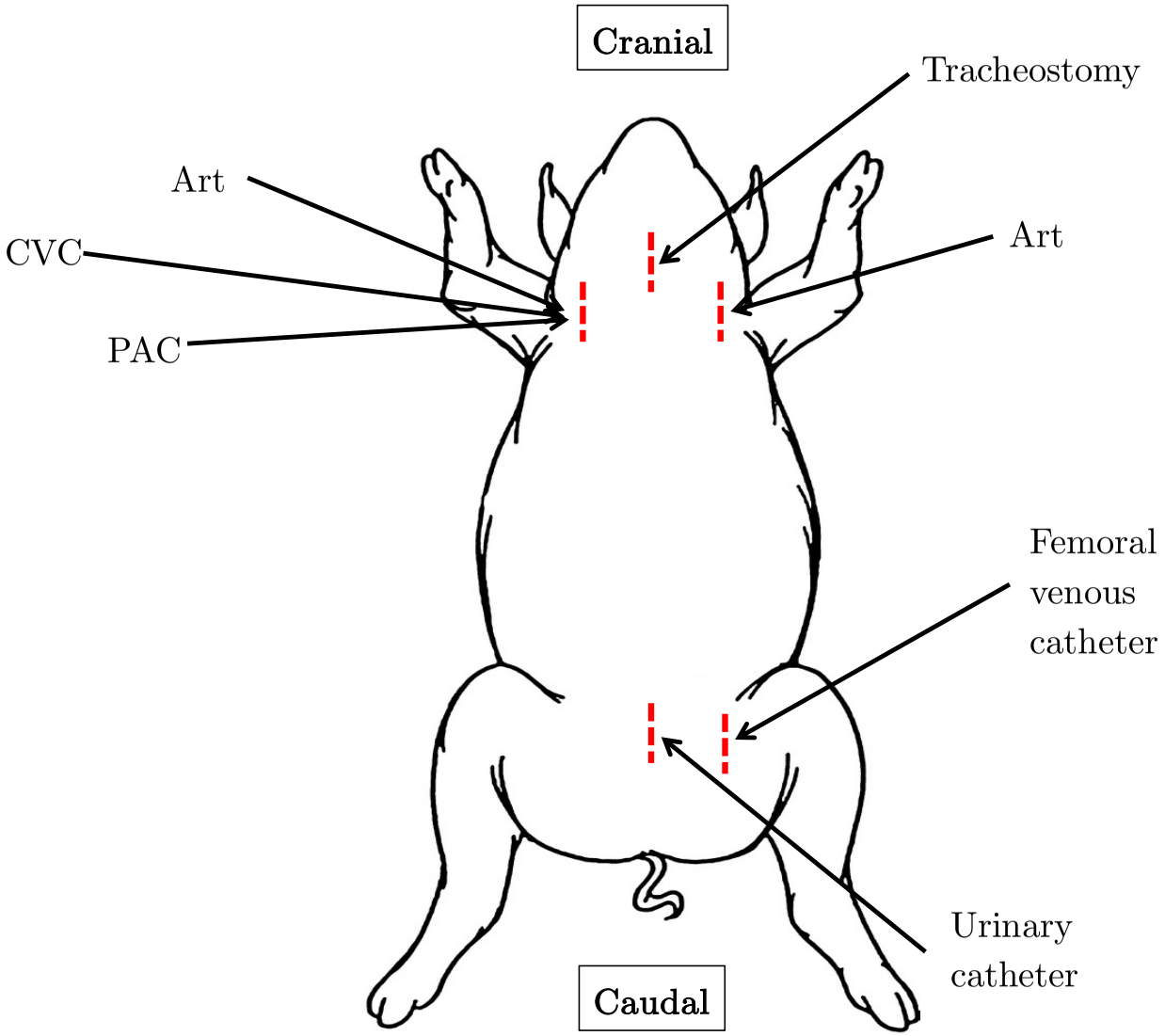


Figure 2.2: Schematic of invasive line placement for each animal. *With the animal in dorsal recumbency, surgical incisions (marked with red dashed lines) were made and tubes/catheters inserted under direct vision. Art = arterial catheter, CVC = central venous catheter, PAC = pulmonary artery catheter.*

2.4 Real time, *in vivo* P_aO_2 measurement using fibre optic photonic sensors

Fluorescence quenching (FQ) describes the ability of a molecule to suppress the photo-luminescence emitted by an excited fluorophore. In the case of sensors used to detect oxygen, it is the O_2 molecule which quenches the fluorescence emitted from a transition metal fluorophore (Formenti et al. 2017b; Chen et al. 2016; Formenti et al. 2014; Chen et al. 2013). The fluorophore is held *in situ* within a polymethylmethacrylate (PMMA) matrix, in the tip of a fibre-optic probe.

When a beam of pulsed light is transmitted down the core of a fibre-optic cable, it travels by means of total internal reflection to the end of the cable. In the case of the PO_2 probes, the end of the cable is tapered and doped with an excitable platinum fluorophore. On reaching the tip, light escapes from its channel, penetrates the fluorophore-doped matrix and excites electrons within the compound to a higher energy level. Upon returning to their base state, the electrons release quanta of energy as photons. The released photonic energy returns back up the fibre-optic cable to a spectrophotometer where it is measured. This process is illustrated in Figure 2.3. (Chen et al. 2012a; Chen et al. 2013; Formenti et al. 2014; Formenti et al. 2017b)

An increase in the concentration of O_2 within the matrix causes greater quenching of this process and less light to be returned to the spectrophotometer. The relationship is represented mathematically by the Stern-Volmer equation:

$$\frac{I}{I_0} = \frac{1}{1 + k_{SV}[O_2]} \tag{2.1}$$

In equation 2.1, I is light intensity and I_0, the intensity of light when there is no O_2, k_{SV} is the Stern-Volmer constant and $[O_2]$ is the concentration of O_2.

The first published *in vivo* use of a FQ probe to measure P_aO_2 was by Baumgardner et al. (2002). The transition metal used in the fluorophore of that probe was ruthenium which precluded its use in humans due to toxicity. Further development aimed at producing a clinically applicable probe has been undertaken using Pt in the fluorophore (Chen et al. 2013; Formenti et al. 2014; Chen et al. 2016; Formenti et al.

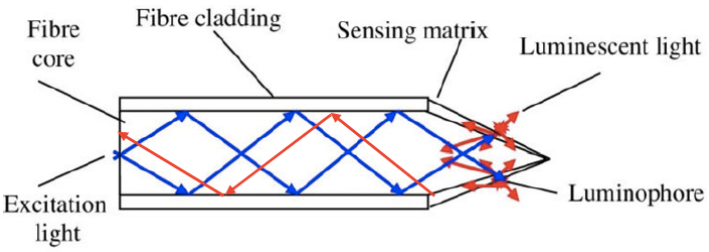
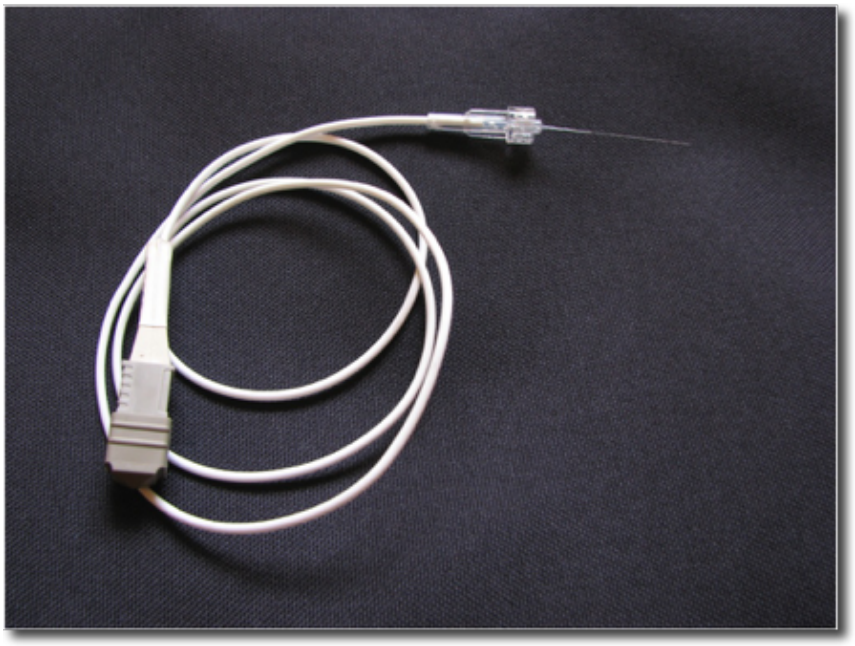


Figure 2.3: Illustration of the process of light transmission at the end of the fibre-optic P_aO_2 probe. *The probe has a response time of 100 ms to step changes in PO_2, as tested in vitro in the liquid phase (Chen et al. 2016). Blue and red arrows represent light travelling within the core of the fibre-optic cable. Loss of light is limited by the insulating cladding which maintains total internal reflection. Blue arrows represent light travelling towards the tip to excite the fluorophore. Red arrows represent the photonic energy released from the fluorophore, some of which are returned back down the cable to the spectrophotometer. Modified from Chen et al. (2016) with permission.*

2017b). This has led to the availability of the potentially clinically safe probes (Oxford Optronix, UK), with a response time of 0.1 s, that have been used to measure real-time P_aO_2 in this thesis. Figure 2.4 is an example of one such probe.



a *Example P_aO_2 probe with leur lock connector for attaching to areterial cannula.*



b *Micrograph of fibreoptic P_aO_2 probe tip.*

Figure 2.4: Example fibreoptic P_aO_2 probe. *(a) An example of one of the probes demonstrating the Luer lock connector close to its distal end for connection to a standard arterial cannula. (b) A micrograph of the end of one of the probes showing its tapered tip, where the platinum fluorophore is embedded within a polymethylmethacrylate matrix. Reproduced from Formenti et al. (2017b) and Chen et al. (2014) with permission.*

2.5 Computed Tomography (CT) image analysis

CT images were segmented using 3D Slicer v4.6.219 (Fedorov et al. 2012) with exclusion of the mediastinum, diaphragm, inferior vena cava and hilar vessels. Exclusion of intrapulmonary vessels within regions of increased voxel density was not possible and these, along with the conducting airways up to the level of the clavicles, were included in the analysis. All images were then sub-segmented according to voxel density (Gattinoni et al. 1988; Lundquist et al. 1995; Vieira et al. 1998):

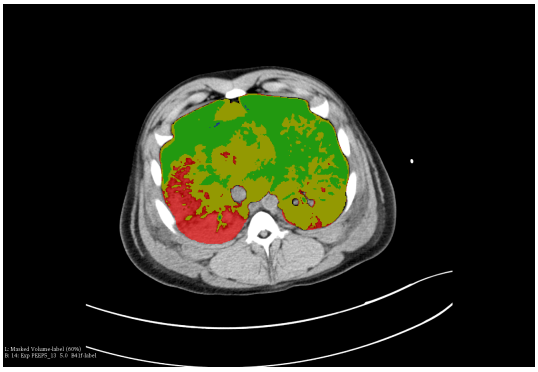
- Collapse: −100 to +100 Hounsfield Units (HU)
- Poorly aerated lung: −101 to −500 HU
- Normally aerated lung: −900 to −501 HU
- Over-distended lung: −1000 to −901 HU

The mass of each lung fraction (e.g. collapse) was then calculated using the mean density and volume of each fraction assuming the lung is composed solely of air and water (Gattinoni et al. 1988). The fractional mass of each region was then calculated as per Equation 2.2.

$$\frac{mass\ of\ fraction}{total\ mass\ of\ all\ fractions} \times 100\% \tag{2.2}$$

2.5.1 Masking of CT images

a



b

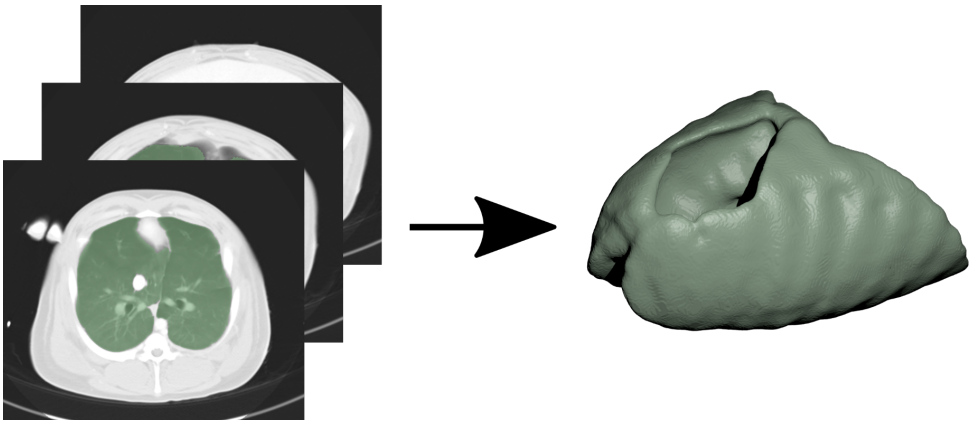


Figure 2.5: Reconstitution of single slice CT images into a completely segmented scan of the entire lung. ***(a)*** *shows a an example of single slice of thorax. The lung field is masked and segmented according to Hounsfield unit density. Red = Collapse (HU -100 to +100), Yellow = Poorly aerated (HU -500 to -100), Green = Normally aerated (HU -900 to -500).* ***(b)*** *shows how individually masked slices are reconstituted to form a complete representation of the entire lung volume.*[*]

[*]Figure 2.5 (b) was created by Dr J Cronin and reproduced with his permission.

2.6 The Inspired Sinewave Technique

The name "Inspired Sinewave Technique" (IST) describes a method based on forcing sinusoids of a tracer gas into inspired airway gases to recover estimates of an alveolar compartment taking part in gas exchange (V_A), a dead-space volume (V_D) and a blood flow to the alveolar compartment ($\dot{Q}_P$). It is based on work by Zwart et al., (Zwart et al. 1976; Zwart et al. 1978) with major contributions to its development coming from Hahn and colleagues. The most significant steps in IST's development are reviewed below.

2.6.1 Development of IST

Zwart et al. (1976) wanted to find a solution to the problem of interference caused by recirculation when inert indicator based methods were used to measure blood flow. They chose to study the use of sinusoids because they are unique amongst linear waves in that when transformed the frequency of a sinewave remains unchanged. Thus, the alterations in the linear sinewave signal is limited to those of wave amplitude and phase. Using a continuous ventilation model of the lung, with no shunt, Aart Zwart et al. demonstrated analytically that effects of venous recirculation were negligible (when halothane was the indicator). They named their approach the alveolar amplitude response technique (AART) (Zwart et al. 1978). Further analysis of the model was limited by the availability of rapid gas analysers at that time. Barton et al. (1988) adapted the Zwart model to include deadspace, an inhomogeneous alveolar compartment and pulmonary shunt. The authors used N_2O (rather than halothane) as a tracer gas because it allowed a higher mean concentration (5 - 7%) to be used and they analytically solved their model in the forward direction by considering compartments as electrical components.

Simplifying the Barton model, Hahn et al. (1993) examined a basic three compartment, continuous ventilation model. Hahn et al. were addressing a fundamental concept in the clinical application of mathematical modelling. That is, the difference between the forward and inverse processes. Up until this paper, only the forward process of using forcing sinusoids had been examined. In the forward process, values

for physiological parameters are chosen (for example, alveolar volume and pulmonary blood flow) and placed in a model of the cardiopulmonary system. The input variables (the inspired sinusoidal concentrations of tracer gas) are known and the output variables (the expired sinusoidal concentrations of tracer gas) are predicted by the model. Comparison of predicted versus measured output variables allows estimation of the validity of the model.

The importance of testing an inverse model is that the physiological variables of interest can be estimated from the measured "outputs" of the system. However, the analytic solutions to a multi-compartmental model of ventilation require complex mathematical inversion to recover the parameters of interest. (Gavaghan et al. 1996; Farmery 2008). Using a simpler model allowed Hahn et al. (1993) to formulate simpler analytic solutions for the inverse model.

Before Hahn's model, physiological dead-space and venous admixture had been measured with steady-state arterial and expired gas sampling, requiring gas collection and cooperation of the subject, with the effect of perturbing the O_2 and CO_2 homeostasis during measurements. One argument for developing the sinusoid model was to develop a technique for making several simultaneous gas exchange measurements where the parameters (F_IO_2, respiratory rate and V_T) were not effected by the measurement procedure itself.

Incorporating the phase change of the sinusoidal signal, Williams et al. (1994a) and Williams et al. (1994b) used two tracer gases simultaneously. Hypothesising that because argon is virtually insoluble ($\lambda = 0.03$), the blood flow signal could be ignored and therefore Ar would best estimate V_A. The authors used N_2O for pulmonary blood flow as described by the group previously (Hahn et al. 1993) and tested their model in a bench lung and anaesthetised dogs. Argon insolubility meant that it can be used to extract ventilation-volume information as described by Hahn et al. (1993) without the interference from $\dot{Q}_P$. The authors tested their theoretical model in 9 ventilated dogs and compared results for dead-space against single-breath washout, for alveolar volume against N_2 washout, and for $\dot{Q}_P$ against thermodilution.

One of the assumptions Zwart et al. made was that using shorter forcing periods with gases of higher solubility would reduce the effect of recirculation on the mixed venous signal and thus provide more faithful adherence to their model. Using a theoretical analysis in a continuous ventilation model, Gavaghan et al. (1995) compared

four tracer gases with different solubilities (Ar, N_2O, acetylene and halothane) at different sinusoidal forcing periods (30, 60, 90, 120 and 180 s). The authors found that in a noisy system with experimental error (akin to real physiology), N_2O based measurements of V_A were significantly more robust than with halothane or acteylene and that measurements of $\dot{Q}_P$ were similar for all three gases. Gavaghan hypothesised that whilst calculation errors were reduced by less recirculation signal, the information recovered from the alveolar compartment was also reduced and thus recovery of compartment parameters would have increased error.

Gavaghan et al. (1996) went on to compare parameter recovery from a tidal ventilation model against their previous continuous ventilation approach (Gavaghan et al. 1995). The authors showed that model choice made negligible difference to recovery of $\dot{Q}_P$. However, on recovery of alveolar and dead-space volumes, the tidal and continuous ventilation models differed. Sainsbury et al. (1997) compared the continuous and tidal ventilation models to recover V_A. Sainsbury et al. found that the continuous ventilation model overestimated V_A, but with a simple adjustment ($(V_T + V_D)/2$), the volumes recovered from the models were in agreement.

Investigating the use of a tidal model to estimate $\dot{Q}_P$, Williams et al. (1998) used N_2O and Ar in anaesthetised dogs. Introducing a modification to take into account the signal from recirculation, the authors demonstrated good agreement between measurements of pulmonary blood flow recovered from the tidal ventilation model and measurements of cardiac output taken with thermodilution. Furthermore, the tidal model of ventilation allows examination of the effects of respiratory rate, I:E ratio, alveolar and dead-space volume on model outputs (Hahn et al. 2003).

Having considered that the predicted venous oscillatory amplitude was small enough to be negligible (Gavaghan et al. 1995), Farmery (2008) proposed a breath-by-breath analysis. The advantage was that the complex equations which considered the concentration of the tracer gas as a function of time, could be integrated to produce single time-point estimates for each breath. This novel solution allowed a simplified inversion of the measured outputs from a tidal ventilation model to recover estimates of V_A, V_D and $\dot{Q}_P$.

Clifton et al. (2013) proceeded to test Farmery's model against the continuous ventilation model in healthy human subjects. Testing the tidal model at several

forcing periods, their results suggested that recovery of V_A, V_D and $\dot{Q}_P$ were optimised at a forcing period of between 120 - 240 s. The recovery of parameters at these periods was reliable and avoided the effects of recirculation. It is on the Farmery breath-by-breath model that the software within the current version of IST is based (Farmery 2008).

2.6.2 The contemporary Inspired Sinewave Technique

More recently, IST has continued to develop (Phan et al. 2017a; Bruce et al. 2018; Bruce et al. 2019). A schematic of IST's current design is shown in Figure 2.6, an example output from IST is shown in Figure 2.7 and its mathematical principles are described below. In the iteration of IST used throughout this thesis, N_2O is used as the tracer gas.

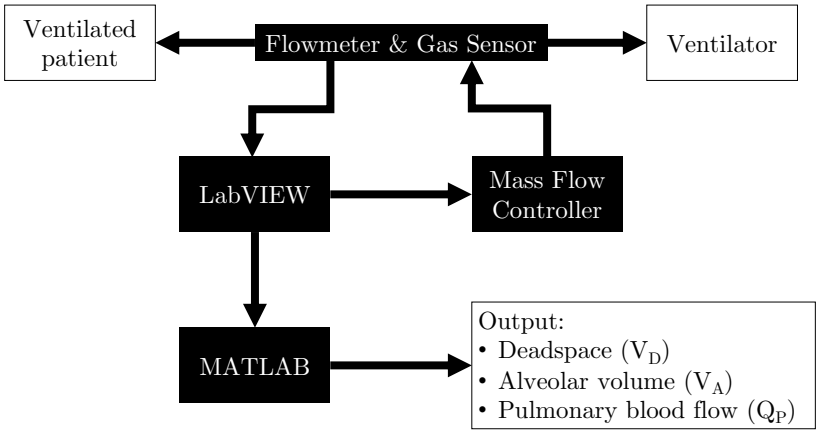


Figure 2.6: Schematic representation of IST. *The ventilated patient has a flowmeter and gas sensor attached in series within their breathing circuit, between an heat-moisture exchange filter (HME) and the ventilator. Gas composition and flow are measured and processed with LabVIEW software. The inspiratory flow is measured in real time and is used by the LabVIEW software to estimate the volume of N_2O required to achieve the desired inspired concentration. This specific volume is then delivered by the mass flow controller into the inspired breath. The delivered volume changes such that a sinusoidally varying concentration of N_2O is delivered with each inspiration (Phan et al. 2017a).*

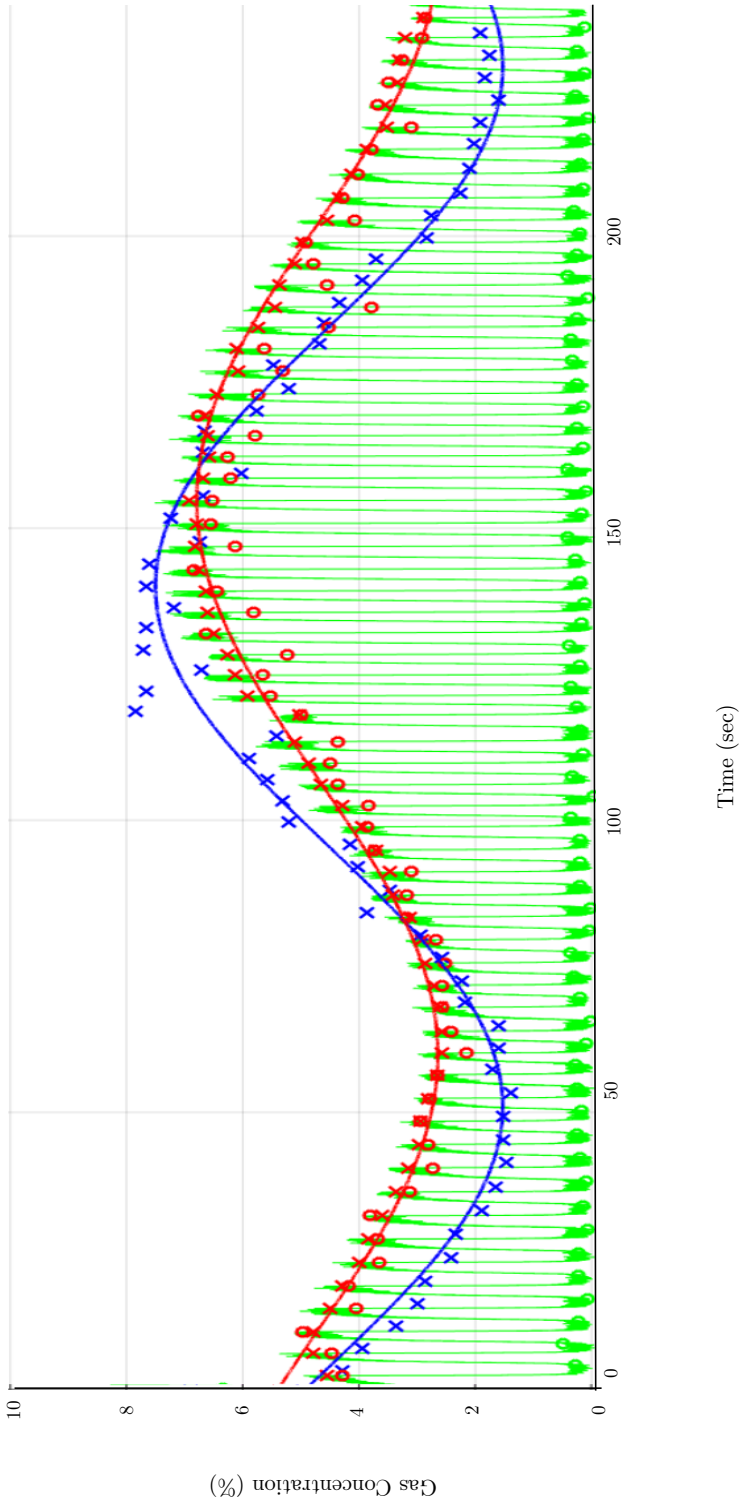


Figure 2.7: Example output from the inspired sinewave technique. *The green line represents end-tidal N_2O concentration. The blue line and crosses show the inspired sinewave produced by changing the inspiratory concentration of N_2O on a breath-breath basis. The red line and open circles show the expired concentration of N_2O, demonstrating the reduction in amplitude and phase-shift.*

2.6.2.1 The current IST lung model

For the purposes of the experiments described in this thesis, the lung model for IST is of tidal ventilation of a simple three compartment model. This is akin to the "balloon on straw" model (Hahn et al. 2003). In this model airway gases pass through an anatomical deadspace (V_D) (the "straw") of fixed volume. Gas then enters the single alveolar compartment (V_A), the volume of which expands as the added tidal volume (V_T) mixes with the already present gas. Pulmonary venous blood is circulated around a single body compartment and returns to the alveolar compartment as pulmonary capillary blood flow ($\dot{Q}_P$). This model is shown in Figure 2.8.

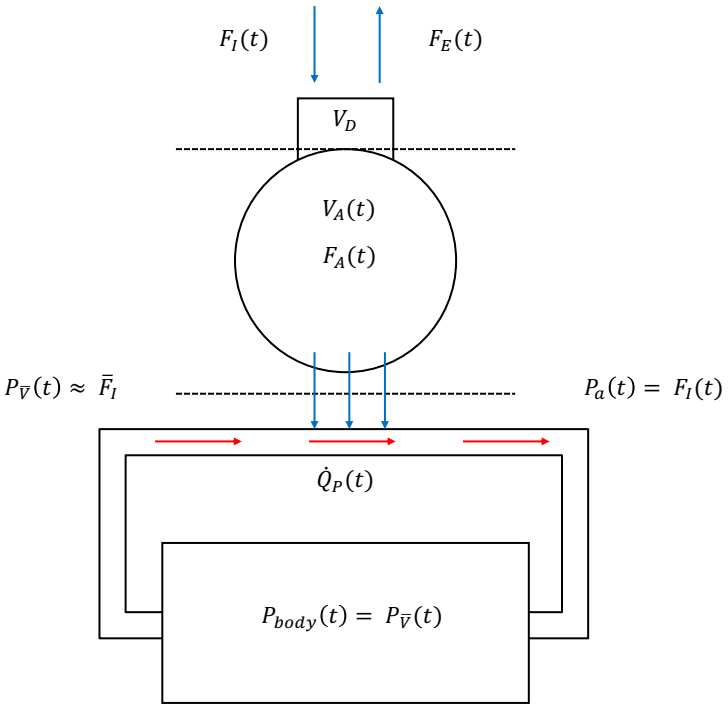


Figure 2.8: Schematic diagram showing the tidal ventilation, three compartment lung model on which the inspired sinewave technique is based. *Blue arrows represent transfer of N_2O in the gas phase and red arrows represent the blood phase. Dotted horizontal lines delineate the boundaries between the three compartments. Abbreviations are explained in the text. Reproduced from Bruce et al. (2019) with permission.*

2.6.2.2 The mass balance equation of the inspired N_2O signal

On inspiration N_2O passes through the dead-space compartment and into the alveolar compartment, where homogeneous mixing of gases is assumed. With a solubility coefficient (λ) of 0.47, the N_2O gas diffuses into the pulmonary capillary blood and is circulated to the single body compartment. The N_2O signal is returned to the alveolar compartment by diffusion out of the returning mixed venous blood. From the alveolar compartment the N_2O passes through the dead-space again to be exhaled.

During an IST test, the fraction of inspired N_2O at time = t ($F_I(t)$) is oscillated sinusoidally as described by Equation 2.3 and after a short period the mean concentration of tracer gas at time = t is assumed to be the same in the alveolar compartment ($F_A(t)$), the arterial supply to the body compartment ($P_a(t)$) and the mixed venous blood returning to the lung from the body ($P_{\bar{V}}(t)$).

$$F_I(t) = \bar{F}_I + \Delta F_I sin\left(\frac{2\pi}{T}t + \phi\right) \tag{2.3}$$

where:

$\bar{F}_I$ = the mean amplitude of the sinewave,

ΔF_I = the oscillation amplitude,

T = the period of the sinewave and

ϕ = the phase shift.

2.6.2.3 The mass balance equation for N_2O in the mixed venous blood

The mixed venous concentration at time = t, $P_{\bar{V}}(t)$, can be described by:

$$P_{\bar{V}}(t) = \bar{F}_I + \Delta P_{\bar{V}} sin\left(\frac{2\pi}{T}t + \phi_{\bar{V}}\right) \tag{2.4}$$

In which,

$\bar{F}_I$ = the mean inspired concentration of N_2O,

$\phi_{\bar{V}}$ = the phase shift of the oscillating sinewave in the mixed venous blood.

The systemic circulation (flowing through the single body compartment in the model shown in Figure 2.8) acts as a low pass filter to diminish the amplitude of the sinusoidal signal in the mixed venous blood. When the period of the sine-wave is < 300 s duration, the amplitude is heavily attenuated and so can be considered to be a constant so $P_{\bar{V}}(t) \approx \bar{F}_I$ where $\bar{F}_I$ is the mean gas concentration of the inspired sine-wave.

2.6.2.4 IST's deadspace calculation

The volume of dead-space is calculated using Bohr method:

$$V_D = V_T \left(\frac{F_E - F_{\bar{E}}}{F_E - \bar{F}_I} \right) \tag{2.5}$$

Where:
$F_{\bar{E}}$ = the mean expired concentration of N_2O and
$\bar{F}_I$ = the mean inspired concentration of N_2O.

2.6.2.5 The mass balance equation of N_2O in the lung.

The mass balance equation for N_2O in the lung can be written as:

$$N_2O \text{ mass inhaled} - N_2O \text{ mass exchanged with blood} = N_2O \text{ mass exhaled} \tag{2.6}$$

Which is equivalent to:

$$\overbrace{\left(F_{E_{n-1}}.V_A\right)}^{1} + \overbrace{\bar{F}_{I_n}(V_{T_n} - V_D) + F_{E_{n-1}}.V_D)}^{2} - \overbrace{\left(\Delta t_n.\lambda.\dot{Q}_P(F_{E_n} - P_{\bar{V}})\right)}^{3} = \underbrace{\left(V_A.F_{E_n}\right)}_{4} + \underbrace{V_{T_n}.F_{E_n}\big)}_{5} \tag{2.7}$$

in which the numbers 1 - 5 represent the mass of tracer gas where:
1 = gas already present in the alveolar compartment before inspiration,
2 = the inhaled mass,

3 = the mass exchanged with the blood,
4 = the mass remaining in the alveolar compartment at the end of expiration,
5 = the mass exhaled from the alveolar compartment,
and,
F_{E_n} and $F_{E_{n-1}}$ = the end-expired concentrations of N_2O in the n^{th} and its preceding breath,
V_A = the volume of the alveolar compartment,
$\bar{F}_{I_n}$ = the mean inspired concentration of N_2O in the n^{th} breath,
V_{T_n} = the tidal volume of the n^{th} breath,
V_D = the volume of the dead-space compartment (estimated from the Bohr method),
Δt_n = the duration of the n^{th} breath,
λ = the blood-gas partition coefficient of N_2O,
$\dot{Q}_P$ = the pulmonary blood flow and
$P_{\bar{V}}$ = the mixed venous concentration of N_2O, which is assumed to be equal to the mean inspired and expired concentration ($\bar{F}_A$) in the steady state.

The mass balance equation then becomes:

$$V_A(F_{E_n} - F_{E_{n-1}}) + \Delta t_n.\lambda.\dot{Q}_P(F_{E_n} - \bar{F}_A) = V_D(F_{E_{n-1}} - \bar{F}_{I_n}) + V_{T_n}(\bar{F}_{I_n} - F_{E_n}) \quad (2.8)$$

Considering Equation 2.8, the unknown variables of V_A and $\dot{Q}_P$ can be recovered over the course of several breaths by producing multiple simultaneous equations. It is on this basis that IST provides estimations of lung volume and pulmonary blood flow. In Chapters 5 and 6, IST's measurements are experimentally compared against established methods of quantifying lung volume and cardiac output.

2.6.2.6 Assumptions of the model on which IST is based

- The mean concentration of N_2O in all body compartments over the oscillation period is the same as the mean inspired concentration ($\bar{F}_I$) over the same period. The mean time-varying partial pressure for any part of the system is measured as a deviation from the mean P_{N_2O}.

- Tidal ventilation:
  - any dead-space is series dead-space
  - an homogeneous alveolar gas phase in which the concentration of tracer remains constant during expiration
  - no alveolar-capillary diffusion limitation
  - equality of inspired and expired ventilation
  - no transport lags
  - CO_2 output equals O_2 uptake, *i.e.* the respiratory quotient = 1.

2.7 Multiple breath sulphur hexafluoride (SF_6) washout

As previously discussed, SF_6-washout was originally described by Jonmarker et al. (1985) and developed by Larsson et al. (1987). Its clinical adoption has been limited by the availability of equipment, however, it provides accurate and repeatable measurements and has been tested in ventilated lungs (Jonmarker et al. 1985; Larsson et al. 1987; Vilstrup et al. 1992; Schulze et al. 1994; Schibler et al. 2002). It is used as one of the techniques against which IST is compared in Chapter 5.

At the time of the initial development of the SF_6 washout technique, methods of measuring FRC in ventilated patients relied upon disconnection of the patient from the ventilator and collection of the expired gases in a bag to calculate the expired concentration of tracer gas. Jonmarker et al. (1985)'s major step forward was to use a rapid gas analyser and flowmeter both connected to a computer which allowed calculation of the expired concentration of tracer gas. The main limitation of Jonmarker's system was a reliance on constant inspiratory flow to deliver a constant rate of SF_6 during inspiration. Consequently, in situations where there are inspiratory patterns that did not have a constant flow, there would be varying inspiratory concentrations of SF_6 and uneven distribution to inhomogeneously ventilated lungs. This limitation was overcome by Larsson et al. (1987) who included microprocessor

control of the SF_6 valve to deliver a volume of tracer gas proportional to the inspiratory flow. This modification allowed the concentration of inspired SF_6 to be maintained irrespective of the inspiratory flow pattern.

2.7.1 Process of measuring FRC with SF_6 multiple breath washout

2.7.1.1 Tracer gas washin and washout

The SF_6 is introduced via a catheter controlled by a piezoelectric valve. In sync with the inspiratory gas flow, the valve opens and a pulsed flow of SF_6 is introduced into the inspired gases. The pulse frequency and duty cycle is controlled by a microprocessor and changed in proportion to the inspiratory flow. To eliminate rebreathing, the microprocessor resets the SF_6 analyser to zero when SF_6-free gas has passed the analyser for 0.5 s. Additionally a correction to the expired concentration of SF_6 is made to account for the effect of CO_2 concentration on measured SF_6 concentration. SF_6 washin is continued until the expired concentration of SF_6 is constant. SF_6 washout is commenced by stopping the supply of SF_6 between breaths and is continued until the expired concentration of a consecutive five breaths is $<$ 0.001%.

2.7.1.2 Calculation of end-expiratory lung volume

Signals from the rapid SF_6 analyser, CO_2 analyser and ventilator flowmeter are collected in real time by a bespoke computer programme. SF_6 elimination is calculated every 10 ms as the product of the measured SF_6 concentration with the expiratory flow and the tidal elimination of SF6 is obtained by integration. An estimation of FRC is obtained as shown in Equation 2.9:

$$FRC = \frac{V_{SF6}}{[Alv]_{SF6}} \times k - V_{app} \tag{2.9}$$

where:

V_{SF6} = the total volume of SF_6 washed out
$[Alv]_{SF6}$ = the alveolar concentration of SF_6 at the end of washin
k = conversion factor to BTPS conditions (1.09 in this case)
V_{app} = the apparatus deadspace volume

2.7.1.3 Choice of SF_6 washout as a comparison method for validation of IST measured lung volumes.

The technique described above was the one used to calculate measurements of lung volume for comparison with IST in Chapter 5. The method was chosen for the following reasons:

- **Proven accuracy and repeatability in ventilated subjects.** Jonmarker et al. (1985) and Larsson et al. (1987) showed that compared against the techniques of body plethysmography and N_2 washout, lung volumes measured with SF_6 were not significantly different in spontanesouly ventilating human subjects. In anaethetised, mechanically ventilated patients, the technique was highly repeatable, with a coefficient of variation of 0.6%. SF_6 has also been applied to paediatric medicine, where its use to measure lung volumes was proven reliable and precise (Vilstrup et al. 1992; Schulze et al. 1994; Schibler et al. 2002).
- **Familiarity and expertise with the equipment.** Data collection for Chapter 5 was carried out at the Hedenstierna Laboratory in Uppsala with collaboration from Professor Anders Larsson. Professor Larsson was one of the main contributors to the development of the method and his experience with the equipment meant the method could be reliably applied.

Like every method, SF_6 washout has its limitations. Firstly, concentration and flow measurements are sensitive to humidity and temperature. To overcome this two modifications must be made:

- a patient-end heat moisture exchange filter must be used (HME) and accounted for in the manual input of the apparatus deadspace

- a heated pneumotachograph must be used to ensure constant viscosity of the tracer gas within the airway gases

Secondly, because SF_6 washout needs relatively specialist equipment and use of potent greenhouse gas, it is not a clinically used tool for bedside lung volume measurement in the adult intensive care population. However, for the purposes of experimental validation of IST and in combination with the second reference technique of CT imaging, its limitations are easily overcome.

2.7.2 Comparing lung volumes measured with different techniques.

In Chapters 4 and 5 the techniques of SF_6 washout and CT are used as "gold standard" methods against which to compare experimental techniques to quantify lung volume. A gas dilution technique and CT were chosen because each quantifies a different volume of gas within the lung. SF_6, as a gas dilution technique, measures the volume of gas within the thorax communicating with the conducting airways. CT measures the entire thoracic gas volume, including gas trapped behind closed airways.

IST and P_aO_2 rate-of-decline (as used in Chapters 4 and 5 respectively) quantify the volume of gas in alveolar units that are both ventilated and perfused. This "effective lung volume" (ELV) is a potentially different volume compared to those measured by SF_6 or CT. However, there is no equivalent "gold standard" method to measure ELV and so both a gas dilution technique and an imaging technique have been used.

2.7.3 Statistics

In the following experimental chapters analysis of variance (ANOVA) has been applied as a statistical test. When conducting this analysis, post-hoc tests have only been carried out where the initial ANOVA demonstrated a significant interaction.

CHAPTER 3

Investigating the relationship between respiratory oscillations in P_aO_2 and cyclical recruitment/derecruitment of atelectasis

Abstract

This chapter examines the hypothesis that respiratory oscillations in P_aO_2 are directly related to cyclical recruitment/derecruitment of atelectasis (CA) and that the amplitude of these oscillations is proportional to the amount of CA. A collapse-prone and recruitable model of lung injury was used to investigate this in mechanically ventilated pigs. Measurements of atelectasis were made using both single slice dynamic CT (dCT) (during tidal ventilation) and whole lung CT scans (during breath-hold manoeuvres). Simultaneously, continuous recordings of P_aO_2 were taken using fibre optic P_aO_2 probes (as described in the Methods chapter). The presented results suggest that P_aO_2 oscillation amplitude is not clearly related to CA and that there may be contribution from other competing pathophysiological mechanisms in the injured lung.*

*The work presented in this chapter forms the basis of a published research paper which is attached in Appendix A (Crockett et al. 2019).

3.1 Introduction

It has been over a century since Krogh et al. (1914) investigated the composition of alveolar gas, suggesting that the alveolar concentration of O_2 may change throughout the course of the respiratory cycle. Forty years later DuBois (1952) demonstrated those cyclical variations in alveolar O_2. The next steps were to address whether or not the alveolar oscillations in O_2 were transferred to the arterial blood and whether they could be measured in the blood phase.

3.1.1 Detection of respiratory O_2 oscillations in arterial blood.

The advent of the arterial oxyhaemoglobin saturation (S_aO_2) monitor (Matthes 1935) allowed Bergman (1961) to demonstrate the predicted arterial O_2 oscillations. Bergman showed that S_aO_2 oscillated by $\pm$ 10% at a frequency identical to the imposed respiratory rate in anaesthetised, ventilated dogs.

With technological advancement came the possibility to measure P_aO_2 using electrochemical probes with a sufficiently rapid response time that might allow detection of perturbations in P_aO_2 within the course of a single breath. In the same year as Bergman had shown S_aO_2 oscillations, Staub (1961) presented a polarographic electrode which could measure P_aO_2 in an exteriorised flow-through cuvette with a response time of < 0.5 s. Within the space of 5 years, Purves (1966) proceeded to use a modified Staub electrode to become the first author to measure oscillations in P_aO_2 with the same frequency as respiration. Since that study, several authors have demonstrated P_aO_2 oscillations in anaesthetised animals without lung injury (see Table 3.1).

The polarogrpahic technique's tendency for measurement drift and electrode fouling hampered its uptake into clinical practice. It was not until development of optical sensing technology (see the Methods chapter, section 2.4 for details) that interest in the clinical applications of real-time, rapid response P_aO_2 measurement regained interest (Williams et al. 2000; Baumgardner et al. 2002).

3.1.2 Causes of respiratory P_aO_2 oscillations.

Factors which cause and therefore affect the amplitude of respiratory P_aO_2 oscillations can be split into two main categories:

1. *Ventilation related*:
   As predicted from the earliest studies of alveolar gas composition, the tidal nature of alveolar ventilation causes fluctuations in alveolar gas composition which are transferred to the blood phase and Folgering et al. (1978) demonstrated all of the following affected respiratory P_aO_2 oscillation amplitude:
   - V_T
   - mean P_aO_2 (and F_IO_2)
   - respiratory rate
2. *Perfusion related*:
   On the other side of the alveolar-capillary membrane the role of several components of pulmonary perfusion were shown to affect respiratory P_aO_2 oscillation amplitude:
   - Left ventricular mixing (Yokota et al. 1973)
   - Pulmonary "dispersion" (transit) time (Yokota et al. 1973)
   - Pulmonary shunt fraction ($\dot{Q}_S/\dot{Q}_T$) (Bergman 1961; Yokota et al. 1973; Williams et al. 2000; Baumgardner et al. 2002)

Indeed, most recently, Formenti et al. (2017a) demonstrated the influence of both factors on respiratory P_aO_2 oscillations in the uninjured lung. The authors showed that the amplitude of the oscillations can be predicted by a mass balance equation of a single alveolar compartment that takes into account the oxygen uptake from the lung, the inspiratory flow rate, the end-expiratory alveolar volume and the tidal volume (Formenti et al. 2017a).

3.1.3 The relationship between pulmonary shunt, cyclical recruitment/derecruitment of atelectasis and respiratory P_aO_2 oscillations.

Williams et al. (2000) hypothesised that if oscillations in P_aO_2 were caused by a variable shunt fraction within the course of a breath, then changing the reversible shunt fraction would change P_aO_2 oscillation amplitude. The authors considered that if $\dot{Q}_S/\dot{Q}_T$ varied with the degree of cyclical recruitment/derecruitment of atelectasis (CA) then the amplitude of P_aO_2 oscillations would be sensitive to the application of PEEP (acting to alter the degree of CA). Using a polarographic electrode in a saline-lavage model of lung injury in dogs, the authors demonstrated respiratory P_aO_2 oscillation amplitude was PEEP dependent and took this as evidence to suggest that $\dot{Q}_S/\dot{Q}_T$ was different during inspiration and expiration in this model of atelectasis. William et al.'s investigation was important for two reasons. Firstly, the authors examined the effect of changing $\dot{Q}_S/\dot{Q}_T$ on P_aO_2 oscillation amplitude, and secondly, they used an injured lung model to study the respiratory P_aO_2 oscillations. Neither of these had been done before.

After this, Baumgardner et al. (2002), using an optical P_aO_2 probe, demonstrated much larger respiratory P_aO_2 oscillations ($\leq$ 439 mmHg vs $\leq$ 69 mmHg) in rabbits with saline-lavage lung injury. The authors, suggesting their results supported the Williams' hypothesis, attributed the variable $\dot{Q}_S/\dot{Q}_T$ and thus amplitude of the oscillations to CA. Subsequent studies used respiratory P_aO_2 oscillation amplitude (measured by fast-response P_aO_2 probes) as a surrogate marker of the amount of CA (Otto et al. 2008; Pfeiffer et al. 2006; Syring et al. 2007). Table 3.1 summarises the main studies examining respiratory O_2 oscillations.

Paper	Species	n	Injury model	Probe
Bergman (1961)	Canine	8	Uninjured	S_aO_2
Purves (1966)	Ovine, feline	6	Uninjured	Polarographic
Yokota et al. (1973)	Canine	15	Uninjured	Polarographic
Folgering et al. (1978)	Feline	23	Uninjured	Polarographic
Williams et al. (2000)	Canine	7	Saline lavage	Polarographic
Baumgardner et al. (2002)	Leporine	6	Saline lavage	FQ-Ru
Herweling et al. (2005)	Porcine	4	Cardiac arrest	FQ-Ru
Otto et al. (2008)	Leporine	23	Saline lavage	FQ-Ru
Pfeiffer et al. (2006)	Leporine	6	Saline lavage	FQ-Ru
Syring et al. (2007)	Leporine	7	Saline lavage	FQ-Ru
Bodenstein et al. (2010)	Porcine	3	Saline lavage, oleic acid, pneumonia	S_pO_2, FQ-Ru
Hartmann et al. (2012)	Porcine	16	Saline lavage	FQ-RU
Bodenstein et al. (2013)	Porcine	14	Uninjured	FQ-Ru
K. Klein et al. (2013)	Porcine	7	Saline lavage	FQ-Ru & S_pO_2
Formenti et al. (2015)	Ovine, porcine	2	Saline lavage	FQ-Pt
Formenti et al. (2017a)	Porcine	8	Uninjured	FQ-Pt

Table 3.1: Comparison of previous *in vivo* studies examining respiratory oscillations in arterial oxygenation. *S_aO_2 = arterial oxyhaemoglobin saturation, S_pO_2 = Peripheral oxyhaemoglobin saturation, FQ-Ru = ruthenium based fluorescence quenching (FOXY AL-300, Ocean Optics, Dunedin, FL), FQ-Pt = platinum based fluorescence quenching (Oxford Optronix, Oxford, UK).*

3.1.4 The importance of cyclical recruitment/derecruitment of atelectasis (CA).

As discussed in the Introduction chapter, section 1.4.1, CA is important because of its putative role in contributing to ventilator-induced lung injury (VILI) via atelectrauma (Slutsky et al. 2013). Bedside detection of CA during MV remains difficult because there is no method of direct measurement. Instead the existence and contribution of CA to VILI is inferred by a number of techniques.

3.1.4.1 Methods of detecting cyclical atelectasis.

Computed Tomography (CT). Clinically, the use of CT is commonly employed in both the diagnosis and prognostication of ARDS (Gattinoni et al. 1988; Gattinoni et al. 2001). Experimentally, repeated CT imaging allows measurement of atelectasis in the ventilated lung and quantification of its temporal changes throughout the respiratory cycle (Markstaller et al. 2003). CT imaging also been demonstrated to be able to quantify cyclical atelectasis and shunt (David et al. 2005).

CT has several limitations in its use to detect CA. The dose of ionising radiation and inherent risks associated with the transfer of a mechanically ventilated, critically unwell patient to a remote site make routine CT to detect CA an unfeasible candidate at the bedside. Evidence suggests that recruitment and derecruitment are dynamic processes (Albert et al. 2009) and a single CT scan represents a static representation of the lung at the time of that scan. The optimum technique requires temporal resolution sufficient to detect this in the course of a single breath (5 s). Thus the application of CT imaging to detect CA throughout the entire lung volume is not possible. Consequently, a single slice of CT must be chosen that may or may not be representative of the entire lung. The single slice chosen does not account for the parenchymal movement of lung tissue with ventilation, thus it may move into and out of the CT slice with each breath (Helm et al. 2009). However, recent work by Cronin et al. (2019) supports the suggestion that the single slice method provides a reasonable representation of the whole lung. Finally, after acquisition of the image, each reconstituted voxel is assigned a density based on its CT opacity. With unenhanced CT there is no way of determining if the constituent of a voxel is

collapsed alveolus or alveolus containing fluid (Baumgardner et al. 2013). However, despite its limitations CT remains the gold standard for detection of CA.

Fibre-optic P_aO_2 sensor. Full details of the fibre-optic fluorescence quenching (FQ) technique of PO_2 measurement can be found in the Methods chapter, section 2.4. In summary, FQ relies on the ability of O_2 to quench photoluminescence emitted by a transition metal fluorophore. Increased O_2 concentration causes greater quenching of fluorescence. The fluorophore is embedded in an inert matrix at the tip of a fibre-optic probe which can be inserted via a cannula into the bloodstream. As discussed previously and shown in Table 3.1 these sensors have been widely used in the detection of CA (Baumgardner et al. 2002; Syring et al. 2007; Otto et al. 2008; Formenti et al. 2015). Recent development has lead to the manufacture a non-toxic, fibre-optic indwelling probe with the ability to measure P_aO_2 with a response time of $0.1s$ (Chen et al. 2012b; Chen et al. 2013; Formenti et al. 2014). Images of a probe and an illustrative example of its tip are shown in Figures 2.3 and 2.4.

Intra-vital microscopy (IVM). Developed by Nieman et al. (Nieman et al. 1981; Lutz et al. 1999), IVM allows direct visualisation of alveoli across the respiratory cycle in real time. The technique involves general anaesthesia and placement, via thoracotomy, of a dark-field microscope with a cover-slip suction head to the lung surface. Studies conducted in a surfactant deactivation model of lung injury (Tween instillation) provided evidence that during the course of a single breath cyclical recruitment and derecruitment of alveoli occurred (Schiller et al. 2001; Halter et al. 2003) and that it could be identified by IVM. However, a recognised drawback was that negative pressure had to be applied to the alveoli of interest in order to obtain images. It was thought that the applied negative pressure may well interfere with the alveolar mechanics that the technique was designed to examine. Indeed, Mertens et al. (2009) proceeded to use a modified IVM setup without the negative pressure tip in an attempt to eliminate the contribution this may have to alveolar mechanics. The main drawback of IVM is that its potential for clinical translation is limited by requirement for thoracotomy. Limitations as a research tool are that the subpleural alveoli imaged are restricted to a microscopic area that those may not represent either the rest of the alveoli in general, nor specifically more central alveoli which may have different characteristics to subpleural alveoli.

Electrical Impedance Tomography (EIT). EIT relies on the fact that body tissue has inherent impedance to alternating electrical current. An EIT belt contains an array of electrodes which are applied to the chest wall. Pairs of electrodes within the belt generate small alternating electrical currents, and the resultant changes in potential difference are measured by the rest of the electrodes in the belt. The pair of electrodes delivering the current sequentially changes, cycling through each pair in the belt. The changes in impedance are processed to produce a pixelated image of the tissue plane within the circumference of the EIT belt (Consuelo-Bachmann et al. 2018). The EIT output has a temporal resolution of up to 50 images per second and its ability to detect regional changes in ventilation and perfusion have been demonstrated (Blankman et al. 2016; Frerichs et al. 2017). Whether or not EIT has sufficient spatial resolution to detect CA is debatable. Bodenstein et al. (2014) and Liu et al. (2016) suggest measurements made with EIT could be interpreted as representing CA in experimental lung injury, but the method cannot yet quantify CA.

Advantages of EIT are that it is non-invasive, carries limited risk and has been translated successfully to human medicine (Consuelo-Bachmann et al. 2018). Its main limitation is that it does not yet provide the spatial resolution required to quantify CA within the lung.

3.1.5 Clinical importance of respiratory P_aO_2 oscillations.

As discussed, respiratory oscillations in P_aO_2 are associated with injurious mechanical ventilation and specifically the phenomenon of CA which may cause atelectrauma (Muscedere et al. 1994; Sugiura et al. 1994; Slutsky et al. 2013). Whilst these oscillations in P_aO_2 might be caused by the pathological process of CA, there is evidence they may be pathogenic themselves. Several authors have noted oscillations in P_aO_2 in end-organs (K. Klein et al. 2016; Thomas et al. 2017) and their presence has been associated with brain injury (Thomas et al. 2017). Furthermore, respiratory P_aO_2 oscillations have been shown to cause both endothelial and myocyte inflammation (Wu et al. 2016a; Wu et al. 2016b). More recently, respiratory P_aO_2 oscillations have been shown to produce lung inflammation (Boehme et al. 2019).

3.1.6 Aims and hypotheses.

Despite numerous studies examining CA measured with dCT or respiratory P_aO_2 oscillations independently, no investigation has been undertaken to confirm the direct association of one with the other. Therefore, the aim of this study was to establish the role of CA (quantified by dCT) as a determinant of respiratory P_aO_2 oscillations (measured with a fast response P_aO_2 probe) in a surfactant depletion, porcine model of lung injury.

It was hypothesised that in this collapse-prone lung injury model:

1. respiratory P_aO_2 oscillations would be co-incident with CA
2. the amplitude of respiratory P_aO_2 oscillations would be proportional to the degree of CA
3. larger increases in atelectasis during expiratory breath-hold manoeuvres would be associated with a larger drop in P_aO_2.

3.2 Methods

3.2.1 Ethical approval

This study of five domestic pigs (3 male, 2 female, mean weight (SD) = 29.6 (1.7) kg) at the Hedenstierna laboratory, Uppsala University, Sweden was approved by the regional animal welfare ethics committee (Ref: C98/16).

3.2.2 Animal preparation

Induction and maintenance of anaesthesia was carried out as described in the Methods, section 2.3.3.[†] Notably, anaesthesia was maintained with intravenous infusions rather than volatile agents. Table 3.2 shows baseline characteristics of each animal. Once anaesthetised, bilateral surgical dissections of the neck were performed. The exposed right internal jugular vein was cannulated with a pulmonary artery catheter. This was used for continuous pulmonary artery pressure monitoring, intermittent thermodilution cardiac output monitoring and core temperature monitoring. The right and left internal carotid arteries were cannulated with 20G Leadercath arterial cannulae (Vygon, UK) for the introduction of fibre-optic P_aO_2 probes.

3.2.3 Lung injury

Lung injury was induced with a technique modified from Lachmann et al. (1980). This model was chosen because of its tendency for collapse. Pre-oxygenation with a F_IO_2 of 1.0 preceded ventilator disconnection and lavage of the lungs by instillation of 0.9% saline solution (at 37 ^oC) via the endotracheal tube. After 30 s the saline was drained out of the lungs and ventilation recommenced. This process was repeated until a PFR of less than 40 kPa was achieved.

[†]Important considerations are repeated in this section for clarity.

Variable	Animal Number					Mean (SD)
	1	2	3	4	5	
Gender	♂	♀	♂	♀	♂	-
Weight (kg)	31.1	29.0	29.8	31.2	26.7	29.6 (1.7)
F_IO_2	0.5	0.8	0.7	0.7	0.9	0.7 (0.1)
PFR	288	285	232	105	276	237 (77)
pH	7.29	7.35	7.32	7.23	7.37	7.31 (0.05)
P_aO_2 (kPa)	19.2	38.1	21.7	9.8	33.0	24.4 (11.2)
P_aCO_2 (kPa)	8.2	7.3	7.8	8.9	6.8	7.8 (0.8)
Hb $(g\ l^{-1})$	91	80	81	86	76	82 (5)
CO $(l\ min^{-1})$	3.7	4.8	3.5	4.2	3.2	3.9 (0.6)

Table 3.2: Baseline characteristics and post-injury blood gas data for each animal. *Pre-lavage blood gas values were within normal limits. Blood gas data presented were measured post-saline lavage. ♂= male, ♀= female, F_IO_2 = fraction of inspired O_2, PFR = P_aO_2:F_IO_2 ratio, Hb = haemoglobin, CO = cardiac output.*

3.2.4 Data collection and processing

Cardio-respiratory variables including peripheral oxyhaemoglobin saturations (S_pO_2), electrocardiography (ECG), invasive arterial blood pressure (BP) (AS/3 Multi-Parameter Patient Monitor, Datex-Ohmeda, Madison, WI, USA), airway gas composition, flow and pressure (Capnomac Ultima, Datex-Ohmeda, Madison, WI, USA) were continuously monitored and recorded as analogue signals throughout the protocol. P_aO_2 signals from the fibre-optic probes were continuously collected with OxyLitePro monitors (Oxford Optronix, Didcot, UK), converted to digital form using PowerLab (ADInstruments, Dunedin, NZ) and displayed/recorded with LabChart v8.1.5 (ADInstruments, Dunedin, NZ) with a sampling rate of 10 Hz. Physiological data were processed using R v3.4.1 (R Development Core Team 2017).

3.2.5 Study protocol

Animals were positioned in dorsal recumbency on the CT scanner table. F_IO_2 (mean (SD) = 0.7 (0.1)) was set depending on the lung injury achieved with saline lavages (see Table 3.2) and P_aO_2 was recorded continuously.

3.2.5.1 Tidal ventilation

A first set of measurements considered tidal ventilation. Animals were ventilated in both PCV and VCV modes at I:E ratios of 1:2, 2:1, 1:4 and 4:1 to explore the effects of different ventilatory modes on P_aO_2 and its dynamic changes. Upon each change of ventilator setting the P_aO_2 trace was monitored until its mean value was stable and then recorded for 120 s. dCT images were recorded in the last 30 s of this period as described in Section 3.2.6.

3.2.5.2 Breath-hold manoeuvres

A second set of experiments considered breath-hold manoeuvres. Whole lung CT scans (as described in Section 3.2.6) were recorded during the first and last 5 s of an imposed 30 s breath-hold at:

- End expiration – the expiratory and inspiratory valves were closed at an initial airway pressure of 5 cmH_2O airway pressure (Ve)
- End inspiration – the valves were closed after inspiration of V_T 10 ml kg^{-1} (V_T10)
- End large inspiration – the valves were closed after inspiration of V_T 20 ml kg^{-1} (V_T20)

To control for the effect the preceding breath-hold may have on the subsequent breath-hold manoeuvre, a sequence of breath-hold manoeuvres was designed to ensure all permutations of manoeuvre-order were achieved, without serial duplication of one type of manoeuvre. The sequence of manoeuvres is shown in Table 3.3. Upon completion of the protocol, anaesthetised animals were euthanized with a bolus dose of potassium chloride.

Sequence No.	Manoeuvre
1	Ve
2	V_T10
3	V_T20
4	Ve
5	V_T20
6	V_T10
7	V_T20
8	Ve
9	V_T10
10	V_T20
11	V_T10
12	Ve
13	V_T10
14	Ve
15	V_T20
16	V_T10
17	V_T20
18	Ve

Table 3.3: Sequence of breath-hold manoeuvres in each animal. *Ve = expiratory breath-hold manoeuvre, V_T10 = breath-hold after V_T 10 ml kg^{-1} inspiration, V_T20 = breath-hold after V_T 20 ml kg^{-1} inspiration.*

3.2.6 CT image acquisition

A Somatom Definition Flash or Somatom Definition Edge (Siemens, Germany) were used to acquire all images as series of transverse sections with a reconstituted voxel size of 0.5 x 0.5 x 5 mm.

3.2.6.1 Single-slice dCT during tidal ventilation.

Scans of a single juxta-diaphragmatic thoracic slice were acquired at 50 ms intervals with 70 kV tube voltage, 246 mA current and collimation of 64 x 0.6 mm in order to analyse dynamic changes during ventilation.

3.2.6.2 Whole lung scans during breath-hold manoeuvres.

A whole lung scan was conducted at the start and immediately before the end of each breath-hold manoeuvre using a tube voltage of 80 kV, 364 mA current and 64 x 60 mm collimation.

3.2.7 CT image analysis

CT images were segmented using 3D Slicer v4.6.219 (Fedorov et al. 2012) as detailed in the Methods chapter, Section 2.5. Collapsed lung was considered to have a voxel density of −100 to +100 HU. For single-slice dCT studies, every fifth image was analysed producing a final sampling rate of 4 Hz. For breath-hold manoeuvres, the entire lung was segmented as described. CA was defined as the difference between the maximum and minimum measured mass of collapsed lung during the course of a single breath.

3.2.8 Statistical analysis

Statistical analyses were performed in GraphPad Prism (version 7.00 for Windows, GraphPad Software, La Jolla California USA, www.graphpad.com). Before ana-

lysis, all data were tested for normality and homogeneity of variance. Parametric data were compared with paired, two-tailed, Student's t-test and non-parametric with Wilcoxon matched-pairs signed rank test. The level of significance was set at $p < 0.05$ for all tests.

3.2.8.1 Tidal ventilation

CT measurements from all animals were compared using a one-way ANOVA with multiple comparisons and Greenhouse-Geisser correction (parametric) or using a Wilcoxon matched-pairs signed rank test (non-parametric). A two-way ANOVA with Sidak correction for multiple comparisons was used for analysis of CT measurements of inter- and intra-animal variability during tidal ventilation under different conditions.

3.2.8.2 Breath-hold manoeuvres

The effect of type of breath-hold manoeuvre on the change in lung collapse was compared using a Kruskal-Wallis test with Dunn's correction for multiple comparisons. Two-way ANOVA was used to examine the effects of individual animal and type of breath-hold manoeuvre on the change in P_aO_2. Spearman correlations were used to assess the relationship between change in collapse and change in P_aO_2.

3.3 Results

3.3.1 Single slice dCT and P_aO_2 during tidal ventilation.

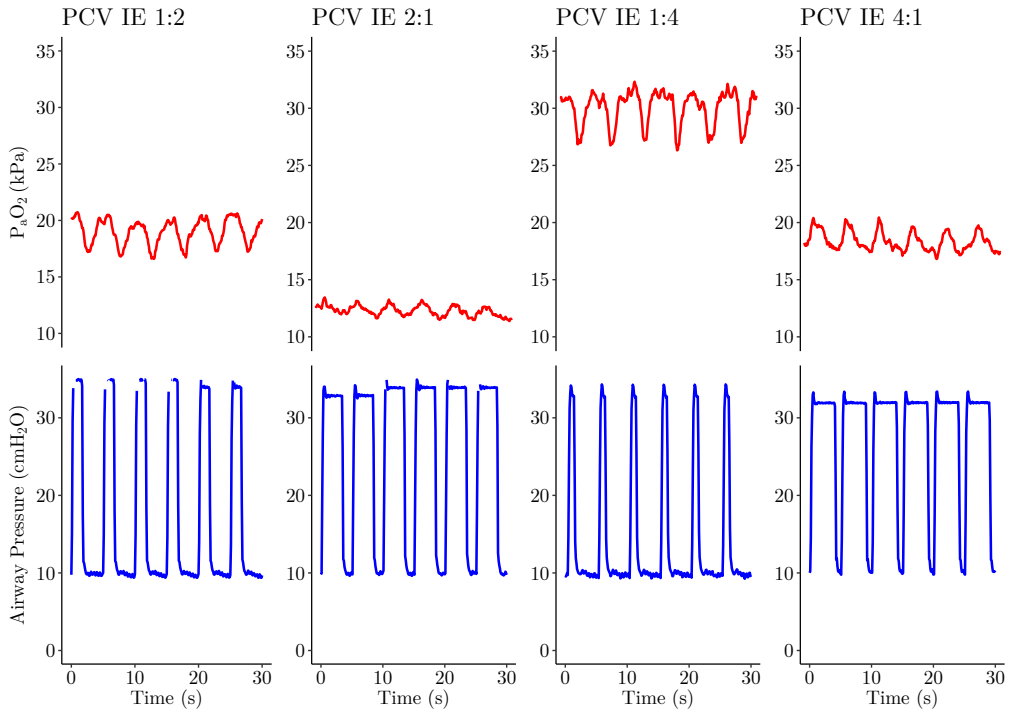
An example of the real-time measurements of P_aO_2 and P_{AW} that were recorded in each ventilatory condition are shown in Figure 3.1. The changes in aerated, poorly aerated and atelectatic fractions of lung as determined by dCT are shown in Figure 3.2.

3.3.1.1 Tidal CA measured by dCT was detected when the expiratory time was longer than the inspiratory time during tidal ventilation.

As demonstrated in Figure 3.2, the maximum fraction of collapse was significantly larger ($p < 0.05$) than the minimum fraction when I:E was below 1 (PCV 1:2 (11.6 – 19.5 %), PCV 1:4 (11.5 – 19.9 %), VCV 1:2 (12.6 – 20.4 %), VCV 1:4 (12.9 - 20.6 %)), as quantified by single-slice dCT at a temporal resolution of 250 ms. This effect was consistent between PCV and VCV. There was no significant difference between the maximum and minimum fraction of collapse when I:E was higher than 1.

The mean fraction of atelectasis was compared during inspiration versus expiration at respiratory rate = 12 /min and V_T 10 ml kg^{-1} . The mean fraction of atelectasis during inspiration was not significantly different ($p < 0.05$) to the mean fraction of atelectasis during expiration in any of the conditions other than PCV 1:2 (PCV 1:2 (13.8 – 17.3 %)).

a Pressure Controlled Ventilation



b Volume Controlled Ventilation

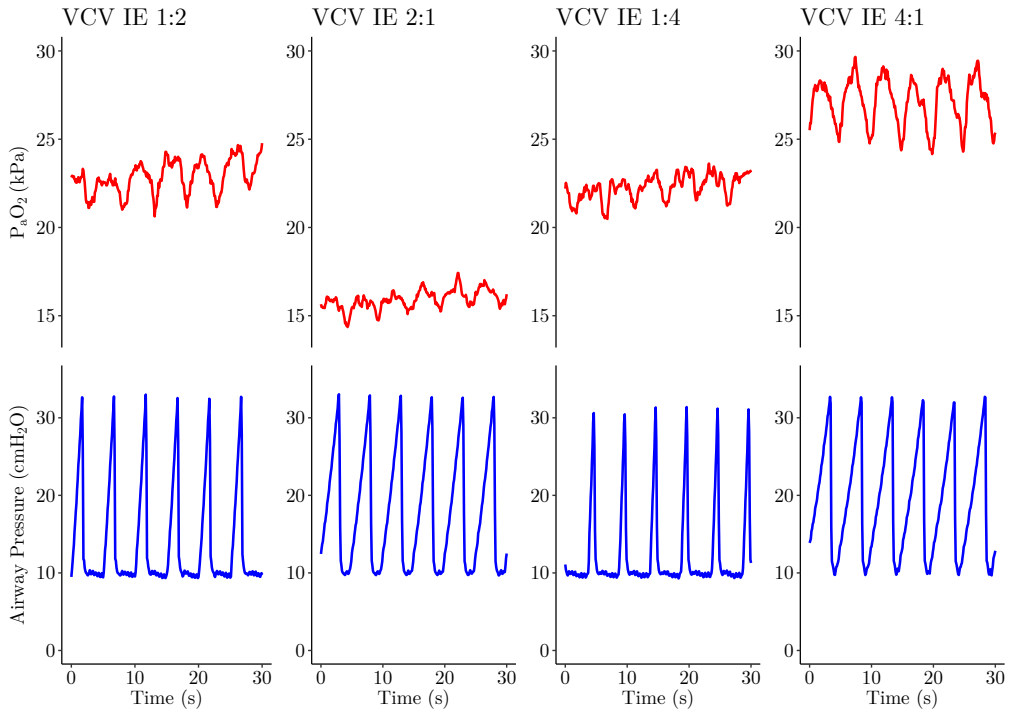


Figure 3.1: Example recordings of P_aO_2 and airway pressure during tidal ventilation under different conditions. *All the displayed recordings were taken in the same animal, after saline lavage lung injury. Ventilator settings were V_T 10 ml kg^{-1}, RR = 12 bpm and PEEP = 10 cmH_2O. The changes in mean P_aO_2 and P_aO_2 oscillation amplitude are not meant for interpretation. The aim of this figure is simply to provide a visual representation of the data which were analysed. PCV: Pressure Controlled Ventilation, VCV: Volume Controlled Ventilation, IE: Inspiratory:Expiratory ratio.*

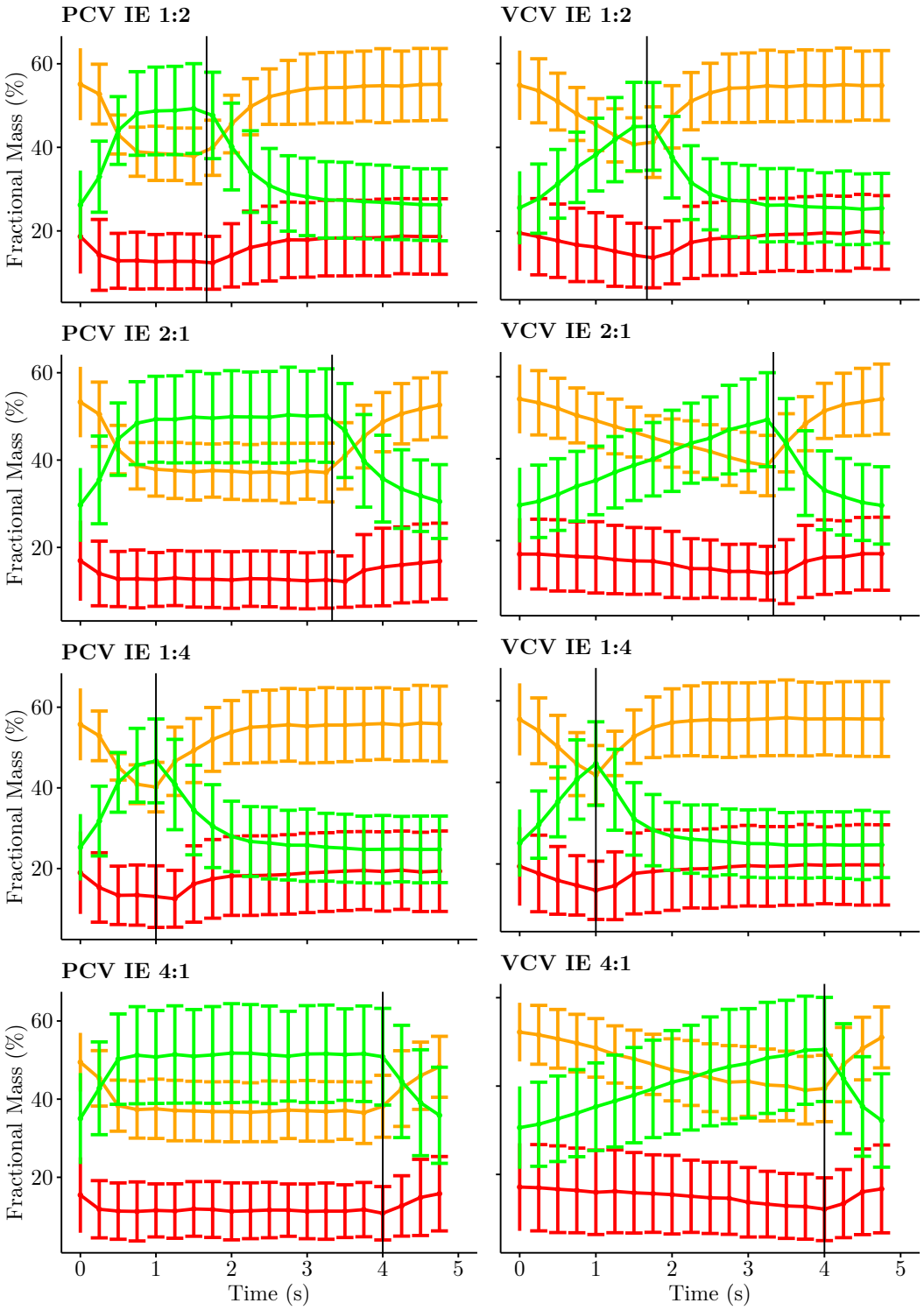


Figure 3.2: Changes in compartmental mass over the course of a single breath. *Red = atelectasis, yellow = poorly aerated, green = normally aerated. PCV = pressure controlled ventilation, VCV = volume controlled ventilation, I:E = inspiratory:expiratory ratio. Error bars represent standard deviation. Only in conditions where the expiratory time exceeds inspiratory time is there a significant difference between the mean maximum and minimum fractions of atelectasis, PCV 1:2 (*11.6 – 19.5% *), PCV 1:4 (* 11.5 – 19.9%*), VCV 1:2 (*12.6 – 20.4%*), VCV 1:4 (*12.9 – 20.6%*). Overdistended mass represented <* 2 % *of total mass and remained unchanged throughout the breath in all condition. It is therefore not shown.*

3.3.1.2 Respiratory P_aO_2 oscillation amplitude was not clearly related to CA.

A total of $n = 148$ different 30 s sections of respiratory P_aO_2 oscillation data were analysed, all of which were with $V_T = 10\ ml\ kg^{-1}$ and RR = 12 bpm. Figure 3.3(A) illustrates the relationship between the change in lung collapse and the respiratory P_aO_2 oscillation amplitude. Mean P_aO_2 and respiratory P_aO_2 oscillation amplitude for each ventilator condition are shown in Table 3.4 and Figure 3.3(B).

There was not a strong correlation between mean airway pressure and mean P_aO_2 during tidal ventilation, with a 0.55 kPa reduction in P_aO_2 for 1 cmH_2O increase in airway pressure ($r^2 = 0.21$). A one-way repeated measures ANOVA with multiple comparisons supported a significant effect of ventilatory mode on mean P_aO_2 during tidal ventilation. ($F_{(3,57)} = 7.6, p = 0.0002$).

I:E Ratio	PCV				VCV			
	Mean P_aO_2 (kPa)	Oscillation Amplitude (kPa)	Mean Airway Pressure (cmH_2O)	Peak Airway Pressure (cmH_2O)	Mean P_aO_2 (kPa)	Oscillation Amplitude (kPa)	Mean Airway Pressure (cmH_2O)	Peak Airway Pressure (cmH_2O)
1:2	25.2 (4.7)	2.6 (0.8)	11 (8)	24 (5)	26.4 (4.6)	2.1 (0.6)	8 (5)	23 (4)
2:1	19.7 (6.6)	1.6 (0.5)	16 (8)	24 (5)	25.9 (5.5)	2.1 (0.7)	11 (6)	23 (5)
1:4	27.1 (2.5)	2.8 (1.0)	8 (7)	25 (4)	26.3 (3.6)	2.1 (0.5)	7 (5)	23 (4)
4:1	22.7 (3.9)	2.0 (0.5)	18 (6)	24 (4)	26.4 (3.2)	2.3 (0.9)	13 (5)	23 (4)

Table 3.4: Mean P_aO_2, amplitude of respiratory P_aO_2 oscillations and mean airway pressure during different ventilatory conditions. *Respiratory P_aO_2 oscillation amplitude was significantly lower during PCV 2 : 1 when compared to PCV 1 : 2, PCV 1 : 4, VCV 1 : 2 and significantly higher during PCV 1 : 4 compared to PCV 4 : 1, PCV 2 : 1 and VCV 1 : 4. The tidal volume was monitored throughout each experiment by a Capnomac Ultima. The measured tidal volume for the presented data was 10 ml^{-1} kg^{-1}. Values shown are mean (SD). PCV = pressure controlled ventilation, VCV = volume controlled ventilation.*

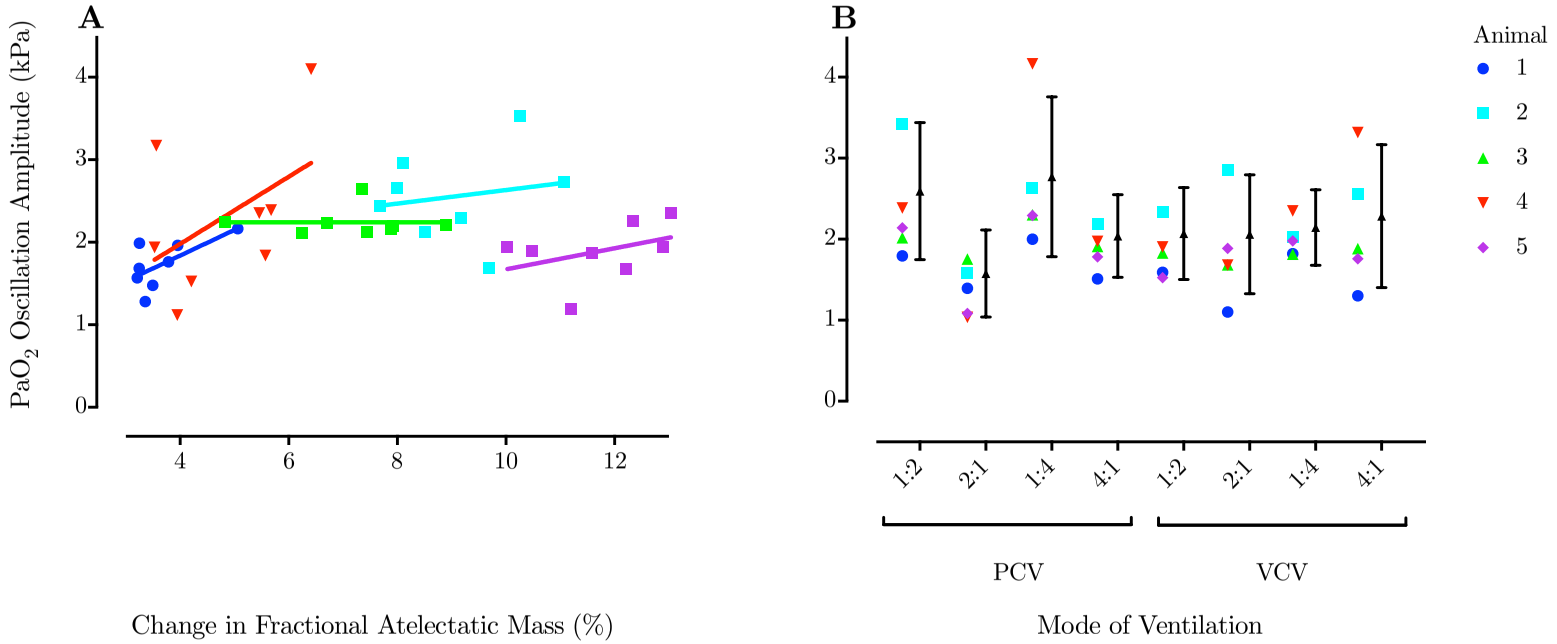


Figure 3.3: Mean respiratory P_aO_2 oscillation amplitude during tidal ventilation under different ventilatory conditions. ***(A)*** *Correlation between the mean respiratory P_aO_2 oscillation amplitude (kPa) recorded during CT scanning and the relevant associated CT-measured change in fractional atelectasis during that ventilatory condition. Linear regression analysis results gave: Pig 1 r^2 = 0.44, gradient = 2.33. Pig 2 r^2 = 0.31, gradient = 0.62. Pig 3 r^2 = 0.00, gradient = 0.00. Pig 4 r^2 = 0.23, gradient = 3.06. Pig 5 r^2 = 0.15, gradient = 0.96.* ***(B)*** *Mean amplitude (kPa) with error bars representing SD (black dots & lines). Amplitudes are calculated from tidal ventilation both before and during CT for each ventilator condition. Each animal is represented by a different coloured symbol. PCV = pressure controlled ventilation, VCV = volume controlled ventilation, x-axis ratios in (B) represent different I:E ratios.*

3.3.2 Whole lung CT and P_aO_2 during breath-hold manoeuvres

Measurements of continuous P_aO_2 and airway pressure were recorded throughout each breath-hold manoeuvre. Some animals did not complete the full sequence of manoeuvres due to time constraints. The numbers of each breath-hold manoeuvre completed in each experiment are shown in Table 3.5. An example of the traces recorded during each type of manoeuvre is shown in Figure 3.4.

Pig	Pre-CT			CT			Total
	Ve	V_T10	V_T20	Ve	V_T10	V_T20	
1	3	3	3	6	6	6	27
2	6	6	6	3	3	3	27
3	6	6	6	6	6	6	36
4	6	6	6	4	4	4	30
5	3	3	3	6	5	6	26
							146

Table 3.5: Number of breath-hold manoeuvres carried out per animal. *Pre-CT: laboratory based manoeuvres without CT imaging. CT = Experiments conducted in the CT scanner.*

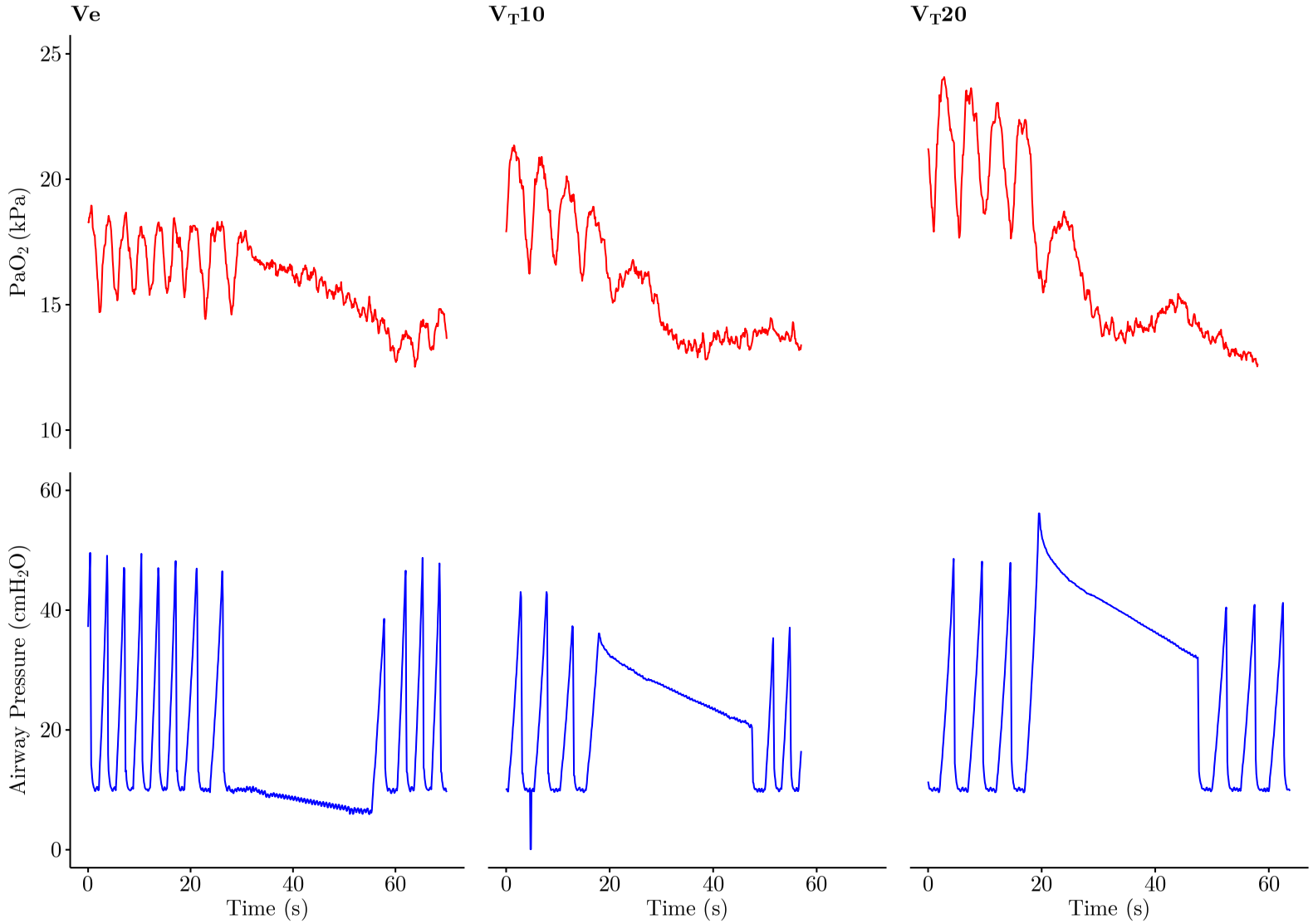


Figure 3.4: Example P_aO_2 and airway pressure traces for breath-hold manoeuvres. *These traces demonstrate when and how the P_aO_2 trace deviates from its preceding oscillations during each type of breath-hold manoeuvre. Additionally, these traces demonstrate the ongoing loss of pressure that occurred consistently throughout each breath-hold manoeuvre. This is discussed further in Section 3.4.2 and represents a potential limitation to interpreting these data from the breath-hold experiments.*

3.3.2.1 Whole lung collapse did not decrease during a 30 second breath-hold manoeuvre with large tidal volume.

Analysis of $n = 74$ breath-hold manoeuvres undertaken with simultaneous CT showed a significant increase in the fraction of collapse from the start to the end of an imposed breath-hold manoeuvre as shown in Table 3.6 and Figure 3.5(A). Mean (SD) airway pressure decreased concurrently during breath-hold manoeuvres at end-expiration by 4 (2) cmH_2O, V_T10 by 11 (6) cmH_2O and V_T20 by 11 (6) cmH_2O. The fractional increase in collapse during end-expiratory breath-hold manoeuvres was significantly larger compared to the other two conditions (14% *vs* 0.9 – 2.1%, $p < 0.0001$). There was no statistical difference between the change in collapse with V_T10 and V_T20 end-inspiratory breath-hold manoeuvres.

Animal number	Fractional Collapse (%)					
	Ve		V_T10		V_T20	
	Start	End	Start	End	Start	End
1	18.4 (2.1)	23.8 (2.0)	16.8 (1.4)	17.5 (2.1)	15.3 (1.7)	16.0 (1.3)
2	37.1 (2.9)	55.3 (3.6)	22.5 (7.7)	28.3 (9.4)	13.0 (2.3)	15.8 (1.8)
3	25.4 (1.1)	37.8 (1.4)	19.9 (0.7)	22.5 (0.5)	16.1 (0.6)	17.0 (1.4)
4	19.8 (1.2)	36.8 (3.0)	8.7 (1.6)	10.2 (2.5)	7.0 (0.6)	9.6 (3.2)
5	32.8 (0.9)	53.1 (0.7)	25.6 (3.4)	27.1 (0.7)	19.1 (1.1)	20.0 (1.4)
Combined	26.0 (7.1)	40.1 (12.0)	18.6 (6.5)	20.7 (7.1)	14.8 (4.1)	16.1 (3.7)
Difference	14.1* (6.1)		2.1** (3.0)		0.9 (0.6 – 1.5)†	

Table 3.6: Mean fractional mass of collapsed lung measured by CT at the start and the end of breath-hold manoeuvres. *The increase was significant under each of the three conditions. Ve = end-expiratory, V_T10 = end-inspiratory (10 ml kg^{-1}), V_T20 = end-inspiratory (20 ml kg^{-1}). *Ve: $t(24) = 12$, $p < 0.0001$. **V_T10: $t(24) = 3.2$, $p < 0.005$. †V_T20: 95% CI 0.6 – 1.5%.*

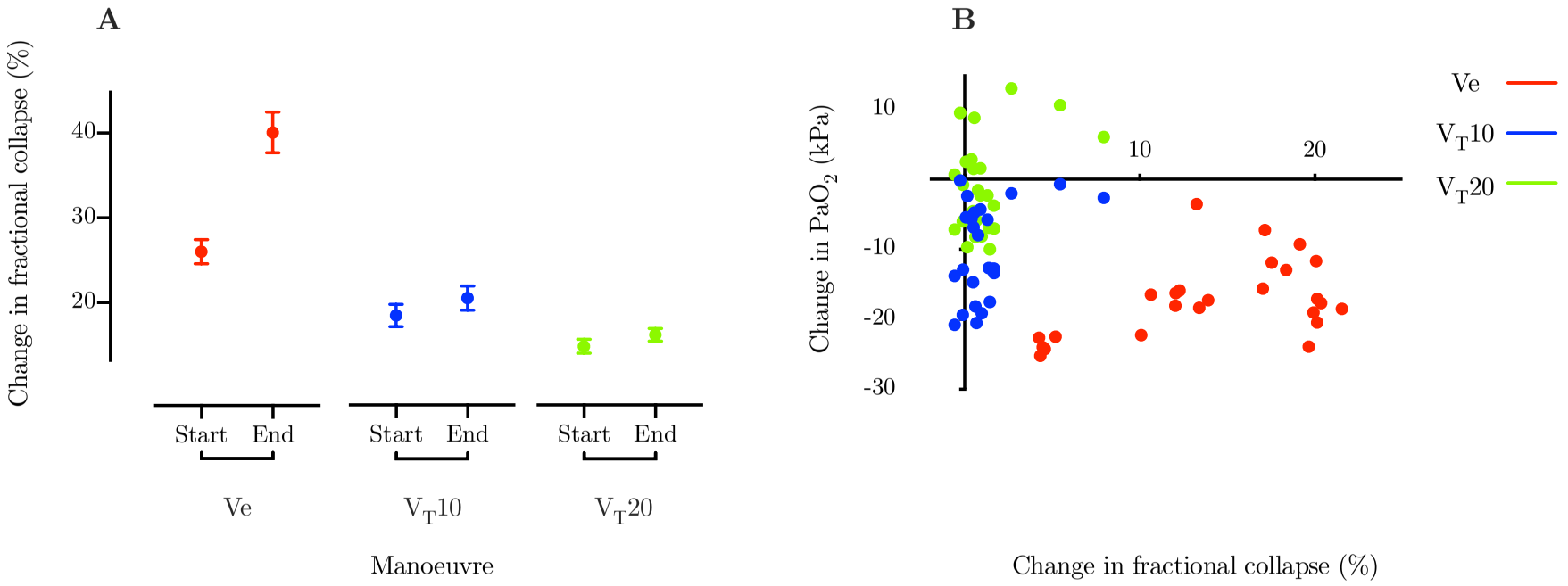


Figure 3.5: Changes in fractional lung collapse during breath-hold manoeuvres. (A) Change in mean fractional collapse. *Points represent the mean (±SE) fraction of lung collapse measured by whole lung CT at the start and the end of a 30 s breath-hold.* **(B) Relationship between change in lung collapse and change in P_aO_2.** *Mixed effects linear modelling was used to take into account the effect of the individual animal on the relationship between the change in collapse and the change in P_aO_2 (using animal as a random effect). This yielded linear equations of $y = -0.14x - 14.2$ for Ve, $y = 0.14x - 8.9$ for V_T10 and $y = 0.50x - 0.7$ for V_T20. Conditional r^2 values were < 0.1 for all three models. Red represents end-expiratory (Ve) breath-hold manoeuvres, blue and green represent end-inspiratory breath-hold manoeuvres with V_T 10 ml kg^{-1} (V_T10) and 20 ml kg^{-1} (V_T20).*

3.3.2.2 Change in P_aO_2 during breath-hold manoeuvres could not be predicted from the change in fractional lung collapse with a linear model.

The change in P_aO_2 during the course of a breath-hold manoeuvre was predicted from the change in fractional lung collapse using a linear mixed effects model with animal as a random effect. As can be seen from Figure 3.5(B) and the presented r^2 values, the change in fractional lung collapse accounts for little of the variance observed in the change in P_aO_2 across the course of a breath-hold manoeuvre (r^2 = 0.23, 0.15, 0.14 for Ve, V_T10 and V_T20 breath-hold manoeuvres respectively).

3.3.2.3 There was significant variation in the P_aO_2 change between different breath-hold manoeuvres within and between individual animals.

Figure 3.6 shows mean continuous P_aO_2 recordings from the animals ($n = 5$) during each breath-hold manoeuvre studied before and during CT scanning ($n = 146$). For each individual manoeuvre, the change in P_aO_2 was calculated from the start of the breath-hold manoeuvre (measured from the start of the imposed airway pressure change) to the subsequent nadir in the trace. Mean (SD) change in P_aO_2 was -16.5 (6.3) kPa during end-expiratory breath-hold manoeuvres, -10.5 (5.0) kPa and -4.8 (3.4) kPa for V_T10 and V_T20 end-inspiratory breath-hold manoeuvres respectively. A repeated measures ANOVA with Greenhouse-Geisser correction determined these P_aO_2 changes were significantly different between each condition ($F_{(2,38)} = 110,\ p < 0.0001$).

As can be seen on inspection of the P_aO_2 traces in Figure 3.7 and the post-hoc analysis shown in Table 3.7, comparisons of manoeuvres between animals was significantly different. The P_aO_2 traces during breath-hold manoeuvres demonstrate high variability between each animal and manoeuvre in the majority of cases. Notably, animal No. 4 has large deviations in its traces and this is the animal with PFR suggestive of the most severe lung injury (PFR 105 mmHg compared to PFR >200 mmHg for other animals).

Animal comparison	breath-hold manoeuvre		
	Ve	V_T10	V_T20
1 vs 2	****	****	****
1 vs 3	*	*	ns
1 vs 4	***	****	****
1 vs 5	ns	****	ns
2 vs 3	**	****	****
2 vs 4	ns	ns	**
2 vs 5	****	*	***
3 vs 4	ns	***	**
3 vs 5	ns	*	ns
4 vs 5	**	ns	ns

Table 3.7: Results of two-way ANOVA with Tukey's multiple comparison test on the difference between the change in P_aO_2 during different breath-hold manoeuvres in different animals. *Significant differences in the change in P_aO_2 are denoted against the relative comparison. Ve = end-expiratory, V_T10 = end-inspiratory (10 ml kg^{-1}), V_T20 = end-inspiratory (20 ml kg^{-1}). Significant differences in the change in P_aO_2 are denoted against the relative comparison; * = $p < 0.05$, ** = $p < 0.01$, *** = $p < 0.005$, **** = $p < 0.0001$, ns = not significant.*

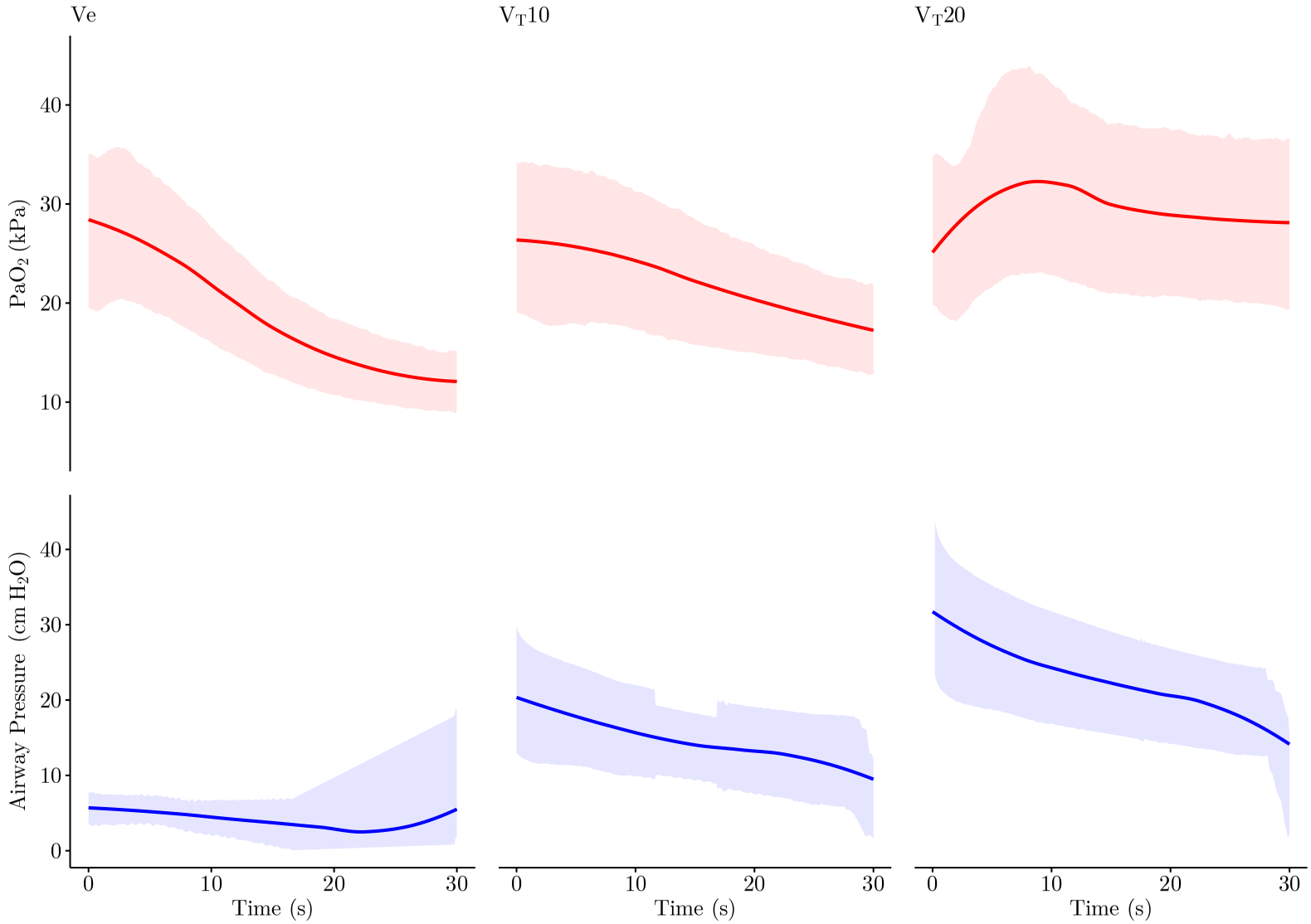


Figure 3.6: Mean P_aO_2 and airway pressure traces during breath-hold manoeuvres. *P_aO_2 and airway pressure traces during breath-hold manoeuvres. The left column shows end-expiratory breath-hold manoeuvres (Ve), the middle column 10 $ml\ kg^{-1}$ end-inspiratory breath-hold-manoeuvres (V_T10) and the right column 20 $ml\ kg^{-1}$ end-inspiratory breath-hold manoeuvres (V_T20). Red represents P_aO_2 and blue mean airway pressure. Solid lines represent mean of $n = 5$ animals' manoeuvres associated with CT imaging. The shaded area represents SD. P_aO_2 traces have been corrected for the effect of O_2 uptake ($\dot{V}O_2$) over time.*

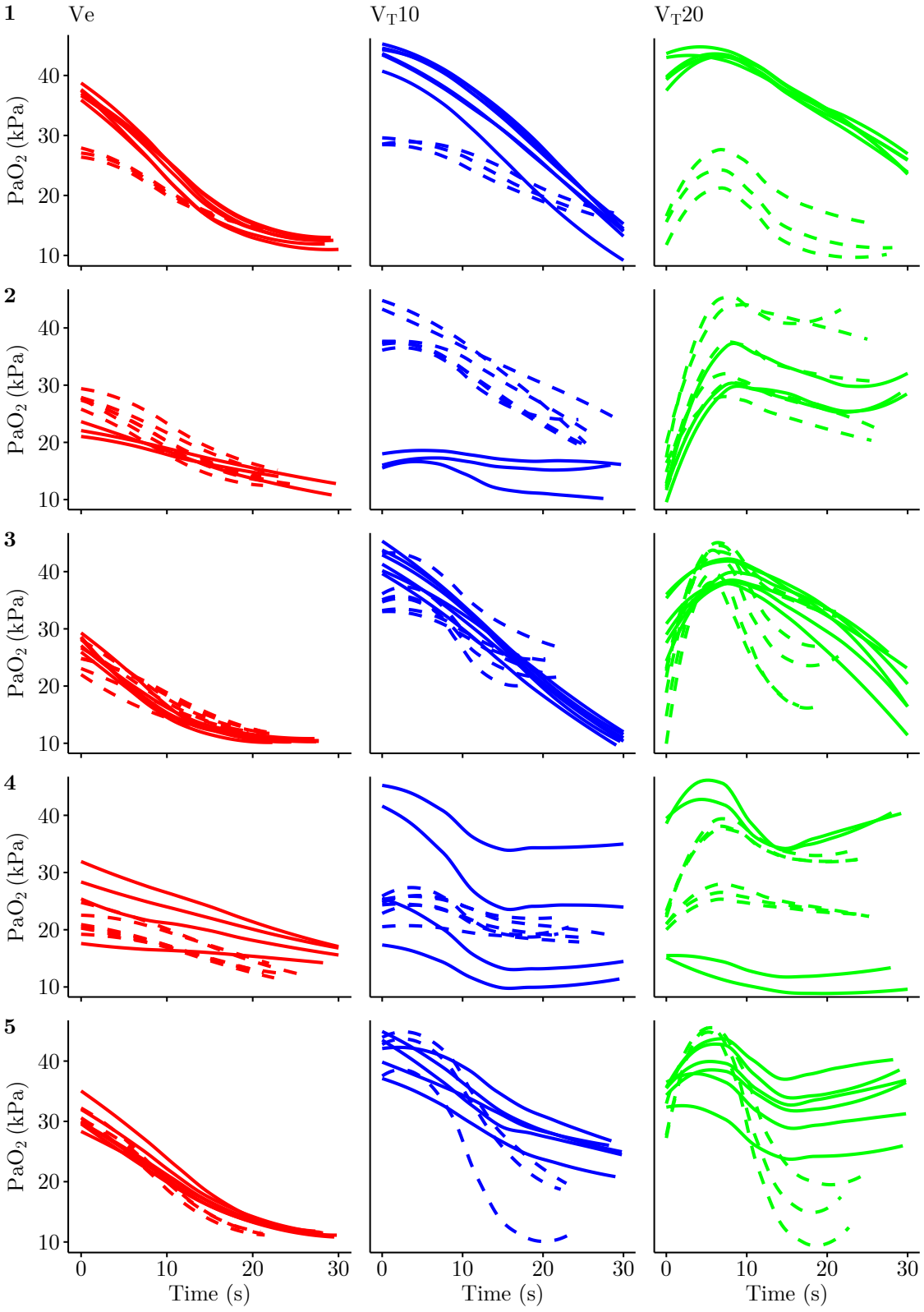


Figure 3.7: P_aO_2 traces during breath-hold manoeuvres for each animal. *In the left column, red traces show end-expiratory breath-hold manoeuvres (Ve). In the middle column, blue traces show* 10 *ml* kg^{-1} *end-inspiratory breath-hold-manoeuvres (*V_T10*) and in the right column, green traces show* 20 *ml* kg^{-1} *end-inspiratory breath-hold manoeuvres (*V_T20*). Dashed lines represent measurements undertaken in the laboratory before transfer to the CT scanner. Solid lines are manoeuvres associated with CT imaging. Each animal is represented by the number to the left of each set of plots. All traces have been corrected for the effect of* O_2 *uptake (*$\dot{V}O_2$*).*

3.4 Discussion

This chapter investigates the relationship between dynamic changes in P_aO_2 and atelectasis in anaesthetised, mechanically ventilated pigs with saline lavage lung injury. Dynamic respiratory P_aO_2 oscillations were demonstrated during tidal ventilation which increased when CT markers of tidal CA increased. However, the magnitude of this association was not as large as expected. Additionally, there was a significant CA only during tidal ventilation when the expiratory time was longer than the inspiratory time (I:E <1). During all types of imposed breath-hold manoeuvres, there was an increase in lung collapse. This was true even during a 30 s large inspiratory breath-hold manoeuvre (with a V_T of 20 ml kg^{-1}). The increase in lung collapse was associated with significant reduction in P_aO_2 during these manoeuvres.

3.4.1 The relationship between respiratory P_aO_2 oscillations and cyclical atelectasis.

Analysis of the respiratory P_aO_2 oscillation amplitude showed that there were significant differences in the amplitudes for some conditions, however these did not match the conditions in which CA was detected by dCT.

The minimum and maximum amounts of mean fractional collapse (mean (SD)) were 14 (7)% and 17 (9)% measured in PCV 2 : 1 and PCV 1 : 4 respectively. Given the small differences and large variability in these values it is likely that while technically measurable, they do not represent a meaningful physiological or clinical difference. These results suggest a lack of a strong association between CA and respiratory P_aO_2 oscillations. This finding does not support the hypothesised strong causal relationship between them (Williams et al. 2000; Baumgardner et al. 2002; Syring et al. 2007; Boehme et al. 2015) and suggests the presence of other contributing determinants of variable shunt fraction within each breath. This proposition is supported by results from studies in the uninjured porcine lung, where respiratory P_aO_2 oscillations (with an amplitude of c0.6 - 1.3 kPa with V_T 10 ml kg^{-1}) were demonstrated in the absence of CA (Formenti et al. 2017a). The measured mass of collapse (mean (SD) = 16 (9)%) is lower than that reported in other studies using

dCT (Neumann et al. 1998; Markstaller et al. 2003; David et al. 2005) in lung injury, the details of which are shown in Table 3.8. Notably, some of these studies considered different HU ranges and used different lung injury models.

Paper	Injury Model	HU Range	Fractional Atelectasis (%)
Neumann et al. (1998)	Oleic acid	-100 to +100	c 25 - 40
Markstaller et al. (2003)	Saline lavage	-300 to +200	c 60
David et al. (2005)	Saline lavage	-300 to +200	c 20 - 50

Table 3.8: Dynamic CT studies examining fractional lung collapse in porcine lung-injury models. *HU = hounsfield unit.*

However, in the current study, the measured atelectasis was mean (SD) = 88 (59)% higher than that measured in a similar study (Formenti et al. 2017a). In this set of experiments Formenti et al. (2017a) used a similar protocol, with the same HU ranges, in the the same species without lung injury. This suggests that the saline lavage lung injury used in my experiments was effective in producing lung collapse. This collapse however, did not cyclically recruit and derecruit as previously hypothesised and this is consistent with findings from intravital microscopy (Mertens et al. 2009). This result suggests that other determinants of respiratory P_aO_2 oscillations should be considered. Whilst CA is likely to cause an increase in the amplitude of respiratory P_aO_2 oscillations, in the context of a complex physiological system, the effect may be obscured by other competing variables such as the redistribution of pulmonary blood flow to regions with different ventilation:perfusion ratios (Vimlati et al. 2011). This hypothesis is supported by the finding in these experiments that the mean P_aO_2 did not increase with an increase in mean airway pressure, as reported previously (Brower et al. 1985; Musch et al. 2004). Additionally, CT measured voxel density used as a surrogate marker of collapse assumes that the higher density voxels are true collapse and not another radiodense material such as fluid (alveolar flooding) or blood. This may have lead to an overestimation of the degree of true atelectasis.

In addition to demonstrating the change in compartmental masses during tidal ventilation, Figure 3.2 shows that those changes occur within less than 1 s of the change from inspiration to expiration. This occurs in both VCV and PCV modes

and supports findings from other authors that recruitment occurs within the first few seconds of increasing airway pressure (Markstaller et al. 2001; Albert et al. 2009).

The mean (SD) amplitude of oscillations (2.2 (0.8) kPa) was smaller than had been previously demonstrated by other authors (Williams et al. 2000; Baumgardner et al. 2002), where P_aO_2 oscillations of up to 40 kPa were measured. This may be partially explained by the smaller V_T (10 vs ∼30 ml kg^{-1}) and lower peak P_{AW} (< 35 vs > 45 cmH_2O) during tidal ventilation in the present study. Whilst the V_T is larger than the recommended human clinical V_T (Acute Respiratory Distress Syndrome Network et al. 2000), it is smaller than those used in studies showing respiratory P_aO_2 oscillations with amplitudes of > 13 kPa, and equivalent to V_T measured in spontaneously ventilating pigs (Hannon et al. 1990). In addition, peak pressure was < 30 cmH_2O throughout the experiments, which is in contrast to previous studies where peak pressure exceeded 45 cmH_2O (Baumgardner et al. 2002).

Changes in atelectasis during the course of a single breath were not detected in either PCV or VCV when a positive I:E ratio was used. However, when the expiratory time was greater than the inspiratory time there was a significant difference between the maximum and minimum measured fraction of atelectasis. This observation aligns with the findings during breath-hold manoeuvres in that they similarly demonstrate the effect of expiratory time on change in atelectasis.

3.4.2 The relationship P_aO_2 and fractional lung collapse during breath-hold manoeuvres.

The amount of lung collapse, unexpectedly, did not decrease during imposed inspiratory (V_T = 10 ml kg^{-1} and 20 ml kg^{-1}) breath-hold manoeuvres. In the context of evidence demonstrating that the majority of recruitment occurs within the first few seconds of application of inflation pressure (Markstaller et al. 2001; Albert et al. 2009), this result may represent CT measurement of "starting" collapse being taken at a time point already on the plateau of the recruitment curve. Indeed, the starting mass of collapse recorded in Ve (26.0%) was 76% greater than that recorded in V_T20 (14.8%). As demonstrated in the representative traces (Figure 3.4) airway pressure is not maintained during a prolonged breath-hold. This is because both the expiratory and inspiratory ventilator valves close at the start of manoeuvre, and

the measured airway pressure (representing the pressure in the lungs) decreases due to:

- "pendelluft" phenomena (Tabuchi et al. 2016) and
- oxygen consumption ($\dot{V}O_2$)

I attempted to correct for effect of $\dot{V}O_2$ in analysis of the continuous P_aO_2 recordings during breath-hold manoeuvres by subtracting calculated $\dot{V}O_2$ at each 100 ms time point. The reduction in airway pressure throughout the course of a breath-hold will increase the amount of both poorly aerated and collapsed lung regions. This will in turn will reduce P_aO_2 by increasing shunt and $\dot{V}/\dot{Q}$ mismatch. Indeed, we found a decrease in airway pressure during all breath-hold manoeuvres

3.4.3 Limitations

The animal model. One main limitation of this study is that the porcine model does not comprise all the features observed in human ARDS. Additionally, the PFRs attained were consistent with only mild to moderate lung injury. However, the saline lavage model is prone to collapse and easily recruitable (Boehme et al. 2015). Thus, this model of lung injury was chosen because it would potentially exaggerate the phenomenon of CA and CA dependent P_aO_2 oscillations.

Voxel density thresholds. Different compartments of lung (normally aerated, poorly aerated, atelectatic and overdistended) were segmented based on their voxel density. The thresholds for each compartment were based on previous literature using CT studies of lung parenchyma (Gattinoni et al. 1988; Lundquist et al. 1995; Vieira et al. 1998). Any chosen thresholds leave open the possibility that clusters of voxels exist on one side or another of a cut-off value and although a voxel cluster may tend towards collapse, for example, it may have not been counted in the analysis.

The timing of the "start" of a breath-hold. Analyses of the P_aO_2 traces in this report were carried out from the start of the change in the airway pressure trace. Whether or not this represents where the oscillating P_aO_2 signal truly deviates

secondary to the imposed change in airway pressure is not clear. Qualitative visual examination of the P_aO_2 traces during imposed breath-hold manoeuvres suggests there is a variable delay in when deviation in the P_aO_2 signal responds. However, the timing/effect is not consistent and thus the fixed/defined point of change in P_{AW} was chosen in this study.

Ventilation vs Perfusion. Whilst rapid measurement of P_aO_2 is a potentially translatable technology with growing supportive evidence it is unable to take into account of spatial pulmonary heterogeneity and there remains a question of whether or not oscillations as observed are caused by changes in ventilation or perfusion, or indeed by heterogeneous changes in both.

3.4.4 Conclusions

This study is the first to contemporaneously measure dynamic CA and real-time P_aO_2 in a collapse-prone ARDS model. It demonstrates a limited association between CA and respiratory P_aO_2 oscillations, much smaller than expected from the published literature. The results challenge the accepted hypothesis that CA is the main determinant of respiratory P_aO_2 oscillations in ARDS, where reductions of P_aO_2 oscillations are mostly expected from reductions in CA. The findings warrant further investigation into the dynamic role of pulmonary perfusion within the context of complex pulmonary responses to mechanical ventilation (Pelosi et al. 2015; Formenti et al. 2017b).

CHAPTER 4

Measuring lung volumes using real-time changes in P_aO_2: Comparison with Computed Tomography

Abstract

This chapter tests the hypothesis that real-time measurements of P_aO_2 can be used to measure lung volume. Estimates of lung volume predicted from P_aO_2 rate-of-decline are compared against measurements made with CT in mechanically ventilated pigs with uninjured lungs and with a saline-lavage model of ARDS. The results show that real time P_aO_2 rate-of-decline tends to under-estimate lung volume compared to CT in the uninjured lung. The trending ability of the P_aO_2 rate-of-decline method demonstrates it can track direction of change, but that measurements of the change in lung volume are less than those measured with CT. These results support the hypothesis that P_aO_2 rate-of-decline can be used to quantify the volume of lung taking part in gas exchange and that a formal protocol to further study this hypothesis would be valuable.

4.1 Introduction

The previous chapter examined the application of real-time P_aO_2 measurement in a porcine ARDS model and challenged the existing hypothesis that the main determinant of large oscillations in P_aO_2 was cyclical recruitment and derecruitment of atelectasis. The intra-arterial O_2 sensors used in that chapter have previously been applied to test whether a simple lung model could predict oscillations in arterial P_aO_2 measured with the intra-arterial O_2 sensors.

Formenti et al. (2017a) examined a simple, two-compartment tidal ventilation model of P_aO_2 decline in the mechanically ventilated, uninjured porcine lung. The authors considered that at any time, t, the volume of O_2 in the alveolar compartment is equal to the product of the total volume of the alveolar compartment ($V_A(t)$) and the fraction of O_2 within that compartment ($F_A(t)$). The rate of change of O_2 within the alveolar compartment is thus:

$$\frac{d\big(V_A(t).F_A(t)\big)}{dt} = V_A(t)\frac{dF_A(t)}{dt} + F_A(t)\frac{dV_A(t)}{dt} \tag{4.1}$$

During inspiration, the change in O_2 within the alveolar compartment is represented by the difference between the rate of O_2 ingress and the rate of oxygen uptake by the pulmonary circulation ($\dot{V}_{O_2}$):

$$\frac{dV_A(t).F_A}{dt} - \dot{V}_{O_2} \tag{4.2}$$

During expiration, O_2 is removed from the alveolar compartment by both exhalation of alveolar gas and $\dot{V}_{O_2}$:

$$-\frac{dV_A(t).F_A}{dt} - \dot{V}_{O_2} \tag{4.3}$$

The authors then developed mass balance equations for O_2 in both inspiration and expiration by combining expressions 4.2 and 4.3 to give:

Inspiration :

$$\frac{dF_A(t)}{dt} = \frac{-\dot{V}_{O_2} + \frac{dV_A(t)}{dt}.F_I}{V_A(t)} = \frac{-\dot{V}_{O_2} + \dot{V}_{insp}(t).F_I}{EELV + V_{insp}(t)} \tag{4.4}$$

Expiration :

$$\frac{dF_A(t)}{dt} = \frac{-\dot{V}_{O_2}}{V_A(t)} = \frac{-\dot{V}_{O_2}}{EELV + V_T - V_{exp}(t)} \tag{4.5}$$

where:

$\dot{V}_{insp}(t)$ = the inspiratory flow rate,

EELV = the end-expiratory lung volume,

$V_{insp}(t)$ = the inspired volume at time t,

$V_{exp}(t)$ = the expired volume at time t.

Assuming that in the uninjured lung P_AO_2 and P_aO_2 were similar and that the gradient between them was constant, Formenti et al. (2017a) considered a modification to equations 4.4 and 4.5, so that during a breath-hold manoeuvre, the rate of decline in P_aO_2 could be modelled by:

$$\frac{dF_A(t)}{dt} = \frac{-\dot{V}_{O_2}}{EELV + V_T} \tag{4.6}$$

Using lung volumes measured by CT and $\dot{V}_{O_2}$ measured by Fick's principle (with thermodilution cardiac output and paired P_aO_2 and $P_{\bar{V}}O_2$ measurements), the authors solved equation 4.6 to predict the rate of decline in P_aO_2 during breath-hold manoeuvres at end-expiration and end-inspiration with tidal volumes of 10 and 20 ml kg^{-1}. They compared their predicted rate of P_aO_2 decline with real time measurement of P_aO_2 made with intra-arterial fibreoptic P_aO_2 sensors of the type described in Section 2.4 and used in Chapter 3. Formenti et al. (2017a) showed that their model could predict the change in P_aO_2 measured in real time.

4.1.1 Inverting the P_aO_2 rate of decline model to predict lung volume.

The model represented by equation 4.6 can predict changes in P_aO_2 over the course of breath-hold manoeuvres (Formenti et al. 2017a). If the rate of change in P_aO_2 can be measured in real-time and $\dot{V}_{O_2}$ can be quantified separately, then the model can be inverted and equation 4.6 solved to provide an estimate of the lung volume.

As discussed in Section 1.5, measurements of lung volume in mechanically ventilated patients have the potential to allow personalised ventilatory strategies and reduce mortality in patients with ARDS. If the imposed V_T can be titrated to the underlying volume of "baby lung" then this has the potential to reduce ΔP and mortality in ARDS (Acute Respiratory Distress Syndrome Network et al. 2000; Gattinoni et al. 2005; Gattinoni et al. 2016a; Amato et al. 2015; Mancebo et al. 2019).

Quantification of lung volumes by imaging techniques requires transfer of the patient and, for CT, exposure to ionising radiation. This makes the application of these techniques unsuitable for repeated measurement of lung volume in the mechanically ventilated intensive care patient. Bedside techniques, such as those described in Section 1.6 have not been widely adopted. They either rely on bulky equipment, which cannot easily be applied at the bedside (Larsson et al. 1987), are too time consuming or have not proven reliable in assisted ventilation (Larsson et al. 1987; Di Marco et al. 2007; Maisch et al. 2007; Patroniti et al. 2008; Heinze et al. 2009; Richard et al. 2014).

The majority of mechanically ventilated intensive care patients have invasive arterial blood pressure monitoring as a standard of care. This is achieved by introduction of an intra-vascular catheter into a peripheral artery. The same type of catheters are used as introducers for intra-arterial P_aO_2 probes (Section 2.4). Therefore, estimation of the lung volume taking part in gas exchange (the effective lung volume, ELV) could be made by inserting a fibreoptic P_aO_2 probe into an already existing arterial cannula. This would require no movement of the patient and no alteration to standard care.

The aim of the pilot study presented in this chapter was to determine the agreement between measurements of ELV taken with real-time P_aO_2 (ELV_{O_2}) and measurements taken with CT (ELV_{CT}). This aim was achieved by comparing paired measurements of ELV_{O_2} and ELV_{CT} during breath-hold manoeuvres in a mechanically ventilated porcine model.

4.2 Methods

4.2.1 Ethical approval

Studies were carried out at the Hedenstierna laboratory, Uppsala University, Sweden. Ethical approval was granted by the regional animal welfare ethics committee (Ref: C98/16) and reporting in this chapter adheres to Animal Research: Reporting of In Vivo Experiments guidelines (Kilkenny et al. 2013).

4.2.2 Data selection

A total of $n = 26$ porcine experiments with a total of $n = 190$ breath-hold manoeuvres were identified as having simultaneous capture of real-time P_aO_2 and whole lung volume, single-energy CT data.

P_aO_2 traces of the 190 breath-hold manoeuvres were analysed and excluded if:

1. mean P_aO_2 was < 13.3 kPa
2. signal to noise ratio (SNR) was < 30 dB (determined by wavelet transform)

This provided $n = 146$ breath-hold manoeuvres from $n = 19$ animals (mean weight (SD) = 30 (2) kg) with paired measurements of ELV_{O_2} and ELV_{CT}. Table 4.1 compares baseline characteristics of the uninjured and ARDS model animals and Tables 4.2 and 4.3 provide baseline characteristics for each individual animal in the uninjured and ARDS model groups.

4.2.3 Animal preparation

Animals were prepared and anaesthetised as described in Section 2.3.3. In all cases, anaesthesia was maintained using a total intravenous technique and baseline mechanical ventilation delivered at 20 - 25 breaths per minute in volume controlled mode

with V_T 10 ml kg^{-1} to maintain pH > 7.2 and end-tidal CO_2 (E_TCO_2) < 8 kPa (Servo-I, Maquet, Rastatt, Germany).

Parameter	Uninjured	ARDS Model
	Mean (SD)	Mean (SD)
Weight (kg)	31 (2)	30 (2)
HR	97 (24)	91 (16)
SBP (mmHg)	111 (7)	100 (10)
DBP (mmHg)	71 (8)	59 (12)
CO (l min^{-1})	3.9 (1.2)	3.4 (0.6)
PASP (mmHg)	32 (5)	35 (5)
PADP (mmHg)	13 (6)	18 (6)
Hb (g dl^{-1})	8.4 (0.8)	8.4 (0.7)
F_IO_2	0.4 (0.1)	0.8 (0.1)
S_PO_2	99 (1)	95 (7)
pH	7.42 (0.03)	7.28 (0.09)
P_aO_2 (kPa)	19.9 (3.2)	16.4 (7.5)
P_aCO_2 (kPa)	6.1 (0.8)	8.5 (2.1)
PFR*	425 (100)	160 (84)
n	6	13

Table 4.1: Summary baseline characteristics pre- and post- lung injury. ** = signifies a $p < 0.05$ when comparing uninjured and ARDS model characteristics using a Kruskal-Wallis test with Dunn's correction for multiple comparisons. HR = heart rate, SBP = systolic arterial blood pressure, DBP = diastolic arterial blood pressure, CO = cardiac output, PASP = pulmonary artery systolic pressure, PADP = pulmonary artery diastolic pressure, Hb = haemoglobin concentration, F_IO_2 = fraction of inspired O_2, S_aO_2 = arterial oxyhaemoglobin saturation, P_aO_2 = arterial O_2 partial pressure, P_aCO_2 = arterial CO_2 partial pressure, PFR = P_aO_2:F_IO_2 ratio*

4.2.4 Lung injury

A collapse-prone model of ARDS was induced with a technique modified from Lachmann et al. (1980) in the animals listed in Table 4.3. Pre-oxygenation with an F_IO_2 = 1.0 preceded ventilator disconnection and lavage of the lungs by instillation of 0.9% saline solution (at 37^{o}C) via the endotracheal tube. After 30 s, the saline was drained out of the lungs by gravity and ventilation was recommenced. This process was repeated until a P_aO_2:F_IO_2 ratio (PFR) of < 300 was achieved.

Parameter	Animal Number						Mean	SD
	1	2	19	20	22	24		
Weight (kg)	31	29	30	33	30	33	31	2
HR	101	78	83	94	83	143	97	24
SBP (mmHg)	103	106	116	121	111	106	111	7
DBP (mmHg)	72	57	77	76	76	66	71	8
CO (l min^{-1})	3.2	3.1	3.9	4.1	2.8	6.1	3.9	1.2
PASP (mmHg)	27	32	30	40	29	35	32	5
PADP (mmHg)	15	16	15	19	5	6	13	6
Hb (g dl^{-1})	8.8	8.6	9.0	7.0	7.9	9.3	8.4	0.8
F_IO_2	0.3	0.3	0.4	0.4	0.4	0.4	0.4	0.1
S_PO_2	100	100	98	98	100	97	99	1
pH	7.44	7.45	7.38	7.43	7.40	7.43	7.42	0.03
P_aO_2 (kPa)	18.8	19.8	19.0	23.1	23.7	14.8	19.9	3.2
P_aCO_2 (kPa)	6.4	5.4	6.6	5.9	5.2	7.3	6.1	0.8
PFR	470	571	356	433	444	278	425	100

Table 4.2: Baseline characteristics of n = 6 uninjured animals. *HR = heart rate, SBP = systolic arterial blood pressure, DBP = diastolic arterial blood pressure, CO = cardiac output, PASP = pulmonary artery systolic pressure, PADP = pulmonary artery diastolic pressure, Hb = haemoglobin concentration, F_IO_2 = fraction of inspired O_2, S_PO_2 = peripheral oxyhaemoglobin saturation, P_aO_2 = arterial O_2 partial pressure, P_aCO_2 = arterial CO_2 partial pressure, PFR = P_aO_2:F_IO_2 ratio*

Parameter	Animal Number													Mean	SD
	3	5	6	7	8	9	11	12	13	15	18	23	25		
Weight (kg)	31	30	31	27	32	31	30	27	27	27	29	33	31	30	2
HR	76	87	115	77	80	67	88	95	85	80	116	113	101	91	16
SBP (mmHg)	106	104	83	102	96	99	101	91	102	85	120	114	99	100	10
DBP (mmHg)	66	58	43	56	50	54	59	50	67	45	78	81	62	59	12
CO (l min^{-1})	3.7	3.7	3.8	2.6	3.3	3.0	3.1	2.7	2.7	3.4	3.7	4.7	4.5	3.4	0.7
PASP (mmHg)	30	34	34	35	32	34	32	29	42	34	35	34	48	35	5
PADP (mmHg)	19	17	18	14	16	17	19	10	13	22	19	21	35	19	6
Hb (g dl^{-1})	9.1	8.0	8.3	8.2	8.8	9.7	8.5	7.8	7.5	7.3	9.4	8.3	7.8	8.4	0.7
F_IO_2	1.0	0.7	1.0	0.8	0.7	0.7	0.7	0.9	0.9	0.9	0.7	0.7	0.7	0.8	0.1
S_PO_2	100	100	95	99	99	100	93	74	94	91.1	96	100	94	95	7
pH	7.33	7.32	7.23	7.41	7.2	7.3	7.14	7.18	7.26	7.23	7.42	7.31	7.35	7.28	0.09
P_aO_2 (kPa)	19.9	21.7	9.8	29.2	10.0	26.0	11.8	12.3	11.3	11.4	10.6	28.2	10.3	16.4	7.5
P_aCO_2 (kPa)	7.2	7.8	8.9	5.9	10.5	8.7	13.7	7.1	8.4	9.3	6.2	7.2	9.7	8.5	2.1
PFR	149	233	73	292	107	279	126	103	94	101	114	302	114	160	84

Table 4.3: Baseline characteristics of n = 13 ARDS model animals. *HR = heart rate, SBP = systolic arterial blood pressure, DBP = diastolic arterial blood pressure, CO = cardiac output, PASP = pulmonary artery systolic pressure, PADP = pulmonary artery diastolic pressure, Hb = haemoglobin concentration, F_IO_2 = fraction of inspired O_2, S_PO_2 = peripheral oxyhaemoglobin saturation, P_aO_2 = arterial O_2 partial pressure, P_aCO_2 = arterial CO_2 partial pressure, PFR = P_aO_2:F_IO_2 ratio*

4.2.5 CT image acquisition, analysis and calculation of $\mathbf{ELV}_{O_2}$

CT scans were conducted during imposed breath-holds by closing both the expiratory and inspiratory airway valves at end-expiration or end-inspiration. A Somatom Definition Flash or Somatom Definition Edge (Siemens, Munich, Germany) were used to acquire whole-lung scans using a tube voltage of 80 kV, 364 mA current, and 64 x 60 mm collimation. Images were collected as series of transverse sections and reconstituted with a voxel size of 0.5 x 0.5 x 5 mm. CT images were segmented using 3D Slicer (Fedorov et al. 2012) with exclusion of the mediastinum, diaphragm, inferior vena cava, and hilar vessels. ELV_{CT} was calculated as the aerated mass of the whole lung according to equation 4.7:

$$ELV_{CT} = \frac{-\text{mean voxel density (HU)}}{1000} \times \text{segmented volume} \tag{4.7}$$

4.2.6 Continuous measurement of $\mathbf{P_aO_2}$ and calculation of $\mathbf{ELV}_{O_2}$

The P_aO_2 was measured continuously throughout each breath-hold manoeuvre using intra-arterial fibre optic oxygen sensors with a response time of < 0.1 s, such as the type described in Section 2.4 (Chen et al. 2013; Formenti et al. 2014; Formenti et al. 2017a; Crockett et al. 2019). The last 5 s of each breath-hold manoeuvre's trace was analysed to calculate to rate of decline in P_aO_2. This period was chosen because it was assumed that at the end of the breath-hold, gas pressures between inhomogeneous regions would have equilibrated and there would be no further movement of gas within the lung at this time. Paired measurements of P_aO_2 and $P_{\bar{V}}O_2$ and the mean of three consecutive thermodilution cardiac output measurements were used to calculate $\dot{V}_{O_2}$. ELV_{O_2} was subsequently calculated using a modification of equation 4.6 (Formenti et al. 2017a):

$$ELV_{O_2} = \dot{V}_{O_2} / \frac{dP_aO_2}{dt} \tag{4.8}$$

4.2.7 Statistical Analyses

Data were tested for normality using D'Agostino-Pearson's test and Shapiro-Wilk's tests. Baseline characteristics were compared with a repeated measures Kruskal-Wallis test with Dunn's correction for multiple comparisons. Change in ELV between PEEP levels (ΔELV) was calculated by subtracting one absolute ELV from its value at the preceding PEEP level. The linear relationship between measurements was tested using linear mixed effects modelling with variation caused by different animals considered a random effect. Conditional r^2 values based on the entire model are reported (Nakagawa et al. 2013).

4.2.7.1 Measuring agreement between ELV_{O_2} and ELV_{CT}

Agreement in measurements between techniques was assessed with Bland-Altman analysis corrected for multiple comparisons using a single factor analysis of variance (ANOVA) with individual animal as the factor (where appropriate) (Bland et al. 1986; Bland et al. 1999; Bland et al. 2007). Normally distributed differences are presented as the mean bias ± 95% limits of agreement calculated as 1.96 SD. Non-normally distributed differences that could not be meaningfully transformed to conform to the assumption of normality are presented as the median bias ± 95% limits of agreement. These were calculated as the range between the 2.5 - 97.5^{th} quantiles.

4.2.7.2 Comparing changes in lung volume using ELV_{O_2} and ELV_{CT}

Measured changes in lung volume (ΔELV) were compared using four quadrant plots with direction of change concordance analysis and polar plots (Critchley et al. 2010; Critchley et al. 2011). Radial measurements lying close to the centre of the plot (< 100 ml ΔELV) were excluded from analysis.

Analyses were carried out using R v3.5.1 (R Development Core Team 2017), Graphpad Prism v8.1.2 (GraphPad Software, USA, www.graphpad.com) and SigmaPlot (Systat Software, CA).

4.3 Results

A total number of $n = 146$ paired ELV measurements in 19 different animals were analysed. Figure 4.1 shows the changes in ELV_{O_2} and ELV_{CT} by PEEP as measured during breath-hold manoeuvres, in both the uninjured and ARDS models. There were $n = 62$ paired ΔELV measurments. Table 4.4 shows descriptive statistics for absolute ELV and ΔELV measurements and statistical analyses of difference at each PEEP level during breath-hold manoeuvres in the uninjured and ARDS models.

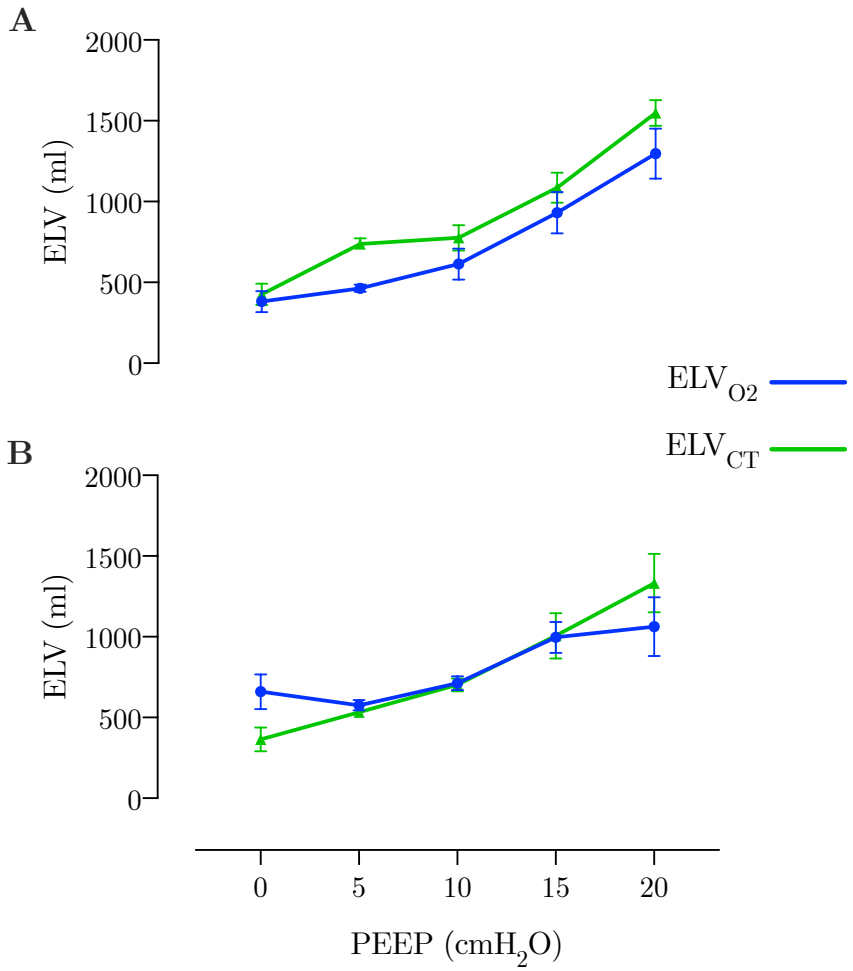


Figure 4.1: Mean absolute ELV measurements using ELV_{O_2} and ELV_{CT} at each PEEP level. *Mean ($\pm$SEM) absolute ELV measurements at each PEEP level. Panel **A)** shows results from the uninjured animal model. Panel **B)** shows results from the ARDS model. Table 4.4 provides full details of the measured volumes and statistical tests of difference.*

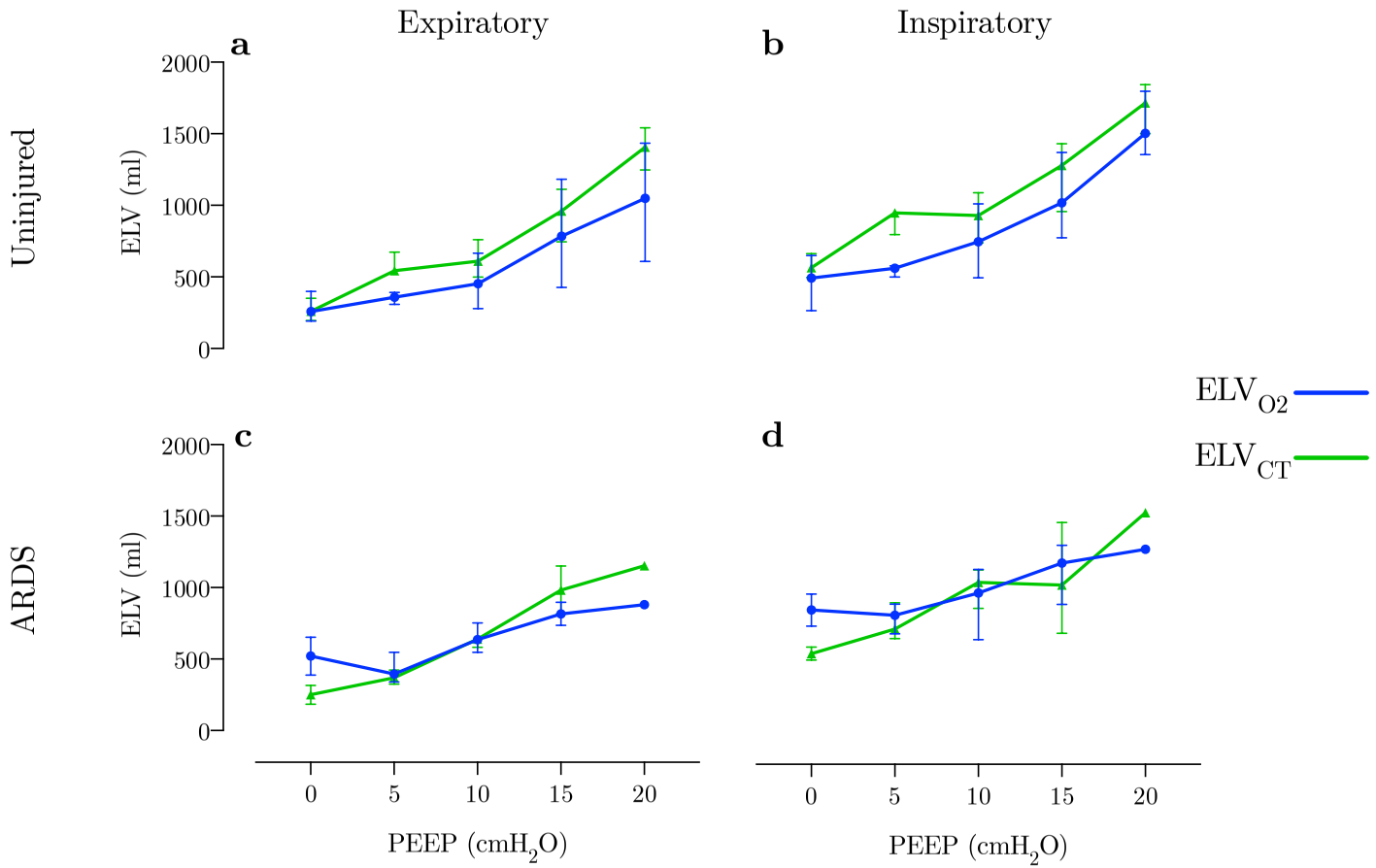


Figure 4.2: Median (± IQR) ELV measurements using ELV_{O_2}, and ELV_{CT} at each PEEP level. *Panels **a)** and **b)** present paired measurements from the uninjured model. Panels **c)** and **d)** present paired measurements from the ARDS model. Table 4.4 provides full details of volumes measured and probabilities of difference.*

PEEP (cmH_2O)	Uninjured				ARDS Model			
	n	ELV_{O_2}	ELV_{CT}	p	n	ELV_{O_2}	ELV_{CT}	p
0	8	382 (184)	427 (186)	0.99	4	660 (216)	365 (148)	0.21
5	35	464 (130)	739 (203)	< 0.0001	44	576 (212)	534 (187)	0.88
10	8	613 (273)	776 (221)	0.57	23	712 (203)	702 (193)	0.99
15	8	931 (360)	1086 (261)	0.62	6	996 (234)	1006 (344)	0.99
20	8	1297 (438)	1548 (225)	0.14	2	1062 (258)	1333 (255)	0.66

PEEP Change (cmH_2O)	Uninjured				ARDS Model			
	n	ΔELV_{O_2}	ΔELV_{CT}	p	n	ΔELV_{O_2}	ΔELV_{CT}	p
$0 \rightarrow 5$	8	90 (47)	136 (26)	0.90	4	140 (33 - 176)	143 (130 - 280)	0.99
$5 \rightarrow 10$	8	142 (79)	214 (50)	0.64	20	136 (78 - 157)	243 (194 - 283)	0.0005
$10 \rightarrow 15$	8	318 (149)	310 (70)	0.99	4	222 (78 - 312)	365 (289 - 482)	0.36
$15 \rightarrow 20$	8	435 (242)	506 (121)	0.66	2	85 (25 - 144)	344 (337 - 351)	0.04

Table 4.4: Descriptive statistics for comparisons of absolute lung volume (ELV) and changes in lung volume (ΔELV) measured in both the uninjured lung and the ARDS model at each PEEP level. *Mean (SD) or median (IQR) volumes are shown in ml. PEEP = Positive end-expiratory pressure, n = number of observations, ELV_{O_2} = PaO_2 measured absolute volume, ELV_{CT} = CT measured absolute volume, ΔELV_{O_2} = P_aO_2 measured change in lung volume, ΔELV_{CT} = CT measured change in lung volume, p = probability from either one-way ANOVA with Sidak's correction for multiple comparisons or Kruskal-Wallis with Dunn's correction for multiple comparisons that mean or median measurements at each PEEP level are from different samples.*

PEEP (cmH_2O)	Uninjured								ARDS Model							
	Expiratory				Inspiratory				Expiratory				Inspiratory			
	n	ELV_{O_2}	ELV_{CT}	p	n	ELV_{O_2}	ELV_{CT}	p	n	ELV_{O_2}	ELV_{CT}	p	n	ELV_{O_2}	ELV_{CT}	p
0	4	269 (83)	283 (112)	>0.9	4	585 (87)	480 (201)	0.85	2	250 (185-315)	521 (388-653)	-	2	479 (431-527)	799 (681-917)	-
5	16	566 (125)	355 (77)	0.01	19	958 (806-969)	571 (510-587)	0.0003	25	370 (326-422)	396 (341-547)		19	709 (116)	736 (147)	>0.9
10	4	623 (136)	466 (208)	0.73	4	930 (182)	761 (270)	0.49	17	640 (583-659)	636 (546-753)		6	953 (191)	860 (264)	>0.9
15	4	939 (191)	797 (394)	0.81	4	1233 (254)	1064 (316)	0.49	2	983 (815-1150)	817 (736-897)		4	983 (629-1441)	1144 (840-1275)	>0.9
20	4	1398 (159)	1031 (449)	0.03	4	1698 (181)	1563 (238)	0.68	1	112	880	-	1	1513	1244	-

Table 4.5: Descriptive statistics for comparisons of absolute lung volume (ELV) and changes in lung volume (ΔELV) made in both the uninjured lung and the ARDS model at each PEEP level. *Mean (SD) volumes are shown in ml. PEEP = Positive end-expiratory pressure, n = number of observations, ELV_{O_2} = PaO_2 measured absolute volume, ELV_{CT} = CT measured absolute volume. ΔELV_{O_2} = PaO_2 measured change in lung volume, ΔELV_{CT} = CT measured change in lung volume, p = probability from either two-way ANOVA or Kruskall-Wallis that mean measurements at each PEEP level are from different samples.*

4.3.1 Repeatability of ELV_{O_2} measurements

A subset of the paired ELV measurements ($n = 84$ out of the total of $n = 146$) represented repeated measurements taken in the same subject at the same PEEP level. These were analysed to estimate the repeatability of the ELV_{O_2} technique. The coefficient of variation for ELV_{O_2} for each subject at each PEEP level was 5.4% in the uninjured lung and 10.5% in the ARDS model. The overall mean coefficient of variation was 9.5%.

4.3.2 Correlation between ELV_{O_2} and ELV_{CT}

The left column of Figure 4.3 (panels **A** and **C**) shows scatter plots and linear mixed effects regression for each comparison. There was a strong linear relationship between ELV_{O_2} and ELV_{CT} in the uninjured model ($r^2 = 0.93$), which was not as strongly reproduced in the ARDS model ($r^2 = 0.75$).

4.3.3 Agreement between ELV_{O_2} and ELV_{CT}

The right column of Figure 4.3 (panels **B** and **D**) shows Bland-Altman plots demonstrating the agreement between ELV_{O_2} and ELV_{CT} in the uninjured and ARDS models. Figure 4.3, panel **B** shows that in the uninjured model, ELV_{O_2} had a median bias of 232 ml less (- 25%) than the ELV_{CT} and limits of agreement ranging from -637 ml to + 71 ml. Figure 4.3, panel **D** demonstrates that in the ARDS model ELV_{O_2} had minimal bias (median bias = + 8 ml (+12%)) compared to ELV_{CT} with limits of agreement ranging from -269 ml to +487 ml.

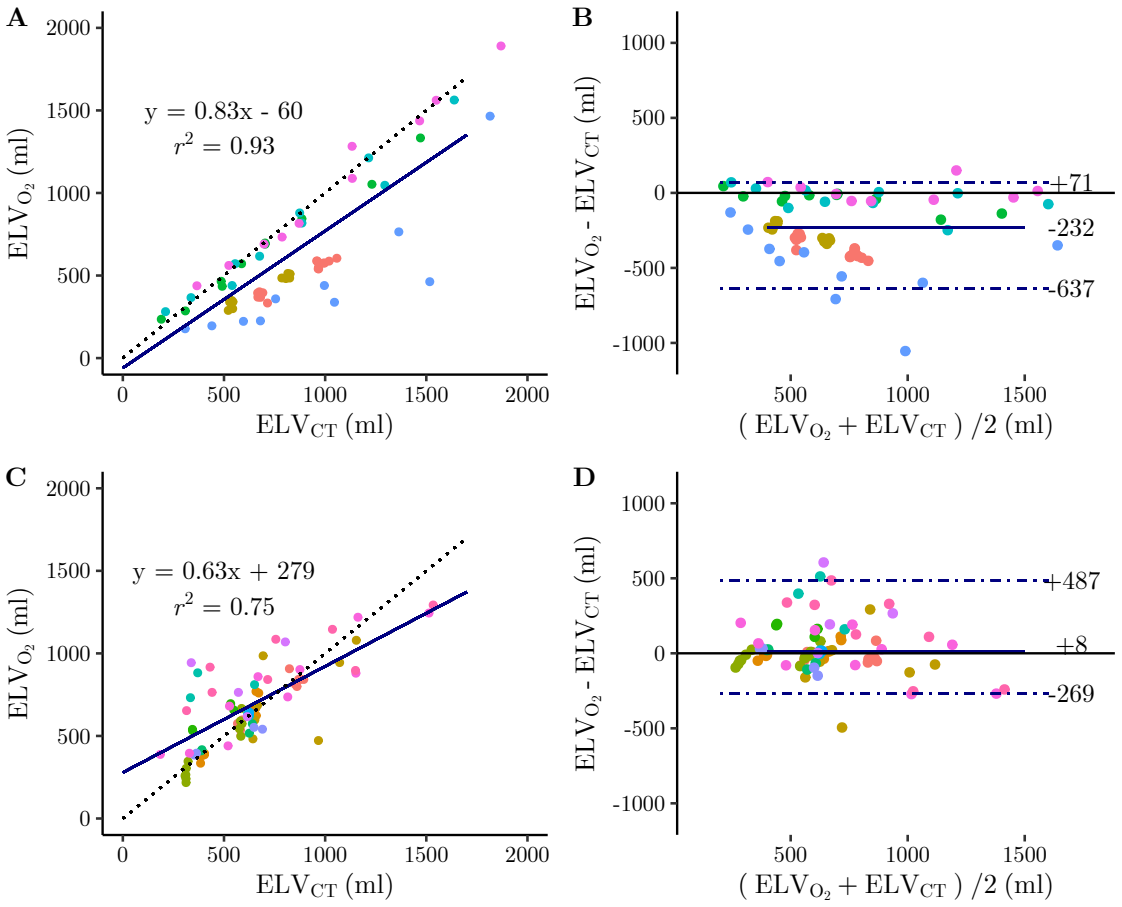


Figure 4.3: Linear regression and Bland-Altman plots for ELV_{O_2} vs ELV_{CT}. *Panels **A)** and **B)** present paired measurements of ELV_{O_2} and ELV_{CT} taken in the uninjured model. Panels **C)** and **D)** present measurements taken in the ARDS model. In the left column, panels **A)** and **C)** show scatter plots with solid lines and their equations representing mixed-effects linear modelling, taking the individual animal into account as a random effect. The dotted lines in the left column represent the line of identity. The right column (panels **B)** and **D)**) show Bland-Altman plots. For these data, the difference in measurements could not be meaningfully transformed to satisfy the assumption of normality, thus, the solid line represents the median bias and the dotted lines represent the limits of agreement (95% confidence interval around the median). Individual points represent a paired set of measurements and different colours represent different animals.*

4.3.4 Correlation between ΔELV_{O_2} and ΔELV_{CT}

Figure 4.4 panels **A** and **C** show four quadrant plots demonstrating the concordance of the relationship of ΔELV_{O_2} with ΔELV_{CT}. The linear relationship between ΔELV_{O_2} vs ΔELV_{CT} in the uninjured lung yielded an $r^2 = 0.62$, and $r^2 = 0.00$ in the ARDS model.

4.3.5 Agreement between ΔELV_{O_2} and ΔELV_{CT}

Direction of change concordance analysis showed that ΔELV_{O_2} had a concordance rate of 100% in the uninjured model and 93% in the ARDS model (97% overall) with ΔELV_{CT}. This is reflected in Figure 4.4, panels **A** and **C** where 97% of the data are in the top right quadrant of each four quadrant plot. Figure 4.4 panels **B** and **D** show Bland–Altman plots. In the uninjured lung model, ΔELV_{O_2} had a mean bias (± limits of agreement) of -45 ml (± 237 ml) compared to ΔELV_{CT}. In the ARDS model, ΔELV_{O_2} had a mean bias of -121 ml (± 198 ml) compared to ΔELV_{CT}. Figure 4.5 shows polar agreement in paired measurements of ΔELV. In the uninjured model, measurements of ΔELV_{O_2} had a mean angular bias of -8^o with $\pm\ 32^o$ radial limits of agreement and an angular concordance of 94% compared to ΔELV_{CT}. In the ARDS model, measurements of ΔELV_{O_2} had a mean angular bias of -12^o with radial limits of agreement of $\pm 41^o$ and an angular concordance rate of 75% compared to ΔELV_{CT}.

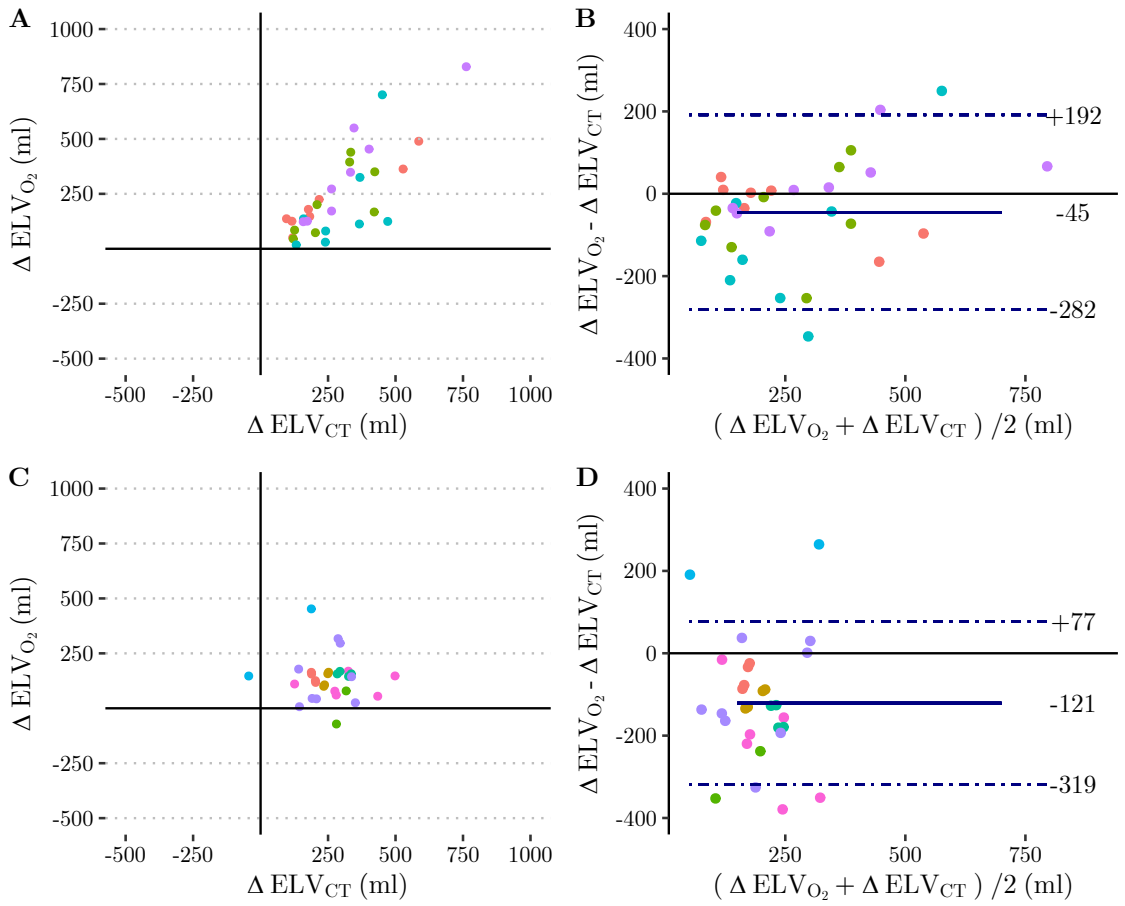


Figure 4.4: Four-quadrant and Bland-Altman plots for changes in volume (ΔELV$_{O_2}$ and ΔELV$_{CT}$.) *Panels **A** and **B** are measurements from the uninjured lung and panels **C**, and **D** represent experiments conducted the ARDS model. In the left column, four-quadrant plots show changes in volume. In the right column, solid lines in the Bland-Altman plots represent the mean bias and the dashed lines show the upper and lower limits of agreement (± 1.96 SD). Individual points represent a paired set of measurements and different colours represent different animals.*

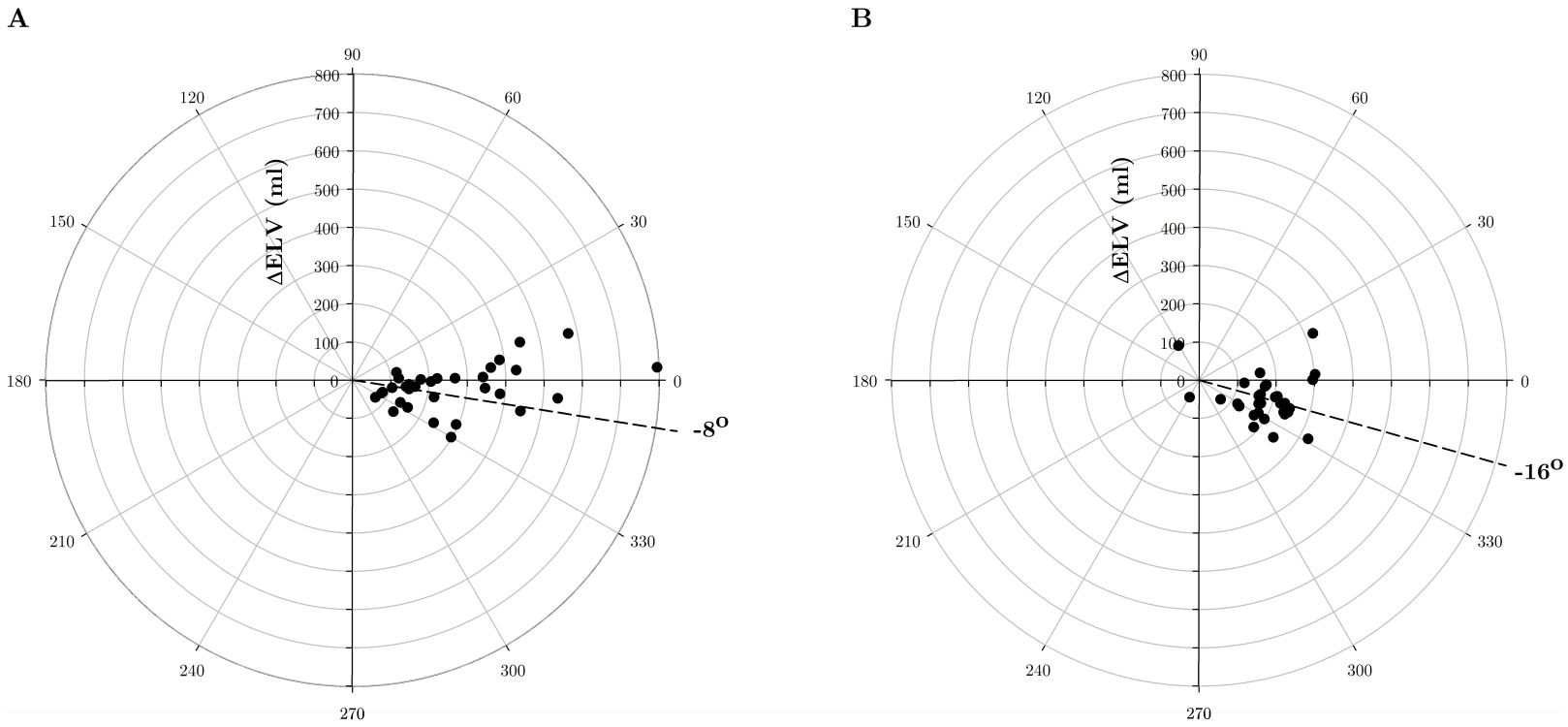


Figure 4.5: Polar plot analysis of measured changes in ELV (ΔELV). *The larger the mean ΔELV the greater the distance between the point and the centre of the plot. The better the agreement between a pair of measurements, the closer the point lies to the horizontal (0°). 95% radial limits of agreement describe the angle within which 95% of the data lie. Concordance rate (%) describes the number of points that lie within the assumed limits of adequate agreement, set at ± 30°.* ***A*** *Comparison of ΔELV_{O_2} vs ΔELV_{CT} in the uninjured lung. Mean angular bias = -8°, 95% radial limits of agreement = ± 32°, angular concordance rate = 94%.* ***B*** *Comparison of ΔELV_{O_2} vs ΔELV_{CT} in the ARDS model. Mean angular bias = -12°, 95% radial limits of agreement = ± 41°, angular concordance rate = 75%.*

4.4 Discussion

This chapter examines the ability of a previously undescribed method to estimate the volume of the lung taking part in gas exchange in a mechanically ventilated porcine model. Comparing ELV measurements estimated with P_aO_2 rate-of-decline and CT, it has been shown that there is a positive linear relationship in absolute measurements of ELV between techniques (ELV_{O_2} and ELV_{CT}) and that ELV_{O_2} underestimates lung volume compared to ELV_{CT} in the uninjured lung. In both the ARDS model and uninjured lungs, ΔELV_{O_2} can reliably track direction of change in volume with 93 - 100% concordance compared to ΔELV_{CT}. Additionally, in the uninjured lung, ΔELV_{O_2} shows good agreement with ΔELV_{CT}, having minimal bias (- 45 ml) and within limits of agreement of $\pm$ 237 ml.

There is no reference standard against which to compare this specific type of lung volume measurement. However, Robinson et al. (2013) sets out the international ERS/ATS consensus for the acceptable reliability of gas dilution techniques to measure lung volume. The bias of ELV_{O_2} was - 25% (- 232 ml) and + 12% (8 ml) in the uninjured and ARDS models respectively. These measurements are outside the $<$ 5% recommendation (Robinson et al. 2013). Measurements of absolute and changes in ELV_{O_2} tended to be less than those made with CT. This finding is consistent with tests of other bedside lung volume measurement techniques such as He dilution and the Inspired Sinewave Technique (Chiumello et al. 2008b; Albu et al. 2014; Bruce et al. 2018). One reason for ELV_{O_2}'s relatively lower measurements is that CT measures the entire thoracic gas volume, thus including areas of gas which may not be taking part in gas exchange. ELV_{O_2} relies on the diffusion of alveolar gas into the circulation and thus measures the volume of the alveolar compartment taking part in gas exchange and excludes areas of dead-space.

The repeatability of ELV_{O_2} in the same subject under the same conditions in the uninjured lung (5.4%) is within the reported international acceptable limits of coefficient of variation of $<$ 10%, but falls just outside these limits in the ARDS model (10.5%) (Wanger et al. 2005). Clinically, the ability of a monitor to detect a difference (or not) in a measured parameter after an imposed change is arguably more valuable than the absolute value itself. In this respect, ΔELV_{O_2} has good repeatability and minimal bias compared to ΔELV_{CT} (mean bias = - 45 ml) when

measuring changes in lung volume in the uninjured model. However, the bias in the ARDS model (- 421 ml) is outside the range where a change to care would be made based on a reported ΔELV_{O_2}.

Lung heterogeneity is another factor which likely contributes to the discrepancy in measurement between ELV_{O_2} and ELV_{CT}. The model used to calculate ELV_{O_2} is of a single alveolar compartment. It does not take into account deadspace nor the possibility of multiple alveolar compartments, each with a unique ventilation, perfusion and diffusion capacity. In the ARDS model, the bias of ELV_{O_2} was + 8 ml compared to - 232 ml in the uninjured lung. This might partially be explained by increased shunt fraction ($\dot{Q}_s/\dot{Q}_T$) in the ARDS model. Increased $\dot{Q}_s/\dot{Q}_T$ would cause relatively greater rate-of-decline in P_aO_2 and therefore dominance of the denominator in equation 4.8. Thus, the reduced ELV_{O_2} bias measured in the ARDS model may not reflect a better representation of physiology, but instead a minimisation of the expected underestimation compared to ELV_{CT}.

4.4.1 Limitations of the presented study

The data presented in this chapter constitute a secondary analysis of data collected by protocols designed with other questions in mind. This has lead to an imbalance in the number of measurements between the uninjured and ARDS model groups as well as in the number of measurements at different PEEP levels. Where no difference was detected between measurements of ELV_{O_2} and ELV_{CT} this could be attributed to the small number of repetitions and Type II error. Indeed, as shown in Table 4.4 when comparing measurements of absolute ELV in the uninjured lung, there were $n = 35$ paired measurements at PEEP 5 cmH_2O compared to $n = 8$ pairs at the other PEEP levels. PEEP 5 cmH_2O was the only PEEP level in the uninjured lung in which a "significant" difference in ELV_{O_2} and ELV_{CT} was found.

As discussed in Section 4.2.2, $n = 54$ paired measurements (23%) were excluded from analysis because either the mean P_aO_2 was less than 13.3 kPa or the signal:noise ratio was < 30 dB. This means that the analysed data were not affected by desaturation of Hb and were of good quality. However, an attrition rate of 23% would preclude bedside application of the technique in its current form. The attrition of data could potentiall be improved. The exclusion of data where the mean P_aO_2 is

$>$ 13.3 kPa is necessary because beneath this value desaturation of Hb occurs and changes in P_aO_2 are buffered by Hb binding. In the intensive care setting, patients usually have their F_IO_2 reduced to target a mean P_aO_2 of 10 kPa, a value where Hb desaturation may well occur. To ensure Hb saturation and allow ELV measurement, temporarily increasing the F_IO_2 may be possible. SNR may be improved by further technological development.

Another potential limitation in translation of the P_aO_2 rate-of-decline method for measuring lung volume is that it currently requires imposition of breath-hold manoeuvres. Whilst these are easily made in the paralysed mechanically ventilated patients, they are not so in sedated patients receiving assisted mechanical ventilation. This limitation could be overcome by temporarily increasing sedation to allow ELV measurement.

4.4.2 Further development of the ELV_{O_2} method

The results presented in this Chapter are supportive of further development of the P_aO_2 rate-of-decline method to measure ELV. This should begin with a study specifically designed to test the approach in a pre-clinical model. Development of a more complex ventilation model which could take into account multiple alveolar compartments and their $\dot{V}/\dot{Q}$ ratios might strengthen the ability of ELV_{O_2} to measure lung volume in clinical conditions.

The main strengths of the P_aO_2 rate-of-decline technique are that it would be easily applied at the bedside of the patient and does not require their cooperation. The P_aO_2 probe can be inserted into an existing arterial cannula and does not mandate a change to standard care of the mechanically ventilated patient.

4.4.3 Conclusions

The results in this chapter have demonstrated that as well as a tool to give real-time measurements of P_aO_2, intra-arterial probes can also be applied to estimate lung volume in a mechanically ventilated porcine model, both with uninjured lungs and

with an ARDS model. This is the first study of its kind and provides strong evidence to support undertaking of further research to test the hypothesis.

CHAPTER 5

Measuring lung volumes with the Inspired Sinewave Technique: Comparison with Computed Tomography and SF_6

Abstract

This chapter investigates the application of the inspired sinewave technique (IST) in mechanically ventilated lungs. Using a porcine model, lung volume was changed by altering the amount of positive end-expiratory pressure (PEEP) and IST's measurements of lung volume were compared against those made with the reference techniques of sulphur hexafluoride washin-washout (SF_6) and computed tomography (CT). Measurements were taken both in an uninjured model and in a saline-lavage model of the acute respiratory distress syndrome (ARDS). The presented results suggest that IST's measurements are repeatable, that it underestimates absolute lung volume and has minimal bias when tracking PEEP-induced changes in lung volume. .*

*The work presented in this chapter has been accepted for publication in the *British Journal of Anaesthesia* (Crockett et al. 2020)

5.1 Introduction

The full rationale for the importance of measuring lung volume in mechanically ventilated patients is discussed in Section 1.5. The acute respiratory distress syndrome (ARDS) affects c10% of critical care patients and has an associated in-hospital mortality of 46% (Bellani et al. 2016). Patients with ARDS have a smaller aerated lung volume ("baby lung") and one of the few interventions shown to reduce mortality in ARDS is ventilating patients with 6 – 8 ml kg^{-1} tidal volume (V_T) (Acute Respiratory Distress Syndrome Network et al. 2000; Gattinoni et al. 2005; Gattinoni et al. 2016a). More recently, driving pressure (ΔP) has been shown to be the ventilator parameter which best stratifies risk of mortality in ARDS (Amato et al. 2015). ΔP is dependent on V_T and respiratory system compliance (C_{RS}) ($\Delta P = V_T$ / C_{RS}). C_{RS} is dependent on the size of the "baby lung" and thus, so too is ΔP (Hubmayr et al. 2018). It is thought that reduced mortality from low V_T ventilation may be secondary to reducing the effect that driving pressure (ΔP) has on the ARDS "baby lung" (Gattinoni et al. 2016b).

There would, therefore, be potential benefit in measuring the effective lung volume (ELV) at the bedside of the mechanically ventilated ARDS patient. This would allow personalised titration of V_T to the underlying aerated lung volume, with limitation of lung stress caused by ΔP. Currently ELV can be measured clinically in ventilated patients either by imaging (computed tomography, CT), with washin-washout techniques or gas dilution techniques. CT imaging puts patients at risk by necessitating a transfer to the scanner and exposure to ionising radiation. Current bedside gas-based techniques have not proven reliable in assisted ventilation or require equipment that is too bulky or too time consuming for bedside clinical use (Larsson et al. 1987; Di Marco et al. 2007; Maisch et al. 2007; Patroniti et al. 2008; Heinze et al. 2009; Richard et al. 2014).

The inspired sinewave technique (IST) has the potential to provide bedside measurement of ELV. IST was initially developed by Zwart et al. (1978) and uses a low concentration of tracer gas ($<$ 5% nitrous oxide (N_2O)) injected into the inspired airway gases in a sinusoidally oscillating concentration (Zwart et al. 1976; Hahn et al. 1993).(Hahn 1996) Sinewave amplitude and phase of the concentration of tracer gas measured in the expiratory airway gases are used to recover values of

ELV (ELV_{IST}) and pulmonary blood flow ($\dot{Q}_{IST}$. IST uses commercially available components commonly used in anaesthetic/intensive care practice and has proven efficacy in spontaneously ventilating healthy volunteers (Phan et al. 2017a; Bruce et al. 2018). To date, IST's ability to measure ELV in mechanically ventilated lungs has not been tested.

The aim of the work presented in this chapter was to conduct a comparison of methods, measuring the relationship and limits of agreement between ELV measured by IST compared to SF_6 washin-washout and CT. To do this, absolute ELV and changes in ELV (ΔELV) at and between different positive end-expiratory pressures (PEEP) were compared in mechanically ventilated pigs both before and after induction of ARDS by saline-lavage (Gattinoni et al. 1986a; Gattinoni et al. 1987; Larsson et al. 1987).

5.2 Methods

5.2.1 Ethical approval

This study of thirteen domestic pigs (mean weight (SD) = 29 (2) kg) at the Hedenstierna laboratory, Uppsala University, Sweden was approved by the regional animal welfare and ethics committee (Ref: C98/16). Reporting in this paper adheres to Animal Research: Reporting of in vivo Experiments (ARRIVE) guidelines (Kilkenny et al. 2013).

5.2.2 Animal Preparation

Table 5.1 shows the summary comparison of baseline characteristics pre- and post-lung injury and Table 5.2 shows the individual animal characteristics. Animals were prepared and anaesthetised using total intravenous anaesthesia as described in the Methods chapter, section 2.3.3. During preparation, mechanical ventilation was delivered in volume-controlled ventilation (VCV) mode at 20 - 25 breaths per minute (to maintain end-tidal CO_2 (E_TCO_2) between 4.5 – 6 kPa), with a V_T of 10 ml kg^{-1}, PEEP of 5 cmH_2O and an inspiratory:expiratory ratio (I:E) of 1:2 (Servo-I, Maquet, Germany). Airway leaks were excluded by analysis of spirometry data. Depth of anaesthesia was confirmed by lack of spontaneous movements, absence of reaction to painful stimulation between the front hooves and absence of cardiovascular signs of sympathetic stimulation (increases in heart rate or arterial blood pressure). Subsequent muscle relaxation was achieved with a bolus of rocuronium 0.2 mg kg^{-1} followed by 0.1 mg kg^{-1} boluses when spontaneous ventilatory efforts were detected from the airway gas and pressure traces. Maintenance IV crystalloid fluids were administered (Ringerfundin; B. Braun Melsungen AG, Melsungen, Germany) at a rate of 10 ml kg^{-1} hr^{-1} during the preparation phase and 7 ml kg^{-1} hr^{-1} for the rest of the protocol. Once anaesthetised, the right internal jugular vein was cannulated with a pulmonary artery catheter used for continuous pulmonary artery pressure, intermittent thermodilution cardiac output and core temperature monitoring.

Parameter	Pre-injury	Post-injury	p
Weight (kg)	29 (2)	-	
HR	86 (70 - 100)	85 (80 - 95)	0.42
SBP (mmHg)	100 (8)	98 (14)	0.57
DBP (mmHg)	67 (12)	54 (8)	0.0006
CO (l min^{-1})	3.4 (0.8)	3.2 (0.4)	0.26
PASP (mmHg)	28 (25 - 33)	32 (29 - 36)	0.03
PADP (mmHg)	16 (4)	19 (5)	0.004
Hb (g dl^{-1})	85 (5)	84 (6)	0.93
F_IO_2	0.4 (0.3 - 0.4)	0.8 (0.7 - 0.9)	0.0002
S_aO_2 (%)	100 (99 - 100)	98 (91 - 99)	0.0001
pH	7.38 (0.07)	7.25 (0.08)	0.0004
P_aO_2 (kPa)	19.2 (15.9 - 21.5)	12.8 (11.3 - 26.0)	0.39
P_aCO_2 (kPa)	6.7 (1.1)	8.4 (2.0)	0.003
PFR	(304 - 513)	128 (101 - 248)	0.0002

Table 5.1: Comparison of baseline characteristics pre- and post- lung injury. *HR = heart rate, SBP = systolic arterial blood pressure, DBP = diastolic arterial blood pressure, CO = cardiac output, PASP = pulmonary artery systolic pressure, PADP = pulmonary artery diastolic pressure, Hb = haemoglobin, F_IO_2 = fraction of inspired O_2, S_aO_2 = arterial oxyhaemoglobin saturation, P_aO_2 = arterial O_2 partial pressure, P_aCO_2 = arterial CO_2 partial pressure, PFR = P_aO_2:F_IO_2 ratio*

Timing	Parameter	Animal Number												
		1	2	3	4	5	6	7	8	9	10	11	12	13
Pre-injury	Weight (kg)	31	32	30	27	27	27	27	31	32	28	28	31	31.6
	HR	68	74	76	70	90	80	63	95	103	86	106	100	99
	SBP (mmHg)	95	92	104	106	118	96	90	99	112	100	105	97	88
	DBP (mmHg)	47	49	60	70	80	78	60	80	72	70	70	81	57
	CO (l min^{-1})	3.8	3.3	3.0	2.2	2.8	3.4	3.3	3.3	5.2	3.0	4.5	3.5	3.3
	PASP (mmHg)	25	28	26	44	44	30	33	29	30	27	20	25	21
	PADP (mmHg)	10	10	15	11	15	20	23	16	18	17	10	13	12
	Hb (g dl^{-1})	87	80	81	83	80	86	70	83	83	88	86	87	88
	F_IO_2	0.4	0.4	0.4	0.3	0.3	0.3	0.4	0.4	0.4	0.4	0.4	0.4	0.3
	S_aO_2 (%)	99	100	100	100	98	100	100	100	99	98	100	100	99
	pH	7.33	7.33	7.29	7.28	7.42	7.53	7.42	7.37	7.43	7.33	7.42	7.39	7.42
	P_aO_2 (kPa)	14.2	17.8	24.0	21.5	20.5	21.0	23.5	15.9	19.2	17.2	20.1	16.2	14.9
	P_aCO_2 (kPa)	7.6	7.6	8.9	5.6	5.6	5.2	6.5	7.3	6.2	8.0	6.2	6.6	5.4
	PFR	304	381	450	538	513	525	441	298	360	323	377	301	373
Post-injury	HR	79	70	88	95	85	81	80	134	80	87	81	95	120
	SBP (mmHg)	95	99	101	91	102	115	85	136	85	95	94	89	80
	DBP (mmHg)	50	52	59	50	67	49	45	64	50	66	46	60	40
	CO (l min^{-1})	3.2	3.0	3.1	2.7	2.7	3.1	3.4	4.0	3.2	3.2	2.9	3.7	3.1
	PASP (mmHg)	32	36	32	29	42	34	34	39	32	30	28	30	25
	PADP (mmHg)	16	17	19	10	13	20	22	24	23	24	17	17	14
	Hb (g dl^{-1})	79	87	85	78	75	77	73	90	77	88	75	89	112
	F_IO_2	0.7	0.7	0.7	0.9	0.9	0.75	0.85	0.8	0.8	0.75	0.75	0.8	0.8
	S_aO_2 (%)	99	100	93.2	74	94.4	83.7	91.1	98.1	98.3	97	99.9	98.3	98.2
	pH	7.2	7.3	7.14	7.18	7.26	7.15	7.23	7.24	7.35	7.36	7.34	7.29	7.18
	P_aO_2 (kPa)	10.0	26.0	11.8	12.3	11.3	12.8	11.4	28.6	26.4	15.6	23.9	10.3	20.6
	P_aCO_2 (kPa)	10.5	8.7	13.7	7.1	8.4	8.9	9.27	8.01	7.12	6.3	6.7	7.06	7.86
	PFR	107	279	126	103	94	128	101	268	248	156	239	97	193

Table 5.2: Baseline characteristics for each individual animal pre- and post- lung injury. *HR = heart rate, ABP = arterial blood pressure, CO = cardiac output, PAP = pulmonary artery pressure, Hb = haemoglobin, F_IO_2 = fraction of inspired O_2, S_aO_2 = arterial oxyhaemoglobin saturation, P_aO_2 = arterial O_2 partial pressure, P_aCO_2 = arterial CO_2 partial pressure, PFR = P_aO_2:F_IO_2 ratio*

5.2.3 Data Collection and processing

Cardio-respiratory variables including peripheral oxyhaemoglobin saturation (SpO_2), electrocardiography (ECG), invasive arterial blood pressure (BP) (AS/3 Multi-Parameter Patient Monitor, Datex-Ohmeda, USA), airway gas composition, flow and pressure (Capnomac Ultima, Datex-Ohmeda, USA) were continuously monitored and acquired as analogue signals throughout the protocol. Analogue data were converted using PowerLab (ADInstruments, New Zealand) and displayed/recorded with LabChart version 8.1.5 (ADInstruments). Physiological data were processed using R v3.5.1 (R Development Core Team 2017).

5.2.4 The Inspired Sinewave Technique (IST)

A mainstream infrared N_2O and CO_2 sensor (IRMA, Sweden) and an ultrasonic flowmeter (VenThor – 22/2A, Hungary) were placed in the breathing circuit between a patient-end heat-moisture exchange filter (HME) (Intersurgical, UK) and the ventilator tubing as described in Section 2.6. At the start of each inspiration, a set volume of N_2O was injected into the inspired gas by a mass flow controller (Alicat Scientific, USA). The volume of N_2O injected was proportional to the inspiratory flow and oscillated sinusoidally over consecutive breaths around a set mean concentration of 5%, with an amplitude of 4% and a period of 180 s for a duration of 270 s. The test duration of 270 s was the maximum duration which would allow repetition of each test within the permitted time frame of the protocol.

5.2.5 SF_6 Washin-Washout

The use of SF_6 as a tracer gas for washin-washout measurement of lung volume is described by Larsson et al. (1987) and described in Section 2.7. The apparatus was attached between the endotracheal tube and the D-Lite spirometer attachment.

5.2.6 CT Image Acquisition and Analysis

A Somatom Definition Flash (Siemens, Munich, Germany) was used to acquire images as series of transverse sections with a reconstituted voxel size of 0.5 x 0.5 x 5 mm. Whole-lung volume scans were conducted during a 20 s end-expiratory pause without ventilator disconnection. Scans were taken using a tube voltage of 80 kV, 364 mA current, and 64 x 60 mm collimation. Reconstituted whole lung scans were segmented using 3D Slicer v4.10.2 (Fedorov et al. 2012). The mediastinum, diaphragm, inferior vena cava, and hilar vessels were not included in segmentation. Exclusion of intrapulmonary vessels within regions of increased voxel density was not possible as they were not distinguishable from lung tissue, and these, along with the conducting airways up to the level of the clavicles, were included in the analysis. The aerated volume of each whole lung scan was calculated from the Hounsfield unit (HU) density of each voxel according to eqation 5.1 (Chiumello et al. 2008b):

$$Aerated\ volume = \frac{-\ mean\ CT\ density\ (HU)}{1000} \times segmented\ volume \tag{5.1}$$

5.2.7 Lung Injury

Lung injury was induced with a technique modified from Lachmann et al. (1980). Following pre-oxygenation, the ventilator was disconnected and the lungs lavaged by instillation of 0.9% saline solution (at 37 ^{o}C) via the endotracheal tube. After 30 s the saline was drained out of the lungs and ventilation recommenced. This process was repeated until a P_aO_2:F_IO_2 ratio (PFR) of less than 40 kPa was achieved.

5.2.8 Study Protocol

Throughout all phases of the protocol animals were positioned in dorsal recumbency, F_IO_2 was titrated to $P_aO_2 > 10$ kPa and animals were mechanically ventilated with VCV, V_T 10 ml kg^{-1} and I:E 1:2. Respiratory rate was adjusted to 15 – 20 breaths per minute to maintain $E_TCO_2 < 8$ kPa. In all cases, measurements were taken after 2 mins of ventilation at the studied PEEP level and the ETT was clamped during airway disconnection (for example to change equipment for measuring ELV_{IST} to

ELV_{SF6}). Figure 5.1 shows a summary timeline of an individual experiment. An example of a full experimental protocol can be found in Appendix B.

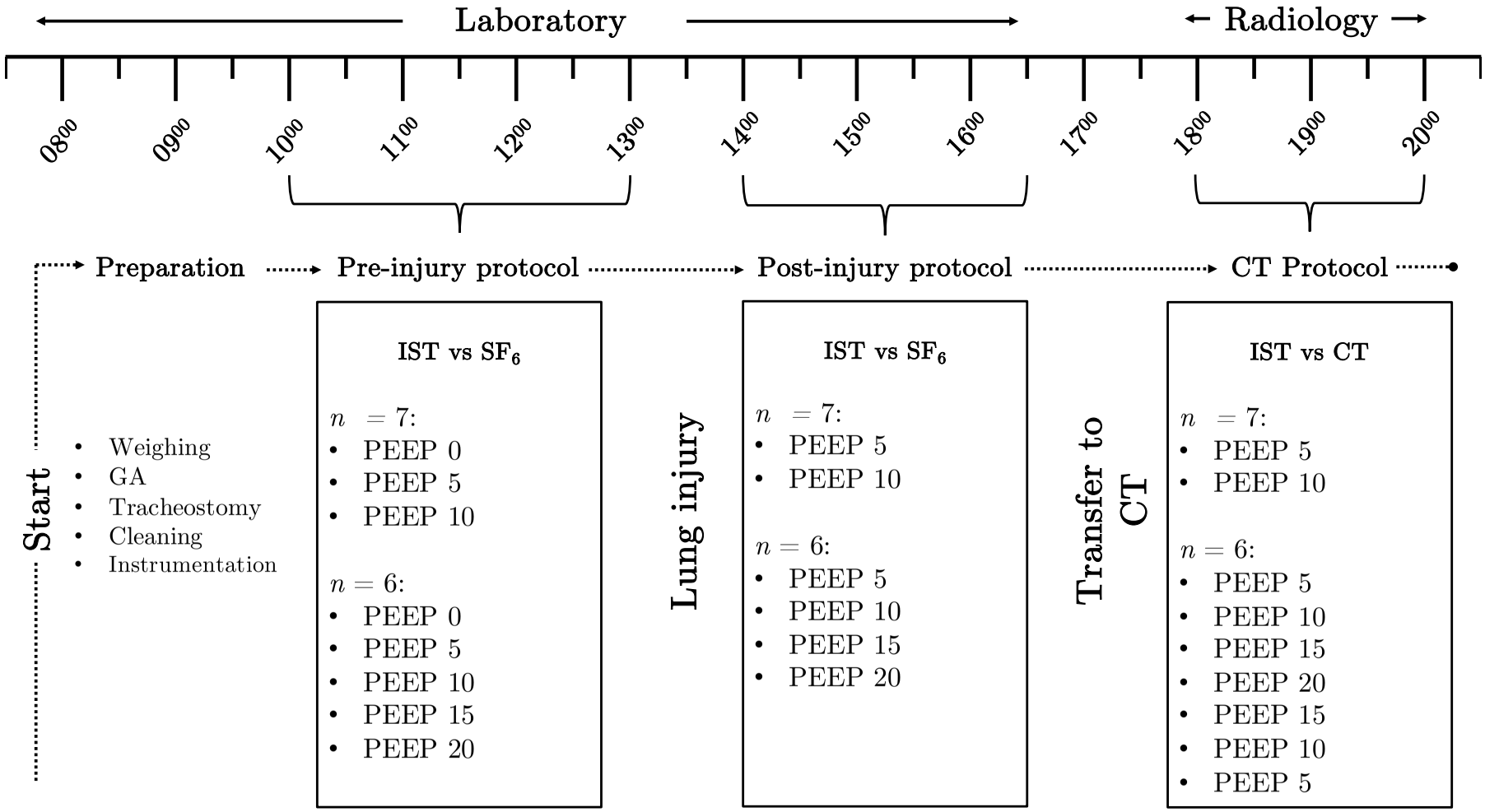


Figure 5.1: Timeline of experimental protocol: validation of IST to measure lung volume. *Paired measurements of ELV were taken with IST and either SF_6 or CT.* ***Pre-Injury and post-injury comparison with SF6:*** *All measurements were taken using incremental steps in PEEP as shown.* ***Post-injury comparison with CT:*** *In n = 7 animals comparisons were made at two different lung volumes (PEEP 5 and PEEP 10), in n = 6 animals PEEP was incremented up to 20 cmH_2O and then decremented back down to 5 cmH_2O. GA = induction of general anaesthesia.*

5.2.8.1 Pre- and post-injury ELV_{IST} vs ELV_{SF6}

Measurements of ELV were taken with IST (ELV_{IST}) and SF_6 washin-washout (ELV_{SF6}). Two sets of paired measurements were taken at each PEEP level studied. Measurements were taken first with IST and then with SF_6. After completion of experiments in the uninjured model, lung injury was induced as described in section 5.2.7 (above) and a further two paired measurements of ELV_{IST} and ELV_{SF6} repeated at each PEEP level. In all 13 animals the studied PEEP levels were 0, 5, and 10 cmH_2O. In 6 of these animals, PEEP levels of 15 and 20 cmH_2O were additionally included. In all comparisons of ELV_{IST} and ELV_{SF6} PEEP was incrementally increased from low to high. The protocol comparing ELV_{IST} and ELV_{SF6} was the same pre- and post- saline lavage except that 0 cmH_2O PEEP was not studied post-injury because of the risk that this would not be tolerated.

5.2.8.2 Post-injury ELV_{IST} vs ELV_{CT}

Upon completion of the ELV_{IST} vs ELV_{SF6} comparisons, animals were transferred to the CT scanner. Two paired measurements of ELV_{IST} and ELV estimated from CT (ELV_{CT}) were made at each PEEP level. In all 13 animals PEEP levels studied were 5 and 10 cmH_2O. In 6 of these animals PEEP was titrated from 5 cmH_2O up to 20 cmH_2O and then back down again. For the reason stated above, zero PEEP was not studied post-injury. Upon completion of the study protocol anaesthetised animals were humanely euthanised with potassium chloride.

5.2.9 Statistical Analyses

Paired measurements of ELV_{IST}, ELV_{SF6} and ELV_{CT} at each PEEP level were tested for normality using D'Agostino-Pearson's test and QQ plots. Datasets were compared with a repeated measures two-way ANOVA, with Sidak's multiple comparison test. ΔELV was calculated by subtracting one absolute ELV from its value at the preceding PEEP level. The linear relationship between measurements was tested using linear mixed effects modelling with variation caused by different animals considered a random effect. Conditional r^2 values based on the entire model

are reported (Nakagawa et al. 2013). Analyses were carried out using R v3.5.1 (R Development Core Team 2017), Graphpad Prism v8.1.2 (GraphPad Software, USA, www.graphpad.com) and SigmaPlot (Systat Software, CA).

5.2.9.1 Measuring agreement between $\mathbf{ELV}_{IST}$, $\mathbf{ELV}_{CT}$ and $\mathbf{ELV}_{SF_6}$.

Agreement in measurements between techniques was assessed with Bland-Altman analysis corrected for multiple comparisons using a single factor analysis of variance (ANOVA) with individual animal as the factor (Bland et al. 1986; Bland et al. 1999; Bland et al. 2007). Non-normally distributed data were transformed (by using a ratio of measurements) to conform to the assumption of normality and 95% limits of agreement were calculated as ± 1.96 SD from the mean bias.

5.2.9.2 Comparing ability to measure trends using $\mathbf{ELV}_{IST}$, $\mathbf{ELV}_{CT}$ and $\mathbf{ELV}_{SF_6}$.

Measured changes in lung volume were compared using four quadrant plots with direction of change concordance analysis and polar plots (Critchley et al. 2010).

5.3 Results

A total of n = 271[†] paired ELV measurements in 13 animals at five different PEEP levels were analysed. Figure 5.2 demonstrates that the protocolised changes in PEEP induced changes in ELV and that these changes were tracked by IST, SF_6 and CT. Figure 5.2 and Table 5.3 show the comparisons of paired ELV and ΔELV measurements at each PEEP level. Statistical analyses suggested that ELV_{IST} at 0, 5 and 10 cmH_2O PEEP was not significantly different from ELV_{SF6} or ELV_{CT} in both the uninjured lung and ARDS model. At 15 and 20 cmH_2O PEEP, measured ELV_{IST} was significantly lower than ELV_{SF6} and ELV_{CT} in all comparisons (p-values are reported in Table 5.3).

[†]n = 271 out of a total possible number of 283. The 4% of measurements excluded were because of lack of paired measurement with the other technique.

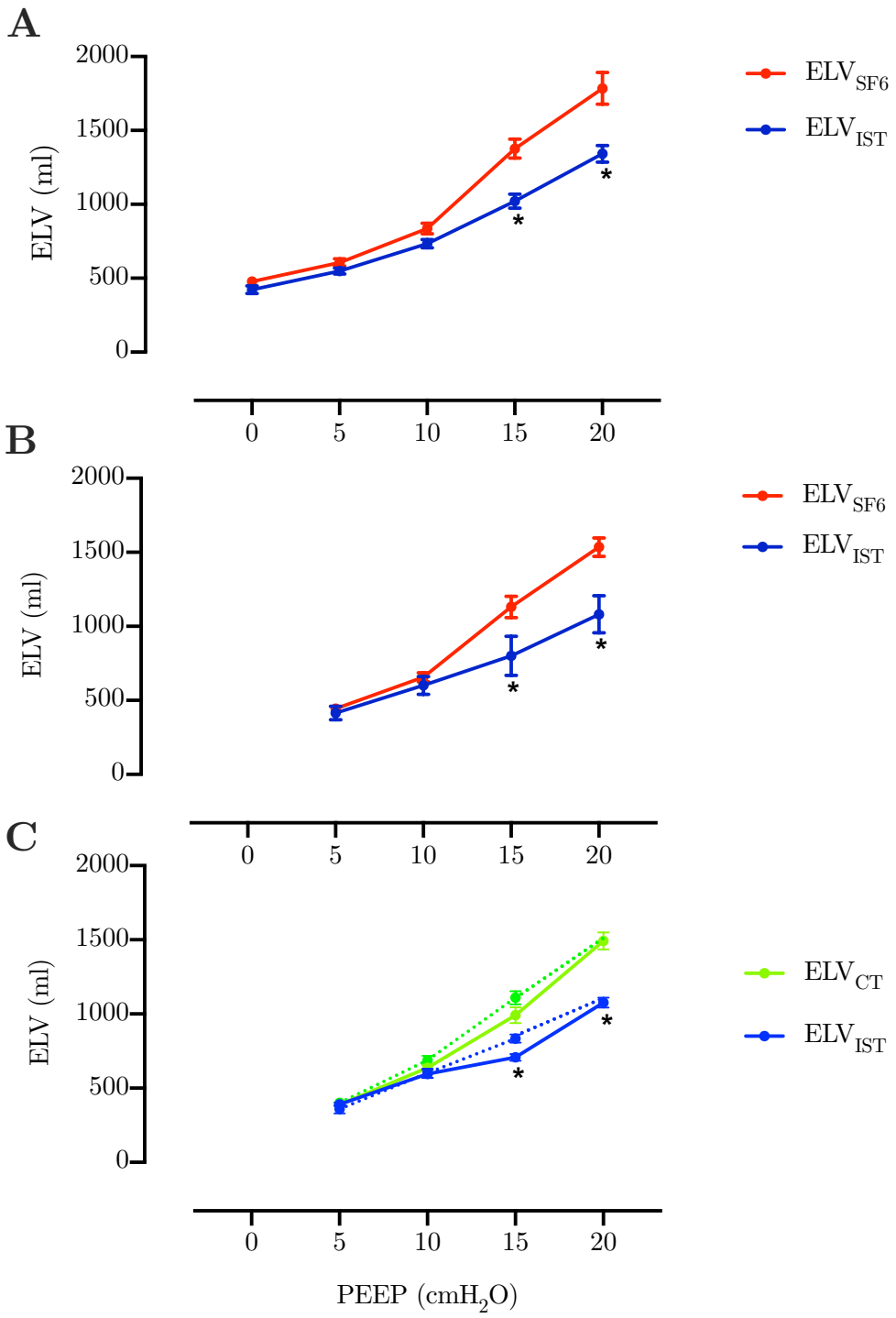


Figure 5.2: Mean ELV measurement (± SE) using ELV_{IST}, ELV_{SF6} and ELV_{CT} at each PEEP level. ***(A)*** *Paired ELV_{IST} and ELV_{SF6} measurements in the uninjured lung.* ***(B)*** *Paired ELV_{IST} and ELV_{SF6} measurements in the ARDS model.* ***(C)*** *Paired ELV_{IST} and ELV_{CT} measurements in the ARDS model. PEEP = 0 cmH_2O was not studied post-injury, PEEP levels of 15 and 20 cmH_2O were studied in 6 of the total n = 13 animals. Solid lines represent volumes measured during incremental PEEP titration, dashed lines represent volumes measured during decremental PEEP titration. * = the probability of ELV_{IST} being the same as ELV_{SF6} or ELV_{CT} was < 0.05. Table 5.3 provides full details of volumes measured and probabilities of difference.*

PEEP (cmH_2O)	Uninjured				ARDS Model							
	n	ELV_{IST}	ELV_{SF6}	p	n	ELV_{IST}	ELV_{SF6}	p	n	ELV_{IST}	ELV_{CT}	p
0	17	422 (106)	477 (66)	0.35	-	-	-	-	-	-	-	-
5	24	548 (99)	607 (119)	0.31	25	415 (108)	444 (113)	0.84	38	381 (76)	394 (49)	0.86
10	22	734 (132)	837 (169)	0.14	26	601 (149)	657 (157)	0.26	36	598 (124)	654 (99)	0.14
15	11	1022 (159)	1377 (213)	0.002	12	801 (207)	1132 (249)	0.01	24	771 (107)	1051 (177)	< 0.0001
20	12	1342 (194)	1785 (373)	0.01	12	1081 (197)	1535 (214)	< 0.0001	12	1077 (113)	1493 (199)	< 0.0001

a *Comparison of absolute measurements of volume in the uninjured and ARDS models. (ELV_{IST} vs ELV_{SF6}, ELV_{IST} vs ELV_{CT}.*

PEEP change (cmH_2O)	Uninjured				ARDS Model							
	n	ΔELV_{IST}	ΔELV_{SF6}	p	n	ΔELV_{IST}	ΔELV_{SF6}	p	n	ΔELV_{IST}	ΔELV_{CT}	p
$0 \rightarrow 5$	17	118 (60)	180 (57)	0.02	-	-	-	-	-	-	-	-
$5 \rightarrow 10$	24	190 (87)	240 (71)	0.13	26	191 (127)	216 (91)	0.81	24	209 (105)	245 (58)	0.60
$10 \rightarrow 15$	11	313 (90)	423 (111)	0.07	12	252 (73)	399 (91)	0.0008	12	196 (77)	371 (90)	0.0002
$15 \rightarrow 20$	12	312 (92)	412 (233)	0.56	12	281 (102)	403 (70)	0.008	12	370 (88)	500 (75)	0.005
$20 \rightarrow 15$	-	-	-	-	-	-	-	-	12	-243 (92)	-383 (100)	0.01
$15 \rightarrow 10$	-	-	-	-	-	-	-	-	12	-233 (69)	-422 (67)	< 0.0001
$10 \rightarrow 5$	-	-	-	-	-	-	-	-	12	-242 (51)	-287 (64)	0.37

b *Comparison of changes in volume measurement between PEEP levels in the uninjured and ARDS models. (ΔELV_{IST} vs ΔELV_{SF6}, ΔELV_{IST} vs ΔELV_{CT}*

Table 5.3: Descriptive statistics for comparisons of absolute lung volume (ELV) and changes in lung volume (ΔELV) made in both the uninjured lung and the ARDS model at each PEEP level. *Mean (SD) volumes are shown in ml. PEEP = Positive end-expiratory pressure, n = number of observations, ELV_{IST} = IST measured absolute volume, ELV_{SF6} = SF_6 measured absolute volume, ELV_{CT} = CT measured absolute volume. ΔELV_{IST} = IST measured change in lung volume, ΔELV_{SF6} = SF_6 measured change in lung volume, ΔELV_{CT} = CT measured change in lung volume, p = probability from either two-way ANOVA or Kruskall-Wallis that mean measurements at each PEEP level are from different samples.*

5.3.1 Repeatability of ELV_{IST} measurements.

The mean coefficient of variation for ELV_{IST} for each subject at each PEEP level was $< 5\%$ in both the uninjured lung and in the ARDS model. 90% of coefficients of variation for replicate measurements were $< 10\%$.

5.3.2 Correlation between ELV_{IST}, ELV_{SF6} and ELV_{CT}.

The left column of Figure 5.3 (panels **A**, **C** and **E**) shows scatterplots and linear mixed effects regression for each of the comparisons. There was a robust linear relationship between ELV_{IST} and ELV_{SF6} in both uninjured lungs ($r^2 = 0.97$) and in the ARDS model ($r^2 = 0.87$) which was also demonstrated between ELV_{IST} and ELV_{CT} in the ARDS model ($r^2 = 0.92$).

5.3.3 Agreement between ELV_{IST}, ELV_{SF6} and ELV_{CT}.

Figure 5.3 (panels **B**, **D**, and **F**) and Figure 5.4 show that in each comparison ELV_{IST} has a mean bias of 12 – 13% less (-129 to -161 ml) than the reference technique in both the uninjured lung and the ARDS model. ELV_{IST} has limits of agreement with ELV_{SF6} of $\pm 17\%$ (± 139 ml) in the uninjured lung and $\pm 20\%$ (± 298 ml) in the ARDS model. The limits of agreement between ELV_{IST} and ELV_{CT} were $\pm 25\%$ (± 294 ml) in the ARDS model.

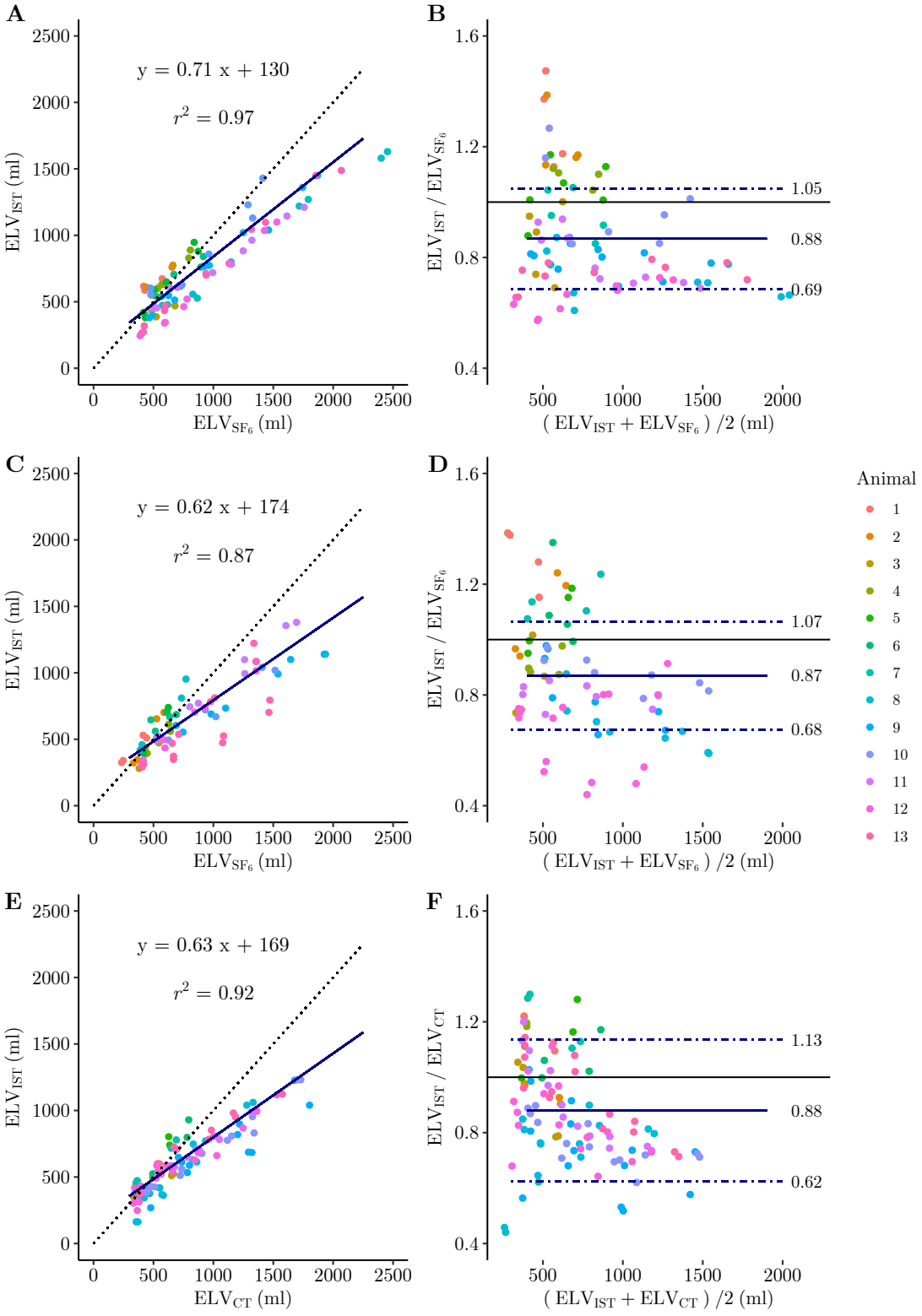


Figure 5.3: Scatter and Bland-Altman plots for changes in volume (ELV_{IST}, ELV_{SF6} and ELV_{CT}). *Panels **A** and **B** are measurements from the uninjured lung, panels **C**, **D**, **E** and **F** represent experiments conducted the ARDS model. In the left column, scatterplots show changes in volume. In the right column, solid lines in the Bland-Altman plots represent the mean bias and the dashed lines show the upper and lower limits of agreement (±1.96 SD). In all plots, individual points represent a paired set of measurements and different colours represent different animals.*

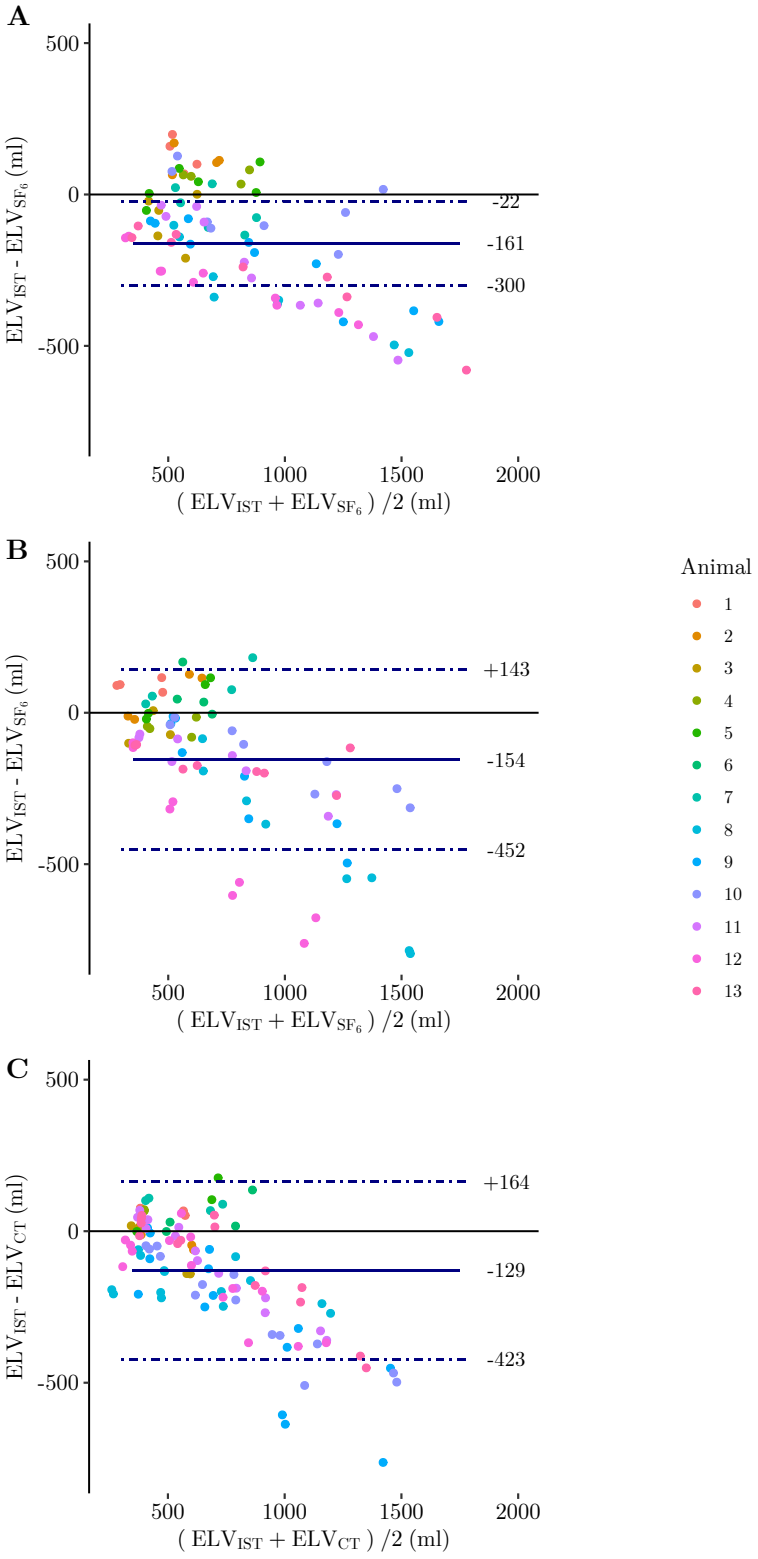


Figure 5.4: Conventional Bland-Altman plots for changes in volume (ELV_{IST}, ELV_{SF6} and ELV_{CT}). *Panel **A** shows measurements from the uninjured lung, panels **B** and **C** represent experiments conducted the ARDS model. Solid lines in the Bland-Altman plots represent the mean bias and the dashed lines show the upper and lower limits of agreement (±1.96 SD). In all plots, individual points represent a paired set of measurements and different colours represent different animals.*

5.3.4 Correlation between ΔELV_{IST}, ΔELV_{SF6} and ΔELV_{CT}.

Figure 5.5 panels **A**, **C** and **E** show four quadrant plots demonstrating the relationship of ΔELV_{IST} with ΔELV_{SF6} and ΔELV_{CT}. The linear relationship between ΔELV_{IST} vs ΔELV_{SF6} in the uninjured lung yielded an $r^2 = 0.58$, and $r^2 = 0.83$ in the ARDS model. The linear relationship between ΔELV_{IST} and ΔELV_{CT} in the ARDS model had an $r^2 = 0.16$.

5.3.5 Agreement between ΔELV_{IST}, ΔELV_{SF6} and ΔELV_{CT}.

Direction of change concordance showed that ΔELV_{IST} has a concordance rate of 98 – 100% with ELV_{SF6} and ELV_{CT}. This is reflected in Figure 5.5, panels **A**, **C** and **E**, where 98 – 100% of data are in the top right and bottom left quadrants of each four quadrant plot. Panels **B**, **D** and **F** in Figure 5.5 show Bland–Altman plots with a mean bias (± limits of agreement) of -73 ml (± 186 ml) for ΔELV_{IST} vs ΔELV_{SF6} in the uninjured, -77 ml (± 128 ml) for ΔELV_{IST} vs ΔELV_{SF6} in the ARDS model and -1 ml (± 333 ml) for ΔELV_{IST} vs ΔELV_{CT} in the ARDS model. Figure 5.6 demonstrates polar agreement in paired measurements of ΔELV. Mean angular bias ranged from 8^o – 11^o and radial limits of agreement from $\pm 30^o$ – 37^o.

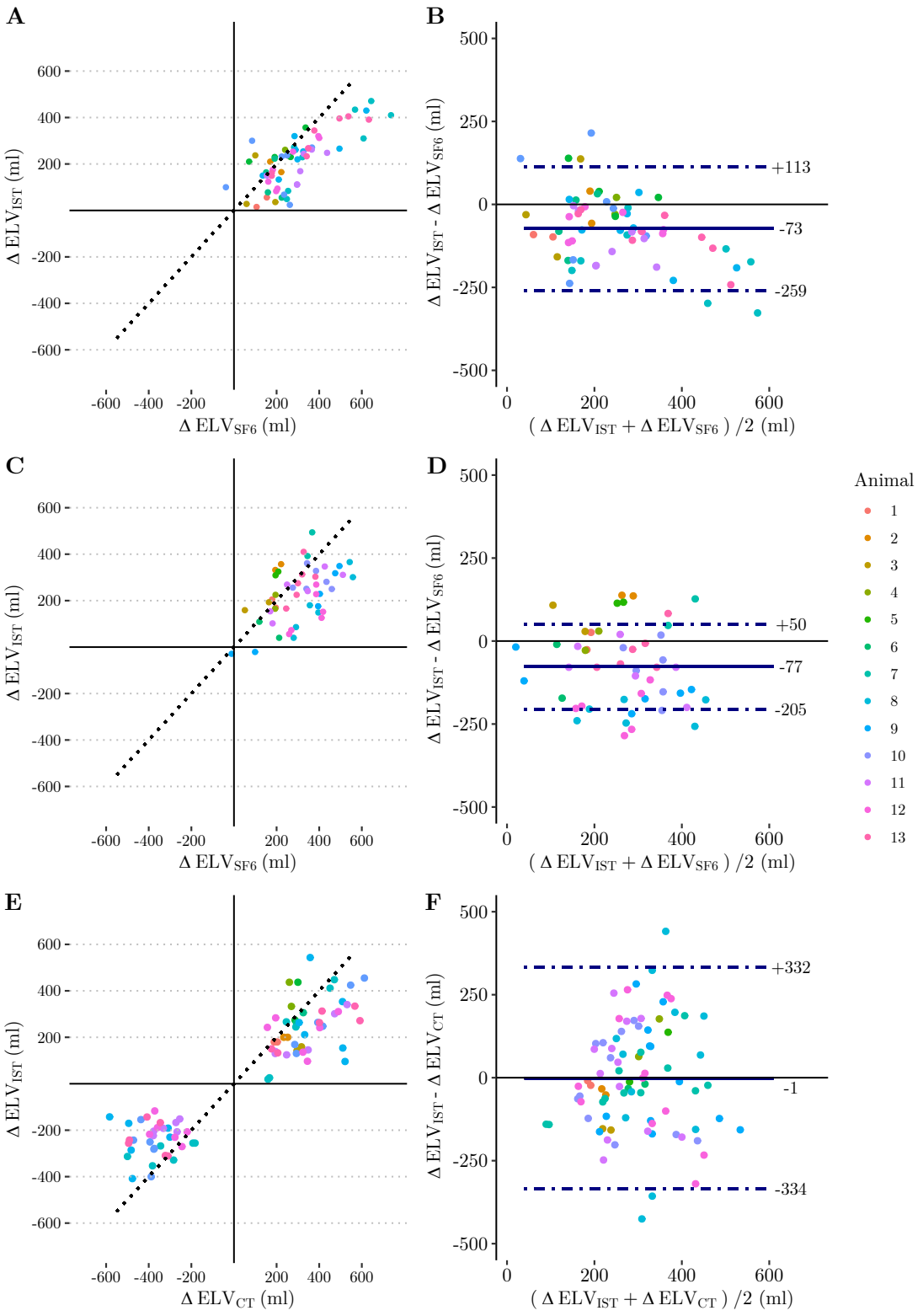


Figure 5.5: Scatter and Bland-Altman plots for changes in volume (ΔELV_{IST}, ΔELV_{SF6} and ΔELV_{CT}). *Panels **A** and **B** are measurements from the uninjured lung, panels **C**, **D**, **E** and **F** represent experiments conducted the ARDS model. In the left column, scatterplots show changes in volume. In the right column, solid lines in the Bland-Altman plots represent the mean bias and the dashed lines show the upper and lower limits of agreement (± 1.96 SD). In all plots, individual points represent a paired set of measurements and different colours represent different animals.*

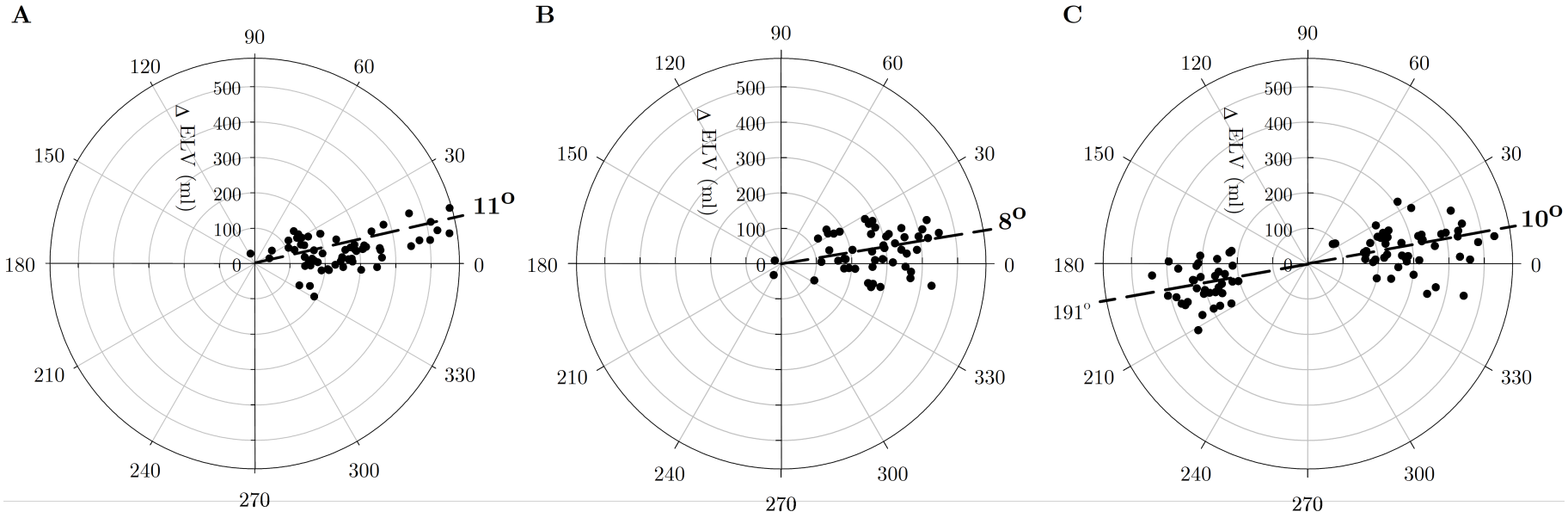


Figure 5.6: Polar plot analysis of measured changes in ELV (ΔELV). *The larger the mean ΔELV the greater the distance between the point and the centre of the plot. The better the agreement between a pair of measurements, the closer the point lies to the horizontal (0°). 95% radial limits of agreement describe the angle within which 95% of the data lie. Concordance rate (%) describes the number of points that lie within the assumed limits of adequate agreement, set at ± 30°.* ***A*** *Comparison of ΔELV_{IST} vs ΔELV_{SF6} in the uninjured lung. Mean angular bias = 11°, 95% radial limits of agreement = ± 35°, concordance = 91%.* ***B*** *Comparison of ΔELV_{IST} vs ΔELV_{SF6} in the ARDS model. Mean angular bias = 8°, 95% radial limits of agreement = ± 37°, concordance rate 90%.* ***C*** *Comparison of ΔELV_{IST} vs ΔELV_{CT} in the ARDS model. Mean angular bias = 10°, for positive changes in volume and 191° for negative changes in volume. 95% radial limits of agreement = ± 30°, concordance rate = 95%.*

5.4 Discussion

This chapter presents an investigation into the ability of IST to measure absolute ELV and changes in ELV compared to SF_6 washin-washout (ELV_{SF6}) and CT (ELV_{CT}) in uninjured lungs and in an ARDS model of lung injury. In both uninjured lungs and in a saline-lavage model of ARDS, IST can reliably measure absolute ELV comparably to SF_6 and CT ($r^2 = 0.87$ - 0.97), with a bias of -12 to -13% and within limits of agreement of ± 17 – 25%. Additionally, when comparing PEEP-induced changes in lung volume, IST is $> 98\%$ concordant with SF_6 and CT.

IST's measurements of absolute ELV, which underestimate ELV by 12 – 13%, do not fall within 5% of the reference method recommended by the ERS/ATS Consensus Statement (Robinson et al. 2013). These results are consistent with a previous study of IST in which Bruce et al. (2018) showed that IST underestimated functional residual capacity (FRC) by 32% (1080 ml) compared to body plethysmography in humans where the mean FRC was 3.4 L. The underestimation was smaller in the present study, with a mean bias of -12 to -13% (-129 ml to -161 ml) where the overall mean ELV was 809 ml. IST measures the volume of ventilated regions of lung and it is expected that IST will underestimate lung volume compared to CT, which estimates the entire thoracic gas volume. One reason for IST's underestimation of ELV compared to SF_6 may be that multiple breath washout techniques recover tracer gas from the slowest compartments if the washout period is long enough, whereas for IST, the contribution of the slowest compartment is limited by the chosen period of the sinewave.

There is no previous study assessing IST's ability to measure changes in lung volume. The linear relationship between ΔELV_{IST} and ΔELV_{SF6} is stronger than for ΔELV_{CT} and the limits of agreement are narrower for ΔELV_{SF6} ($\pm$ 186 ml in the uninjured lung and $\pm$ 128 ml in the ARDS model) compared to ΔELV_{CT} ($\pm$ 333 ml). One proposed explanation for the narrower limits of agreement in the ARDS model compared to the uninjured model with SF_6 was that the measured ΔELV was less in the ARDS model. Further analyses showed that the measured changes in volume (based on ΔELV_{SF6}) were no different in the uninjured and ARDS models (PEEP 5 – 10: $p = 0.11$, PEEP 10 – 15: $p = 0.59$, PEEP 15 – 20: $p = 0.91$).

The repeatability of IST's measurements of ELV in the same subject under the same conditions is within the reported international acceptable limits of coefficient of variation (< 10%) (Wanger et al. 2005) and consistent with studies of IST in other circumstances (Bruce et al. 2018). IST has good repeatability and minimal bias compared to CT (mean bias = - 1 ml) when measuring changes in lung volume. This provides support for the use of IST to monitor trends in lung volume, where the change (or lack of) in volume after a change in ventilator setting is potentially of most interest to the bedside clinician.

5.4.1 Strengths and limitations of the study

When comparing IST to other available methods of bedside lung volume measurement, its strengths are that its component parts are commercially available, it is easy to use at the bedside and does not rely on patient nor operator input. Additionally, because IST does not rely on a fixed inspiratory flow it can be used in spontaneously ventilating patients. The main limitations of the study are that the use of a porcine model does not directly translate to humans and the use of saline-lavage does not necessarily comprise all the features of human ARDS. However saline-lavage does result in reduction in lung volume, which was one reason for its choice in this study. In addition, in this protocol not all PEEP levels were studied in all experiments. This was not feasible due to time restraints because the initial seven experiments including PEEP 0, 5 and 10 cmH_2O were undertaken in parallel with data collection for another study, in keeping with the 3R's principle (Russell et al. 1959).

5.4.2 Future directions for development of IST in the context of measuring lung volume.

Future development of IST should include assessing the feasibility of its use in mechanically ventilated human patients. IST must be able to measure lung volumes when using volume controlled and pressure controlled ventilation modes in paralysed patients and in assisted mechanical ventilation where less regular inspiratory flow patterns exist.

5.4.3 Conclusions

The use of IST to measure lung volume is potentially translatable to human practice and this study is the first to examine its use in mechanically ventilated lungs. Measuring the size of the ARDS baby lung would allow titration of ΔP to the individual by providing a method of scaling V_T to the size of the baby lung. This has the potential to reduce mortality in patients with ARDS. IST measured lung volumes and changes in volume reliably compare to the standard techniques of SF_6 washin-washout and CT in a mechanically ventilated porcine model.

CHAPTER 6

Measuring cardiac output with the Inspired Sinewave Technique: Validation against intermittent thermodilution

Abstract

This chapter examines the use of the inspired sinewave technique (IST) to measure cardiac output ($\dot{Q}$) in a mechanically ventilated porcine model with and without saline-lavage lung injury. Measurements of $\dot{Q}$ taken with IST ($\dot{Q}_{IST}$) are compared against $\dot{Q}$ measured by pulmonary artery thermodilution ($\dot{Q}_T$). To study how well $\dot{Q}_{IST}$ tracks changes in $\dot{Q}$, infusions of esmolol and dobutamine were used to decrease and increase $\dot{Q}$. In the uninjured lung, $\dot{Q}_{IST}$ had a bias of - 0.5 l min^{-1} compared to $\dot{Q}_T$ and had good concordance (93%) when tracking changes in $\dot{Q}$ over time. In the injured lung, IST's measurements of both absolute and changes in $\dot{Q}$ were not as good compared to the uninjured condition.*

*The work presented in this chapter forms the basis of a published research paper which is attached in Appendix A (Bruce et al. 2019).

6.1 Introduction

Cardiac output ($\dot{Q}$) monitoring can improve perioperative outcomes of surgical patients at high risk of haemorrhage or haemodynamic instability and is an essential part of goal directed therapy (GDT) (Abbas et al. 2008; Hamilton et al. 2011; Aya et al. 2013). GDT itself has proved controversial with respect to its impact on patient mortality. In the most comprehensive meta-analysis, Grocott et al. (2012) showed no improvement in mortality compared to control groups. This finding was contrary to several other meta-analyses demonstrating a benefit on mortality by use of GDT (Heyland et al. 1996; Kern et al. 2002; Poeze et al. 2005; Hamilton et al. 2011). However, Grocott et al. (2012) did show reduction in overall post-operative complications (including post-operative kidney injury, respiratory failure and wound infections) and a reduced in-hospital stay. Regardless of its putative effects on mortality, GDT (and measurement of $\dot{Q}$) is of benefit to the high-risk surgical patient and indeed the CardioQ-ODM device is recommended by the UK's National Institute for Heath and Clinical Excellence (NICE) to guide intraoperative fluid therapy in high risk patients (https://www.nice.org.uk/guidance/mtg3).

Intermittent pulmonary artery thermodilution (PATD) remains the 'gold standard' for measuring $\dot{Q}$. However the technique requires the placement of a pulmonary artery catheter (PAC). As discussed in Section 1.7, insertion of a PAC is associated with increased mortality (Harvey et al. 2005; Reuter et al. 2010) and it remains unclear whether or not there is any benefit to inserting a PAC in the critically unwell patient (Connors et al. 1996; Schwann et al. 2011). Recently, the use of the PAC has declined in favour of less invasive techniques to estimate $\dot{Q}$, such as transpulmonary thermodilution (TPTD), pulse contour analysis and trans-oesophageal Doppler (Marik 2013a).

The inspired sinewave technique (IST) has the potential to fulfil the features of an ideal haemodynamic monitor which are detailed in Table 6.1 (Vincent et al. 2011). The background and theory of IST are discussed in detail in Section 2.6. IST is a respiratory-based method for interrogating the cardiopulmonary system. It is based on a tidal model of ventilation to a three compartment model of the lung, comprising a single dead-space volume (V_D), a single alveolar volume (V_A) and the blood flow to that single alveolar compartment (see Figure 2.8). The blood flow

to the single alveolar compartment from the pulmonary artery is equal to the left-sided $\dot{Q}$ provided there is no intra-cardiac shunt. Therefore, IST is able to provide measurements of $\dot{Q}$ ($\dot{Q}_{IST}$).

Provides measurement of relevant variables
Provides accurate and reproducible measurements
Provides interpretable data
Is easy to use
Is readily available
Is operator-independent
Has a rapid response time
Causes no harm
Is cost-effective
Should provide information that is able to guide therapy

Table 6.1: The features of an ideal haemodynamic monitor. *(Vincent et al. 2011)*

Using commercially available equipment integrated into a patient's breathing circuit, IST introduces a sinusoidally varying concentration of tracer gas (N_2O) into the inspired airway gases. The concentration of the tracer in the expired gases is subsequently measured. The phase shift and change in amplitude of the expired sinewave signal are modelled to recover values for the alveolar volume (ELV_{IST}) and $\dot{Q}_{IST}$. (Williams et al. 1998; Farmery 2008; Clifton et al. 2013). IST's measurements of lung volume have proven efficacy in spontaneously ventilating healthy volunteers (Phan et al. 2017a; Bruce et al. 2018) and in a mechanically ventilated porcine model (Crockett et al. 2020). Previous to this work, there has been no study to assess IST's measurements of $\dot{Q}$ during mechanical ventilation.

This chapter presents a proof-of-concept study to determine the level of agreement between paired measurements of $\dot{Q}_{IST}$ and $\dot{Q}_T$ in a mechanically ventilated porcine model with both uninjured lungs and in lungs with saline-lavage induced injury. The ability of IST to track pharmacologically-induced changes in $\dot{Q}$ ($\Delta\dot{Q}_{IST}$) is compared against the same changes measured with PATD ($\Delta\dot{Q}_T$).

6.2 Methods

6.2.1 Ethical approval.

This study of eight domestic pigs (mean weight (SD) = 44 (6) kg) was conducted at the Biomedical Research Centre, University of Bristol, UK. The protocol and its procedures were approved by the UK Home Office, London, UK (PPL: 30/2960) and local ethics committee. Reporting in this chapter adheres to Animal Research: Reporting of in vivo Experiments (ARRIVE) guidelines (Kilkenny et al. 2013). The experiments were designed in accordance with the 3R's principle (Russell et al. 1959), using the minimum number of animals to enable collection of interpretable results. The sample size was calculated using Mead's resource equation (Hubrecht et al. 2010).

6.2.2 Animal preparation and instrumentation.

Summary baseline cardiovascular and respiratory characteristics are shown in Tables 6.2a and 6.2b. Animals were pre-medicated with intramuscular xylazine 2 mg kg^{-1}, ketamine 20 mg kg^{-1} and midazolam 0.5 mg kg^{-1} and underwent induction of anaesthesia with intravenous (IV) propofol titrated to effect (1- 3 mg kg^{-1}). The trachea was intubated orally and mechanical ventilation subsequently commenced. During preparation and throughout the protocol animals were ventilated with volume-controlled ventilation (VCV) using a variable respiratory rate to maintain P_aCO_2 4.5 - 8 kPa, a V_T of 8 ml kg^{-1}, PEEP of 5 cmH_2O and an Inspiratory : expiratory ratio (I:E) of 1:2 (Engström Carestation Ventilator (GE healthcare, Madison USA)). The ventilator tubing and endotracheal tube were checked for leaks by analysis of the spirometry data. Anaesthesia was maintained with continuous IV infusion of ketamine 32 mg kg^{-1} hr^{-1}, fentanyl 4 μg kg^{-1} hr^{-1} and midazolam 0.16 mg kg^{-1} hr^{-1}. General anaesthesia was confirmed by absence of spontaneous movements and by lack of reaction to painful stimulation between the front hooves. After confirmation of general anaesthesia, muscle relaxation was achieved with an initial bolus of pancuronium 0.1 mg kg^{-1} followed by 0.1 mg kg^{-1} hr^{-1} continuous infusion throughout the protocol. Pancuronium boluses (0.1 mg kg^{-1}) were administered

when spontaneous ventilatory efforts were detected from the airway gas and pressure traces. The adequacy of anaesthesia was determined by absence of cardiovascular signs of sympathetic stimulation (increases in heart rate or arterial blood pressure). Hartmann's solution was administered IV at a rate of 10 ml kg^{-1} hr^{-1} throughout the protocol.

Once anaesthetised, the right internal jugular vein was surgically exposed and a balloon-tipped, flow-guided PAC (Edwards Lifesciences, CA, USA) inserted and advanced into the pulmonary artery. Assessment of pulmonary artery pressure (PAP) and waveforms confirmed the correct position of the PAC. A peripheral artery was cannulated (one of either of the superficial brachial, median or saphenous arteries) to provide arterial pressure monitoring and this along with pulmonary artery pressure, electrocardiogram, peripheral oxyhaemoglobin saturation (S_PO_2) and end-tidal CO_2 (E_TCO_2) were continuously recorded (Datex Ohmeda Capnoman Ultima, Datex AS3). $\dot{Q}_{IST}$ and $\dot{Q}_T$ were measured intermittently (as described below). Physiological parameters were recorded on LabChart via a PowerLab AD board (AD Instruments, NZ). At the end of the protocols animals were humanely euthanised under anaesthesia with an overdose of pentobarbital.

6.2.3 The Inspired Sinewave Technique.

Full details of IST are described in Section 2.6. At the beginning of each inspiration, a small volume of N_2O is injected into inspired airway gas by a mass flow controller (Alicat Scientific, Inc., USA). Gas flow is measured by an ultrasonic flowmeter (VenThor 22/2A, Budapest, Hungary), and N_2O concentration by a rapid mainstream infrared sensor (Square One Technology, Boulder, Colorado, USA). The volume of N_2O injected is proportional to inspiratory flow. Over successive breaths, the inspired N_2O concentration is changed so that it oscillates sinusoidally around a fixed mean concentration with a predetermined amplitude and period. Without venous recirculation of the N_2O sinewave, which is assumed negligible at low time periods (*i.e.* < 3 minutes) (Gavaghan et al. 1995), the end-tidal N_2O concentration also oscillates in a sinewave pattern (Figure 2.7). A three-compartment, tidal ventilation model of the lung uses the change in sinewave amplitude and phase shift to estimate pulmonary blood flow ($\dot{Q}_{IST}$). The background principles of IST and the hardware layout are provided in the Section 2.6.

Parameter	Animal								Mean (SD)	n
	1	2	3	4	5	6	7	8		
Weight	47	45	39	53	37	37	47	45	44 (6)	8
HR	75	70	100	87	60	87	70	102	81 (15)	8
SBP (mmHg)	113	101	105	80	130	95	105	95	103 (15)	8
DBP (mmHg)	87	62	71	60	90	85	75	65	74 (12)	8
$\dot{Q}_{IST}$ (l min^{-1})	3.9	6.0	4.1	4.9	8.1	5.6	7.2	9.2	6.1 (1.9)	8
$\dot{Q}_T$ (l min^{-1})	2.9	6.2	5.0	4.4	3.9	3.2	6.7	3.7	4.5 (1.4)	8
PAP (mmHg)	20	16	18	15	17	18	16	21	18 (2)	8
Hb (g dl^{-1})	7.8	8.2	8.9	8.3	10.2	8.3	8.8	9.6	8.8 (0.8)	8
F_IO_2	0.6	0.28	0.4	0.4	0.35	0.4	0.4	0.4	0.4 (0.1)	8
S_aO_2 (%)	99	99	100	99	95	97	100	97	98 (2)	8
pH	7.37	7.48	7.49	7.38	7.31	7.33	7.33	7.24	7.37 (0.08)	8
P_aO_2 (kPa)	40.5	15.3	21.7	21.3	24.8	26.1	21.9	23.3	24.4 (7.3)	8
P_aCO_2 (kPa)	7.9	6.0	5.9	6.1	9.9	7.5	8.5	9.6	7.7 (1.6)	8
PFR	507	411	408	400	531	490	410	438	449 (52)	8

a Pre-injury.

Parameter	Animal								Mean (SD)	n
	1	2	3	4	5	6	7	8		
HR	78	73	84	72	104	96	78	69	82 (12)	8
SBP (mmHg)	94	105	97	70	77	84	103	15	81 (29)	8
DBP (mmHg)	69	47	72	46	40	54	59	47	54 (12)	8
$\dot{Q}_{IST}$ (l min^{-1})	2.8	6.6	6.1	3.2	4.7	4.6	6.7	9.1	5.5 (2.1)	8
$\dot{Q}_T$ (l min^{-1})	2.7	7.2	5.6	3.5	5.2	4.1	4.1	3.3	4.5 (1.5)	8
PAP (mmHg)	37	27	27	35	21	32	24	29	29 (5)	8
Hb (g dl^{-1})	7.2	6.7	7.7	8.3	8.0	6.9	7.6	8.8	7.7 (0.7)	8
F_IO_2	0.6	0.7	0.7	0.8	0.7	0.7	0.9	0.9	0.8 (0.1)	8
S_aO_2 (%)	93	99	100	93	100	99	99	100	97.8 (3.0)	8
pH	7.17	7.33	7.25	7.39	7.19	7.21	7.23	7.15	7.24 (0.08)	8
P_aO_2 (kPa)	12	24	31	12	33	23	29	40	25.5 (9.8)	8
P_aCO_2 (kPa)	10	7	9	11	10	10	10	11	9.8 (1.4)	8
PFR	153	255	331	116	355	241	245	331	254 (86)	8

b Post-injury.

Table 6.2: Baseline characteristics of individual animals pre- and post-lung injury. *HR = heart rate, SBP = systolic arterial blood pressure, DBP = diastolic arterial blood pressure, CO = cardiac output, PASP = pulmonary artery systolic pressure, PADP = pulmonary artery diastolic pressure, Hb = haemoglobin concentration, F_IO_2 = fraction of inspired O_2, S_PO_2 = peripheral oxyhaemoglobin saturation, P_aO_2 = arterial O_2 partial pressure, P_aCO_2 = arterial CO_2 partial pressure, PFR = P_aO_2:F_IO_2 ratio*

6.2.4 Data collection and processing.

Automated measurements of $\dot{Q}_{IST}$ continued throughout the entire protocol. $\dot{Q}_{IST}$ was calculated every 30 s as a rolling average of the previous 3 minutes. $\dot{Q}_T$ was calculated as the average of three 10 ml injections of normal saline (4^oC) through the PAC at end-expiration (Datex Ohmeda). Three repeated $\dot{Q}_T$ measurements were taken every 3 - 5 minutes. Individual $\dot{Q}_T$ measurements $\leq 10\%$ apart were used to calculate $\dot{Q}_T$.

$\dot{Q}_{IST}$ measurements were collected as a rolling average. Consequently, a linear regression analysis between paired $\dot{Q}_T$ and $\dot{Q}_{IST}$ measurements was used to determine the time lag between the two methods (Saugel et al. 2015). The time lag of $\dot{Q}_{IST}$ measurements was shown to be around 60 seconds. After correction, paired $\dot{Q}$ measurements were used for the subsequent analysis.

6.2.5 Pre-injury experimental protocol.

After a stabilisation period of approximately 20 minutes, baseline measurements were recorded for 10 minutes. Stabilisation was judged as adequate when $\dot{Q}_T$ measurements did not fluctuate by more than 15%. Continuous measurement of $\dot{Q}_{IST}$ and intermittent measurement of $\dot{Q}$ were continued for a period of 60 - 90 mins during which time $\dot{Q}$ was pharmacologically manipulated. $\dot{Q}$ was first reduced using an infusion of esmolol (300 - 400 μg kg^{-1} min^{-1}) to decrease $\dot{Q}_T$ by $\geq$ 1 l min^{-1}. Following cessation of the esmolol infusion, $\dot{Q}$ was increased using an infusion of dobutamine (15 - 20 μg kg^{-1} min^{-1}) to raise $\dot{Q}_T$ by $\geq$ 3 l min^{-1} above its baseline measurement. Paired measurements of the partial pressure of mixed venous $P_{\bar{V}}O_2$ and arterial P_aO_2 were taken at the peak and trough of $\dot{Q}$ as measured by $\dot{Q}_T$.

6.2.6 Lung injury.

Lung injury was induced with a technique modified from Lachmann et al. (1980). Following pre-oxygenation, the ventilator was disconnected and the lungs lavaged by instillation of 30 ml kg^{-1} 0.9% saline solution (at 37 ^{o}C) via the endotracheal tube.

After 30 s the saline was drained out of the lungs and ventilation recommenced. This process was repeated until a P_aO_2:F_IO_2 ratio (PFR) of less than 300 mmHg was achieved.

6.2.7 Post-injury experimental protocol.

After lung-injury, animals were re-stabilised for a period of approximately 20 minutes, following which baseline measurements were recorded for 10 minutes. Physiological parameters for the animals post-injury are shown in Table 6.2b. The same protocol that was carried out pre-injury (as described in Section 6.2.5) was then repeated. An example of a full experimental protocol can be found in Appendix C.

6.2.8 Statistical analyses.

Normality of data was assessed using d'Agostino-Pearson's test. Differences between baseline characteristics were tested using a one-way ANOVA with Sidak's correction for multiple comparisons.

Agreement between paired measurements of absolute $\dot{Q}_{IST}$ and $\dot{Q}_T$ was assessed with Bland-Altman analysis adjusted for repeated measurements (Myles et al. 2007) and by caluclating their interchangeability rate (Lorne et al. 2018).

Trending ability of $\dot{Q}_{IST}$ was assessed by comparing changes in $\dot{Q}_{IST}$ ($\Delta\dot{Q}_{IST}$) and $\dot{Q}_T$ ($\Delta\dot{Q}_T$). $\Delta\dot{Q}$ values were calculated by subtracting one value from its preceding value. Agreement between $\Delta\dot{Q}_{IST}$ and $\Delta\dot{Q}_T$ was assessed using Bland-Altman analysis, direction of change concordance on four-quadrant plots and polar plot analysis. An exclusion zone of 15% was excluded from the centre of both four-quadrant and polar plots (Critchley et al. 2010; Critchley et al. 2011).

Analyses were carried out using R v3.5.1 (R Development Core Team 2017), Graphpad Prism v8.1.2 (GraphPad Software, USA, www.graphpad.com) and SigmaPlot (Systat Software, CA).

6.3 Results

The intended protocol was completed in all animals. A total of $n = 248$ paired measurements of $\dot{Q}_{IST}$ and $\dot{Q}_T$ were recorded. Figures 6.1 and 6.2 demonstrate the changes in $\dot{Q}$ over the course of the protocol in each animal relative to their baseline $\dot{Q}$. These figures show that the protocol designed to induce changes in $\dot{Q}$ did so effectively, as can be seen from the $\dot{Q}_T$ measurements (red dots and lines). Likewise, the protocol of repeated saline lavages designed to induce lung injury was effective. This is shown in Tables 6.2a and 6.2b where there was significant reduction in baseline PFR between the pre- and post-injury measurements (mean (SD) PFR = 447 (49) vs 250 (81) respectively).

6.3.1 Relationship between measurements of $\dot{Q}_{IST}$ and $\dot{Q}_T$ in the uninjured lung.

Qualitatively, in the uninjured lung, $\dot{Q}_{IST}$ follows the measurements of $\dot{Q}_T$ well. This is seen in Figure 6.1 where the red and blue dots/lines follow eachother with relative fidelity. This is reflected in Figure 6.3 panels **A** and **B** which show scatter-plots and Bland-Altman plots of $\dot{Q}_{IST}$ and $\dot{Q}_T$ in the pre-injury period. These demonstrate a strong linear relationship between $\dot{Q}_{IST}$ and $\dot{Q}_T$, with an equation of $y = 0.68x - 0.45$ and $r^2 = 0.88$. Bland-Altman analysis showed a mean bias of - 0.5 l min^{-1} with limits of agreement from - 2.4 to + 1.3 l min^{-1}. The interchangeability rate was poor at 41 %.

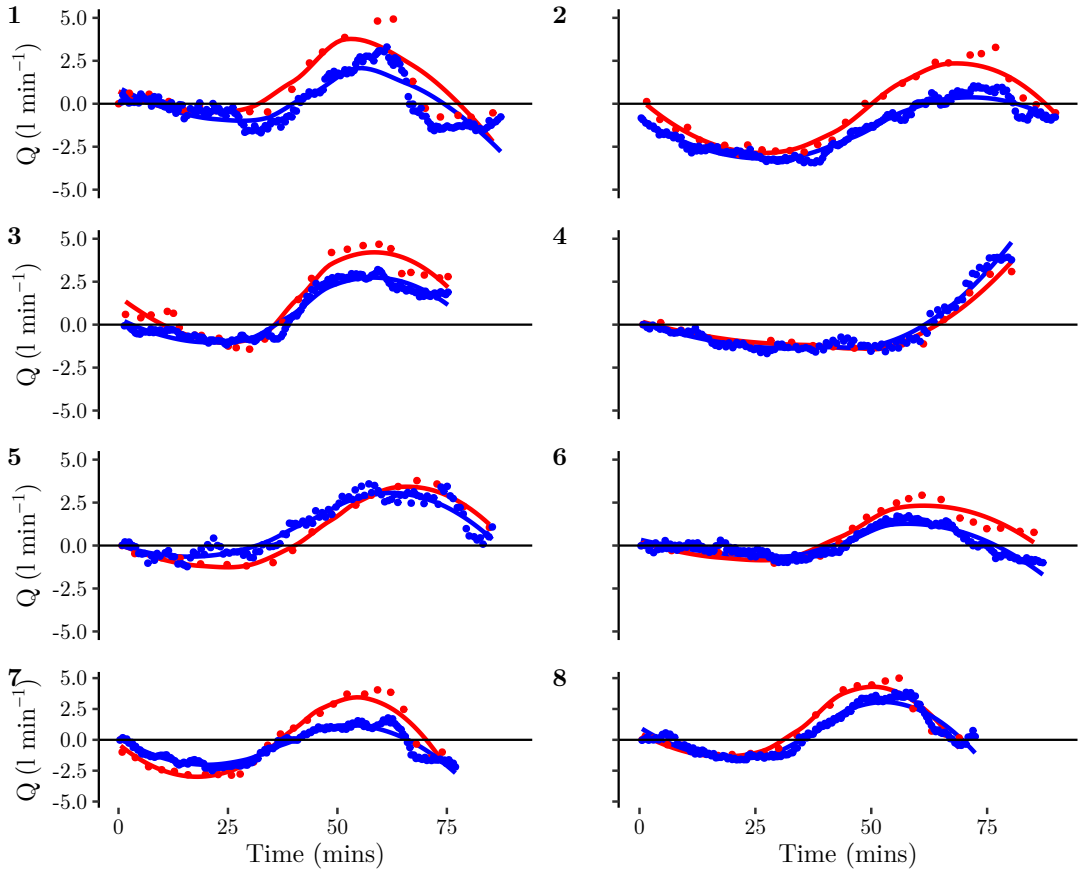


Figure 6.1: Pre-injury: Absolute measurements of cardiac output measured with $\dot{Q}_{IST}$ and $\dot{Q}_T$ in each animal over the period of the protocol. *Panels **1** to **8** show the changes in $\dot{Q}_{IST}$ (blue dots and lines) and $\dot{Q}_T$ (red dots and lines) over the course of the pre-injury protocol. The numbers 1 - 8 represent each individual animal. The points demonstrate values of $\dot{Q}$ normalised to each individual's baseline. Low cardiac output was induced from minutes 0 - 30 with an esmolol infusion (300 - 400 $\mu g\ kg^{-1}\ min^{-1}$). High cardiac output was induced from minutes 30 - 60 with an infusion of dobutamine (15 -20 $\mu g\ kg^{-1}\ min^{-1}$) before returning to baseline in preparation for the lung injury phase of the protocol.*

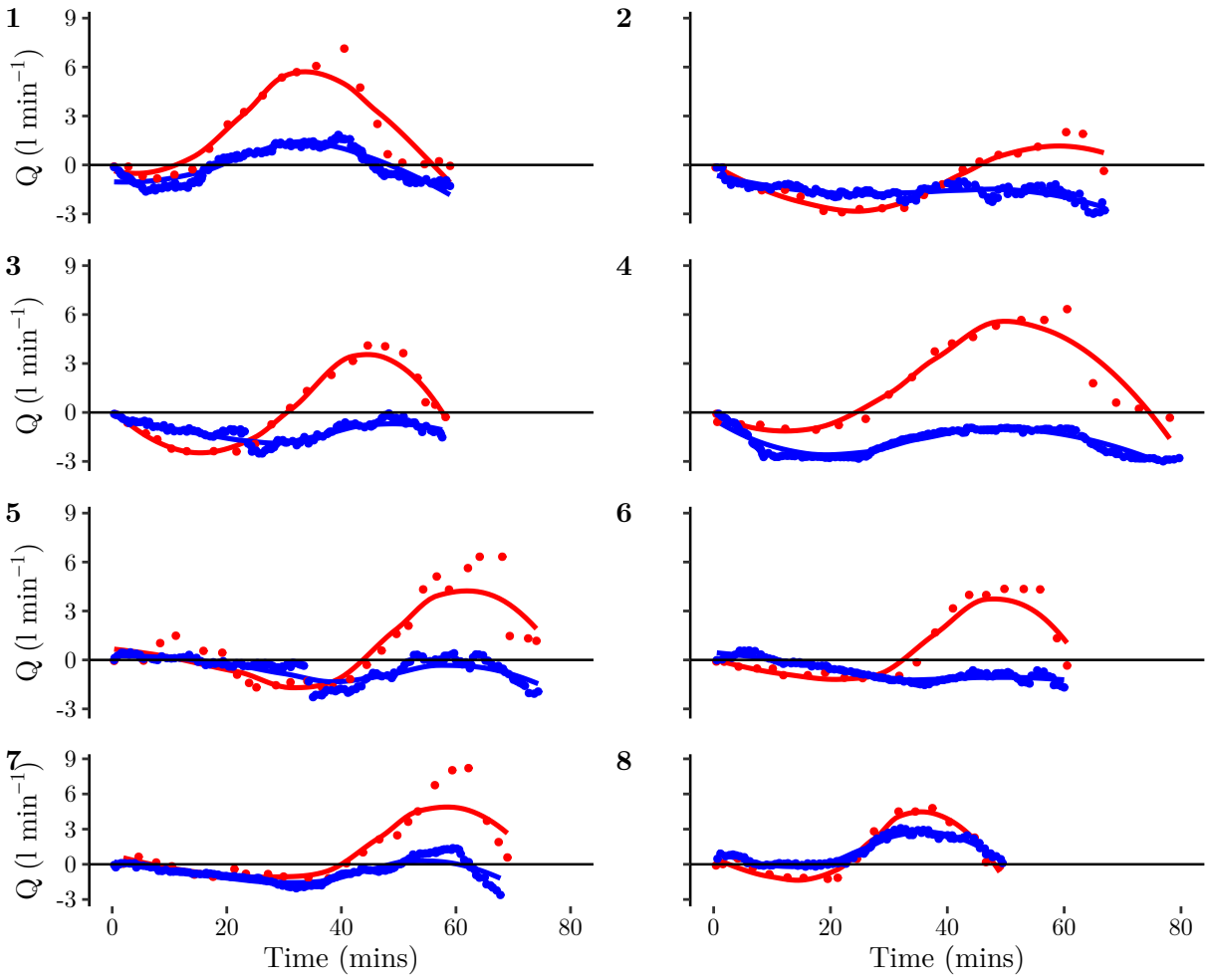


Figure 6.2: Post-injury: Absolute measurements of cardiac output measured with $\dot{Q}_{IST}$ and $\dot{Q}_T$ in each animal over the period of the protocol. *Panels **1** to **8** show the changes in $\dot{Q}_{IST}$ (blue dots and lines) and $\dot{Q}_T$ (red dots and lines) over the course of the post-injury protocol. The numbers 1 - 8 represent each individual animal. The points demonstrate values of $\dot{Q}$ normalised to each individual's baseline. The protocol for timings of low and high cardiac output states were not as rigidly adhered to as in the pre-injury phase of the protocol. This was due to laboratory logistics and lack of time. In keeping with the pre-injury protocol, low cardiac output was induced first, (usually from minutes 0 - 30) with an esmolol infusion (300 - 400 $\mu g\ kg^{-1}\ min^{-1}$). High cardiac output was subsequently induced with an infusion of dobutamine (15 -20 $\mu g\ kg^{-1}\ min^{-1}$) before termination of the experiment.*

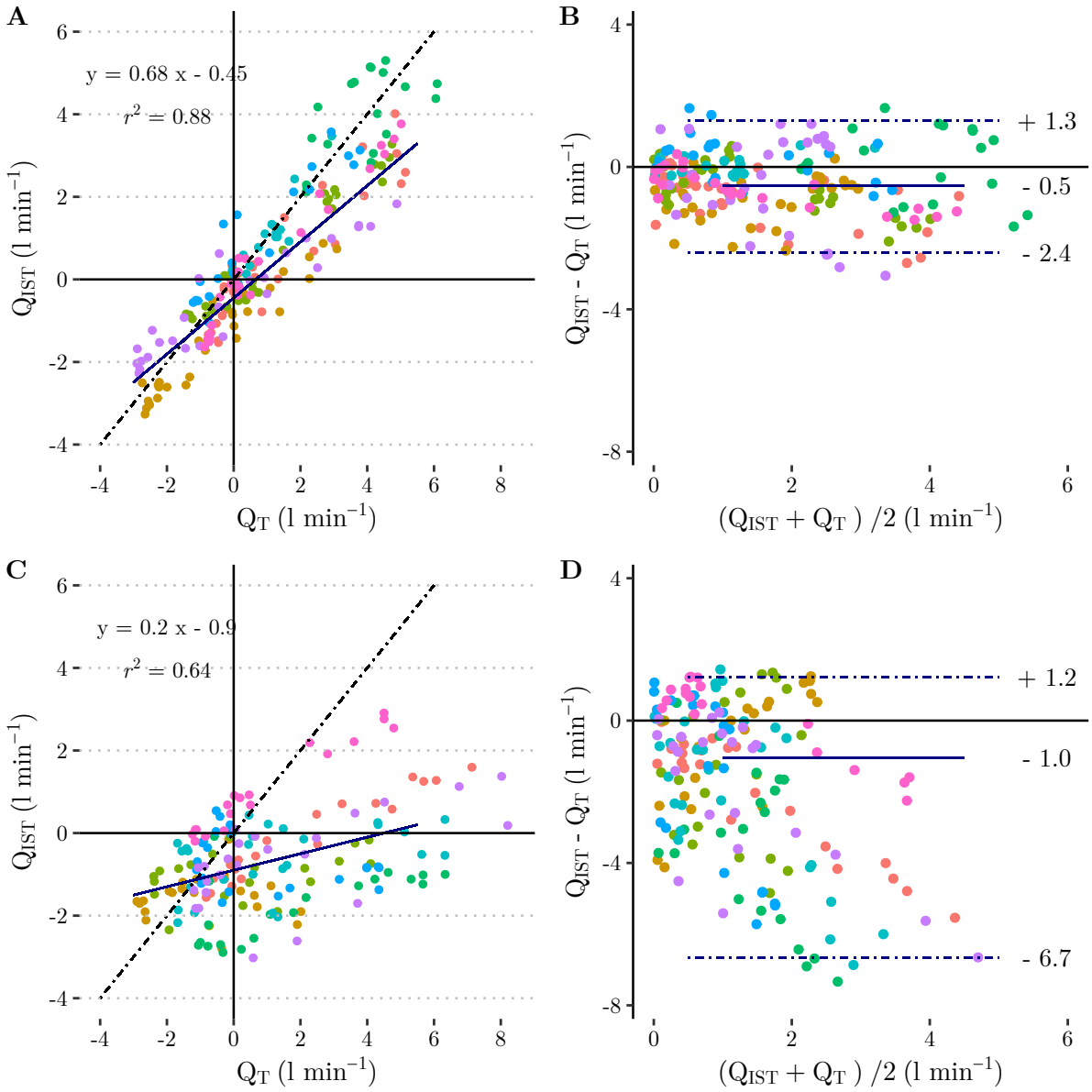


Figure 6.3: Scatter and Bland-Altman plots comparing paired measurements of $\dot{Q}_{IST}$ and $\dot{Q}_T$ pre- and post- lung injury. *Panels **A** and **B** represent measurements taken pre-injury and panels **C** and **D** measurements taken post-injury. In the left column, scatter-plots show results of linear regression analysis, where the solid line represents the reported equation. In the right column, solid lines in the Bland-Altman plots represent the bias and dashed lines show the upper and lower limits of agreement. In all plots, individual points represent a paired set of measurements and different colours represent different animals.*

6.3.2 Relationship between measurements of $\dot{Q}_{IST}$ and $\dot{Q}_T$ in the injured lung.

The ability of $\dot{Q}_{IST}$ to measure and track changes $\dot{Q}_T$ is demonstrated qualitatively in Figure 6.2. Examining the plots compared to those pre-injury (Figure 6.1), it can be seen that $\dot{Q}_{IST}$, shown in blue, fails to follow the induced changes in $\dot{Q}$, which are measured by $\dot{Q}_T$. Figure 6.3 panels C and D show the linear relationship and Bland-Altman plots of agreement between measurements of $\dot{Q}_{IST}$ and $\dot{Q}_T$ from the post-injury period. The linear relationship between $\dot{Q}_{IST}$ and $\dot{Q}_T$ was represented with the equation $y = 0.2x - 0.9$ and an $r^2 = 0.64$. Assessing the agreement in the injured lung showed median bias of -1 l min $^{-1}$ with 95 % limits of agreement ranging from -6.7 to +1.2 l min^{-1}.

6.3.3 The effect of shunt fraction on $\dot{Q}_{IST}$.

Shunt fraction ($\dot{Q}_S/\dot{Q}_T$) ranged from 0% to 53%. Figure 6.4 demonstrates the negative relationship between increasing $\dot{Q}_S/\dot{Q}_T$ and $\dot{Q}_{IST}$ measurements as a proportion of $\dot{Q}_T$. The equation generated by simple linear regression was $y = -172x + 100$ with a Pearson's correlation coefficient r = - 0.79.

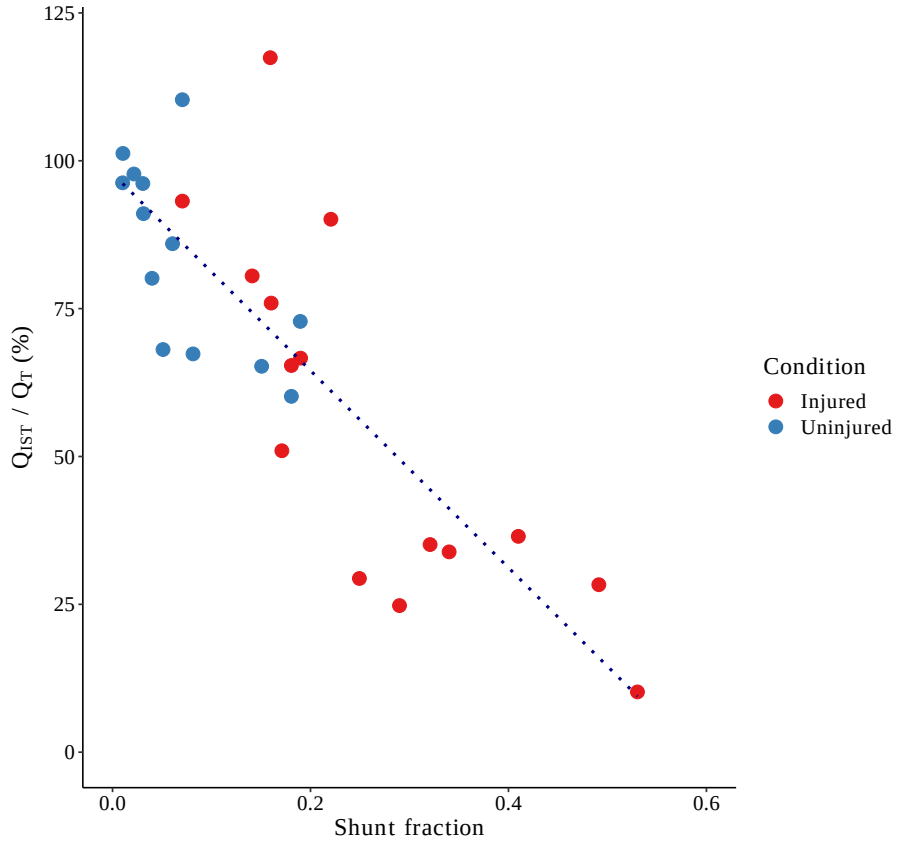


Figure 6.4: The effect of shunt fraction on $\dot{Q}_{IST}$. *The relationship between shunt fraction and $\dot{Q}_{IST}$ as expressed as a percentage of $\dot{Q}_T$. Red dots represent measurements taken in the injured lung and blow dots those from the uninjured lung. The dotted line shows the simple linear relationship between ($y = -172x + 100$), r = -0.79.*

6.3.4 Relationship between measurements of $\Delta\dot{Q}_{IST}$ and $\Delta\dot{Q}_T$ in the uninjured lung.

Figure 6.5 panels **A** and **B** show a four-quadrant plot and Bland-Altman plot assessing the trending ability of $\Delta\dot{Q}_{IST}$ compared to $\Delta\dot{Q}_T$ in the uninjured lung. Linear regression yielded an equation of $y = 0.65x + 0.01$ with an $r^2 = 0.71$. Bland-Altman analysis showed that compared to $\Delta\dot{Q}_T$, $\Delta\dot{Q}_{IST}$ had a median bias of - 0.1 l min^{-1} and 95 % limits of agreement between - 0.9 to + 1.2 l min^{-1}. Polar plot analysis is shown in Figure 6.6, which demonstrates a mean angular bias of + 6^o and an angular concordance rate of 92%.

6.3.5 Relationship between measurements of $\Delta\dot{Q}_{IST}$ and $\Delta\dot{Q}_T$ in the injured lung.

Figure 6.5 panels **C** and **D** show a four-quadrant plot and Bland-Altman plot assessing the trending ability of $\Delta\dot{Q}_{IST}$ compared to $\Delta\dot{Q}_T$ in the injured lung. Linear regression yielded an equation of $y = 0.3x + 0.10$ with an $r^2 = 0.62$. Bland-Altman analysis showed that compared to $\Delta\dot{Q}_T$, $\Delta\dot{Q}_{IST}$ had a median bias of - 0.2 l min^{-1} and 95 % limits of agreement between - 1.7 to + 1.7 l min^{-1}. Polar plot analysis is shown in Figure 6.6, which demonstrates a mean angular bias of + 22^o and an angular concordance rate of 70%.

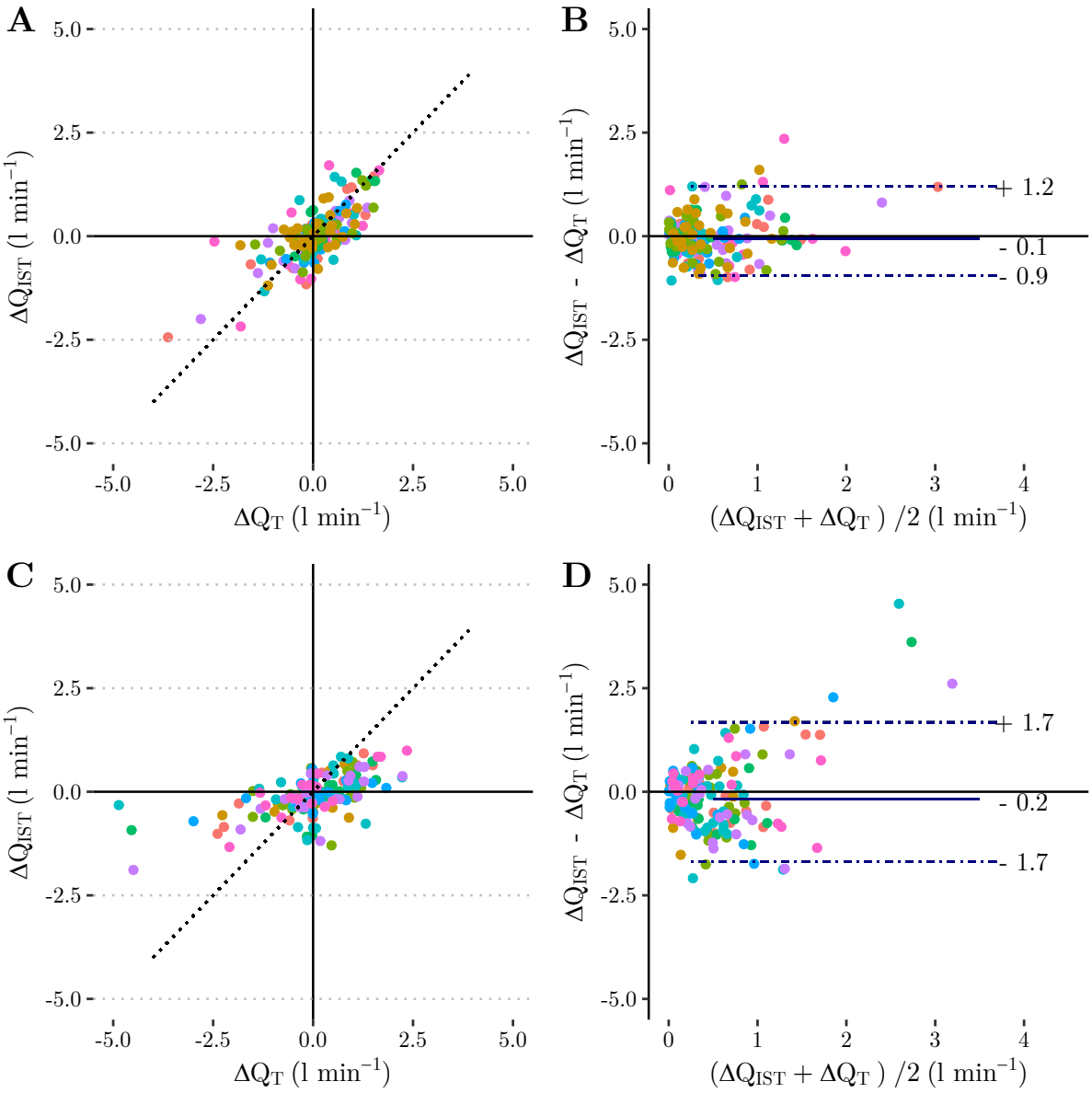


Figure 6.5: Four-quadrant and Bland-Altman plots comparing paired measurements of $\Delta\dot{Q}_{IST}$ and $\Delta\dot{Q}_{T}$ pre- and post- lung injury. *Panels **A** and **B** represent measurements taken pre-injury and panels **C** and **D** measurements taken post-injury. In the left column, four-quadrant plots demonstrate trending ability by swhowing changes in volume measured with each technique. In the right column, solid lines in the Bland-Altman plots represent the bias and dashed lines show the upper and lower limits of agreement. In all plots, individual points represent a paired set of measurements and different colours represent different animals.*

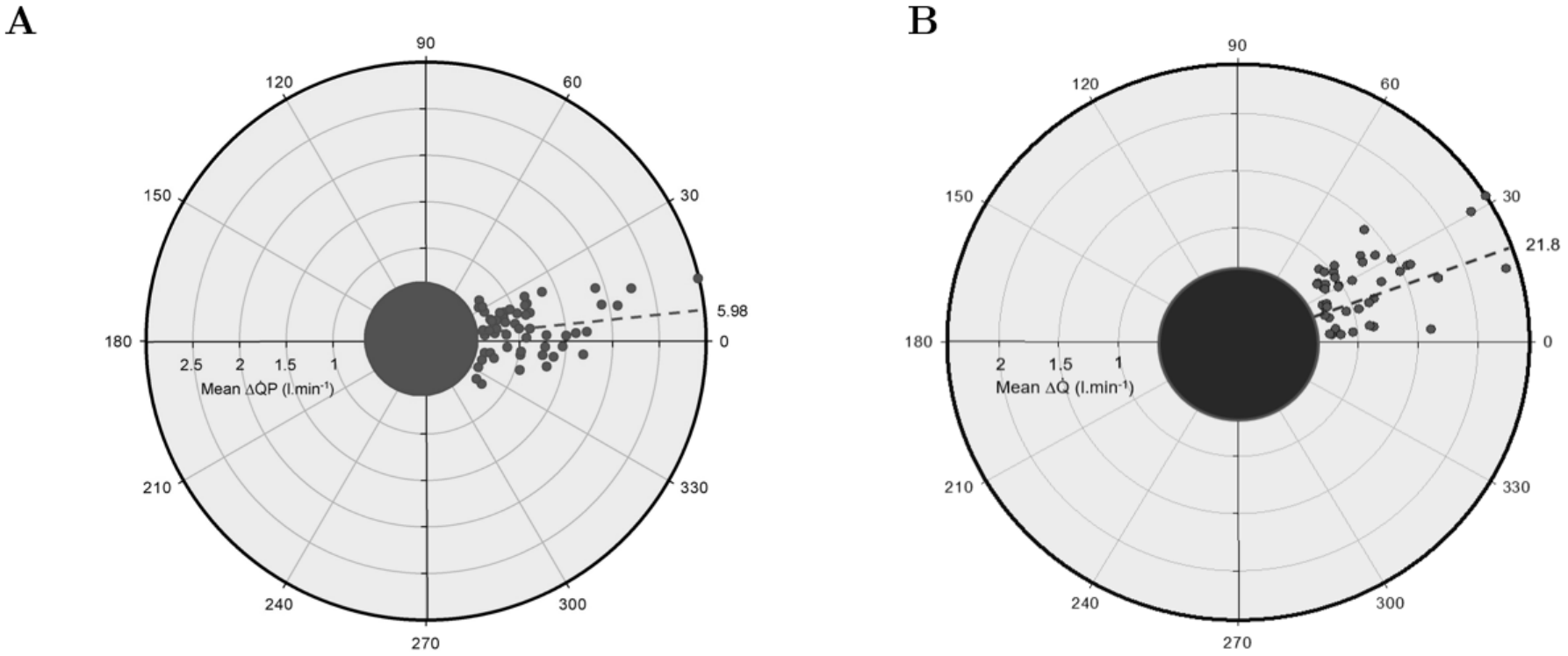


Figure 6.6: Polar plots comparing $\Delta\dot{Q}_{IST}$ and $\Delta\dot{Q}_T$ in uninjured and injured lung. *The larger the mean $\Delta\dot{Q}$ the greater the distance between the point and the centre of the plot. The better the agreement between a pair of measurements, the closer the point lies to the horizontal (0º). Concordance rate (%) describes the number of points that lie within the assumed limits of adequate agreement, set at ± 30º.* ***A*** *Comparison of $\Delta\dot{Q}_{IST}$ vs $\Delta\dot{Q}_T$ in the uninjured lung. Mean angular bias = +6º, angular concordance rate = 92%.* ***B*** *Comparison of $\Delta\dot{Q}_{IST}$ vs $\Delta\dot{Q}_T$ in the injured lung. Mean angular bias = +22º, angular concordance rate = 70%.*

6.4 Discussion

This chapter presents the first study investigating the application of IST to continuously monitor $\dot{Q}$ in a mechanically ventilated porcine model with and without lung injury. In the uninjured lung, there was a strong linear relationship between $\dot{Q}_{IST}$ and $\dot{Q}_T$ (r^2 = 0.88) and good agreement (bias = - 0.5 l min^{-1}, LOA -2.4 to +1.3 l min^{-1}). Likewise, in the uninjured lung, IST tracked changes in lung volume ($\Delta\dot{Q}_{IST}$) with good agreement to $\Delta\dot{Q}_T$ (bias - 0.1 l min^{-1}, LOA - 0.9 to + 1.2 l min^{-1}). In the injured lung, the linear relationship between $\dot{Q}_{IST}$ and $\dot{Q}_T$ was weaker (r^2 = 0.64) with a bias of - 1.0 l min^{-1} (LOA - 6.7 to + 1.2 l min^{-1}. Similarly, in the injured lung, the agreement between $\Delta\dot{Q}_{IST}$ and $\Delta\dot{Q}_T$ was weaker (bias = - 0.2 l min^{-1}, LOA -1.7 to + 1.7 l min^{-1}).

The ability of IST to track the induced changes in $\dot{Q}$ compares well with other non-invasive or minimally invasive methods of monitoring $\dot{Q}$. The concordance rate of $\dot{Q}_{IST}$ with $\dot{Q}_T$ of $>$ 92% in the current study is good (Myles et al. 2007; Critchley et al. 2011). This rate is similar to that observed in human participants with transoesophageal Doppler (Perrino et al. 1994; Møller-Sørensen et al. 2017) and certain pulse contour techniques (Jansen et al. 2001; Wilde et al. 2007). Indeed, the 92% concordance between $\dot{Q}_{IST}$ and $\dot{Q}_T$ is better than non-calibrated pulse contour $\dot{Q}$ measurement (Breukers et al. 2007; Biancofiore et al. 2009).

Measurements of $\dot{Q}_{IST}$ are similar to other recently developed respiratory based approaches using the Fick principle, (Hallsjo-Sander et al. 2014; M. Klein et al. 2015) the trending ability of which have also been examined in pigs. In the current investigation polar plot analysis revealed a mean angular bias of 6^o, which is the same as or better than other respiratory based methods (- 6^o and - 7^o respectively (Hallsjo-Sander et al. 2014; M. Klein et al. 2015)). The angular concordance rate of 92 % is similar to these other respiratory based techniques and is considered as a 'marginal' trending ability (Myles et al. 2007).

IST, as a respiratory technique, has the potential to provide an entirely non-invasive method to monitor $\dot{Q}$. Whilst PAC thermodilution remains the gold-standard technique against which other techniques are tested, because of its invasive nature and associated complications, clinical use of the PAC is becoming less

frequent (Harvey et al. 2005; Marik 2013a). Although the use of less invasive techniques, such as those based on pulse contour analysis or Doppler ultrasound, have increased, they are dependent on the skill of the user and require a some degree of invasive procedure (an arterial line or oesophageal probe) (Marik 2013a). IST is non-invasive and has other qualities of an ideal $\dot{Q}$ monitor. IST arguably meets all of the requirements set out by Vincent et al. (2011), as shown in Table 6.3. As well as meeting the criteria for a good haemodynamic montitor, IST like other respiratory based methods (Hallsjo-Sander et al. 2016), has the benefit of simultaneously estimating other aspects of cardiopulmonary function such as effective lung volume (Bruce et al. 2018; Crockett et al. 2020).

Criterion	Satisfied
Provides measurement of relevant variables	✓
Provides accurate and reproducible measurements	≈
Provides interpretable data	✓
Is easy to use	✓
Is readily available	✓
Is operator-independent	✓
Has a rapid response time	✓
Causes no harm	✓
Is cost-effective	✓
Should provide information that is able to guide therapy	≈

Table 6.3: How IST satisfies the criteria for an ideal haemodynamic monitor. *(Vincent et al. 2011)*

The agreement between $\dot{Q}_{IST}$ and $\dot{Q}_T$ was weaker than agreement between $\Delta\dot{Q}_{IST}$ and $\Delta\dot{Q}_T$. Clinically, absolute values only offer limited information, whereas the temporal variation in values (the % change in $\dot{Q}$) from what is 'normal' for each individual patient provides greater clinical insight (Le Manach et al. 2014). $\dot{Q}_{IST}$ tends to underestimate $\dot{Q}$ to a greater degree at higher $\dot{Q}$. This is seen in the time series comparisons of $\dot{Q}$ (Figures 6.1 and 6.2) and in Bland-Altman analysis (Figure 6.3. This proportional bias could be a consequence of the recirculation of the N_2O sinewave emerging at higher cardiac outputs. This recirculation would violate the assumptions of the model presented in Figure 2.8. Further adjustments to the model are needed to improve the trending (and absolute agreement) of $\dot{Q}_{IST}$ vs $\dot{Q}_T$.

6.4.1 Limitations.

$\dot{Q}_{IST}$ was calculated as a rolling average over a 3 min period, with an updated value produced every 30 s. The window time of 3 min was chosen because it captures three full sinewave periods and allows production of robust solutions from the model. This approach has two potential consequences:

1. The dynamic component of the the $\dot{Q}$ time series will be damped. However, discounting acute emergencies, $\dot{Q}$ changes over the course of minutes rather than seconds and the impact of using a 3 min window to calculate a rolling average should not have a significant impact.

2. There will be a lag-time between real-time $\dot{Q}$ changes and their registration by IST. The lag-time is accounted for in the current analysis by comparing measurements of $\dot{Q}_{IST}$ against measurement of $\dot{Q}_T$ taken 60s previously. This correction is common to other systems which use a rolling average (LiDCO, Deltex) and needs to be taken into consideration.

Another limitation is that the presented data were collected in a mechanically ventilated animal model with no spontaneous ventilatory effort. They may, therefore, not necessarily translate to mechanically ventilated humans, nor to those who are spontaneously breathing or having assisted ventilation. A dedicated trial in humans is required to validate IST masurements of $\dot{Q}$ in humans.

There are certain limitations with the statistical approaches used in the current study. Four-quadrant and polar analyses assume that small changes in $\Delta\dot{Q}$ are caused by noise, but the definition of that noise is arbitrarily defined. Furthermore the polar analysis exclusion zone may inadvertently remove the most discordant measurements *i.e.* those that have similar absolute values but in opposite directions (Saugel et al. 2015). The direction of change concordance rate calculation used in four quadrant plot analysis does not account for the magnitude of variation, only its direction (Saugel et al. 2015).

As with other respiratory based approaches, the presence of lung injury will likely impair aspects of the performance of IST to emsure $\dot{Q}$. The saline lavage model of acute lung injury in the current study reduced the trending ability and concordance

of $\dot{Q}_{IST}$. The mean polar angle became wider (6^o uninjured vs 22^o injured), and the concordance from a four-quadrant plot became poorer (93% uninjured vs 90% injured). There was also a much flatter linear relationship between measurement of $\Delta\dot{Q}_{IST}$ and $\Delta\dot{Q}_T$ in the injured lung compared to the uninjured lung ($y = 0.30x+0.1$ vs $y = 0.65x + 0.01$ respectively). These equations reflect $\Delta\dot{Q}_{IST}$'s underestimation of changes in $\dot{Q}$ relative to $\Delta\dot{Q}_T$ in the injured lung. Any portion of $\dot{Q}$ that bypasses ventilated regions of the lung cannot be quantified by IST. This is likely to be the main explanation for the impaired ability of IST to measure $\dot{Q}$ and is supported by the finding of a significant negative correlation of $\dot{Q}_{IST}$ with shunt fraction (Figure 6.4). However, it might be possible to account for the effect of shunt on measurements of $\dot{Q}_{IST}$ with further refinement of the lung model. Taking the measurements as they are, without correction for $\dot{Q}_S/\dot{Q}_T$, they estimate 'effective' $\dot{Q}$, *i.e.* blood flow that participates in pulmonary gas exchange. This is common to all respiratory based techniques and might provide important clinical information in the critically ill patient. For example, a measured increase in $\dot{Q}_{IST}$ should improve oxygenation and CO_2 elimination independently of any change in $\dot{Q}$. Thus, changes in $\dot{Q}_{IST}$ might provide important additional information in the optimisation of ventilator settings.

6.4.2 Conclusions.

This chapter presents a novel, non-invasive and continual method (IST) to monitor $\dot{Q}$. It was shown that during pharmacologically-induced haemodynamic changes in 8 anaesthetised pigs, $\dot{Q}_{IST}$ demonstrated a marginal-good trending ability, based upon four-quadrant plot and polar analysis, compared to the reference method of PAC thermodilution ($\dot{Q}_T$). Consistent with other respiratory based methods, a saline-lavage model of lung injury impaired the performance of $\dot{Q}_{IST}$ and the impairment was related to the degree of shunt fraction. This study supports refinement of the lung model used in IST with the aims of improving $\dot{Q}_{IST}$ measurements and the performance of $\dot{Q}_{IST}$ in the presence of significant pulmonary shunt.

CHAPTER 7

General discussion and conclusions

7.1 General discussion

This thesis extends our understanding of the application of real-time P_aO_2 measurements and IST to the measurement of cyclical atelectasis, functional lung volume and $\dot{Q}$ in a mechanically ventilated porcine model of ARDS.

Chapter 3 presents the results of experiments investigating the relationship between dynamic changes in P_aO_2 and atelectasis in anaesthetised, mechanically ventilated pigs with saline-lavage lung injury. Dynamic respiratory P_aO_2 oscillations were demonstrated during tidal ventilation and increased in amplitude when CT markers of tidal CA increased. The magnitude of this association was not as large as expected. Additionally, significant CA was found only during tidal ventilation when the expiratory time was longer than the inspiratory time. During all types of imposed breath-hold manoeuvre, there was an increase in lung collapse. This was true even during a 30 s large inspiratory breath-hold manoeuvre (with a V_T of 20 ml kg^{-1}). The increase in lung collapse was associated with significant reduction in P_aO_2 during these manoeuvres. The study presented in Chapter 3 is important for two reasons (Crockett et al. 2019):

1. it is the first to contemporaneously measure dynamic CA and real-time P_aO_2
2. the results challenge the accepted hypothesis that CA is the main determinant of respiratory P_aO_2 oscillations in ARDS

Chapter 4 tests the hypothesis that the change in P_aO_2 measured over the course of imposed breath-hold manoeuvres can be used to estimate the volume of aerated or effective lung (ELV). Comparing ELV measurements estimated with P_aO_2 rate-of-decline and CT, it was shown that there is a strong linear relationship between absolute measurements of ELV taken with both techniques (ELV_{O_2} and ELV_{CT}) and that ELV_{O_2} tended to underestimate lung volume compared to ELV_{CT} in the uninjured lung. In both the ARDS model and uninjured lungs, changes in lung volume between PEEP levels measured by P_aO_2 rate-of-decline (ΔELV_{O_2}) could reliably track direction of change in volume with 93 - 100% concordance compared to CT (ΔELV_{CT}). Additionally, in the uninjured lung, ΔELV_{O_2} showed good agreement with ΔELV_{CT}, having minimal bias (- 45 ml) and within limits of agreement

of ± 237 ml. This method has not previously been experimentally tested. These novel results suggest that with a simple modification to an arterial line, estimation of underlying aerated lung volume of the mechanically ventilated patient could be possible.

Chapter 5 considers the use of IST as an alternative, non-invasive method of quantifying ELV. The presented study investigates the ability of IST to measure absolute ELV and changes in ELV compared to SF_6-washout (ELV_{SF6}) and CT (ELV_{CT}) in uninjured lungs and in an ARDS model of lung injury. In both uninjured lungs and in a saline-lavage model of ARDS, IST reliably measured absolute ELV comparably to SF_6 and CT ($r^2 = 0.87$ - 0.97), with a bias of -12 to -13% and within limits of agreement of ± 17 – 25%. Additionally, when comparing PEEP-induced changes in lung volume, IST's measurements were $> 98\%$ concordant with SF_6 and CT. This study was the first to experimentally test the ability of IST to measure lung volume during mechanical ventilation (Crockett et al. 2020).

Chapter 6 presents the results of experiments comparing IST's measurements of $\dot{Q}$ against those made with PAC thermodilution in a mechanically ventilated porcine model with and without lung injury. In the uninjured lung, there was a strong linear relationship between $\dot{Q}_{IST}$ and $\dot{Q}_T$ ($r^2 = 0.88$) and good agreement (bias = - 0.5 l min^{-1}, LOA -2.4 to +1.3 l min^{-1}). Likewise, in the uninjured lung, IST tracked changes in lung volume ($\Delta\dot{Q}_{IST}$) with good agreement to $\Delta\dot{Q}_T$ (bias - 0.1 l min^{-1}, LOA - 0.9 to + 1.2 l min^{-1}). In the injured lung, the linear relationship between $\dot{Q}_{IST}$ and $\dot{Q}_T$ was weaker ($r^2 = 0.64$) with a bias of - 1.0 l min^{-1} (LOA - 6.7 to + 1.2 l min^{-1}. Similarly, in the injured lung, the agreement between $\Delta\dot{Q}_{IST}$ and $\Delta\dot{Q}_T$ was relatively weaker (bias = - 0.2 l min^{-1}, LOA -1.7 to + 1.7 l min^{-1}). The novelty of this study is in its experimental testing of IST and demonstration that it can monitor changes in $\dot{Q}$ (Bruce et al. 2019).

7.2 Strengths and limitations of the P_aO_2 probes

The fluorescence quenching fibreoptic P_aO_2 probes are proven in their ability to measure PO_2 in fluids, including blood, *in vitro* (Chen et al. 2013; Formenti et al. 2014; Chen et al. 2016; Formenti et al. 2017b). However, their *in vivo* use has

not been formally studied in terms of repeatability and reproducibility of results. Probes are manufactured either out of silica or polymer. Early in the development of the probes silica was used because the tip of the fibre was more easily shaped and doped with luminophore matrix. However, in previous unpublished work, users had found that the shearing forces induced *in vivo* with the probes *in situ* meant that the tips of the probes could break. This makes the silica probes unsuitable for use in humans. Formal assessment of the engineering of the probes is beyond the scope of the research presented here. Qualitatively, however, there are some hurdles to translation which must be overcome to ensure successful adoption to human medicine. One example of this is the signal:noise ratio which appears to be variable between different probes. This is thought to be secondary to the balance of physical properties of the individual probe and is something that can be standardised in the manufacturing process. The probes used in the studies presented here were developed for experimental purposes.

The ability to monitor P_aO_2 continuously in real-time in unwell patients is an attractive prospect. Firstly, it would provide immediate information on the effectiveness of interventions and on deterioration in P_aO_2. Intuitively, this is of interest as a clinical monitor and would allow titration of therapies to optimise P_aO_2. Secondly, real-time P_aO_2 measurements can demonstrate oscillations in P_aO_2. As has been demonstrated here, P_aO_2 oscillations may be both a cause of lung injury (Boehme et al. 2019) and a result of injurious ventilation (Baumgardner et al. 2002). Thirdly, as has been demonstrated in Chapter 4, continuous P_aO_2 monitoring can provide information on the volume of lung partaking in gas exchange. Clearly, whether any or all of these potential applications can impact the outcome of critically unwell patients will require testing with well designed prospective RCT's.

7.3 Strengths and limitations of IST

IST's strengths lie in the commercial availability of its component parts, its of use at the bedside and its independence from input of the operator and patient. IST does not rely on a fixed inspiratory flow and therefore can be used in spontaneously ventilating patients (Phan et al. 2017b; Bruce et al. 2018).

In this thesis, IST's measurements of ELV and $\dot{Q}$ have been experimentally tested. However, IST also provides measurements of deadspace volume. Indeed, a modification of the Bohr method was proposed as a recent development of IST (Phan et al. 2017a). However, this modification is not currently part of IST's software. Despite the proposition that the modified Bohr adaptation would improve the accuracy and repeatability of the airway dead space estimation and therefore the estimation of total lung volume produced by IST.

IST is currently based on a model consisting of a deadspace volume, an alveolar volume and the blood flow to that alveolar volume. The three compartment model does not reflect the complex physiology of the cardiopulmonary system. Recently, a multi-compartmental computational model has been presented which comprises conducting airways and one hundred parallel alveolar compartments, each with its own corresponding set of parameters for stiffness, opening pressure and vascular resistance. The model also includes physiological reflexes such as hypoxic pulmonary vasoconstriction (Das et al. 2015; Chikhani et al. 2016). However, a benefit of IST's simplicity, in terms of its component parts and modelling, is that it can potentially be updated to account for developments in hardware and software.

7.4 Experimental limitations

In addition to the specific limitations of each set of experiments presented in the experimental chapters, some general limitations are discussed below.

7.4.1 The use of an animal model of ARDS

A limitation common to all the conducted experiments is that they were carried out in an animal model of ARDS. Both the use of a porcine model and the chosen saline-lavage model of lung injury have limitations. In general, direct translation of results to human medicine is not possible. However, pre-clinical models, such as that used throughout this thesis, provide crucial information to ensure appropriate and safe translation of new technologies to man. As a model of ARDS, saline-lavage is established, however it cannot reproduce the heterogeneous features of ARDS

seen clinically. The benefit of the saline-lavage model is that it produces recruitable collapse (Boehme et al. 2015), which was the main feature desired for experiments in Chapter 3.

7.4.2 CT image analysis

CT imaging was used as a reference technique in Chapters 3, 4 and 5. Different radiological compartments of lung (normally aerated, poorly aerated, atelectatic and overdistended) were segmented based on their voxel density. The thresholds for each compartment were based on previous literature using CT studies of lung parenchyma (Gattinoni et al. 1988; Lundquist et al. 1995; Vieira et al. 1998). However, this leaves open the possibility that clusters of voxels exist on one side or another of a threshold value and although a voxel cluster may tend towards collapse, for example, it may have not been counted in the analysis.

7.4.3 Does the single slice imaged in dCT represent the rest of the lung?

One limitation of using dynamic CT to study changes in atelectasis is that it can only image a single slice of the lung. Thus, any changes seen may not be representative of changes throughout the lung. During ventilation, the parenchyma imaged changes tidally as the lung moves caudally and cranially within the thorax. The ideal method would be imaging of the whole thorax dynamically during ventilation, however this is not currently possible and in a porcine model, CT densities measured with single-slice dCT agree well with dual-energy whole lung scans (Cronin et al. 2019).

7.4.4 The timing of the "start" of a breath hold.

Analyses of P_aO_2 traces during breath-hold manoeuvres were used in Chapters 3 and 4. One question which has yet to be definitively answered is how the observed change in P_aO_2 temporally aligns with the induced change P_{AW}. In this thesis analyses were carried out either from the start of the change in the airway pressure

trace (Chapter 3) or in the last 5 seconds of P_aO_2 decline (Chapter 4. Whether or not these represent where the continuous P_aO_2 signal truly deviates secondary to the imposed change in airway pressure is not clear. Qualitative visual examination of the P_aO_2 traces during imposed breath hold manoeuvres suggests there is a variable delay in when deviation in the P_aO_2 signal responds to a forced change in P_{AW}, however, the timing/effect is not consistent.

7.5 Future directions

7.5.1 Translating new technologies into human medicine

The main reason to undertake pre-clinical research is to identify methods/techniques that would be of benefit to human medicine. IST has already been used in human subjects (Bruce et al. 2018) and a feasbililty study of the technique is underway in mechanically ventilated intensive care patients (www.ClinicalTrials.gov identifier: NCT03424798). The results from IST presented in this thesis support its translation to the intensive care setting as a clinical monitor of both lung volume and $\dot{Q}$.

Real-time measurement of P_aO_2 has yet to achieved in humans, however, the platinum-doped polymer probes used in the experiments in this thesis are non-toxic and non-breakable. They have, therefore, overcome the problems associated with previous fluorescence quenching probes which were breakable and contained a toxic ruthenium fluorophore. The next step in development of the probes should be to undertake first-in-man studies of safety and feasiblity.

7.5.2 Investigating the role of pulmonary perfusion in understanding P_aO_2 oscillations

The findings from Chapter 3 support the hypothesis that there are other factors contributing to respiratory P_aO_2 oscillations in the ARDS lung besides CA. One of the main factors which has not been examined in this thesis is the dynamic role of pulmonary perfusion within the context of complex pulmonary responses to mechanical

ventilation (Pelosi et al. 2015; Formenti et al. 2017b). Recent evidence demonstrates that during inspiration, in a similar animal model of ARDS, gas distributes to non-dependent lung regions whereas blood volume redistributes to dependent regions (Cronin et al. 2020). This supports the role of dynamic changes in perfusion as a potential contributor to cyclical oscillations in P_aO_2. Whether or not dynamic changes in atelectasis or perfusion are the dominant cause of P_aO_2 oscillations, being able to identify oscillations remains important. P_aO_2 oscillations themselves have induced lung, vascular endothelial and myocyte inflammation (Boehme et al. 2019; Wu et al. 2016a; Wu et al. 2016b) and their presence has been associated with brain injury (Thomas et al. 2017).

7.5.3 Investigating the phenomenon of paradoxical changes in P_aO_2

During the course of collecting data using the fibreoptic P_aO_2 probes, the majority of observed oscillations during tidal ventilation followed the predicted pattern of P_aO_2 increasing during inspiration and decreasing during expiration. These orthodox P_aO_2 oscillations were in contrast to occasionally observed paradoxical oscillations where the P_aO_2 decreased in inspiration and increased in expiration. Paradoxical oscillations have been previously reported in an uninjured, ventilated animal model of hypovolaemia and were attributed to cyclical variation in $\dot{V}/\dot{Q}$ caused by pulmonary blood flow limitation by high inspiratory pressures (Bodenstein et al. 2013). Redistribution of pulmonary blood flow to non-ventilated and non-dependent areas has been demonstrated and is thought to be caused by the transmission of P_{AW} to ventilated alveoli and lack of transmission of P_{AW} to areas that are not ventilated (Musch et al. 2004; Cronin et al. 2020). Full interrogation of the physiological causes of paradoxical P_aO_2 oscillations has not yet been undertaken.

7.5.4 Testing IST's measurements of deadspace

Increased amount of pulmonary deadspace has been demonstrated as an independent predictor of survival in ARDS (Nuckton et al. 2002; Kallet et al. 2004; Gattinoni et al. 2006). Difficulty in bedside quantification of physiological deadspace has

lead to alternative non-invasive capnographic methods (Jonson 2018). IST has the potential to provide non-invasive measurements of deadspace which would help guide ventilation of patients with ARDS. Future work could test IST's ability to estimate deadspace fraction compared to volume capnography.

7.6 Conclusions

The results presented in this thesis demonstrate applications of two relatively novel technologies to measure cardiopulmonary physiology in a mechanically ventilated, saline-lavage model of porcine lung injury. Tidal oscillations in P_aO_2 were not as large as expected and were not as strongly associated with CT estimates of CA as expected. ELV can be estimated minimally-invasively by using a model of P_aO_2 change during the course of imposed breath-hold manoeuvres and non-invasively using IST during tidal ventilation. Likewise, IST can be used to continuously track $\dot{Q}$. Future work should focus on refining the techniques to allow translation to human practice.

References

Abbas, S M and A G Hill (2008). 'Systematic review of the literature for the use of oesophageal Doppler monitor for fluid replacement in major abdominal surgery'. *Anaesthesia* 63.1, pp. 44–51.

Acute Respiratory Distress Syndrome Network, R G Brower, M A Matthay et al. (2000). 'Ventilation with lower tidal volumes as compared with traditional tidal volumes for acute lung injury and the acute respiratory distress syndrome'. *New England Journal of Medicine* 342.18, pp. 1301–1308.

Albert, S P, J DiRocco, G B Allen et al. (2009). 'The role of time and pressure on alveolar recruitment'. *Journal of Applied Physiology* 106.3, pp. 757–765.

Albu, G, F Petak, T Zand et al. (2014). 'Lung volume assessments in normal and surfactant depleted lungs: Agreement between bedside techniques and CT imaging'. *BMC Anesthesiology* 14.1, pp. 1–9.

Amato, M B, C S Barbas, D M Medeiros et al. (1995). 'Beneficial effects of the "open lung approach" with low distending pressures in acute respiratory distress syndrome. A prospective randomized study on mechanical ventilation.' *American Journal of Respiratory and Critical Care Medicine* 152.6, pp. 1835–1846.

Amato, M B, C S Barbas, D M Medeiros et al. (1998). 'Effect of a protective-ventilation strategy on mortality in the acute respiratory distress syndrome'. *New England Journal of Medicine* 338.6, pp. 347–354.

Amato, M B, M O Meade, A S Slutsky et al. (2015). 'Driving pressure and survival in the acute respiratory distress syndrome'. *New England Journal of Medicine* 372.8, pp. 747–755.

Ashbaugh, D G, D B Bigelow, T L Petty et al. (1967). 'Acute respiratory distress in adults'. *Lancet* 2.7511, pp. 319–323.

Avignon, P D, G Hedenstrom and C Hedman (1956). 'Pulmonary complications in respirator patients.' eng. *Acta medica Scandinavica. Supplementum* 316, pp. 86–90.

Aya, H. D., M. Cecconi, M. Hamilton et al. (2013). 'Goal-directed therapy in cardiac surgery: A systematic review and meta-analysis'. *British Journal of Anaesthesia* 110.4, pp. 510–517.

Barton, S, A Black and C Hahn (1988). 'Dynamic Models and Solutions for Evaluating Ventilation, Perfusion, and Mass Transfer in the Lung—Part I: The Models'. *IEEE Transactions on Biomedical Engineering* 35.6, pp. 450–457.

Baumgardner, J, K Markstaller, B Pfeiffer et al. (2002). 'Effects of Respiratory Rate, Plateau Pressure, and Positive End-Expiratory Pressure on PaO2 Oscillations after Saline Lavage'. *American Journal of Respiratory and Critical Care Medicine* 166.12, pp. 1556–1562.

Baumgardner, J, C Otto and K Markstaller (2013). 'Cyclic recruitment of atelectasis - Are there implications for our clinical practice?' *Trends in Anaesthesia and Critical Care* 3.4, pp. 205–210.

Beitler, J R, E C Goligher, M Schmidt et al. (2016). 'Personalized medicine for ARDS: the 2035 research agenda'. *Intensive Care Medicine* 42.5, pp. 756–767.

Bellani, G, J Laffey, T Pham et al. (2016). 'Epidemiology, Patterns of Care, and Mortality for Patients With Acute Respiratory Distress Syndrome in Intensive Care Units in 50 Countries'. *Journal of the American Medical Association* 315.8, pp. 788–800.

Bergman, N A (1961). 'Cyclic variations in blood oxygenation with the respiratory cycle'. *Anesthesiology* 22, pp. 900–908.

Biancofiore, G, L Critchley, A Lee et al. (2009). 'Evaluation of an uncalibrated arterial pulse contour cardiac output monitoring system in cirrhotic patients undergoing liver surgery'. *British Journal of Anaesthesia* 102.1, pp. 47–54.

Bland, J and D Altman (1986). 'Statistical Methods for Assessing Agreement Between Two Methods of Clinical Measurement'. *Lancet* 327, pp. 307–310.

— (1999). 'Measuring agreement in method comparison studies'. *Statistical Methods in Medical Research* 8.2, pp. 135–160.

— (2007). 'Agreement between methods of measurement with multiple observations per individual'. *Journal of Biopharmaceutical Statistics* 17.4, pp. 571–582.

Blankman, P, A Shono, B J Hermans et al. (2016). 'Detection of optimal PEEP for equal distribution of tidal volume by volumetric capnography and electrical impedance tomography during decreasing levels of PEEP in post cardiac-surgery patients'. *British Journal of Anaesthesia* 116.6, pp. 862–869.

Bodenstein, M, S Bierschock, S Boehme et al. (2013). 'Influence of fluid and volume state on PaO2 oscillations in mechanically ventilated pigs'. *Experimental Lung Research* 39.2, pp. 80–90.

Bodenstein, M, S Boehme, H Wang et al. (2014). 'Hints for cyclical recruitment of atelectasis during ongoing mechanical ventilation in lavage and oleic acid lung injury detected by SpO2 oscillations and electrical impedance tomography'. *Experimental Lung Research* 40.9, pp. 427–438.

Bodenstein, M, H Wang, S Boehme et al. (2010). 'Observation of ventilation-induced SpO2 oscillations in pigs: first step to noninvasive detection of cyclic recruitment of atelectasis?' *Experimental Lung Research* 36.5, pp. 270–276.

Boehme, S, A Bentley, E Hartmann et al. (2015). 'Influence of inspiration to expiration ratio on cyclic recruitment and derecruitment of atelectasis in a saline lavage model of acute respiratory distress syndrome'. *Critical Care Medicine* 43.3, pp. 65–74.

Boehme, S, E Hartmann, T Tripp et al. (2019). 'PO2 oscillations induce lung injury and inflammation'. *Critical Care* 23.1, pp. 1–12.

Bone, R C (1993). 'The ARDS Lung: New Insights From Computed Tomography'. *Journal of the American Medical Association* 269.16, pp. 2134–2135.

Branthwaite, M A and R D Bradley (1968). 'Measurement of cardiac output by thermal dilution in man.' *Journal of Applied Physiology* 24.3, pp. 434–438.

Breukers, R M, S Sepehrkhouy, S R Spiegelenberg et al. (2007). 'Cardiac Output Measured by a New Arterial Pressure Waveform Analysis Method Without Calibration Compared With Thermodilution After Cardiac Surgery'. *Journal of Cardiothoracic and Vascular Anesthesia* 21.5, pp. 632–635.

Brewer, L M, J A Orr, M R Sherman et al. (2011). 'Measurement of functional residual capacity by modified multiple breath nitrogen washout for spontaneously breathing and mechanically ventilated patients'. *British Journal of Anaesthesia* 107.5, pp. 796–805.

Briel, M, M Meade, A Mercat et al. (2010). 'Higher vs lower positive end-expiratory pressure in patients with acute lung injury and acute respiratory distress syndrome: systematic review and meta-analysis'. *Journal of the American Medical Association* 303.9, pp. 865–873.

Brower, R, R A Wise, C Hassapoyannes et al. (1985). 'Effect of lung inflation on lung blood volume and pulmonary venous flow'. *Journal of Applied Physiology* 58.3, pp. 954–963.

Bruce, R, D C Crockett, A Morgan et al. (2019). 'Noninvasive cardiac output monitoring in a porcine model using the inspired sinewave technique: a proof-of-concept study'. *British Journal of Anaesthesia* 123.2, pp. 126–134.

Bruce, R, P Phan, E Pacpaco et al. (2018). 'The inspired sine-wave technique: A novel method to measure lung volume and ventilatory heterogeneity'. *Experimental Physiology* 103.5, pp. 738–747.

Cavalcanti, A B (2017). 'Effect of Lung Recruitment and Titrated Positive End-Expiratory Pressure (PEEP) vs Low PEEP on Mortality in Patients With Acute Respiratory Distress Syndrome A Randomized Clinical Trial Writing Group for the Alveolar Recruitment for Acute Respiratory Dist'. *Journal of the American Medical Association* 318.14, pp. 1335–1345.

Chen, R, A Farmery, A Obeid et al. (2012a). 'A Cylindrical-Core Fiber-Optic Oxygen Sensor Based on Fluorescence Quenching of a Platinum Complex Immobilized in a Polymer Matrix'. *IEEE Sensors* 12.1, pp. 71–75.

Chen, R, F Formenti, H McPeak et al. (2014). 'Optimizing design for polymer fiber optic oxygen sensors'. *IEEE Sensors* 14.10, pp. 3358–3364.

— (2016). 'Experimental investigation of the effect of polymer matrices on polymer fibre optic oxygen sensors and their time response characteristics using a vacuum testing chamber and a liquid flow apparatus'. *Sensors and Actuators B: Chemical* 222, pp. 531–535.

Chen, R, F Formenti, A Obeid et al. (2013). 'A fibre-optic oxygen sensor for monitoring human breathing'. *Physiological Measurement* 34.9, pp. 71–81.

Chen, R, C Hahn and A Farmery (2012b). 'A flowing liquid test system for assessing the linearity and time-response of rapid fibre optic oxygen partial pressure sensors'. *Respiratory Physiology and Neurobiology* 183.2, pp. 100–107.

Chikhani, M, A Das, M Haque et al. (2016). 'High PEEP in acute respiratory distress syndrome: quantitative evaluation between improved arterial oxygenation and decreased oxygen delivery'. *British Journal of Anaesthesia* 117.5, pp. 650–658.

Chiumello, D, E Carlesso, P Cadringher et al. (2008a). 'Lung stress and strain during mechanical ventilation for acute respiratory distress syndrome'. *American Journal of Respiratory and Critical Care Medicine* 178, pp. 346–355.

Chiumello, D, M Cressoni, M Chierichetti et al. (2008b). 'Nitrogen washout/washin, helium dilution and computed tomography in the assessment of end expiratory lung volume'. *Critical Care* 12.R150, pp. 1–8.

Ciaffoni, L, D P O'Neill, J H Couper et al. (2016). 'In-airway molecular flow sensing: A new technology for continuous, noninvasive monitoring of oxygen consumption in critical care'. *Science Advances* 2.8, pp. 1–10.

Clausen, J (1997). 'Measurement of absolute lung volumes by imaging techniques'. *European Respiratory Journal* 10.10, pp. 2427–2431.

Clifton, L, D Clifton, C Hahn et al. (2013). 'Assessment of lung function using a non-invasive oscillating gas-forcing technique'. *Respiratory Physiology and Neurobiology* 189.1, pp. 174–182.

Connors, A F, T Speroff, N V Dawson et al. (1996). 'The effectiveness of right heart catheterization in the initial care of critically ill patients'. *Journal of the American Medical Association* 276.11, pp. 889–897.

Consuelo-Bachmann, M, C Morais, G Bugedo et al. (2018). 'Electrical impedance tomography in acute respiratory distress syndrome'. *Critical Care* 22.1, pp. 1–11.

Criée, C P, S Sorichter, H J Smith et al. (2011). 'Body plethysmography - Its principles and clinical use'. *Respiratory Medicine* 105.7, pp. 959–971.

Critchley, L, A Lee and A Ho (2010). 'A Critical Review of the Ability of Continuous Cardiac Output Monitors to Measure Trends in Cardiac Output'. *Anesthesia & Analgesia* 111.5, pp. 1180–1192.

Critchley, L, X Yang and A Lee (2011). 'Assessment of trending ability of cardiac output monitors by polar plot methodology'. *Journal of Cardiothoracic and Vascular Anesthesia* 25.3, pp. 536–546.

Crockett, D C, J N Cronin, N Bommakanti et al. (2019). 'Tidal changes in PaO2 and their relationship to cyclical lung recruitment/derecruitment in a porcine lung injury model'. *British Journal of Anaesthesia* 122.2, pp. 277–285.

Crockett, D C, M T Tran, F Formenti et al. (2020). 'Validating the inspired sinewave technique to measure the volume of the "baby lung" in a porcine lung-injury model'. *British Journal of Anaesthesia* 124.3, pp. 345–353.

Cronin, J N, J B Borges, D C Crockett et al. (2019). 'Dynamic single-slice CT estimates whole-lung dual-energy CT variables in pigs with and without experimental lung injury'. *Intensive Care Medicine Experimental* 7.59, pp. 1–14.

Cronin, J N, D C Crockett, A D Farmery et al. (2020). 'Mechanical Ventilation Redistributes Blood to Poorly Ventilated Areas in Experimental Lung Injury'. *Critical Care Medicine* 48.3, pp. 200–208.

Das, A, L Camporota, J Hardman et al. (2019). 'What links ventilator driving pressure with survival in the acute respiratory distress syndrome? A computational study'. *Respiratory Research* 20.1, pp. 1–10.

Das, A, M Haque, M Chikhani et al. (2015). 'Development of an integrated model of cardiovascular and pulmonary physiology for the evaluation of mechanical ventilation strategies'. *Conference Proceedings: The Annual International Conference of the IEEE Engineering in Medicine and Biology Society.* Vol. 2015, pp. 5319–5322.

David, M, J Karmrodt, C Bletz et al. (2005). 'Analysis of atelectasis, ventilated, and hyperinflated lung during mechanical ventilation by dynamic CT'. *Chest* 128.5, pp. 3757–3770.

Di Marco, F, L Rota Sperti, B Milan et al. (2007). 'Measurement of functional residual capacity by helium dilution during partial support ventilation: In vitro accuracy and in vivo precision of the method'. *Intensive Care Medicine* 33.12, pp. 2109–2115.

Domino, K B, M J Emery, E R Swenson et al. (1998). 'Ventilation heterogeneity is increased in hypocapnic dogs but not pigs'. *Respiration Physiology* 111.1, pp. 89–100.

Dreyfuss, D, J D Ricard and S Gaudry (2015). 'Did studies on HFOV fail to improve ARDS survival because they did not decrease VILI? On the potential validity of

a physiological concept enounced several decades ago'. *Intensive Care Medicine* 41.12, pp. 2076–2086.

Dreyfuss, D, P Soler and G Saumon (1995). 'Mechanical ventilation-induced pulmonary edema: Interaction with previous lung alterations'. *American Journal of Respiratory and Critical Care Medicine* 151.5, pp. 1568–1575.

DuBois, A (1952). 'Alveolar CO2 and O2 during breath holding, expiration, and inspiration.' *Journal of Applied Physiology* 5.1, pp. 1–12.

DuBois, A, S Botelho, G Bedell et al. (1956). 'A rapid plethysmographic method for measuring thoracic gas volume: a comparison with a nitrogen washout method for measuring functional residual capacity in normal subjects.' *The Journal of Clinical Investigation* 35.3, pp. 322–326.

Dunn, J, M Grocott and M Mythen (2016). 'The place of goal-directed haemodynamic therapy in the 21st century'. *British Journal of Anaesthesia Education* 16.6, pp. 179–185.

Emmanuel, G, W A Briscoe and A Cournaud (1961). 'A method for the determination of the volume of air in the lungs: measurements in chronic pulmonary emphysema.' *The Journal of Clinical Investigation* 40.2, pp. 329–337.

Farmery, A (2008). 'Interrogation of the Cardiopulmonary System with Inspired Gas Tension Sinusoids'. PhD thesis. University of London, pp. 1–698.

Farmery, A and J Whiteley (2001). 'A mathematical model of electron transfer within the mitochondrial respiratory cytochromes'. *Journal of Theoretical Biology* 213.2, pp. 197–207.

Fedorov, A, Re Beichel, J Kalpathy-Cramer et al. (2012). '3D Slicer as an image computing platform for the Quantitative Imaging Network'. *Magnetic Resonance Imaging* 30.9, pp. 1323–1341.

Flecknell, P (2002). 'Replacement, Reduction, Refinement'. *Alternatives to Animal Experimentation* 19.2, pp. 73–38.

Folgering, H, F Smolders and F Kreuzer (1978). 'Respiratory oscillations of the arterial PO2 and their effects on the ventilatory controlling system in the cat'. *European Journal of Physiology* 375.1, pp. 1–7.

Formenti, F, N Bommakanti, R Chen et al. (2017a). 'Respiratory oscillations in alveolar oxygen tension measured in arterial blood'. *Scientific Reports* 7.7499, pp. 1–10.

Formenti, F, R Chen, H McPeak et al. (2014). 'A fibre optic oxygen sensor that detects rapid PO2 changes under simulated conditions of cyclical atelectasis in vitro'. *Respiratory Physiology and Neurobiology* 191.1, pp. 1–8.

Formenti, F, R Chen, H McPeak et al. (2015). 'Intra-breath arterial oxygen oscillations detected by a fast oxygen sensor in an animal model of acute respiratory distress syndrome'. *British Journal of Anaesthesia* 114.4, pp. 683–688.

Formenti, F and A Farmery (2017b). 'Intravascular oxygen sensors with novel applications for bedside respiratory monitoring'. *Anaesthesia* 72.1, pp. 95–104.

Frerichs, I, M Amato, A Van Kaam et al. (2017). 'Chest electrical impedance tomography examination, data analysis, terminology, clinical use and recommendations: Consensus statement of the TRanslational EIT developmeNt stuDy group'. *Thorax* 72.1, pp. 83–93.

Fretschner, R, H Deusch, A Weitnauer et al. (1993). 'A simple method to estimate functional residual capacity in mechanically ventilated patients'. *Intensive Care Medicine* 19.1, pp. 372–376.

Fu, Z, M L Costello, K Tsukimoto et al. (1992). 'High lung volume increases stress failure in pulmonary capillaries'. *Journal of Applied Physiology* 73.1, pp. 123–133.

Gattinoni, L, P Caironi, M Cressoni et al. (2006). 'Lung recruitment in patients with the acute respiratory distress syndrome'. eng. *New England Journal of Medicine* 354.17, pp. 1775–1786.

Gattinoni, L, P Caironi, P Pelosi et al. (2001). 'What Has Computed Tomography Taught Us about the Acute Respiratory Distress Syndrome?' *American Journal of Respiratory and Critical Care Medicine* 164.9, pp. 1701–1711.

Gattinoni, L, E Carlesso, P Cadringher et al. (2003). 'Physical and biological triggers of ventilator-induced lung injury and its prevention'. *European Respiratory Journal* 22.47, 15s–25s.

Gattinoni, L, J J Marini, F Collino et al. (2017). 'The future of mechanical ventilation: lessons from the present and the past'. *Critical Care* 21.1, p. 183.

Gattinoni, L, J J Marini, A Pesenti et al. (2016a). 'The "baby lung" became an adult'. *Intensive Care Medicine* 42.5, pp. 663–673.

Gattinoni, L, D Mascheroni, A Torresin et al. (1986a). 'Morphological response to positive end expiratory pressure in acute respiratory failure. Computerized tomography study'. eng. *Intensive Care Med* 12.3, pp. 137–142.

Gattinoni, L and A Pesenti (2005). 'The concept of "baby lung"'. *Intensive Care Med* 31.6, pp. 776–784.

Gattinoni, L, A Pesenti, L Avalli et al. (1987). 'Pressure-Volume Curve of Total Respiratory System in Acute Respiratory Failure. Computed Tomographic Scan Study'. *The American Review of Respiratory Disease* 136.3, pp. 730–736.

Gattinoni, L, A Pesenti, M Bombino et al. (1988). 'Relationships between lung computed tomographic density, gas exchange, and PEEP in acute respiratory failure'. *Anesthesiology* 69.6, pp. 824–832.

Gattinoni, L, A Presenti, A Torresin et al. (1986b). 'Adult respiratory distress syndrome profiles by computed tomography'. *Journal of Thoracic Imaging* 1.3, pp. 25–30.

Gattinoni, L, T Tonetti, M Cressoni et al. (2016b). 'Ventilator-related causes of lung injury: the mechanical power'. *Intensive Care Med* 42.10, pp. 1567–1575.

Gavaghan, D and C Hahn (1995). 'A mathematical evaluation of the alveolar amplitude response technique'. *Respiration Physiology* 102.1, pp. 105–120.

— (1996). 'A tidal breathing model of the forced inspired inert gas sinewave technique'. *Respiration Physiology* 106.2, pp. 209–221.

Goldman, M D, H J Smith and W T Ulmer (2005). 'Whole-body plethysmography'. *European Respiratory Monograph* 31.1, pp. 15–43.

Goligher, E, B Kavanagh, G Rubenfeld et al. (2014). 'Oxygenation response to positive end-expiratory pressure predicts mortality in acute respiratory distress syndrome. A secondary analysis of the LOVS and ExPress trials'. *American Journal of Respiratory and Critical Care Medicine* 190.1, pp. 70–76.

Grieco, D, L Chen, M Dres et al. (2017). 'Should we use driving pressure to set tidal volume?' *Current Opinion in Critical Care* 23.1, pp. 38–44.

Griffiths, M J D, D F McAuley, G D Perkins et al. (2019). 'Guidelines on the management of acute respiratory distress syndrome'. *British Medical Journal Open: Respiratory Research* 6.e000420, pp. 1–27.

Grocott, M, A Dushianthan, M Hamilton et al. (2012). 'Perioperative increase in global blood flow to explicit defined goals and outcomes following surgery'. *Cochrane Database of Systematic Reviews* 2012.11, pp. 1–113.

Guérin, C, L Papazian, J Reignier et al. (2016). 'Effect of driving pressure on mortality in ARDS patients during lung protective mechanical ventilation in two randomized controlled trials'. *Critical Care* 20.384, pp. 1–9.

Hahn, C (1996). 'Oxygen respiratory gas analysis by sine-wave measurement: a theoretical model'. *Journal of Applied Physiology* 81.2, pp. 998–1006.

Hahn, C, A Black, S Barton et al. (1993). 'Gas exchange in a three-compartment lung model analyzed by forcing sinusoids of N2O'. *Journal of Applied Physiology* 75.4, pp. 1863–1876.

Hahn, C and A Farmery (2003). 'Gas exchange modelling: No more gills, please'. *British Journal of Anaesthesia* 91.1, pp. 2–15.

Hallsjo-Sander, C, M Hallback, M Wallin et al. (2014). 'Novel continuous capnodynamic method for cardiac output assessment during mechanical ventilation'. *British Journal of Anaesthesia* 112.5, pp. 824–831.

Hallsjo-Sander, C, P A Lonnqvist, M Hallback et al. (2016). 'Capnodynamic assessment of effective lung volume during cardiac output manipulations in a porcine model'. *Journal of Clinical Monitoring and Computing* 30.6, pp. 761–769.

Halter, J M, J M Steinberg, H J Schiller et al. (2003). 'Positive end-expiratory pressure after a recruitment maneuver prevents both alveolar collapse and re-

cruitment/derecruitment'. *American Journal of Respiratory and Critical Care Medicine* 167.12, pp. 1620–1626.

Hamilton, M A, M Cecconi and A Rhodes (2011). 'A systematic review and meta-analysis on the use of preemptive hemodynamic intervention to improve post-operative outcomes in moderate and high-risk surgical patients'. *Anesthesia and Analgesia* 112.6, pp. 1392–1402.

Hannon, J, C Bossone and C Wade (1990). *Normal physiological values for conscious pigs used in biomedical research.* Tech. rep. 3, pp. 293–298.

Hartmann, E, S Boehme, A Bentley et al. (2012). 'Influence of respiratory rate and end-expiratory pressure variation on cyclic alveolar recruitment in an experimental lung injury model'. *Critical Care* 16.R8, pp. 1–11.

Harvey, S, D A Harrison, M Singer et al. (2005). 'Assessment of the clinical effectiveness of pulmonary artery catheters in management of patients in intensive care (PAC-Man): A randomised controlled trial'. *Lancet* 366.9484, pp. 472–477.

Hedenstierna, G (1993). 'The recording of FRC - is it of importance and can it be made simple?' *Intensive Care Medicine* 19.1, pp. 365–366.

Heinze, H and W Eichler (2009). 'Measurements of functional residual capacity during intensive care treatment: the technical aspects and its possible clinical applications'. *Acta Anaesthesiologica Scandinavica Scand* 53.1, pp. 1121–1130.

Heinze, H, B Schaaf, J Grefer et al. (2007). 'The accuracy of the oxygen washout technique for functional residual capacity assessment during spontaneous breathing'. *Anesthesia and Analgesia* 104.3, pp. 598–604.

Heldt, G P and R M Peters (1978). 'A simplified method to determine functional residual capacity during mechanical ventilation'. *Chest* 74.5, pp. 492–496.

Helm, E, O Talakoub, F Grasso et al. (2009). 'Use of dynamic CT in acute respiratory distress syndrome (ARDS) with comparison of positive and negative pressure ventilation'. *European Radiology* 19.1, pp. 50–57.

Herweling, A, J Karmrodt, A Stepniak et al. (2005). 'A novel technique to follow fast PaO2 variations during experimental CPR'. *Resuscitation* 65.1, pp. 71–78.

Heyland, D K, D J Cook, D King et al. (1996). 'Maximizing oxygen delivery in critically ill patients: A methodologic appraisal of the evidence'. *Critical Care Medicine* 24.3, pp. 517–524.

Hubmayr, R D and R H Kallet (2018). 'Understanding Pulmonary Stress-Strain Relationships in Severe ARDS and Its Implications for Designing a Safer Approach to Setting the Ventilator'. *Respiratory Care* 63.2, pp. 219–226.

Hubrecht, R C and J Kirkwood (2010). *The UFAW handbook on the care and management of laboratory and other research animals.* John Wiley & Sons.

Ingelstedt, S, B Jonson, L Nordström et al. (1972). 'A Servo-Controlled Ventilator Measuring Expired Minute Volume, Airway Flow and Pressure'. *Acta Anaesthesiologica Scandinavica* 16.s47, pp. 7–27.

Jansen, J R C, J J Schreuder, J P Mulier et al. (2001). 'A comparison of cardiac output derived from the arterial pressure wave against thermodilution in cardiac surgery patients'. *British Journal of Anaesthesia* 87.2, pp. 212–222.

Jonmarker, C, L Jansson, B Jonson et al. (1985). 'Measurement of functional residual capacity by sulfur hexaflouide washout'. *Anesthesiology* 63.1, pp. 89–95.

Jonson, B (2018). 'Volumetric capnography for noninvasive monitoring of acute respiratory distress syndrome'. *American Journal of Respiratory and Critical Care Medicine* 198.3, pp. 396–398.

Kacmarek, R M (2011). 'The Mechanical Ventilator: Past, Present, and Future'. *Respiratory Care* 56.8, pp. 1170–1180.

Kallet, R H, J A Alonso, J F Pittet et al. (2004). 'Prognostic value of the pulmonary dead-space fraction during the first 6 days of acute respiratory distress syndrome.' *Respiratory Care* 49.9, pp. 1008–1014.

Kern, J and W Shoemaker (2002). 'Meta-analysis of hemodynamic optimization in high-risk patients'. *Critical Care Medicine* 30.8, pp. 1686–1692.

Kilkenny, C, W J Browne, I C Cuthill et al. (2013). 'Improving bioscience research reporting: The arrive guidelines for reporting animal research'. *Animals* 4.1, pp. 35–44.

Klein, K, E Hartmann, S Boehme et al. (2013). 'PaO2 oscillations caused by cyclic alveolar recruitment can be monitored in pig buccal mucosa microcirculation'. *Acta Anaesthesiologica Scandinavica* 57.3, pp. 320–325.

Klein, K, A Johannes, M Bruckner et al. (2016). 'Systemic PaO2 Oscillations Cause Mild Brain Injury in a Pig Model'. *Critical Care Medicine* 44.5, pp. 253–263.

Klein, M, L Minkovich, M Machina et al. (2015). 'Non-invasive measurement of cardiac output using an iterative, respiration-based method'. *British Journal of Anaesthesia* 114.3, pp. 406–413.

Krogh, A and J Lindhard (1914). 'On the average composition of the alveolar air and its variations during the respiratory cycle'. *Journal of Physiology* 47.6, pp. 431–445.

Kumar, A, H Pontoppidan, K J Falke et al. (1973). 'Pulmonary barotrauma during mechanical ventilation.' eng. *Critical Care Medicine* 1.4, pp. 181–186.

Lachmann, B, B Robertson and J Vogel (1980). 'In Vivo Lung Lavage as an Experimental Model of the Respiratory Distress Syndrome'. *Acta Anaesthesiologica Scandinavica* 24.3, pp. 231–236.

Larsson, A, D Linnarsson, C Jonmarker et al. (1987). 'Measurement of lung volume by sulfur hexafluoride washout during spontaneous and controlled ventilation: further development of a method'. *Anesthesiology* 67.4, pp. 543–550.

Le Manach, Y and G Collins (2014). 'Statistical methods in hemodynamic research'. *Perioperative hemodynamic monitoring and goal directed therapy: from theory to practice.* Chap. 2, pp. 8–13.

Liu, S, L Tan, K Moller et al. (2016). 'Identification of regional overdistension, recruitment and cyclic alveolar collapse with electrical impedance tomography in an experimental ARDS model'. *Critical Care* 20.1, p. 119.

Lobo, S M, E Rezende, M F Knibel et al. (2011). 'Early determinants of death due to multiple organ failure after noncardiac surgery in high-risk patients'. *Anesthesia and Analgesia* 112.4, pp. 877–883.

Lorne, E, M Diouf, R B P de Wilde et al. (2018). 'Assessment of interchangeability rate between 2 methods of measurements: An example with a cardiac output comparison study.' *Medicine* 97.7, pp. 1–7.

Lundquist, H, G Hedenstierna, A Strandberg et al. (1995). 'CT-assessment of dependent lung densities in man during general anaesthesia.' *Acta Radiologica* 36.6, pp. 626–32.

Lutz, C J, D E Carney, A L Picone et al. (1999). 'Videomicroscopy provides accurate in vivo assessment of pulmonary microvascular reactivity in rabbits'. *Shock* 11.5, pp. 367–371.

Maisch, S, S H Boehm, D Weismann et al. (2007). 'Determination of functional residual capacity by oxygen washin-washout: a validation study'. *Intensive Care Med* 33.1, pp. 912–916.

Mancebo, J, A Mercat and L Brochard (2019). 'Maximal Lung Recruitment in ARDS: A Nail in the Coffin'. *American Journal of Respiratory and Critical Care Medicine*, pp. 1331–1333.

Marik, P (2013a). 'Noninvasive cardiac output monitors: A state-of the-art review'. *Journal of Cardiothoracic and Vascular Anesthesia* 27.1, pp. 121–134.

— (2013b). 'Obituary: pulmonary artery catheter 1970 to 2013'. *Annals of Intensive Care* 3.1, p. 38.

Markstaller, K, B Eberle, H Kauczor et al. (2001). 'Temporal dynamics of lung aeration determined by dynamic CT in a porcine model of ARDS'. *British Journal of Anaesthesia* 87.3, pp. 459–468.

Markstaller, K, H Kauczor, N Weiler et al. (2003). 'Lung density distribution in dynamic CT correlates with oxygenation in ventilated pigs with lavage ARDS'. *British Journal of Anaesthesia* 91.5, pp. 699–708.

Matthes, K (1935). 'Untersuchungen über die Sauerstoffsättigung des menschlichen Arterienblutes'. *Naunyn-Schmiedebergs Archiv für experimentelle Pathologie und Pharmakologie* 179.6, pp. 698–711.

Mead, J, T Takishima and D Leith (1970). 'Stress distribution in lungs: a model of pulmonary elasticity.' eng. *Journal of Applied Physiology* 28.5, pp. 596–608.

Meade, M O, D J Cook, G H Guyatt et al. (2008). 'Ventilation strategy using low tidal volumes, recruitment maneuvers, and high positive end-expiratory pressure for acute lung injury and acute respiratory distress syndrome: a randomized controlled trial.' eng. *Journal of the American Medical Association* 299.6, pp. 637–645.

Mercat, A, J Richard and B Vielle (2008). 'Positive end-expiratory pressure setting in adults with acute lung injury and acute respiratory distress syndrome: A randomized controlled trial'. *Journal of the American Medical Association* 299.6, pp. 646–655.

Mertens, M, A Tabuchi, S Meissner et al. (2009). 'Alveolar dynamics in acute lung injury: Heterogeneous distension rather than cyclic opening and collapse'. *Critical Care Medicine* 37.9, pp. 2604–2611.

Mitchell, R R, R M Wilson, L Holzapfel et al. (1982). 'Oxygen wash-in method for monitoring functional residual capacity.' *Critical care medicine* 10.8, pp. 529–533.

Møller-Sørensen, H, J Cordtz, M Østergaard et al. (2017). 'Transesophageal Doppler reliably tracks changes in cardiac output in comparison with intermittent pulmonary artery thermodilution in cardiac surgery patients'. *Journal of Clinical Monitoring and Computing* 31.1, pp. 135–142.

Mountain, J, P Santer, D O'Neill et al. (2018). 'Potential for noninvasive assessment of lung inhomogeneity using highly precise, highly time-resolved measurements of gas exchange'. *Journal of Applied Physiology* 124.3, pp. 615–631.

Muscedere, J G, J B Mullen, K Gan et al. (1994). 'Tidal ventilation at low airway pressures can augment lung injury'. eng. *American Journal of Respiratory and Critical Care Medicine* 149.5, pp. 1327–1334.

Musch, G, R S Harris, M F Vidal Melo et al. (2004). 'Mechanism by which a sustained inflation can worsen oxygenation in acute lung injury'. *Anesthesiology* 100.2, pp. 323–330.

Myles, P S and J Cui (2007). 'I. Using the Bland-Altman method to measure agreement with repeated measures'. *British Journal of Anaesthesia* 99.3, pp. 309–311.

Mythen, M and A Webb (1995). 'Perioperative Plasma Volume Expansion Reduces the Incidence of Gut Mucosal Hypoperfusion During Cardiac Surgery'. *Archives of Surgery* 130.4, pp. 423–429.

Nakagawa, S and H Schielzeth (2013). 'A general and simple method for obtaining R2 from generalized linear mixed-effects models'. *Methods in Ecology and Evolution* 4.2, pp. 133–142.

Neumann, P, J E Berglund, E Fernandez Mondejar et al. (1998). 'Dynamics of lung collapse and recruitment during prolonged breathing in porcine lung injury'. *Journal of Applied Physiology* 85.4, pp. 1533–1543.

Newth, C, P Enright and R Johnson (1997). 'Multiple-breath nitrogen washout techniques: Including measurements with patients on ventilators'. *European Respiratory Journal* 10.9, pp. 2174–2185.

Nieman, G F, C E Bredenberg, W R Clark et al. (1981). 'Alveolar function following surfactant deactivation.' *Journal of Applied Physiology* 51.4, pp. 895–904.

Nuckton, T J, J A Alonso, R H Kallet et al. (2002). 'Pulmonary dead-space fraction as a risk factor for death in the acute respiratory distress syndrome'. *New England Journal of Medicine* 346.17, pp. 1281–1286.

O'Donnell, C R, A A Bankier, L Stiebellehner et al. (2010). 'Comparison of plethysmographic and helium dilution lung volumes: Which is best for COPD?' *Chest* 137.5, pp. 1108–1115.

Older, P and R Smith (1988). 'Experience with the preoperative invasive measurement of haemodynamic, respiratory and renal function in 100 elderly patients scheduled for major abdominal surgery'. *Anaesthesia and Intensive Care* 16.4, pp. 389–395.

Older, P, R Smith, P Courtney et al. (1993). 'Preoperative evaluation of cardiac failure and ischemia in elderly patients by cardiopulmonary exercise testing'. *Chest* 104.3, pp. 701–704.

Olegård, C, S Söndergaard, E Houltz et al. (2005). 'Estimation of functional residual capacity at the bedside using standard monitoring equipment: a modified nitrogen washout/washin technique requiring a small change of the inspired oxygen fraction'. *Anesthesia and Analgesia* 101.1, pp. 206–212.

Olegard, C, S Sondergaard, J Palsson et al. (2010). 'Validation and clinical feasibility of nitrogen washin/washout functional residual capacity measurements in children'. *Acta Anaesthesiologica Scandinavica* 54.3, pp. 370–376.

Otto, C, K Markstaller, O Kajikawa et al. (2008). 'Spatial and temporal heterogeneity of ventilator-associated lung injury after surfactant depletion'. *Journal of Applied Physiology* 104.5, pp. 1485–1494.

Patroniti, N, M Saini, A Zanella et al. (2008). 'Measurement of end-expiratory lung volume by oxygen washin-washout in controlled and assisted mechanically ventilated patients'. *Intensive Care Medicine* 34.1, pp. 2235–2240.

Pearse, R, D Dawson, J Fawcett et al. (2005). 'Early goal-directed therapy after major surgery reduces complications and duration of hospital stay. A randomised, controlled trial.' *Critical Care* 9.6, pp. 687–693.

Pearse, R, D Harrison, N MacDonald et al. (2014). 'Effect of a perioperative, cardiac output-guided hemodynamic therapy algorithm on outcomes following major gastrointestinal surgery a randomized clinical trial and systematic review'. *Journal of the American Medical Association* 311.21, pp. 2181–2190.

Pelosi, P and M G de Abreu (2015). 'Acute respiratory distress syndrome: we can't miss regional lung perfusion!' *BMC Anesthesiology* 15.35, pp. 1–3.

Perrino, A C, T O'Connor and M Luther (1994). 'Transtracheal Doppler Cardiac Output Monitoring: Comparison to Thermodilution During Noncardiac Surgery'. *Anesthesia and Analgesia* 78.1, pp. 1060–1066.

Petousi, N, N P Talbot, I Pavord et al. (2019). 'Measuring lung function in airways diseases: current and emerging techniques'. *Thorax* 74.1, pp. 797–805.

Pfeiffer, B, R Syring, K Markstaller et al. (2006). 'The implications of arterial Po2 oscillations for conventional arterial blood gas analysis'. *Anesthesia and Analgesia* 102.6, pp. 1758–1764.

Phan, P, C Hahn and A Farmery (2017a). 'A modification of the Bohr method to determine airways deadspace for non-uniform inspired gas tensions'. *Physiological Measurement* 38.7, pp. 107–117.

Phan, P, C Zhang, D Geer et al. (2017b). 'The Inspired sinewave technique: A comparison study with body plethysmography in healthy volunteers'. *IEEE Journal of Translational Engineering in Health and Medicine* 5.1, pp. 1–9.

Poeze, M, J W M Greve and G Ramsay (2005). 'Meta-analysis of hemodynamic optimization: relationship to methodological quality.' *Critical Care* 9.6, pp. 771–779.

Purves, M J (1966). 'Fluctuations of arterial oxygen tension which have the same period as respiration'. *Respiration Physiology* 1.3, pp. 281–296.

R Development Core Team (2017). *R: A Language and Environment for Statistical Computing*.

Ranieri, V, G Rubenfeld, B Thompson et al. (2012). 'Acute respiratory distress syndrome: the Berlin Definition.' *Journal of the American Medical Association* 307.23, pp. 2526–33.

Reuter, D A, C Huang, T Edrich et al. (2010). 'Cardiac output monitoring using indicator-dilution techniques: Basics, limits, and perspectives'. *Anesthesia and Analgesia* 110.3, pp. 799–811.

Richard, J, L Brochard, P Vandelet et al. (2003). 'Respective effects of end-expiratory and end-inspiratory pressures on alveolar recruitment in acute lung injury'. *Critical Care Medicine* 31.1, pp. 89–92.

Richard, J, C Pouzot, A Pinzón et al. (2014). 'Reliability of the nitrogen washin-washout technique to assess end-expiratory lung volume at variable PEEP and tidal volumes'. *Intensive Care Medicine Experimental* 2.10, pp. 1–14.

Robinson, P, P Latzin, S Verbanck et al. (2013). 'Consensus statement for inert gas washout measurement using multiple- and single breath tests'. *European Respiratory Journal* 41.3, pp. 507–522.

Russell, W M S, R L Burch and C W Hume (1959). *The Principles of Humane Experimental Technique*. Meuthen, London.

Rylander, C, M Hogman, G Perchiazzi et al. (2004). 'Functional Residual Capacity and Respiratory Mechanics as Indicators of Aeration and Collapse in Experimental Lung Injury'. *Anesthesia & Analgesia* 98.1, pp. 782–789.

Sainsbury, M, Lorenzi, E Williams et al. (1997). 'A reconciliation of continuous and tidal ventilation gas exchange models'. *Respiration Physiology* 108.1, pp. 89–99.

Saugel, B, O Grothe and J Y Wagner (2015). 'Tracking changes in cardiac output: Statistical considerations on the 4-quadrant plot and the polar plot methodology'. *Anesthesia and Analgesia* 121.2, pp. 514–524.

Schaanning, C G and A Gulsvik (1973). 'Accuracy and precision of helium dilution technique and body plethysmography in measuring lung volumes'. *Scandinavian Journal of Clinical and Laboratory Investigation* 32.3, pp. 271–277.

Schibler, A., G. L. Hall, F. Businger et al. (2002). 'Measurement of lung volume and ventilation distribution with an ultrasonic flow meter in healthy infants'. *European Respiratory Journal* 20.4, pp. 912–918.

Schiller, H J, U G McCann, D E Carney et al. (2001). 'Altered alveolar mechanics in the acutely injured lung.' *Critical Care Medicine* 29.5, pp. 1049–1055.

Schulze, A, P Schaller, A Töpfer et al. (1994). 'Measurement of functional residual capacity by sulfur hexafluoride in small-volume lungs during spontaneous breathing and mechanical ventilation'. *Pediatric Research* 35.4, pp. 494–499.

Schwann, N M, Z Hillel, A Hoeft et al. (2011). 'Lack of effectiveness of the pulmonary artery catheter in cardiac surgery'. *Anesthesia and Analgesia* 113.5, pp. 994–1002.

Shoemaker, W, P Appel, H Kram et al. (1988). 'Prospective trial of supranormal values of survivors as therapeutic goals in high-risk surgical patients'. *Chest* 94.6, pp. 1176–1186.

Shoemaker, W, E Montgomery, E Kaplan et al. (1973). 'Physiologic Patterns in Surviving and Nonsurviving Shock Patients: Use of Sequential Cardiorespiratory Variables in Defining Criteria for Therapeutic Goals and Early Warning of Death'. *Archives of Surgery* 106.5, pp. 630–636.

Sivan, Y, T Deakers and C Newth (1990). 'An automated bedside method for measuring functional residual capacity by N2 washout in mechanically ventilated children'. *Pediatric Research* 28.5, pp. 446–450.

Slutsky, A (1999). 'Lung injury caused by mechanical ventilation'. *Chest* 116.6, 9S–15S.

Slutsky, A and V Ranieri (2013). 'Ventilator-induced lung injury'. *New England Journal of Medicine* 369.22, pp. 2126–2136.

Stapleton, R D, B M Wang, L D Hudson et al. (2005). 'Causes and timing of death in patients with ARDS'. *Chest* 128.2, pp. 525–532.

Staub, N C (1961). 'A simple small oxygen electrode'. *Journal of Applied Physiology* 16.1, pp. 192–194.

Sugiura, M, P R McCulloch, S Wren et al. (1994). 'Ventilator pattern influences neutrophil influx and activation in atelectasis-prone rabbit lung.' *Journal of applied physiology* 77.3, pp. 1355–1365.

Swan, H J C, William Ganz, James Forrester et al. (1970). 'Catheterization of the Heart in Man with Use of a Flow-Directed Balloon-Tipped Catheter'. *New England Journal of Medicine* 283.9, pp. 447–451.

Swindle, M M, A Makin, A J Herron et al. (2012). 'Swine as Models in Biomedical Research and Toxicology Testing'. *Veterinary Pathology* 49.2, pp. 344–356.

Syring, R, C Otto, R Spivack et al. (2007). 'Maintenance of end-expiratory recruitment with increased respiratory rate after saline-lavage lung injury'. *Journal of Applied Physiology* 102.1, pp. 331–339.

Tabuchi, A, H Nickles, M Kim et al. (2016). 'Acute Lung Injury Causes Asynchronous Alveolar Ventilation That Can Be Corrected by Individual Sighs'. *American Journal of Respiratory and Critical Care Medicine* 193.4, pp. 396–406.

The National Heart Lung and Blood Institute ARDS Clinical Trials Network (2004). 'Higher versus Lower Positive End-Expiratory Pressures in Patients with the Acute Respiratory Distress Syndrome'. *New England Journal of Medicine* 351.4, pp. 327–336.

Thomas, R, C Mollmann, A Ziebart et al. (2017). 'Cyclic PaO2 oscillations assessed in the renal microcirculation: correlation with tidal volume in a porcine model of lung lavage'. *BMC Anesthesiology* 17.92, pp. 1–7.

Vieira, S R, L Puybasset, J Richecoeur et al. (1998). 'A lung computed tomographic assessment of positive end-expiratory pressure-induced lung overdistension'. *American Journal of Respiratory and Critical Care Medicine* 158.5, pp. 1571–1577.

Vilstrup, C T, L J Bjorklund, A Larsson et al. (1992). 'Functional residual capacity and ventilation homogeneity in mechanically ventilated small neonates'. *Journal of Applied Physiology* 73.1, pp. 276–283.

Vimlati, L, R Kawati, G Hedenstierna et al. (2011). 'Spontaneous breathing improves shunt fraction and oxygenation in comparison with controlled ventilation at a similar amount of lung collapse'. *Anesthesia and Analgesia* 113.5, pp. 1089–1095.

Vincent, J L, A Rhodes, A Perel et al. (2011). 'Clinical review: Update on hemodynamic monitoring - a consensus of 16'. *Critical Care* 15.229, pp. 1–8.

Wanger, J, J L Clausen, A Coates et al. (2005). 'Standardisation of the measurement of lung volumes'. *European Respiratory Journal* 26.3, pp. 511–522.

Weismann, D, H Reißmann, S Maisch et al. (2006). 'Monitoring of functional residual capacity by an oxygen washin/washout; technical description and evaluation'. *Journal of Clinical Monitoring and Computing* 20.4, pp. 251–260.

Wilde, R B P de, J J Schreuder, P C M van den Berg et al. (2007). 'An evaluation of cardiac output by five arterial pulse contour techniques during cardiac surgery'. *Anaesthesia* 62.8, pp. 760–768.

Williams, E, J Aspel, S Burrough et al. (1994a). 'Assessment of cardiorespiratory function using oscillating inert gas forcing signals'. *Journal of Applied Physiology* 76.5, pp. 2130–2139.

Williams, E, D Gavaghan, P Oakley et al. (1994b). 'Measurement of dead–space in a model lung using an oscillating inspired argon signal'. *Acta Anaesthesiologica Scandinavica* 38.1, pp. 126–129.

Williams, E, M Sainsbury, L Sutton et al. (1998). 'Pulmonary blood flow measured by inspiratory inert gas concentration forcing oscillations'. *Respiration Physiology* 113.1, pp. 47–56.

Williams, E, J Viale, R Hamilton et al. (2000). 'Within-breath arterial PO2 oscillations in an experimental model of acute respiratory distress syndrome'. *British Journal of Anaesthesia* 85.3, pp. 456–459.

Wu, J, C Hafner, J P Schramel et al. (2016a). 'Cyclic and constant hyperoxia cause inflammation , apoptosis and cell death in human umbilical vein endothelial cells'. *Acta Anaesthesiologica Scandinavica* 60.1, pp. 492–501.

Wu, J, J Stefaniak, C Hafner et al. (2016b). 'Intermittent Hypoxia Causes Inflammation and Injury to Human Adult Cardiac Myocytes'. *Anesthesia and Analgesia* 122.2, pp. 373–380.

Yokota, H and F Kreuzer (1973). 'Alveolar to arterial transmission of oxygen fluctuations due to respiration in anesthetized dogs'. *European Journal of Physiology* 340.4, pp. 291–306.

Young, D, S E Lamb, S Shah et al. (2013). 'High-Frequency Oscillation for Acute Respiratory Distress Syndrome'. *New England Journal of Medicine* 368.9, pp. 806–813.

Zwart, A, J Bogaard, J Jansen et al. (1978). 'A non-invasive determination of lung perfusion compared with the direct Fick method'. *European Journal of Physiology* 375.2, pp. 213–217.

Zwart, A, R Seagrave and A Van Dieren (1976). 'Ventilation-perfusion ratio obtained by a noninvasive frequency response technique'. *Journal of Applied Physiology* 41.3, pp. 419–424.

APPENDIX A

Published papers

BJA

British Journal of Anaesthesia, 122 (2): 277–285 (2019)

doi: 10.1016/j.bja.2018.09.011
Advance Access Publication Date: 3 November 2018
Respiration and the airway

Tidal changes in PaO_2 and their relationship to cyclical lung recruitment/derecruitment in a porcine lung injury model

D. C. Crockett[1,*], J. N. Cronin[2], N. Bommakanti[1,3], R. Chen[1], C. E. W. Hahn[1], G. Hedenstierna[4], A. Larsson[5], A. D. Farmery[1] and F. Formenti[1,2,6,*]

[1]Nuffield Division of Anaesthetics, University of Oxford, Oxford, UK, [2]Centre for Human and Applied Physiological Sciences, King's College, London, UK, [3]Vagelos College of Physicians and Surgeons, Columbia University, New York, NY, USA, [4]Hedenstierna Laboratory, Department of Medical Sciences, Uppsala University, Uppsala, Sweden, [5]Hedenstierna Laboratory, Department of Surgical Sciences, Uppsala University, Uppsala, Sweden and [6]Department of Biomechanics, University of Nebraska Omaha, Omaha, NE, USA

*Corresponding authors. E-mails: douglas.crockett@ndcn.ox.ac.uk, federico.formenti@outlook.com

Abstract

Background: Tidal recruitment/derecruitment (R/D) of collapsed regions in lung injury has been presumed to cause respiratory oscillations in the partial pressure of arterial oxygen (PaO_2). These phenomena have not yet been studied simultaneously. We examined the relationship between R/D and PaO_2 oscillations by contemporaneous measurement of lung-density changes and PaO_2.

Methods: Five anaesthetised pigs were studied after surfactant depletion via a saline-lavage model of R/D. The animals were ventilated with a mean fraction of inspired O_2 (FiO_2) of 0.7 and a tidal volume of 10 ml kg^{-1}. Protocolised changes in pressure- and volume-controlled modes, inspiratory:expiratory ratio (I:E), and three types of breath-hold manoeuvres were undertaken. Lung collapse and PaO_2 were recorded using dynamic computed tomography (dCT) and a rapid PaO_2 sensor.

Results: During tidal ventilation, the expiratory lung collapse increased when I:E <1 [mean (standard deviation) lung collapse=15.7 (8.7)%; $P<0.05$], but the amplitude of respiratory PaO_2 oscillations [2.2 (0.8) kPa] did not change during the respiratory cycle. The expected relationship between respiratory PaO_2 oscillation amplitude and R/D was therefore not clear. Lung collapse increased during breath-hold manoeuvres at end-expiration and end-inspiration (14% *vs* 0.9–2.1%; $P<0.0001$). The mean change in PaO_2 from beginning to end of breath-hold manoeuvres was significantly different with each type of breath-hold manoeuvre ($P<0.0001$).

Conclusions: This study in a porcine model of collapse-prone lungs did not demonstrate the expected association between PaO_2 oscillation amplitude and the degree of recruitment/derecruitment. The results suggest that changes in pulmonary ventilation are not the sole determinant of changes in PaO_2 during mechanical ventilation in lung injury.

Keywords: diagnostic imaging; dynamic computed tomorgraphy; lung injury; pulmonary atelectasis; respiration; ventilation

Editorial decision: 10 September 2018; **Accepted:** 10 September 2018

© 2018 The Authors. Published by Elsevier Ltd on behalf of British Journal of Anaesthesia. This is an open access article under the CC BY license (http://creativecommons.org/licenses/by/4.0/).
For Permissions, please email: permissions@elsevier.com

Editor's key points

- Tidal recruitment/derecruitment is considered as a mechanism of ventilator-induced lung injury in acute respiratory distress syndrome.
- Respiratory oscillations in PaO_2 have been hypothesised to be indicative of tidal recruitment/derecruitment.
- In a porcine model for lung injury, the authors investigated whether an association between tidal recruitment/decruitment and PaO_2 oscillations existed.
- There was no change in amplitude of PaO_2 oscillations during the respiratory cycle, and an association with tidal recruitment/decruitment was therefore not demonstrated.
- These findings challenge the hypothesis that respiratory oscillations in PaO_2 are indicative of the lung collapse observed in lung injury.

Respiratory oscillations in the partial pressure of arterial oxygen (PaO_2) have been hypothesised to indicate tidal recruitment/derecruitment (R/D) in acute respiratory distress syndrome (ARDS).[1,2] Notably, R/D is one of the proposed mechanisms of ventilator-induced lung injury in this condition.[3–5] In addition, PaO_2 oscillations *per se* could potentially cause or augment organ damage by exposing organs to cyclically varying O_2 levels.[6–9] Despite the leading hypothesis that PaO_2 oscillations are caused by tidal R/D, no study to date has demonstrated their relationship by simultaneous dynamic measurements of both PaO_2 and R/D. Moreover, oscillations in PaO_2 have been found in mechanically ventilated uninjured lungs with no tendency to collapse.[10]

Therefore, the aims of the present study were to explore whether R/D is the underlying reason for PaO_2 oscillations by simultaneously measuring PaO_2 and R/D dynamically in a porcine, collapse-prone ARDS model, and to examine whether larger increases in lung collapse during breath-hold manoeuvres are associated with a larger reduction in PaO_2. For this purpose, we used newly developed fluorescence-quenching fibreoptic PaO_2 probes with a response time of less than 100 ms that allow measurement of PaO_2 oscillations in real time *in vitro* and *in vivo*[11–14] together with a single-slice dynamic CT (dCT) with a sampling interval of 250 ms affording measurements of R/D during mechanical ventilation.[15]

Methods

Ethical approval

This study of five domestic pigs (three males and two females; mean weight [standard deviation (SD)]=29.6 (1.7) kg) at the Hedenstierna laboratory, Uppsala University, Sweden was approved by the regional animal welfare ethics committee (Ref: C98/16) and adhered to Animal Research: Reporting of *In Vivo* Experiments guidelines.[16] Measurements undertaken on the uninjured lungs of animals reported in this study have been published elsewhere.[10]

Animal preparation

Table 1 shows the baseline characteristics of each animal. The animals were premedicated with i.m. xylazine 2 mg kg^{-1}, ketamine 20 mg kg^{-1}, and midazolam 0.5 mg kg^{-1}, and underwent induction of anaesthesia with i.v. propofol titrated to effect (1–3 mg kg^{-1}). The trachea was intubated and mechanical ventilation subsequently commenced. During preparation and before commencement of the study protocol, the animals were ventilated with volume-controlled ventilation (VCV) at 20–25 breaths per minute (bpm) [to maintain end-tidal CO_2 ($EtCO_2$) 4.5–6 kPa], with a tidal volume (V_T) of 10 ml kg^{-1}, positive end-expiratory pressure (PEEP) of 5 cm H_2O, and an inspiratory:expiratory ratio (I:E) of 1:2. The ventilator tubing and tracheal tube were checked for leaks by analysis of the spirometry data. Anaesthesia was maintained with continuous i.v. ketamine 32 mg kg^{-1} h^{-1}, fentanyl 4 μg kg^{-1} h^{-1}, and midazolam 0.16 mg kg^{-1} h^{-1}. General anaesthesia was confirmed by absence of spontaneous movements and by absence of reaction to painful stimulation between the front hooves. After confirmation of general anaesthesia, muscle relaxation was achieved with an initial bolus of rocuronium 0.2 mg kg^{-1} followed by 0.1 mg kg^{-1} boluses when spontaneous ventilatory efforts were detected from the airway gas and pressure traces. The adequacy of anaesthesia was determined during the periods of muscle relaxation by the absence of cardiovascular signs of sympathetic stimulation (increases in heart rate or arterial BP). Maintenance fluids were administered i.v. in the form of isotonic electrolyte solution (Ringerfundin; B. Braun Melsungen AG, Melsungen, Germany) at a rate of 10 ml kg^{-1} h^{-1} during the instrumentation phase and 7 ml kg^{-1} h^{-1} for the rest of the protocol. Once anaesthetised, bilateral surgical dissections of the neck

Table 1 Baseline characteristics and post-injury blood gas data for each animal. Pre-lavage blood gas values were within normal limits. Blood gas data presented were measured post-saline lavage. ♂, male; ♀, female. CO, cardiac output; FiO_2, fraction of inspired O_2; Hb, haemoglobin; PFR, PaO_2:FiO_2 ratio; SD, standard deviation

Variable	Animal number					Mean (SD)
	1	2	3	4	5	
Sex	♂	♀	♂	♀	♂	—
Weight (kg)	31.1	29.0	29.8	31.2	26.7	29.6 (1.7)
FiO_2	0.5	0.8	0.7	0.7	0.9	0.7 (0.1)
PFR	288	285	232	105	276	237 (77)
pH	7.29	7.35	7.32	7.23	7.37	7.31 (0.05)
PaO_2 (kPa)	19.2	38.1	21.7	9.8	33.0	24.4 (11.2)
$PaCO_2$ (kPa)	8.2	7.3	7.8	8.9	6.8	7.8 (0.8)
Hb (g L^{-1})	91	80	81	86	76	82 (5)
CO (L min^{-1})	3.7	4.8	3.5	4.2	3.2	3.9 (0.6)

were performed. The exposed right internal jugular vein was cannulated with a pulmonary artery catheter used for continuous pulmonary artery pressure monitoring, intermittent thermodilution cardiac output monitoring, and core temperature monitoring. The right and left internal carotid arteries were cannulated with 20G Leadercath Arterial cannulae (Vygon, Swindon, UK) for the introduction of fibreoptic PaO_2 probes.

Lung injury

A collapse-prone lung injury was induced with a technique modified from Lachmann and colleagues.[17] Preoxygenation with a fraction of inspired O_2 (FiO_2) of 1.0 preceded the ventilator disconnection and lavage of the lungs by instillation of 0.9% saline solution (at 37°C) via the tracheal tube. After 30 s, the saline was drained out of the lungs and ventilation recommenced. This process was repeated until a PaO_2:FiO_2 ratio (PFR) of <300 mm Hg (40 kPa) was achieved.

Data collection and processing

Cardiorespiratory variables, including peripheral O_2 saturations (SpO_2), ECG, invasive arterial BP (AS/3 Multi-Parameter Patient Monitor; Datex-Ohmeda, Madison, WI, USA), airway gas composition, flow, and pressure (Capnomac Ultima; Datex-Ohmeda), were continuously monitored and recorded as analogue signals throughout the protocol. PaO_2 signals from the fibreoptic probes were continuously collected with OxyLitePro monitors (Oxford Optronix, Abingdon, UK), converted to digital form using PowerLab (ADInstruments, Dunedin, New Zealand) and displayed/recorded with LabChart version 8.1.5 (ADInstruments) with a sampling rate of 10 Hz. Physiological data were processed using R version 3.4.1 (R Core Team, Vienna, Austria).[18]

Study protocol

The animals were positioned in dorsal recumbency on the CT scanner table. FiO_2 [mean (SD)=0.7 (0.1)] was set depending on the lung injury achieved with saline lavages (see Table 1), and PaO_2 was recorded continuously.

A first set of measurements considered tidal ventilation, when animals were ventilated in both pressure-controlled ventilation (PCV) and VCV modes at I:E ratios of 1:2, 2:1, 1:4, and 4:1 to explore the effects of different ventilatory modes on PaO_2 and its dynamic changes. Upon each change of ventilator setting, the PaO_2 trace was monitored until its mean value was stable, and then recorded for 120 s. The dCT images were recorded in the last 30 s of this period.

A second set of experiments considered breath-hold manoeuvres, when whole-lung CT scans were recorded during the first and last 5 s of an imposed 30 s breath hold at:

(i) End expiration: the expiratory and inspiratory valves closed at an initial airway pressure of 5 cm H_2O airway pressure (Ve)
(ii) End inspiration: the valves closed after inspiration of V_T 10 ml kg^{-1} (V_T10)
(iii) End large inspiration: the valves closed after inspiration of V_T 20 ml kg^{-1} (V_T20).

Breath-hold manoeuvres were repeated multiple times in each animal in sequences designed to ensure all permutations of manoeuvre-order were achieved. The anaesthetised animals were euthanised with a bolus dose of potassium chloride (1–2 mmol kg^{-1}) upon completion of the study protocol.

CT image acquisition

A SOMATOM Definition Flash or SOMATOM Definition Edge (Siemens, Munich, Germany) were used to acquire all images as series of transverse sections with a reconstituted voxel size of 0.5 × 0.5 × 5 mm. Scans of a single juxta-diaphragmatic thoracic slice were acquired at 50 ms intervals with a 70 kV tube voltage, 246 mA current, and collimation of 64 × 0.6 mm in order to analyse dynamic changes during ventilation. A whole-lung scan was conducted at the start and immediately before the end of each breath-hold manoeuvre using a tube voltage of 80 kV, 364 mA current, and 64 × 60 mm collimation.

CT image analysis

CT images were segmented using 3D Slicer version 4.6.2[19] (http://www.slicer.org) with exclusion of the mediastinum, diaphragm, inferior vena cava, and hilar vessels. Exclusion of intrapulmonary vessels within regions of increased voxel density was not possible, and these, along with the conducting airways up to the level of the clavicles, were included in the analysis. Every fifth image was analysed producing a final temporal resolution of 250 ms. All images were then subsegmented according to voxel density:[20–22]

(i) Collapse: −100 to +100 Hounsfield units (HU)
(ii) Poorly aerated lung: −500 to −101 HU
(iii) Normally aerated lung: −900 to −501 HU
(iv) Overdistended lung: −1000 to −901 HU.

The mass of each lung fraction (e.g. collapsed) was then calculated using the mean density and volume of each fraction assuming the lung is composed solely of air and water.[20] The fractional mass of each region was then calculated as:

$$(\text{mass of fraction})*100\%/(\text{total mass of all fractions}). \quad (1)$$

Tidal R/D was defined as the difference between the maximum and minimum measured mass of the collapsed lung during the course of a single breath.

Statistical analysis

Statistical analyses were performed in GraphPad Prism (version 7.00 for Windows, GraphPad Software; La Jolla, CA, USA; https://www.graphpad.com). Before analysis, all data were tested for normality and homogeneity of variance. Parametric data were compared with paired, two-tailed, Student's *t*-test, and non-parametric with Wilcoxon matched-pairs signed-rank test. The level of significance was set at $P<0.05$ for all tests.

Tidal ventilation

CT measurements from all animals were compared using a one-way analysis of variance (ANOVA) with multiple comparisons and Greenhouse–Geisser correction (parametric), or using a Wilcoxon matched-pairs signed-rank test (non-parametric). A two-way ANOVA with Šidák correction for multiple comparisons was used for the analysis of CT

measurements of inter- and intra-animal variability during tidal ventilation under different conditions.

Breath-hold manoeuvres

The effect of type of breath-hold manoeuvre on the change in lung collapse was compared using a Kruskal–Wallis test with Dunn's correction for multiple comparisons. A two-way ANOVA was used to examine the effects of individual animal and type of breath-hold manoeuvre on the change in PaO_2. Spearman correlations were used to assess the relationship between change in collapse and change in PaO_2.

Results

Tidal R/D measured by dCT was detected when the expiratory time exceeded the inspiratory time during tidal ventilation

Figure 1 shows the changes in compartmental mass over the course of a single breath. The maximum fraction of collapse was significantly larger than the minimum fraction when I:E was below 1 [PCV 1:2 (11.6–19.5%), PCV 1:4 (11.5–19.9%), VCV 1:2 (12.6–20.4%), VCV 1:4 (12.9–20.6%); $P<0.05$], as quantified by single-slice dCT at a temporal resolution of 250 ms. This effect was consistent between PCV and VCV. There was no difference between the maximum and minimum fractions of collapse when I:E was higher than 1.

Respiratory PaO_2 oscillation amplitude was not clearly related to R/D

A total of $n=148$ different 30 s sections of respiratory PaO_2 oscillation data were analysed, all of which were with $V_T=10$ ml kg^{-1} and ventilatory frequency=12 bpm. Figure 2a illustrates the relationship between the change in lung collapse and the respiratory PaO_2 oscillation amplitude. The mean PaO_2 and respiratory PaO_2 oscillation amplitude for each ventilator condition are shown in Table 2 and Figure 2b. There was not a strong correlation between mean airway pressure and mean PaO_2 during tidal ventilation, with a 0.55 kPa reduction in PaO_2 for 1 cm H_2O increase in airway pressure ($r=-0.46$). A one-way repeated measures ANOVA with multiple comparisons supported a significant effect of ventilatory mode on mean PaO_2 during tidal ventilation ($F_{(3,57)}=7.6$; $P=0.0002$).

Whole-lung collapse did not decrease during a 30 s breath-hold manoeuvre with large tidal volume

The analysis of $n=74$ breath-hold manoeuvres undertaken with simultaneous CT showed a significant increase in the fraction of collapse from the start to the end of an imposed breath-hold manoeuvre, as shown in Table 3. The mean (SD) airway pressure decreased concurrently during breath-hold manoeuvres at end expiration by 4 (2) cm H_2O, V_T10 by 11 (6) cm H_2O, and V_T20 by 11 (6) cm H_2O. The fractional increase in collapse during the end-expiratory breath-hold manoeuvres was significantly larger compared with the other two conditions (14% *vs* 0.9–2.1%; $P<0.0001$). There was no difference between the change in collapse with V_T10 and V_T20 end-inspiratory breath-hold manoeuvres. The change in PaO_2 could not be predicted from the change in collapse with simple linear regression ($r^2=0.23$, 0.15, 0.14 for Ve, V_T10, and V_T20 breath-hold manoeuvres, respectively).

Significant variation in the PaO_2 change for different breath-hold manoeuvres within and between individual animals

Figure 3 shows the mean continuous PaO_2 recordings from the animals ($n=5$) during each breath-hold manoeuvre studied before and during CT scanning ($n=146$). For each individual manoeuvre, the change in PaO_2 was calculated from the start of the breath-hold manoeuvre (measured from the start of the imposed airway pressure change) to the subsequent nadir in the trace. The mean (SD) change in PaO_2 was −16.5 (6.3) kPa during end-expiratory breath-hold manoeuvres, and −10.5 (5.0) kPa and −4.8 (3.4) kPa for V_T10 and V_T20 end-inspiratory breath-hold manoeuvres, respectively. A repeated measures ANOVA with Greenhouse–Geisser correction determined that these PaO_2 changes were significantly different between each condition ($F_{(2,38)}=110$; $P<0.0001$). Supplementary Table S1 shows *post hoc* multiple comparisons, and Supplementary Figure S1 shows all recorded traces for each animal and breath-hold manoeuvre. These demonstrate high variability between each animal and manoeuvre in the majority of cases.

Discussion

This study investigated the relationship between dynamic changes in PaO_2 and collapse in anaesthetised, mechanically ventilated pigs with saline-lavage lung injury. We demonstrated dynamic respiratory PaO_2 oscillations during tidal ventilation, which increased when CT markers of tidal R/D increased. However, the magnitude of this association was not as large as expected. We found a significant tidal R/D only when I:E <1. Additionally, our study showed an increase in lung collapse even during a 30 s large inspiratory breath-hold manoeuvre and that the increase in collapse was associated with a significant reduction in PaO_2 during these manoeuvres, including when the effect of continuous O_2 uptake ($\dot{V}O_2$) was considered.

The analysis of the respiratory PaO_2 oscillation amplitude showed that there were differences in the amplitudes for some conditions; however, these did not match the conditions, in which R/D was detected by dCT. The minimum and maximum amounts of mean fractional collapse (mean (SD)) were 14 (7) % and 17 (9) % measured in PCV 2:1 and PCV 1:4 respectively. Given the small differences and large variability in these values, it is likely that, whilst technically measurable, they do not represent a meaningful physiological or clinical difference. These results suggest a lack of a strong association between R/D and respiratory PaO_2 oscillations. This finding does not support the hypothesised strong causal relationship between them,[1,2,23,24] and suggests the presence of other contributing determinants of variable shunt fraction within each breath. This proposition is supported by results from studies in the uninjured porcine lung, where the presence of respiratory PaO_2 oscillations was demonstrated in the absence of R/D.[10] The measured mass of collapse [mean (SD) = 16 (9)%] was lower than that reported in other studies using dCT[25–27] in lung injury, although some of these studies considered different HU ranges. The measured collapse in our study, however, was 88 (59)% higher than that measured in studies examining a similar protocol in the uninjured lung using the same species and model,[10] and consistent with findings from intra-vital microscopy.[28] This result suggests that other determinants of respiratory PaO_2 oscillations should be considered. Whilst R/D is likely to cause an increase in the amplitude

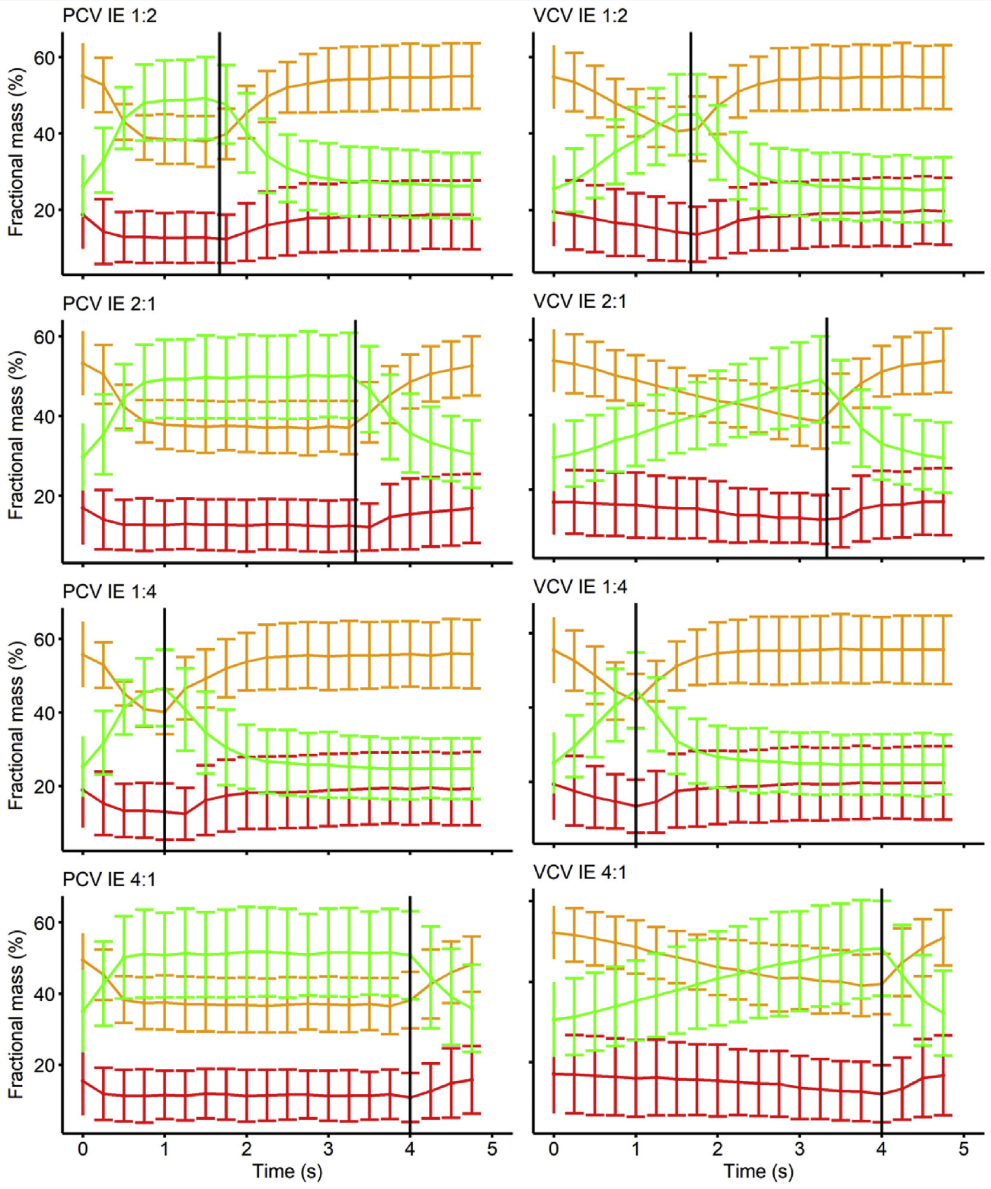


Fig 1. Changes in compartmental mass over the course of a single breath. Red, atelectasis; yellow, poorly aerated; and green, normally aerated. I:E, inspiratory:expiratory ratio; PCV, pressure-controlled ventilation; VCV, volume-controlled ventilation. Error bars represent standard deviation. Only in conditions where the expiratory time exceeded inspiratory time there was a significant difference between the mean maximum and minimum fractions of collapse, PCV 1:2 (11.6–19.5%), PCV 1:4 (11.5–19.9%), VCV 1:2 (12.6–20.4%), VCV 1:4 (12.9–20.6%). Overdistended mass represented <2% of total mass and remained unchanged throughout the breath in all conditions (not shown).

of respiratory PaO_2 oscillations, in the context of a complex physiological system, the effect may be obscured by other competing variables, such as the redistribution of pulmonary blood flow to regions with different ventilation:perfusion ratios.[29] This hypothesis is supported by the finding in our study that mean PaO_2 did not increase with an increase in mean airway pressure, as reported previously.[30,31] Additionally, CT-measured voxel density used as a surrogate marker of collapse assumes that the higherdensity voxels are true collapse and not another high radiodense material, such as fluid (alveolar flooding) or blood, and so may overstate the degree of true collapse.

The observed amplitude of oscillations was smaller than had been demonstrated elsewhere.[1,2] This may be partially

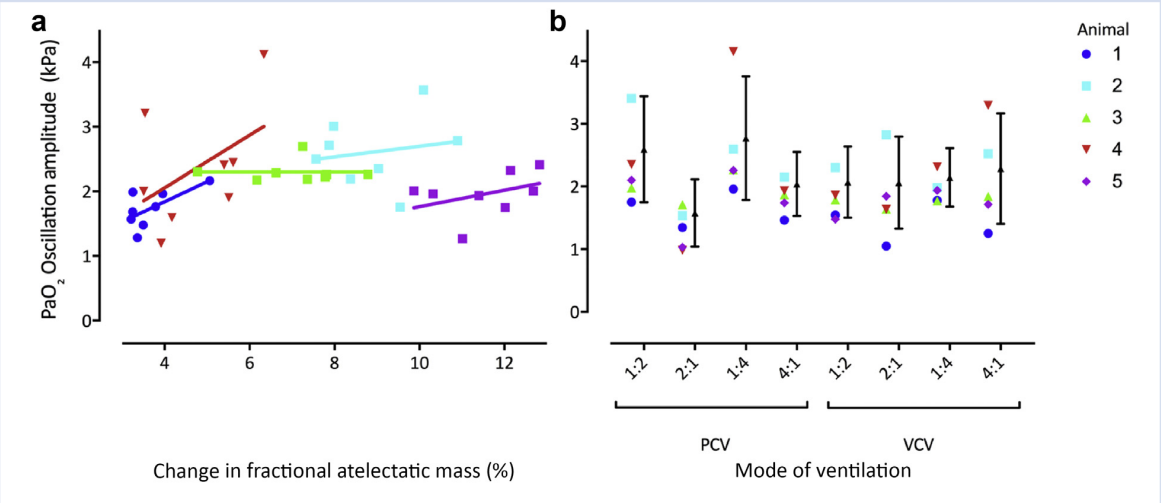


Fig 2. Mean respiratory PaO_2 oscillation amplitude during tidal ventilation under different ventilatory conditions. (a) Correlation between the mean respiratory PaO_2 oscillation amplitude (kPa) recorded during CT scanning and the relevant associated CT-measured change in fractional collapse during that ventilatory condition. The linear regression analysis results gave: Pig 1: r^2=0.44, gradient=2.33; Pig 2: r^2=0.31, gradient=0.62; Pig 3: r^2=0.00, gradient=0.00; Pig 4: r^2=0.23, gradient=3.06; Pig 5: r^2=0.15, gradient=0.96. (b) Mean amplitude (kPa) with error bars representing standard deviation (black dots and lines). Amplitudes are calculated from tidal ventilation both before and during CT for each ventilator condition. Each animal is represented by a different coloured symbol. I:E, inspiratory:expiratory ratio; PCV, pressure-controlled ventilation; VCV, volume-controlled ventilation; x-axis ratios in (b) represent different I:E ratios.

Table 2 Mean PaO_2, amplitude of respiratory PaO_2 oscillations, and mean airway pressure during different ventilatory conditions. Values shown are mean (standard deviation)

I:E ratio	Pressure-controlled ventilation			Volume-controlled ventilation		
	Mean PaO_2 (kPa)	Oscillation amplitude (kPa)	Mean airway pressure (cm H_2O)	Mean PaO_2 (kPa)	Oscillation amplitude (kPa)	Mean airway pressure (cm H_2O)
1:2	25.2 (4.7)	2.6 (0.8)	11 (8)	26.4 (4.6)	2.1 (0.6)	8 (5)
2:1	19.7 (6.6)	1.6 (0.5)	16 (8)	25.9 (5.5)	2.1 (0.7)	11 (6)
1:4	27.1 (2.5)	2.8 (1.0)	8 (7)	26.3 (3.6)	2.1 (0.5)	7 (5)
4:1	22.7 (3.9)	2.0 (0.5)	18 (6)	26.4 (3.2)	2.3 (0.9)	13 (5)

Respiratory PaO_2 oscillation amplitude was significantly lower during PCV 2:1 when compared to PCV 1:2, PCV 1:4, VCV 1:2 and significantly higher during PCV 1:4 compared to PCV 4:1, PCV 2:1 and VCV 1:4.

Table 3 Mean fractional mass of collapsed lung measured by CT at the start and end of breath-hold manoeuvres. Ve, end expiratory; V_T10, end-inspiratory (10 ml kg^{-1}); V_T20, end-inspiratory (20 ml kg^{-1}). *Ve: $t(24)$=12; P<0.0001. †V_T10: $t(24)$=3.2; P<0.005. ‡V_T20: 95% confidence interval: 0.6–1.5%

Animal number	Fractional collapse (%)					
	Ve		V_T10		V_T20	
	Start	End	Start	End	Start	End
1	18.4 (2.1)	23.8 (2.0)	16.8 (1.4)	17.5 (2.1)	15.3 (1.7)	16.0 (1.3)
2	37.1 (2.9)	55.3 (3.6)	22.5 (7.7)	28.3 (9.4)	13.0 (2.3)	15.8 (1.8)
3	25.4 (1.1)	37.8 (1.4)	19.9 (0.7)	22.5 (0.5)	16.1 (0.6)	17.0 (1.4)
4	19.8 (1.2)	36.8 (3.0)	8.7 (1.6)	10.2 (2.5)	7.0 (0.6)	9.6 (3.2)
5	32.8 (0.9)	53.1 (0.7)	25.6 (3.4)	27.1 (0.7)	19.1 (1.1)	20.0 (1.4)
Combined	26.0 (7.1)	40.1 (12.0)	18.6 (6.5)	20.7 (7.1)	14.8 (4.1)	16.1 (3.7)
Difference	14.1* (6.1)		2.1† (3.0)		0.9 (0.6–1.5)‡	

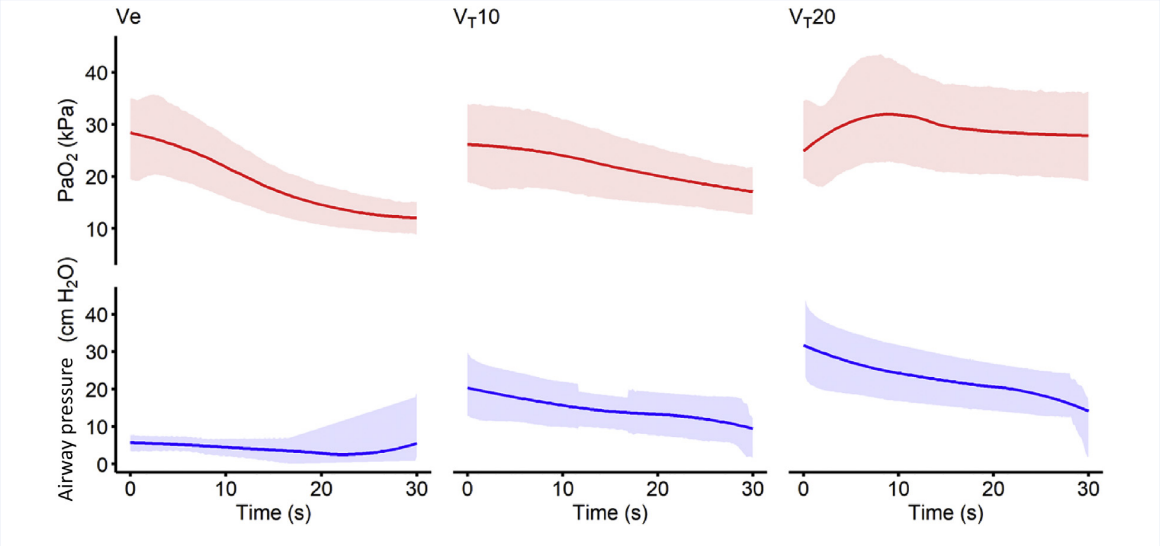


Fig 3. PaO_2 and airway pressure traces during breath-hold manoeuvres. The left column shows end-expiratory breath-hold manoeuvres (Ve), the middle column 10 ml kg^{-1} end-inspiratory breath-hold manoeuvres (V_T10), and the right column 20 ml kg^{-1} end-inspiratory breath-hold manoeuvres (V_T20). Red represents PaO_2 and blue represents mean airway pressure. Solid lines represent mean of n=5 animal manoeuvres associated with CT imaging. The shaded area represents standard deviation. PaO_2 traces have been corrected for the effect of O_2 uptake ($\dot{V}O_2$) over time.

explained by the smaller V_T (10 *vs* ~30 ml kg^{-1}) and lower peak P_{AW} (<35 *vs* >45 cm H_2O) during tidal ventilation in our study. Whilst the V_T is larger than the recommended human clinical V_T,[32] it is smaller than those used in studies showing respiratory PaO_2 oscillations with amplitudes of >13 kPa, and equivalent to V_T measured in spontaneously ventilating pigs.[33] In addition, peak pressure was <30 cm H_2O throughout the experiments, in contrast to previous studies where peak pressure exceeded 45 cm H_2O.[1]

The amount of lung collapse, unexpectedly, did not decrease during imposed inspiratory (V_T=10 and 20 ml kg^{-1}) breath-hold manoeuvres. In the context of evidence demonstrating that the majority of recruitment occurs within the first few seconds of application of inflation pressure,[15,33,34] this result may represent CT measurement of 'starting' collapse being taken at a time point already on the plateau of the recruitment curve. In fact, the starting collapse mass recorded in Ve was 31% greater than that recorded in V_T20 (26.0–14.8%). However, it is important to recognise that the airway pressure is not maintained during a prolonged pause, as both the expiratory and inspiratory ventilator valves close at the start of manoeuvre, and the pressure in the lungs decreases as a result of the 'pendelluft' phenomena[35] and oxygen consumption ($\dot{V}O_2$), although we attempted to correct for the effect of $\dot{V}O_2$ in our analysis by subtracting the calculated $\dot{V}O_2$ at each 100 ms time point. The reduction in airway pressure will increase both the amount of poorly aerated regions and lung collapse, which in turn will reduce PaO_2 by increasing shunt and V/Q mismatch. Indeed, we found a decrease in airway pressure during all breath-hold manoeuvres.

The main limitations of our study are that the porcine model does not comprise all the features observed in human ARDS, and that the PFRs attained were consistent with only mild to moderate lung injury. However, the lavage model is very prone to collapse and is easily recruitable. Thus, this model of lung injury would exaggerate the R/D phenomena and possible R/D dependent PaO_2 oscillations.

In conclusion, to the best of our knowledge, this is the first study to measure contemporaneously dynamic R/D and PaO_2 in a collapse-prone ARDS model. We found a very limited association between R/D and respiratory PaO_2 oscillations, certainly much smaller than expected from the published literature. These results challenge the accepted hypothesis that R/D is the main determinant of respiratory PaO_2 oscillations in ARDS, where reduction of PaO_2 oscillation amplitude is mostly expected from reduction of R/D. Our study warrants further investigation into the dynamic, often overlooked role of pulmonary perfusion within the complex context of pulmonary responses to mechanical ventilation.[10,36]

Authors' contributions

Study design: FF, GH, CH, AF.
Study conduct: FF, NB.
Data analysis: DC.
Data interpretation: DC, FF, JC, AF, AL, GH.
Writing of paper: DC, FF.
Critical revision: all authors.
Financial support: FF, AF, CH, AL.

Acknowledgements

The authors are grateful to H. McPeak, G. Fioroni, A. Roneus, K. Ahlgren, M. Swälas, M. Andersson, and M. Segelsjö for technical support; M. C. Tran for invaluable assistance with data analysis; and L. Camporota for helpful discussions;

additionally, OxSTaR, St Peter's College, and the Nuffield Division of Anaesthetics office for their ongoing support of DC.

Declaration of interest

The authors declare that they have no conflicts of interest.

Funding

Wellcome Trust Translation Award (HMRXGK00) to AF and CH; Swedish Heart and Lung Foundation (20170531); Swedish Research Council (K2015-99X-2273101-4) to AL; Oxford University Medical Research Fund (MRF/LSV2014/2091) to FF; Whitaker International Fellow Grant to NB.

Appendix A. Supplementary data

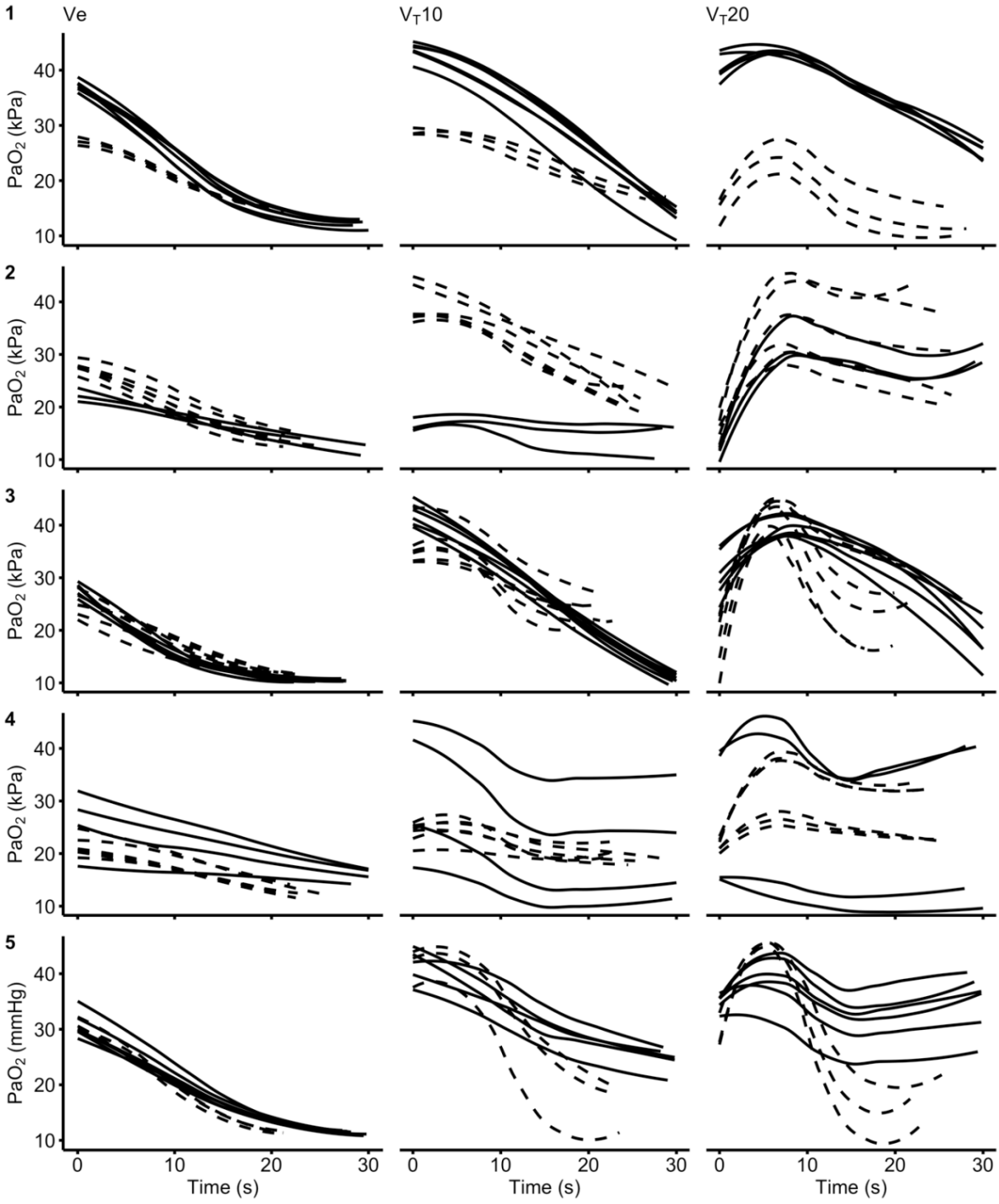
Supplementary data to this article can be found online at https://doi.org/10.1016/j.bja.2018.09.011.

References

1. Baumgardner JE, Markstaller K, Pfeiffer B, Doebrich M, Otto CM. Effects of respiratory rate, plateau pressure, and positive end-expiratory pressure on PaO_2 oscillations after saline lavage. *Am J Respir Crit Care Med* 2002; **166**: 1556–62
2. Williams EM, Viale JP, Hamilton RM, McPeak H, Sutton L, Hahn CE. Within-breath arterial PO_2 oscillations in an experimental model of acute respiratory distress syndrome. *Br J Anaesth* 2000; **85**: 456–9
3. Dreyfuss D, Saumon G. Ventilator-induced lung injury. *Am J Respir Crit Care Med* 1998; **157**: 294–323
4. Ricard JD, Dreyfuss D, Saumon G. Ventilator-induced lung injury. *Eur Respir J Suppl* 2003; **42**: 2s–9s
5. Muscedere JG, Mullen JB, Gan K, Slutsky AS. Tidal ventilation at low airway pressures can augment lung injury. *Am J Respir Crit Care Med* 1994; **149**: 1327–34
6. Klein KU, Johannes A, Bruckner M, et al. Systemic PaO_2 oscillations cause mild brain injury in a pig model. *Crit Care Med* 2016; **44**: e253–63
7. Thomas R, Mollmann C, Ziebart A, Liu T, David M, Hartmann EK. Cyclic PaO_2 oscillations assessed in the renal microcirculation: correlation with tidal volume in a porcine model of lung lavage. *BMC Anesthesiol* 2017; **17**: 92
8. Wu J, Hafner C, Schramel JP, et al. Cyclic and constant hyperoxia cause inflammation, apoptosis and cell death in human umbilical vein endothelial cells. *Acta Anaesthesiol Scand* 2016; **60**: 492–501
9. Wu J, Stefaniak J, Hafner C, et al. Intermittent hypoxia causes inflammation and injury to human adult cardiac myocytes. *Anesth Analg* 2016; **122**: 373–80
10. Formenti F, Bommakanti N, Chen R, et al. Respiratory oscillations in alveolar oxygen tension measured in arterial blood. *Sci Rep* 2017; **7**: 7499
11. Chen R, Hahn CE, Farmery AD. A flowing liquid test system for assessing the linearity and time-response of rapid fibre optic oxygen partial pressure sensors. *Respir Physiol Neurobiol* 2012; **183**: 100–7
12. Chen R, Formenti F, Obeid A, Hahn CE, Farmery AD. A fibre-optic oxygen sensor for monitoring human breathing. *Physiol Meas* 2013; **34**: N71–81
13. Formenti F, Chen R, McPeak H, Matejovic M, Farmery AD, Hahn CE. A fibre optic oxygen sensor that detects rapid PO_2 changes under simulated conditions of cyclical atelectasis in vitro. *Respir Physiol Neurobiol* 2014; **191**: 1–8
14. Formenti F, Chen R, McPeak H, et al. Intra-breath arterial oxygen oscillations detected by a fast oxygen sensor in an animal model of acute respiratory distress syndrome. *Br J Anaesth* 2015; **114**: 683–8
15. Markstaller K, Eberle B, Kauczor HU, et al. Temporal dynamics of lung aeration determined by dynamic CT in a porcine model of ARDS. *Br J Anaesth* 2001; **87**: 459–68
16. Kilkenny C, Browne WJ, Cuthill IC, Emerson M, Altman DG. Improving bioscience research reporting: the ARRIVE guidelines for reporting animal research. *PLoS Biol* 2010; **8**: e1000412
17. Lachmann B, Robertson B, Vogel J. In vivo lung lavage as an experimental model of the respiratory distress syndrome. *Acta Anaesthesiol Scand* 1980; **24**: 231–6
18. R Development Core Team R. *A language and environment for statistical computing*. Vienna, Austria: R Foundation for Statistical Computing; 2017
19. Fedorov A, Beichel R, Kalpathy-Cramer J, et al. 3D Slicer as an image computing platform for the quantitative imaging network. *Magn Reson Imaging* 2012; **30**: 1323–41
20. Gattinoni L, Pesenti A, Bombino M, et al. Relationships between lung computed tomographic density, gas exchange, and PEEP in acute respiratory failure. *Anesthesiology* 1988; **69**: 824–32
21. Lundquist H, Hedenstierna G, Strandberg Å, Tokics L, Brismar B. CT-assessment of dependent lung densities in man during general anaesthesia. *Acta Radiol* 1995; **36**: 626–32
22. Vieira SR, Puybasset L, Richecoeur J, et al. A lung computed tomographic assessment of positive end-expiratory pressure-induced lung overdistension. *Am J Respir Crit Care Med* 1998; **158**: 1571–7
23. Syring RS, Otto CM, Spivack RE, Markstaller K, Baumgardner JE. Maintenance of end-expiratory recruitment with increased respiratory rate after saline-lavage lung injury. *J Appl Physiol (1985)* 2007; **102**: 331–9
24. Boehme S, Bentley AH, Hartmann EK, et al. Influence of inspiration to expiration ratio on cyclic recruitment and derecruitment of atelectasis in a saline lavage model of acute respiratory distress syndrome. *Crit Care Med* 2015; **43**: e65–74
25. Neumann P, Berglund JE, Fernandez Mondejar E, Magnusson A, Hedenstierna G. Effect of different pressure levels on the dynamics of lung collapse and recruitment in oleic-acid-induced lung injury. *Am J Respir Crit Care Med* 1998; **158**: 1636–43
26. David M, Karmrodt J, Bletz C, et al. Analysis of atelectasis, ventilated, and hyperinflated lung during mechanical ventilation by dynamic CT. *Chest* 2005; **128**: 3757–70
27. Markstaller K, Kauczor HU, Weiler N, et al. Lung density distribution in dynamic CT correlates with oxygenation in ventilated pigs with lavage ARDS. *Br J Anaesth* 2003; **91**: 699–708
28. Mertens M, Tabuchi A, Meissner S, et al. Alveolar dynamics in acute lung injury: heterogeneous distension rather than cyclic opening and collapse. *Crit Care Med* 2009; **37**: 2604–11
29. Vimlati L, Kawati R, Hedenstierna G, Larsson A, Lichtwarck-Aschoff M. Spontaneous breathing improves shunt fraction and oxygenation in comparison with controlled ventilation at a similar amount of lung collapse. *Anesth Analg* 2011; **113**: 1089–95

30. Musch G, Harris RS, Vidal Melo MF, et al. Mechanism by which a sustained inflation can worsen oxygenation in acute lung injury. *Anesthesiology* 2004; **100**: 323–30
31. Brower R, Wise RA, Hassapoyannes C, Bromberger-Barnea B, Permutt S. Effect of lung inflation on lung blood volume and pulmonary venous flow. *J Appl Physiol* 1985; **58**: 954–63
32. The Acute Respiratory Distress Syndrome Network. Ventilation with lower tidal volumes as compared with traditional tidal volumes for acute lung injury and the acute respiratory distress syndrome. *N Engl J Med* 2000; **342**: 1301–8
33. Hannon JP, Bossone CA, Wade CE. Normal physiological values for conscious pigs used in biomedical research. *Lab Anim Sci* 1990; **40**: 293–8
34. Albert SP, DiRocco J, Allen GB, et al. The role of time and pressure on alveolar recruitment. *J Appl Physiol (1985)* 2009; **106**: 757–65
35. Tabuchi A, Nickles HT, Kim M, et al. Acute lung injury causes asynchronous alveolar ventilation that can be corrected by individual sighs. *Am J Respir Crit Care Med* 2016; **193**: 396–406
36. Pelosi P, de Abreu MG. Acute respiratory distress syndrome: we can't miss regional lung perfusion! *BMC Anesthesiol* 2015; **15**: 35

Handling editor: C. Boer



Supplementary Figure 1 PaO_2 traces during breath-hold manoeuvres for each animal. The left column shows end-expiratory breath-hold manoeuvres (Ve), the middle column 10 ml kg^{-1} end-inspiratory breath hold-manoeuvres (V_T10) and the right column 20 ml kg^{-1} end-inspiratory breath hold manoeuvres (V_T20). Dashed lines represent measurements undertaken in the laboratory before transfer to the CT scanner. Solid lines are manoeuvres associated with CT imaging. Each animal is represented by the number to the left of each set of plots. All traces have been corrected for the effect of O_2 uptake ($\dot{V}O_2$).

Supplementary Table 1: Change in PaO_2 during breath-hold manoeuvres in different animals.

Animal	Breath-hold Manoeuvre Type		
Comparison	Ve	V_T10	V_T20
1 vs 2	****	****	****
1 vs 3	*	*	ns
1 vs 4	***	****	****
1 vs 5	ns	****	
2 vs 3	**	****	****
2 vs 4	ns	ns	**
2 vs 5	****	*	***
3 vs 4	ns	***	**
3 vs 5	ns	*	ns
4 vs 5	**	ns	ns

Ve = end-expiratory, V_T10 = end-inspiratory (10 ml kg^{-1}), V_T20 = end-inspiratory (20 ml kg^{-1}). Significant differences in the change in PaO_2 are denoted against the relative comparison; * = $p < 0.05$, ** = $p < 0.01$, *** = $p < 0.005$, **** = $p < 0.0001$, ns = not significant.

BJA

British Journal of Anaesthesia, 123 (2): 126–134 (2019)

doi: 10.1016/j.bja.2019.02.025
Advance Access Publication Date: 4 April 2019
Cardiovascular

Noninvasive cardiac output monitoring in a porcine model using the inspired sinewave technique: a proof-of-concept study

Richard M. Bruce[1,2,*], Douglas C. Crockett[2], Anna Morgan[2], Minh Cong Tran[2], Federico Formenti[1,2,3], Phi Anh Phan[2] and Andrew D. Farmery[2]

[1]Centre for Human and Applied Physiological Sciences, School of Basic and Medical Sciences, King's College London, London, UK, [2]Nuffield Department of Clinical Neurosciences, University of Oxford, Oxford, UK and [3]Department of Biomechanics, University of Nebraska, Omaha, NE, USA

*Corresponding author. E-mail: richard.bruce@kcl.ac.uk

Abstract

Background: Cardiac output ($\dot{Q}$) monitoring can support the management of high-risk surgical patients, but the pulmonary artery catheterisation required by the current 'gold standard'—bolus thermodilution ($\dot{Q}_T$)—has the potential to cause life-threatening complications. We present a novel noninvasive and fully automated method that uses the inspired sinewave technique to continuously monitor cardiac output ($\dot{Q}_{IST}$).

Methods: Over successive breaths the inspired nitrous oxide (N_2O) concentration was forced to oscillate sinusoidally with a fixed mean (4%), amplitude (3%), and period (60 s). $\dot{Q}_{IST}$ was determined in a single-compartment tidal ventilation lung model that used the resulting amplitude/phase of the expired N_2O sinewave. The agreement and trending ability of $\dot{Q}_{IST}$ were compared with $\dot{Q}_T$ during pharmacologically induced haemodynamic changes, before and after repeated lung lavages, in eight anaesthetised pigs.

Results: Before lung lavage, changes in $\dot{Q}_{IST}$ and $\dot{Q}_T$ from baseline had a mean bias of −0.52 L min^{-1} (95% confidence interval [CI], −0.41 to −0.63). The concordance between $\dot{Q}_{IST}$ and $\dot{Q}_T$ was 92.5% as assessed by four-quadrant analysis, and polar plot analysis revealed a mean angular bias of 5.98° (95% CI, −24.4°–36.3°). After lung lavage, concordance was slightly reduced (89.4%), and the mean angular bias widened to 21.8° (−4.2°, 47.6°). Impaired trending ability correlated with shunt fraction (r=0.79, P<0.05).

Conclusions: The inspired sinewave technique provides continuous and noninvasive monitoring of cardiac output, with a 'marginal–good' trending ability compared with cardiac output based on thermodilution. However, the trending ability can be reduced with increasing shunt fraction, such as in acute lung injury.

Keywords: cardiac output; haemodynamic; mechanical ventilation; monitoring; nitrous oxide; noninvasive; respiration; thermodilution

Accepted: 11 February 2019

© 2019 The Authors. Published by Elsevier Ltd on behalf of British Journal of Anaesthesia. This is an open access article under the CC BY license (http://creativecommons.org/licenses/by/4.0/).
For Permissions, please email: permissions@elsevier.com

Editor's key points

- The inspired sinewave method can be used to determine cardiac output noninvasively in mechanically ventilated subjects.
- This proof-of-concept study aimed to determine the level of agreement and trending ability of this technique with thermodilution-based cardiac output in a pig model.
- Under control conditions, there was a good level of agreement but with wide limits of agreements between both methods, with marginal–good trending ability.
- The trending ability was reduced by lung lavage-induced acute lung injury.
- Further studies should reveal whether inspired sinewave technology could be developed as an accurate cardiac output monitoring technique.

Cardiac output monitoring can be used to manage surgical patients at high risk of haemorrhage or haemodynamic instability, and is an essential part of goal-directed therapy.[1–3] Bolus thermodilution remains the current 'gold standard' for measuring cardiac output, but the required pulmonary artery catheterisation is highly invasive and has the potential to lead to life-threatening complications.[4] Indeed, it is still uncertain whether its application in critically ill patients improves clinical outcomes.[5–7] As such, the use of pulmonary artery catheterisation has declined in favour of techniques that are less invasive, such as transpulmonary thermodilution and those utilising transoesophageal Doppler and pulse contour analysis.[8]

The ideal cardiac output monitor should be noninvasive and automated, and generate continual, accurate, and precise measurements. Measuring cardiac output via a respiratory based method such as the inspired sinewave technique (IST) has the potential to meet these criteria. The theoretical and experimental basis for the IST originates from the work of Zwart and colleagues[9] and Hahn and colleagues,[10,11] whereby the concentration of a tracer gas (e.g. nitrous oxide [N_2O]) is sinusoidally oscillated in inspired air. A mathematical model of the lung processes the resultant amplitude/phase of the expired sinewave signal and recovers values for cardiopulmonary variables such alveolar volume and pulmonary blood flow ($\dot{Q}_{IST}$).[12–14]

This proof-of-concept study aimed at validating the $\dot{Q}_{IST}$ technique in anaesthetised, mechanically ventilated pigs during pharmacologically induced haemodynamic changes and a saline lavage model of acute lung injury. We particularly examined the trending ability and agreement of $\dot{Q}_{IST}$ with invasive cardiac output measurements based on thermodilution.

Methods

Inspired sinewave technique

Details of the IST and inspired sinewave device (ISD) have been detailed elsewhere,[15] but in brief: at the start of each inhalation a small volume of N_2O is injected into inspired gas by a mass flow controller (Alicat Scientific, Inc., Tucson, AZ, USA). Airflow is measured using an ultrasonic flowmeter (VenThor 22/2A; Thor Laboratories, Budapest, Hungary), and N_2O concentration using a rapid mainstream infrared sensor (Square One Technology, Boulder, CO, USA). The volume injected is proportional to inspiratory flow, and over time (i.e. successive breaths) the inspired N_2O concentration oscillates sinusoidally around a fixed mean (4%), with a predetermined amplitude (3%) and period (60 s). Without venous recirculation of the N_2O sinewave, which is assumed negligible at short periods (i.e. <3 min),[16] the end-tidal N_2O concentration also oscillate in a sinewave pattern (Fig. 1). A single-compartment tidal ventilation model of the lung uses this resulting amplitude and phase of the expired sinewave to estimate cardiopulmonary variables such as pulmonary blood flow ($\dot{Q}_{IST}$). The mathematical principles of the IST and the hardware layout of the ISD are provided in Supplementary Fig. S1.

Animal preparation

Measurements were made in eight female large white pigs with a weight of 37–53 kg (mean=43.6 kg). All procedures in the study were approved by a local ethics committee and the UK Home Office, London, UK (PPL: 30/2960) and performed at

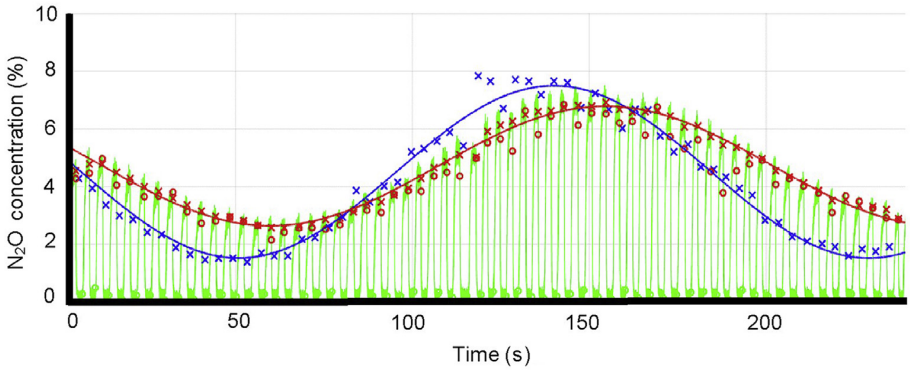


Fig 1. A typical example of recorded data, with inspired N_2O concentration oscillating sinusoidally around a fixed mean (4%), with a predetermined amplitude (3%) and period (180 s). Green line is the expired N_2O concentration; the blue and red crosses are the N_2O concentrations in inspired gas and end-tidal gas, respectively; the blue and red lines are the inspired and expired N_2O sinewaves, respectively (reproduced from Bruce and colleagues[15]).

the school of Veterinary Sciences, University of Bristol, Bristol, UK. At the end of each study, the animals were killed under anaesthesia with an overdose of pentobarbital (~100 mg kg^{-1}). Relevant sections of the Animal Research: Reporting of *In Vivo* Experiments (ARRIVE) guidelines were followed.

All procedures have been detailed elsewhere,[17] but in brief: the pigs lay in dorsal recumbency and received i.v. anaesthesia using ketamine, fentanyl, and midazolam. The trachea was intubated, and ventilation was provided in volume-controlled mode using an Engström Carestation Ventilator (GE Healthcare, Madison, WI, USA), which delivered a tidal volume of 8 ml kg^{-1}, with positive end-expiratory pressure set at 5 cm H_2O. Ventilatory frequency was adjusted to maintain $PaCO_2$ between 4.5 and 8 kPa, and it then remained fixed throughout the protocol. Adequacy of general anaesthesia was established with the absence of movement/reflexes the absence of a reaction to painful stimulation between the front hooves, and haemodynamic monitoring. Pancuronium was then administered for muscle relaxation, and Hartmann's solution (10 ml kg^{-1} h^{-1}) was used for fluid maintenance. Additional boluses of the muscle relaxant were administered when spontaneous ventilatory efforts were detected from the airway gas and pressure traces. The adequacy of anaesthesia was determined during the periods of muscle relaxation by the absence of cardiovascular signs of sympathetic stimulation (increases in heart rate or arterial BP). Anaesthesia was maintained with continuous i.v. ketamine 32 mg kg^{-1} hr^{-1}, fentanyl 4 mg kg^{-1} hr^{-1}, and midazolam 0.16 mg kg^{-1} hr^{-1}.

A pulmonary artery catheter (PAC; Edward Lifesciences, Irvine, CA, USA) was inserted into the internal jugular vein and advanced into the pulmonary artery. Assessment of pulmonary artery pressure (PAP) and wedge waveforms confirmed the correct position of the PAC. Arterial pressure (via a peripheral artery), PAP, ECG, $\%SO_2$, and end-tidal CO_2 were continuously recorded, whereas $\dot{Q}_T$ was measured intermittently (see below). Variables were monitored with standard patient monitors (Datex Ohmeda Capnomac Ultima; multiparameter patient monitor, Datex AS3, Madison, WI, USA) and recorded on a computer via PowerLab and LabChart (AD Instruments, Dunedin, New Zealand).

Experimental protocol

After a stabilisation period of approximately 20 min, baseline measurements were recorded for 10 min, where $\dot{Q}_T$ measurements did not fluctuate by more than 15%. Cardiac output was then pharmacologically manipulated via infusions of esmolol (300–400 μg kg^{-1} min^{-1}), reducing $\dot{Q}_T$ by at least 1 L min^{-1}, followed by infusions of dobutamine (15–20 μg kg^{-1} min^{-1}) increasing $\dot{Q}_T$ by at least 3 L min^{-1} above baseline measurements.

Measurements of $\dot{Q}_{IST}$ are fully automated and continued throughout the entire protocol. $\dot{Q}_{IST}$ is calculated every 30 s as a rolling average of the previous 3 min. $\dot{Q}_T$ was calculated using the Datex cardiac output module, and was obtained as the average of three 10 ml injections of normal saline through the PAC. $\dot{Q}_T$ measurements were obtained every 3–5 min, and only three measurements $\leq$10% apart were used to form the average. As each $\dot{Q}_{IST}$ measurement is a rolling average, linear regression analysis between paired $\dot{Q}_T$ and $\dot{Q}_{IST}$ measurements was used to determine any time delay, as described elsewhere.[18] In these experiments, the time delay of $\dot{Q}_{IST}$ measurements was shown to be around 60 s. After correction, paired cardiac output measurements were used for the subsequent analysis.

After these measurements, repeated warm saline lavages were performed (30 ml kg^{-1} 0.9% NaCl at approximately 38°C) until a PaO_2/F_IO_2 ratio of 200–300 mm Hg was achieved, as determined from arterial blood gas analysis. The above experimental protocol was then repeated.

Statistical analysis

The experiments were designed in accordance with Home Office principles of RRR, essentially minimising animal use whilst preserving data fidelity. Sample sizes were estimated

Table 1 Baseline and respiratory and haemodynamic variables from each animal before repeated saline lavages. DBP, diastolic blood pressure; F_IO_2, fraction of inspired O_2; Hb, haemoglobin; HR, heart rate; IST, inspired sinewave technique; $\dot{Q}_T$, cardiac output from PAC thermodilution; $\dot{Q}_{IST}$, cardiac output from IST; PAC, pulmonary artery catheter; $PaCO_2$, arterial CO_2 partial pressure; PaO_2, arterial O_2 partial pressure; PAP, mean pulmonary artery pressure; Paw Peak, peak airway pressure; PFR, PaO_2/FiO_2 ratio; SaO_2, arterial oxygen saturation; SBP, systolic blood pressure

Uninjured Parameter	Animal number								Mean
	1	2	3	4	5	6	7	8	
Weight (kg)	46.5	45	39	53	37	37	47	44.5	43.6
HR (beats min^{-1})	75	70	100	87	60	87	70	102	81
SBP (mm Hg)	113	101	105	80	130	95	105	95	103
DBP (mm Hg)	87	62	71	60	90	85	75	65	74
$\dot{Q}_T$ (L min^{-1})	2.9	6.2	5	4.4	3.9	3.2	6.7	3.7	4.5
$\dot{Q}_{IST}$ (L min^{-1})	3.9	6	4.1	4.9	8.1	5.6	7.2	9.2	6.1*
PAP (mm Hg)	20	16	18	15	17	18	16	21	18
Haemoglobin (g dl^{-1})	7.8	8.2	8.9	8.3	10.2	8.3	8.8	9.6	8.8
F_IO_2	0.6	0.28	0.4	0.4	0.35	0.4	0.4	0.4	0.4
SaO_2 (%)	99	99	100	99	95	97	100	97	98
pH	7.37	7.48	7.49	7.38	7.31	7.33	7.33	7.24	7.36
PaO_2 (mm Hg)	304	115	163	160	186	196	164	175	182
$PaCO_2$ (mm Hg)	59	45	44	46	60	56	58	60	53.5
PFR	507	411	408	400	531	490	410	438	449
Paw peak (cm H_20)	15	14	16	18	16	16	15	13	15

* significant difference from $\dot{Q}_T$ ($P<0.05$)

using Mead's resource equation, as is typical for laboratory animal studies. We chose the sample size to give a value of E (the error degree of freedom) between 10 and 20. Since we used the same animals for measurements before and after lung injury (paired), and a quasi-factorial 'treatment' design (i.e. changing cardiac output from resting to higher to lower), a sample size of 8 animals yields an E value of 20. Results are displayed as means 95% confidence interval

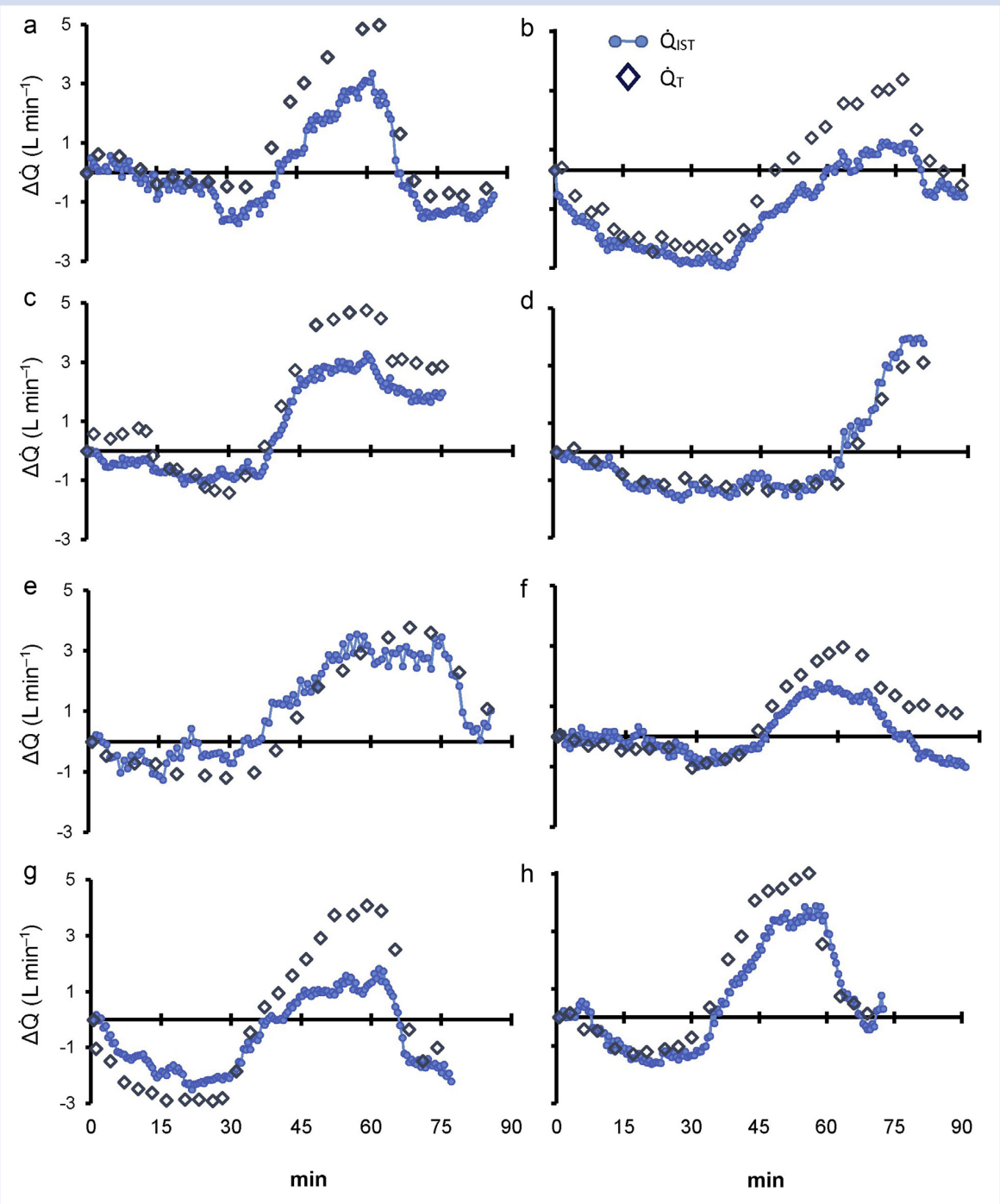


Fig 2. (a–h) $\Delta\dot{Q}$ from baseline in all eight animals throughout the protocol. Dark blue diamonds are $\dot{Q}_T$ measurements, and light blue dots and lines are $\dot{Q}_{IST}$ measurements.

unless otherwise stated. The agreement of paired absolute $\dot{Q}_T$ and $\dot{Q}_{IST}$ values were assessed via calculating their interchangeability rate.[19] Values were considered interchangeable if the difference was less than a maximal acceptable value:

$$\frac{\dot{Q}_T + \dot{Q}_{IST}}{2} \times \sqrt{R\dot{Q}_T^2 + R\dot{Q}_T^2},$$

where RQ_T is the repeatability coefficient for $\dot{Q}_T$ measurements. The agreement between absolute $\dot{Q}_T$ and $\dot{Q}_{IST}$, and between the changes in $\dot{Q}_T$ and $\dot{Q}_{IST}$ from baseline ($\Delta\dot{Q}_T$ and $\Delta\dot{Q}_{IST}$, respectively) were examined via Bland–Altman analysis, and adjusted for multiple measurements within subjects.[20] The trending ability of $\dot{Q}_{IST}$ *vs* $\dot{Q}_T$ was examined by calculating the Pearson correlation coefficient (r) for paired $\Delta\dot{Q}$ from the previous paired measurements and assessing the concordance (% of paired $\Delta\dot{Q}$ with same directional change) using a four-quadrant plot. A concordance >92% is considered a good trending ability.[21,22] In addition to assessing the agreement of the direction of $\Delta\dot{Q}$ with a four-quadrant plot, the agreement of the magnitude of $\Delta\dot{Q}$ has been examined with a half-circle polar plot—both calculated with an exclusion zone of 15% mean $\dot{Q}$.[18,21,22] With polar plots, the radial length of each data point represents the mean of paired $\Delta\dot{Q}_T$ and $\Delta\dot{Q}_{IST}$, and the polar angle (°) signifies the agreement of the magnitude of $\Delta\dot{Q}$ between the two methods. A mean polar angle (angular bias) of approximately ±5° with a concordance of >95% (% data points within ±30°) (radial limits of agreement) is considered to have a good trending ability, and a concordance of 90–95% is considered marginal.[21]

Trending ability was also assessed via the trend interchangeability method (TIM).[23] First, changes in $\dot{Q}_T$ are determined as 'interpretable' if no overlap exists between the confidence intervals ($\dot{Q}_T \pm \dot{Q}_T \times$ repeatability coefficient) of consecutive measurements. Each interpretable $\Delta\dot{Q}_T$ is then either determined as interchangeable with $\Delta\dot{Q}_{IST}$, non-interchangeable, or situated within an uncertain interchangeable zone.[23] Changes are regarded interchangeable if the second pair of measurements ($\dot{Q}_T$ and $\dot{Q}_{IST}$) are found within a predicted precision interval (i.e. within confidence intervals of interchangeable changes), calculated via a predicted line of identity from the first pair of measurements ($\dot{Q}_{T1}$ and $\dot{Q}_{IST1}$) and the repeatability coefficient of $\dot{Q}_T$. These confidence intervals can be defined as follows: $X = Y(1 + RQT) + (1 + RQT)(\dot{Q}_{T1} - \dot{Q}_{IST1})$ and $X = Y(1 - RQT) + (1 + RQT)(\dot{Q}_{T1} - \dot{Q}_{IST1})$. $\Delta\dot{Q}$ is considered uncertain if its interval of precision intersects one of the confidence intervals, but the value itself does not lie within them.

Differences between baseline variables were assessed via two-tailed unpaired Student's t-tests, with statistical significance set at $P<0.05$. All analyses were completed using

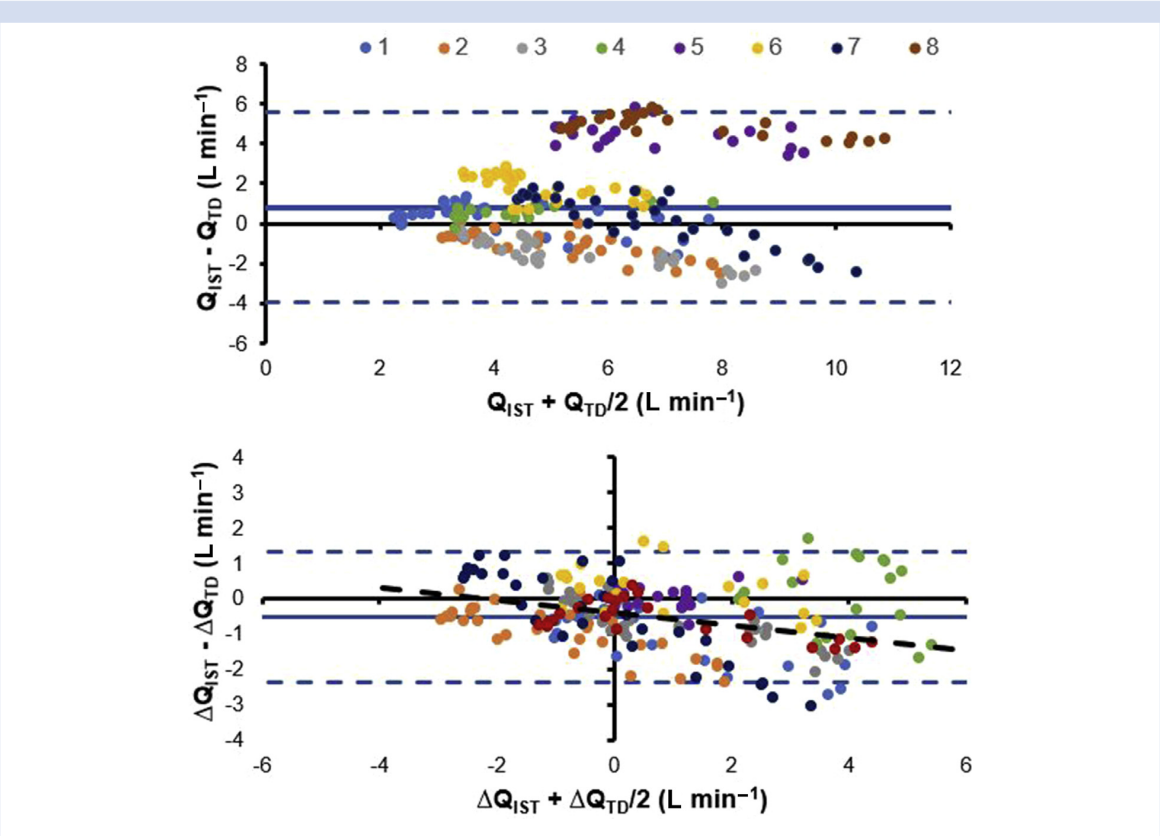


Fig 3. Bland–Altman analysis of the agreement between paired measurements of (a) $\dot{Q}_{IST}$ *vs* $\dot{Q}_T$ and (b) $\Delta\dot{Q}_{IST}$ *vs* $\Delta\dot{Q}_T$ from baseline. Colours represent each animal (1–8). Solid line, mean difference (bias); dotted lines, limits of agreement (LOA).

standard statistical software (Sigma plot version 13; Systat Software, Erkrath, Germany).

Results

Uninjured lung

Baseline haemodynamic and blood gas measurements for each animal are shown in Table 1. All animals survived the protocol, which resulted in marked haemodynamic changes (Fig. 2). A total of 248 paired $\dot{Q}_{IST}$ and $\dot{Q}_T$ measurements were recorded and the $\Delta\dot{Q}$ values from baseline are presented in Figure 2a–h. Linear regression analysis produced the regression equation $\Delta\dot{Q}_{IST} = 0.68 \times \Delta\dot{Q}_T - 0.45$, with r=0.88. Bland–Altman analysis of absolute $\dot{Q}_T$ and $\dot{Q}_{IST}$ values (Fig. 3a) shows a mean bias of 0.79 L min^{-1} (0.51, 1.07) with limits of agreement (LOA) ranging from 5.5 (4.6, 6.4) to −3.9 L min^{-1} (−2.8, −4.7). Despite this wide LOA *between* data points from all animals, the LOA *within* each animal is substantially narrower: the LOA for each animal ranged between 0.31 and 0.8 L min^{-1} (mean=0.61 L min^{-1}). This is reflected in the Bland–Altman analysis of $\Delta\dot{Q}_{IST}$ *vs* $\Delta\dot{Q}_T$ (Fig. 3b), where data were normalised to the individual mean baseline value, showing a mean bias of −0.52 (−0.41, −0.63) with LOA ranging from −2.4 (−2, −2.6) to 1.3 (0.9, 2.6), and linear regression analysis reveals an equation of $\Delta\dot{Q}_{IST} - \Delta\dot{Q}_T = 0.27 \times \text{mean}\ \Delta\dot{Q} - 0.56$, r=0.48. The interchangeability rate was calculated as 41%. As only poor interchangeability was observed, estimating the range of interchangeable measurements was inappropriate.

Trending ability was assessed by calculating the $\Delta\dot{Q}$ from the previous paired measurement values throughout the protocol, with $\Delta\dot{Q}$ <15% mean $\dot{Q}$ excluded. Linear regression shows a high correlation between $\Delta\dot{Q}_{IST}$ and $\Delta\dot{Q}_T$ of 0.84 (P<0.01). The concordance was 92.5% as assessed using four-quadrant analysis (Fig. 4), where data points located in either quadrant of agreement were considered concordant. Linear regression analysis of the four-quadrant plot shows an equation of $\Delta\dot{Q}_{IST} = 0.65 \times \Delta\dot{Q}_T + 0.01$. Half-circle polar plot analysis (Fig. 5) revealed an angular bias of 5.98° (−24.4°, 36.3°), and a concordance of 92.3% (% of data points within ±30° limits). Half-circle polar plot analysis of the %$\Delta\dot{Q}$ (Supplementary Fig. S3) revealed an angular bias of 4.75° (26.8, 36.2) and a concordance of 90.5%. Trending ability assessed via the TIM demonstrated the following: 65.1% of paired measurements were uninterpretable, 13.2% interchangeable, 9.7% uncertain, and 12% non-interchangeable.

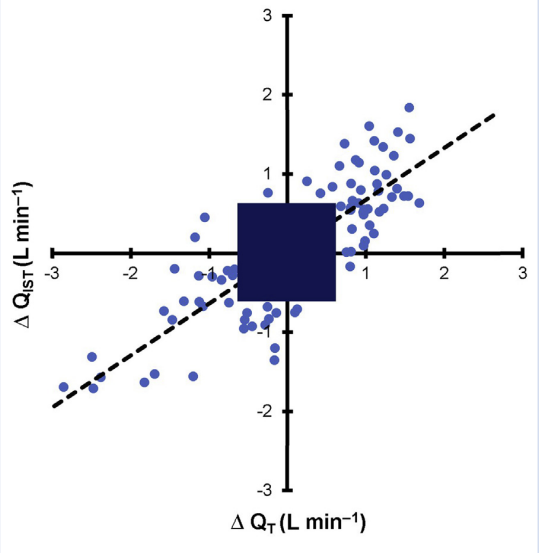


Fig 4. Four-quadrant plot analysis of $\Delta\dot{Q}_{IST}$ *vs* $\Delta\dot{Q}_T$ throughout the protocol, with an exclusion zone of 15% mean $\dot{Q}$ (0.67 L min^{-1}). Linear regression analysis reveals an equation of $\Delta\dot{Q}_{IST}$=0.65×$\Delta\dot{Q}_T$+0.01, where r=0.84. Data points located in either quadrant of agreement were considered concordant (92.5%).

Injured lung model

Repeated saline lavages resulted in significant reductions in the mean baseline PaO_2/F_IO_2 ratio (250.4 mm Hg [201.4, 299.4] *vs* 449 mm Hg [413, 455]; P<0.05). Trending ability was examined using the same approaches discussed above (Supplementary Figs S4 and S5). Four-quadrant analysis revealed a concordance of 89.4%, and polar plot analysis showed a mean angular bias of 21.8° (−4.2°, 47.6°) and a concordance of 69.7%. There was a reduced slope in the linear regression equation of the four-quadrant plot ($\Delta\dot{Q}_{IST} = 0.3 \times \Delta\dot{Q}_T + 0.1$), highlighting that impairments in trending ability after lung injury was the result of underestimations in $\Delta\dot{Q}_{IST}$ relative to $\Delta\dot{Q}_T$. This impaired trending ability was correlated with shunt fraction (Supplementary Fig. S6; r=0.79, P<0.05). The $\Delta\dot{Q}$ from baseline in the injured animals are presented in Supplementary Figure S7a–h. Trending ability assessed via TIM demonstrated: 53.7% of paired measurements were uninterpretable, 7.1% interchangeable, 7.6% uncertain, and 31.5% non-interchangeable.

Discussion

This proof-of-concept study investigated a novel, noninvasive, and fully automated method to continuously monitor changes in cardiac output using the IST. We showed that a prototype device that utilised the IST could be integrated in a breathing circuit of mechanical ventilator, suggesting that it is feasible to use within the perioperative setting. We further demonstrated that a cardiac output based on the IST demonstrated a 'marginal–good' trending ability, based upon four-quadrant plot and polar analysis, compared with the pulmonary artery catheter thermodilution reference method.[21]

Thermodilution is widely considered the gold standard technique for cardiac output monitoring. However, because of its highly invasive nature and the associated complications, its clinical use is becoming less frequent.[6,8] In contrast, the use of less invasive techniques such as those utilising pulse contour analysis or Doppler ultrasound have increased, yet they remain dependent on the skill of the user and their application still requires a somewhat invasive procedure such as an arterial line[8] (although arterial vascular access is often routinely required in critically ill patients). Respiratory techniques, such as the IST, have the potential to provide an entirely noninvasive method to monitor cardiac output. The IST also has other qualities of an idealised cardiac output monitor,[24] such as its ability to deliver automated and continual measurements that are independent from the skill of the operator. In addition the IST, like other respiratory-based methods,[25] can simultaneously estimate other aspects of cardiopulmonary function such as effective lung volume,[15]

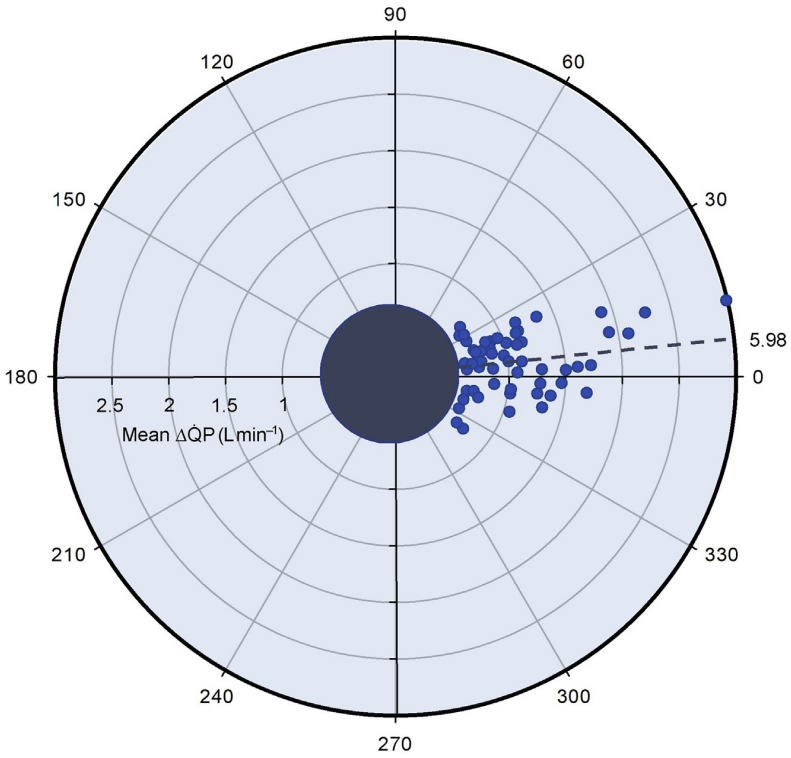


Fig 5. Half-circle polar-plot analysis of $\dot{Q}_{IST}$ *vs* $\dot{Q}_T$ throughout the protocol, with an exclusion zone of 15% mean cardiac output (0.67 L min^{-1}). Mean angular bias=5.98° (radial limits, ±30.2°). Data points located within ±30° limits were considered concordant (92.3%). Data points distributed near the polar axis (0°) indicate good trending.

a parameter which may provide additional clinically important information for mechanically ventilated patients.

The trending ability of the IST compares well with other noninvasive or minimally invasive methods of monitoring cardiac output. Examining concordance using a four-quadrant plot against thermodilution has been commonly used. The concordance of >92% in the current investigation is commonly regarded as a 'good' or clinically acceptable trending ability,[21,22] and this is similar to that observed in human participants with transoesophageal Doppler[26,27] and certain pulse contour techniques,[28,29] and is superior to non-calibrated pulse contour.[30,31] Furthermore, analysis via TIM revealed a similar percentage of paired interchangeable measurements in comparison with pulse contour techniques such LiDCO and PiCCO.[23]

The findings are also similar to other recently developed respiratory-based approaches utilising the Fick principle,[32,33] the trending ability of which have also been examined in pigs. In the current investigation polar plot analysis revealed a mean angular bias that was comparable with other respiratory-based methods,[32,33] and a concordance that was similar to other respiratory-based techniques and considered a 'marginal' trending ability.[21] Altogether, IST seems to have a marginal–good trending ability relative to PAC thermodilution, and is comparable with other respiratory-based or minimally invasive techniques.

Despite the encouraging trending ability, the absolute agreement between $\dot{Q}_{IST}$ and $\dot{Q}_T$ was weaker. This can be easily observed from the examination of the baseline variables where offset errors have occurred, and from the poor interchangeability rate. Bland–Altman analysis of absolute values revealed an acceptable bias. A wide LOA could make it impossible to achieve good trending ability between $\Delta\dot{Q}_{IST}$ and $\Delta\dot{Q}_T$, but a closer inspection reveals that the majority of bias variability occurs *between* animals, not *within* each animal. Indeed, the LOA for each individual animal was low, and so normalisation of values to each animal results in a lower bias and narrower LOA and a good trending ability, which clearly demonstrates the potential of the technique. From a practical perspective, when monitoring patients in many clinical settings absolute values only offer limited information, whereas the temporal variation in values (e.g. the % change in cardiac output) from what is 'normal' for each individual patient provides greater clinical insight.[34] Indeed, polar plot analysis reveals an even smaller angular bias when $\Delta\dot{Q}_{IST}$ and $\Delta\dot{Q}_T$ are presented as percentage changes.

Bland–Altman analysis of $\Delta\dot{Q}$ from baseline also shows the existence of greater degrees of $\dot{Q}_{IST}$ underestimation with higher mean $\Delta\dot{Q}$. Indeed, it is likely that the LOA at these higher $\Delta\dot{Q}$ is underestimated. This scaling error could be a consequence of the recirculation of the N_2O sinewave emerging at higher cardiac outputs and so conflicts with

assumptions made by the lung model. Clearly, further work and adjustments to the model are needed to improve the trending (and absolute agreement) of $\dot{Q}_{IST}$ *vs* $\dot{Q}_T$ and, as a first step, simulations using single and multi-compartmental tidal lung models are being developed to investigate these questions.

Data from the IST measurements are averaged over a 3 min rolling window and updated to the monitor every 30 s. The time of 3 min was chosen because it captures three full sinewave periods and gives robust solutions, although a shorter period could be used depending on the degree of stability required. Theoretically this approach has two potential clinical consequences. The first is that it will dampen the dynamic component of the cardiac output time series, and the second is that it results in a lag between real-time cardiac output changes and their registration. Given that even under the most challenging clinical circumstances (other than sudden cardiac arrest), cardiac output changes over a time course of minutes and the ultra-dynamic component of the time series is small; so the 3 min moving average should have so significant impact. In contrast, the 'lag' effect will clearly result in a delay in the registration of real-time CO values. In the data presented here, this was measured as being approximately 60 s (cf. contemporaneously measured $\dot{Q}_T$). This property is common to many other similar monitors where averaging is used (Lidco, Deltex) and needs to be taken into consideration.

The current experiment collected data from mechanically ventilated animals and so may not necessarily apply to human participants or those spontaneously breathing. Previous work has shown that IST measures of cardiopulmonary function are both accurate and reproducible in young healthy volunteers,[15] but further work is necessary to validate the technique in human patients/participants by comparing the trending ability of $\dot{Q}_{IST}$ with an appropriate reference method during haemodynamic changes.

There are several limitations with the statistical approaches used in the current study. The exclusion zone in the four-quadrant plot and polar analysis aims to remove small $\Delta\dot{Q}$ which may be attributed to noise, but its definition (e.g. an absolute value or % change) is rather arbitrary. Furthermore, the polar analysis exclusion zone may inadvertently remove the most discordant measurements, that is those that have similar absolute values but in opposite directions.[18] The concordance rate calculation in the four-quadrant plot does not account for the range of variation as, for example, a plot will be still be considered concordant if one method records $\Delta\dot{Q}$ of 100% and the other only 1%.[18] The TIM[23] may redress some of the limitations; however, as four-quadrant plots and polar analysis are the most commonly used approaches, and we want to compare the performance of IST with other techniques, they form the basis of our data analysis.

As with other respiratory-based approaches, the presence of lung disease or injury will likely impair aspects of $\dot{Q}_{IST}$ performance. The saline lavage model of acute lung injury in the current investigation reduced the trending ability of $\dot{Q}_{IST}$ and the concordance from a four-quadrant plot became slightly poorer. The reduced slope clearly revealed that impairments in trending ability were the result of underestimations in $\Delta\dot{Q}_{IST}$ relative to $\Delta\dot{Q}_T$. Any cardiac output that bypasses ventilated regions of the lung cannot be quantified by approaches relying on gas exchange measurements, and we have shown that the impaired trending of $\Delta\dot{Q}_{IST}$ was significantly correlated with shunt fraction. Further refinement of the lung model is required to address this issue; nevertheless, the estimation of 'effective' cardiac output—that is, blood flow that participates in pulmonary gas exchange—by respiratory-based techniques might also provide important clinical information in the critical care setting. For example, as increases in $\dot{Q}_{IST}$ should improve oxygenation and CO_2 elimination independently of any change in cardiac output, $\dot{Q}_{IST}$ might provide important additional information in the optimisation of ventilator settings.

Authors' contributions

Conception of the protocol: AF.
Design of the protocol: RB, PP, AF.
Acquisition of data: RB, DC, AM, FF, PP, AF.
Analysis and interpretation of the data: all authors.
Development of the new technique: RB, MT, PP.
Writing paper: RB.
Contributed to the production of the manuscript: DC, AM, MT, FF, PP, AF.

Acknowledgements

The authors are grateful for the important work from veterinary anaesthetists Christian Dancker and William McFadzean, and for the technical assistance from Hanne McPeak and Kristina Britchford.

Appendix A. Supplementary data

Supplementary data to this article can be found online at https://doi.org/10.1016/j.bja.2019.02.025.

Declaration of interests

ADF and PP have a patent pending which is relevant to this work (Method and apparatus for measurement of cardiopulmonary function; European patent no. EP 3122249 A1, US patent no. US20170100043 A1).

Funding

The UK Department of Health, National Institute of Health Research (II-LA-0214-20005) grant funded the development of the sensing unit used in the technology. A Wellcome Trust (HMRXGK00) grant funded the experimental costs.

References

1. Abbas SM, Hill AG. Systematic review of the literature for the use of oesophageal Doppler monitor for fluid replacement in major abdominal surgery. *Anaesthesia* 2008; **63**: 44–51
2. Aya HD, Cecconi M, Hamilton M, Rhodes A. Goal-directed therapy in cardiac surgery: a systematic review and meta-analysis. *Br J Anaesth* 2013; **110**: 510–7
3. Hamilton MA, Cecconi M, Rhodes A. A systematic review and meta-analysis on the use of preemptive hemodynamic intervention to improve postoperative outcomes in moderate and high-risk surgical patients. *Anesth Analg* 2011; **112**: 1392–402
4. Reuter DA, Huang C, Edrich T, Shernan SK, Eltzschig HK. Cardiac output monitoring using indicator-dilution

techniques: basics, limits, and perspectives. *Anesth Analg* 2010; **110**: 799–811
5. Connors Jr AF, Speroff T, Dawson NV, et al. The effectiveness of right heart catheterization in the initial care of critically ill patients. SUPPORT Investigators. *JAMA* 1996; **276**: 889–97
6. Harvey S, Harrison DA, Singer M, et al. Assessment of the clinical effectiveness of pulmonary artery catheters in management of patients in intensive care (PAC-Man): a randomised controlled trial. *Lancet (London, England)* 2005; **366**: 472–7
7. Schwann NM, Hillel Z, Hoeft A, et al. Lack of effectiveness of the pulmonary artery catheter in cardiac surgery. *Anesth Analg* 2011; **113**: 994–1002
8. Marik PE. Noninvasive cardiac output monitors: a state-of the-art review. *J Cardiothorac Vasc Anesth* 2013; **27**: 121–34
9. Zwart A, Seagrave RC, Van Dieren A. Ventilation–perfusion ratio obtained by a noninvasive frequency response technique. *J Appl Physiol* 1976; **41**: 419–24
10. Hahn CE, Black AM, Barton SA, Scott I. Gas exchange in a three-compartment lung model analyzed by forcing sinusoids of N_2O. *J Appl Physiol (Bethesda, Md: 1985)* 1993; **75**: 1863–76
11. Hahn CE. Oxygen respiratory gas analysis by sine-wave measurement: a theoretical model. *J Appl Physiol (Bethesda, Md: 1985)* 1996; **81**: 985–97
12. Williams EM, Sainsbury MC, Sutton L, et al. Pulmonary blood flow measured by inspiratory inert gas concentration forcing oscillations. *Respir Physiol* 1998; **113**: 47–56
13. Farmery A. *Interrogation of the cardiopulmonary system with inspired gas tension sinusoids*. University of London; 2008
14. Clifton L, Clifton DA, Hahn CEW, Farmery AD. Assessment of lung function using a non-invasive oscillating gas-forcing technique. *Respir Physiol Neurobiol* 2013; **189**: 174–82
15. Bruce RM, Phan PA, Pacpaco E, Rahman NM, Farmery AD. The inspired sine-wave technique: a novel method to measure lung volume and ventilatory heterogeneity. *Exp Physiol* 2018; **103**: 738–47
16. Gavaghan DJ, Hahn CE. A mathematical evaluation of the alveolar amplitude response technique. *Respir Physiol* 1995; **102**: 105–20
17. Formenti F, Bommakanti N, Chen R, et al. Respiratory oscillations in alveolar oxygen tension measured in arterial blood. *Sci Rep* 2017; **7**: 7499
18. Saugel B, Grothe O, Wagner JY. Tracking changes in cardiac output: statistical considerations on the 4-quadrant plot and the polar plot methodology. *Anesth Analg* 2015; **12**: 514–24
19. Lorne E, Diouf M, de Wilde RBP, Fischer MO. Assessment of interchangeability rate between 2 methods of measurements: an example with a cardiac output comparison study. *Medicine* 2018; **97**: e9905
20. Myles PS, Cui J. Using the Bland–Altman method to measure agreement with repeated measures. *Br J Anaesth (England)* 2007; **99**: 309–11
21. Critchley LA, Yang XX, Lee A. Assessment of trending ability of cardiac output monitors by polar plot methodology. *J Cardiothorac Vasc Anesth* 2011; **25**: 536–46
22. Critchley LA, Lee A, Ho AM. A critical review of the ability of continuous cardiac output monitors to measure trends in cardiac output. *Anesth Analg* 2010; **111**: 1180–92
23. Fischer MO, Diouf M, Wilde RB, Dupont H, Hanouz JL, Lorne E. Evaluation of cardiac output by 5 arterial pulse contour techniques using trend interchangeability method. *Medicine* 2016; **95**: e3530
24. Sangkum L, Liu GL, Yu L, Yan H, Kaye AD, Liu H. Minimally invasive or noninvasive cardiac output measurement: an update. *J Anesth* 2016; **30**: 461–80
25. Hallsjo Sander C, Lonnqvist PA, Hallback M, et al. Capnodynamic assessment of effective lung volume during cardiac output manipulations in a porcine model. *J Clin Monit Comput* 2016; **30**: 761–9
26. Perrino Jr AC, Harris SN, Luther MA. Intraoperative determination of cardiac output using multiplane transesophageal echocardiography: a comparison to thermodilution. *Anesthesiology* 1998; **89**: 350–7
27. Møller-Sørensen H, Cordtz J, Østergaard M, Nilsson JC, Hansen KL. Transesophageal Doppler reliably tracks changes in cardiac output in comparison with intermittent pulmonary artery thermodilution in cardiac surgery patients. *J Clin Monit Comput* 2017; **31**: 135–42
28. Jansen JR, Schreuder JJ, Mulier JP, Smith NT, Settels JJ, Wesseling KH. A comparison of cardiac output derived from the arterial pressure wave against thermodilution in cardiac surgery patients. *Br J Anaesth* 2001; **87**: 212–22
29. de Wilde RB, Schreuder JJ, van den Berg PC, Jansen JR. An evaluation of cardiac output by five arterial pulse contour techniques during cardiac surgery. *Anaesthesia* 2007; **62**: 760–8
30. Breukers RM, Sepehrkhouy S, Spiegelenberg SR, Groeneveld AB. Cardiac output measured by a new arterial pressure waveform analysis method without calibration compared with thermodilution after cardiac surgery. *J Cardiothorac Vasc Anesth* 2007; **21**: 632–5
31. Biancofiore G, Critchley LA, Lee A, et al. Evaluation of an uncalibrated arterial pulse contour cardiac output monitoring system in cirrhotic patients undergoing liver surgery. *Br J Anaesth* 2009; **102**: 47–54
32. Hallsjo Sander C, Hallback M, Wallin M, Emtell P, Oldner A, Bjorne H. Novel continuous capnodynamic method for cardiac output assessment during mechanical ventilation. *Br J Anaesth* 2014; **112**: 824–31
33. Klein M, Minkovich L, Machina M, et al. Non-invasive measurement of cardiac output using an iterative, respiration-based method. *Br J Anaesth* 2015; **114**: 406–13
34. Le Manach Y, Collins G. Statistical methods in hemodynamic research. In: *Perioperative hemodynamic monitoring and goal directed therapy: from theory to practice*. Cambridge: Cambridge University Press; 2014

Handling editor: C. Boer

NON-INVASIVE MONITORING OF CARDIAC OUTPUT USING THE INSPIRED SINEWAVE TECHNIQUE

Supplementary material

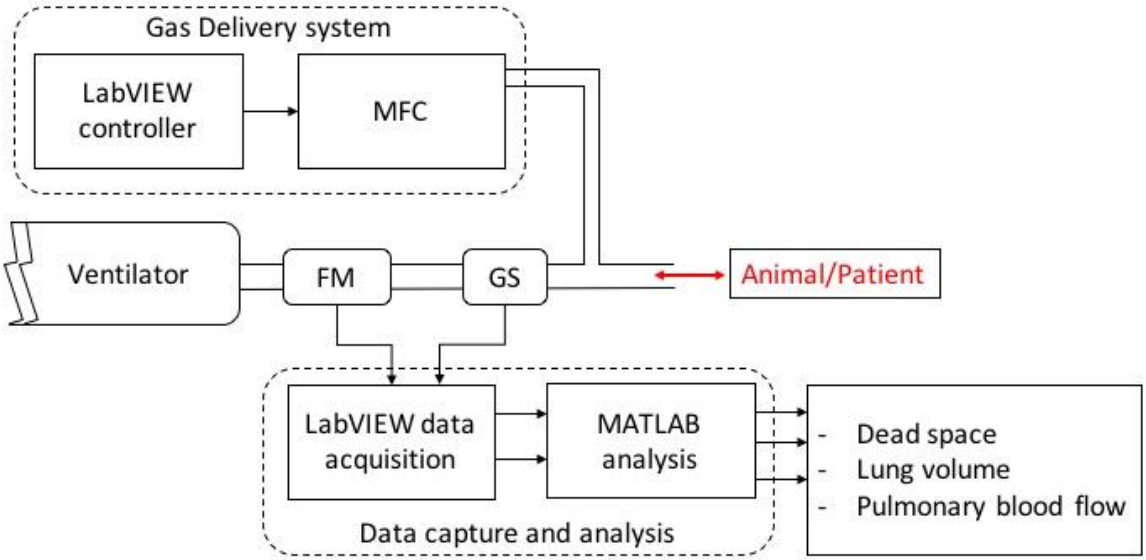


Figure 1S. Schematic representation of the Inspired Sinewave Device. Air is inhaled and exhaled through the flow meter (FM) and gas sensor (GS). Small volumes of N_2O are delivered into inspired gas at the beginning of each inspiration via a mass flow controller (MFC). Flow and gas concentration data are recorded, and cardiorespiratory variables are recovered using a mathematical model of the lung.

Mathematical principles of the IST

The oscillating inspired N_2O concentration can be defined by the equation:

$$F_I(t) = \bar{F}_I + \Delta F_I \sin\left(\frac{2\pi}{T}t + \phi\right) \qquad (eq.1)$$

where $\bar{F}_I$ is the mean amplitude, ΔF_I is the oscillation amplitude, T is the time period (60 seconds) and ϕ is the phase shift.

Figure 2S illustrates the lung model used for parameter recovery. The lung consists of one dead space compartment (V_D) and one lung compartment $V_A(t)$. The body is also considered as one compartment. The total pulmonary capillary blood flow through the lung is $\dot{Q}_P(t)$. N_2O tracer gas is inhaled through the dead-space into the lung and diffuses into pulmonary blood. After being distributed to different body compartments, the tracer gas renters the pulmonary circulation in mixed venous blood. It passes through dead space, before being exhaled.

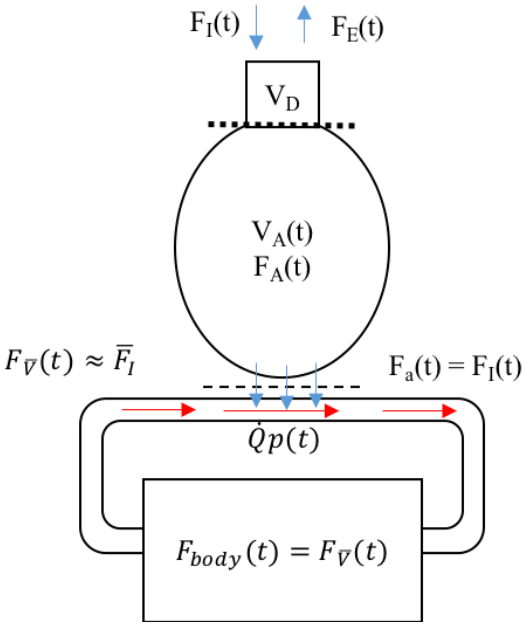


Figure 2S: The single compartment "balloon and straw" model of the lung and circulatory system

During the IST test, the $F_I(t)$ follows the sinewave pattern described by equation (eq.1). After an initial transient period, the alveolar concentration $F_A(t)$, the arterial concentration $F_a(t)$ and the mixed venous concentration $F_{\bar{v}}(t)$ all reach steady-state and follow sinusoidal patterns. The mixed venous concentration can then be described as:

$$F_{\bar{v}}(t) = \bar{F}_I + \Delta F_{\bar{v}} \sin\left(\frac{2\pi}{T}t + \phi_{\bar{v}}\right) \quad (eq.2)$$

From Figure 2S, the mass balance of the N_2O in the lung can be writen as:

$$Change\ of\ mass\ in\ lung = mass\ inhaled - mass\ exhaled - mass\ exchanged\ with\ the\ blood$$

So, the mass balance equation of the tracer gas of two consecutive breaths (*n*-1 and *n*) is:

$$F_{E,n-1} \times V_A + F_{\bar{I},n} \times \left(V_{T,n} - V_D\right) + F_{E,n-1} \times V_D - \lambda \times \dot{Q}_P \times \left(F_{E,n} - F_{\bar{v}}\right) \times \Delta t_n = V_A \times F_{E,n} + V_{T,n} \times F_{E,n} \quad (eq.3)$$

in which:

V_A: the alveolar lung volume;

$\dot{Q}_P$: the pulmonary blood flow;

V_D: the deadspace, estimated from the Bohr method;

$F_{\bar{I},n}$: the mean inspired concentration of breath n_{th};

$F_{E,n-1}$, $F_{E,n}$: the end expired concentrations of breath (n-1) and n;

λ: the solubility of N_2O, 0.47;

$F_{\bar{v}}$: the mixed venous concentration, assumed to equal to the mean of the inspired sinewave concentration at steady state F_I^0;

Δt_n: the duration of breath n_{th};

$V_{t,n}$: the tidal volume of breath n_{th}.

The mixed-venous concentration, $F_{\bar{v}}$, is assumed to be heavily damped by the body compartments and so to oscillate only negligibly at periods less than 3 minutes. Therefore, it can be considered as a constant $F_{\bar{v}}$ .which approximates to the mean inspired concentration, $\overline{F_I}$. The mass balance equation then becomes:

$$\begin{aligned} &\Leftrightarrow V_A \times \left(F_{E,n} - F_{E,n-1}\right) + \lambda \times \dot{Q}_P \times \left(F_{E,n} - \overline{F_I}\right) \times \Delta t_n \\ &= V_D \times \left(F_{E,n-1} - F_{\bar{I},n}\right) + V_{T,n} \times \left(F_{\bar{I},n} - F_{E,n}\right) \qquad (eq.4) \end{aligned}$$

The volume of dead-space was calculated using Bohr method:

$$V_D = V_T \frac{F_E - F_{\bar{E}}}{F_E - \overline{F_I}}$$

where $F_{\bar{E}}$ is the average expired tracer gas concentration and $\overline{F_I}$ is the mean inspired concentration. A modified Bohr method has also been proposed to further improve the accuracy and repeatability of the airway dead space estimation[17]. This method also increases the accuracy of Q_P and V_A estimation. With V_D and all the other parameters determined, effective lung volume (ELV = V_D + V_A) and $\dot{Q}_P$ (i.e. $\dot{Q}_{IST}$) are estimated by solving a set of mass balance equations (eq.4).

SUPPLEMENTARY FIGURES

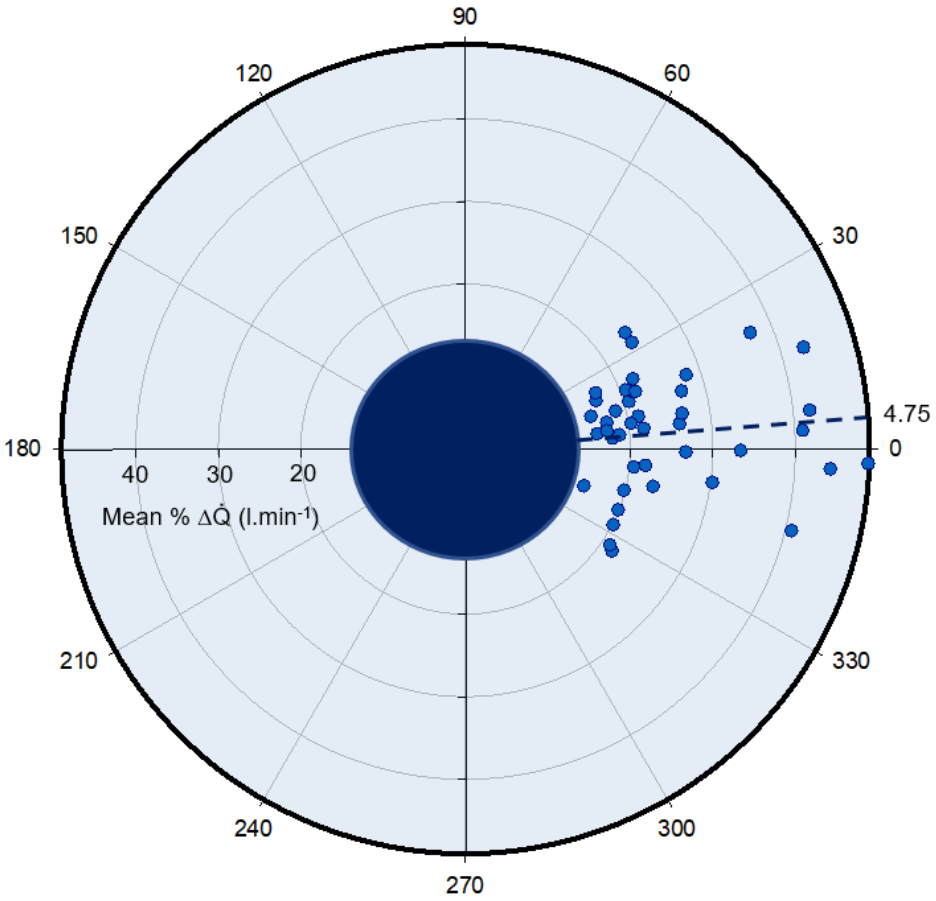


Figure 3S. Half circle polar-plot analysis of $\%\Delta\dot{Q}_{IST}$ vs. $\%\Delta\dot{Q}_{T}$ throughout the protocol pre-saline lung lavage, with an exclusion zone of 15% mean $\dot{Q}$. Mean angular bias = 4.75° (-26.8°, 36.3°). Data points located within ±30° limits were considered concordant (90.5%). Data points distributed near the polar axis (0°) indicate good trending.

SALINE LAVAGE MODEL TABLES/FIGURES

Injured									
Parameter	**Animal Number**								**Mean**
	1	**2**	**3**	**4**	**5**	**6**	**7**	**8**	
Weight (kg)	46.5	45	39	53	37	37	47	44.5	**43.0**
HR	78	73	84	72	104	96	78	69	**81**
SBP (mmHg)	94	105	97	70	77	84	103	15	**83**
DBP (mmHg)	69	47	72	46	40	54	59	47	**54**
$\dot{Q}_T$ (l min^{-1})	2.7	7.2	5.6	3.5	5.2	4.1	4.1	3.3	**4.5**
$\dot{Q}_{IST}$ (l min^{-1})	2.8	6.6	6.1	3.2	4.7	4.6	6.7	9.1	**5.5**
PAP (mmHg)	37	27	27	35	21	32	24	29	**29.1**
Hb (g dl^{-1})	7.2	6.7	7.7	8.3	8	6.9	7.6	8.8	**7.6**
FiO_2	0.6	0.7	0.7	0.8	0.7	0.7	0.9	0.9	**0.8**
SaO_2 (%)	93	99	100	93	100	99	99	100	**98**
pH	7.17	7.33	7.25	7.39	7.19	7.21	7.23	7.15	**7.23**
PaO_2 (mmHg)	92	178	232	93	249	169	221	298	**193**
$PaCO_2$ (mmHg)	78	50	69	80	78	73	73	85	**73**
PFR	153	255	331	116	355	241	245	331	**250**
Paw Peak (cmH_20)	38	28	26	39	18	28	26	33	**29**

Table 2. Baseline and respiratory and haemodynamic variables from each animal following repeated saline lavages. HR = heart rate, SBP = systolic blood pressure, DBP = diastolic blood pressure, $\dot{Q}_T$ = cardiac output from PAC thermodilution, $\dot{Q}_{IST}$ = cardiac output from IST; PAP = mean pulmonary artery pressure, Hb = haemoglobin, F_IO_2 = fraction of inspired O_2, SaO_2 = arterial oxygen saturation, PaO_2 = arterial O_2 partial pressure, $PaCO_2$ = arterial CO_2 partial pressure, PFR = PaO_2:FiO_2 ratio, Paw Peak = peak airway pressure. * Difference between baseline $\dot{Q}_{IST}$ and $\dot{Q}_T$ was 1.0 l.min^{-1} (-1.1, 3.1), P = 0.28).

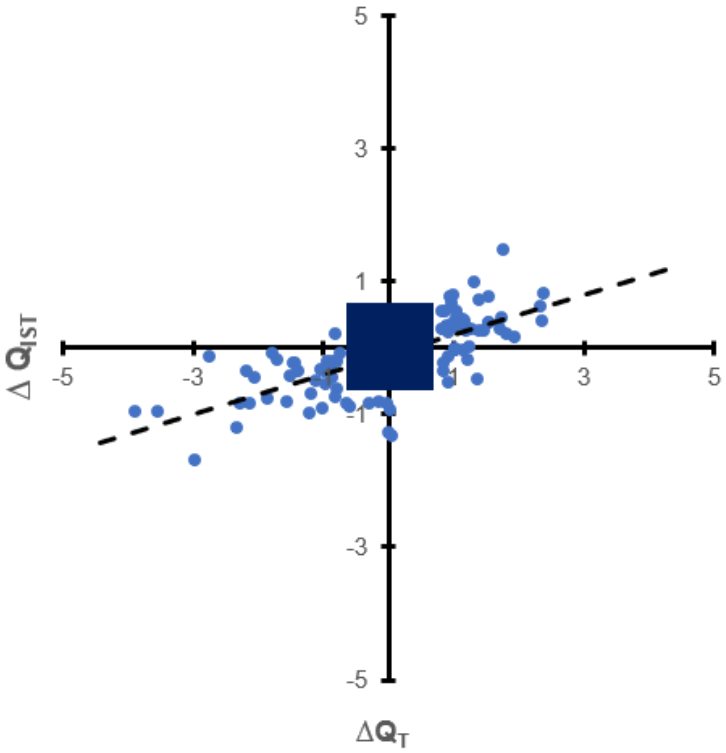


Figure 4S. Four-quadrant plot analysis of ΔQ̇IST vs. ΔQ̇T throughout the protocol post saline lung lavage, with an exclusion zone of 15% mean $\dot{Q}_T$ (0.75 l min^{-1}). Linear regression analysis reveals an equation of $\Delta\dot{Q}_{IST}$ 0.3 x $\Delta\dot{Q}_T$ + 0.1, with r = 0.72. Data points located in either quadrant of agreement were considered concordant (89.4%)

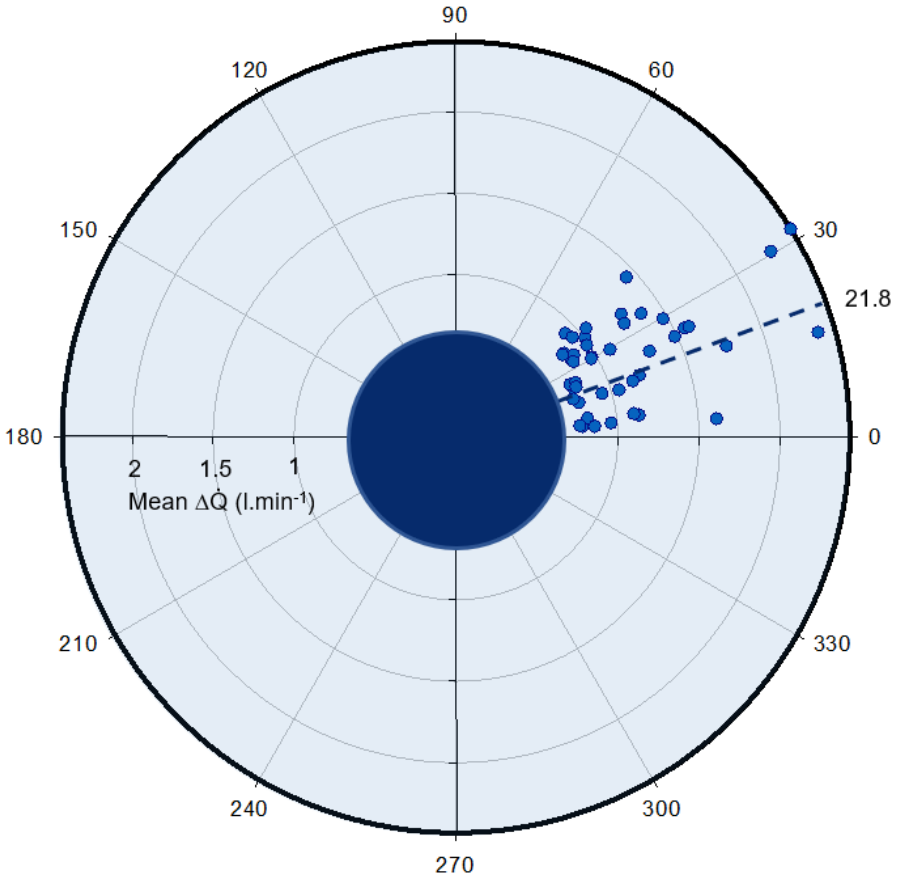


Figure 5S. Half circle polar-plot analysis of $\%\Delta\dot{Q}_{IST}$ vs. $\%\Delta\dot{Q}_{T}$ throughout the protocol post-saline lung lavage, with an exclusion zone of 15% mean $\dot{Q}_{T}$ (0.75 l.min^{-1}). Mean angular bias = 21.8° (-4.2°, 47.6°) Data points distributed near the polar axis (0°) indicate good trending.

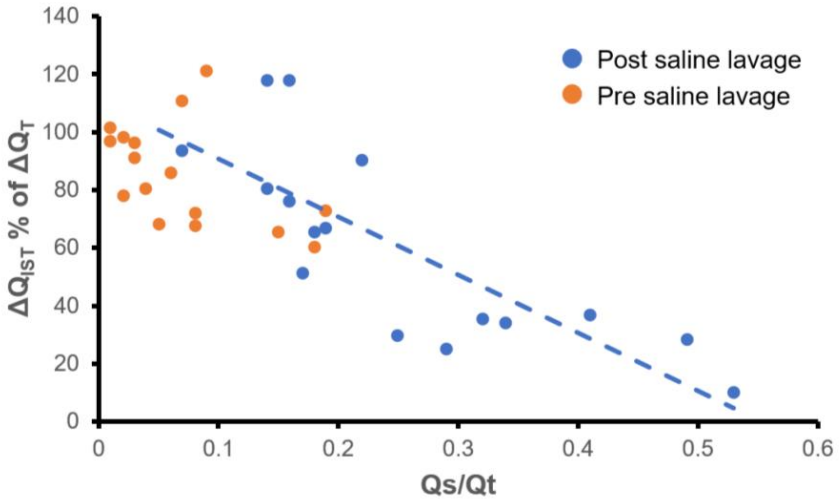


Figure 6S. The correlation, between shunt fraction ($\dot{Q}s/\dot{Q}t$) and the change in $\dot{Q}_{IST}$ expressed as a percentage of the change in $\dot{Q}_T$ ($\Delta\dot{Q}_{IST}$ % of $\Delta\dot{Q}_T$). Orange dots = pre-lavage; Blue dots = Post lavage; r = 0.79, $P<0.05$. Arterial blood gas samples, needed for the calculation of $\dot{Q}s/\dot{Q}t$, were collected on two occasions during each protocol: 1) during the nadir of $\dot{Q}_T$ and 2) during peak $\dot{Q}_T$. As such, $\Delta\dot{Q}_{IST}$ and $\Delta\dot{Q}_T$ were calculated as 1) the change in $\dot{Q}$ from baseline to nadir and 2) the change in $\dot{Q}$ from nadir to peak.

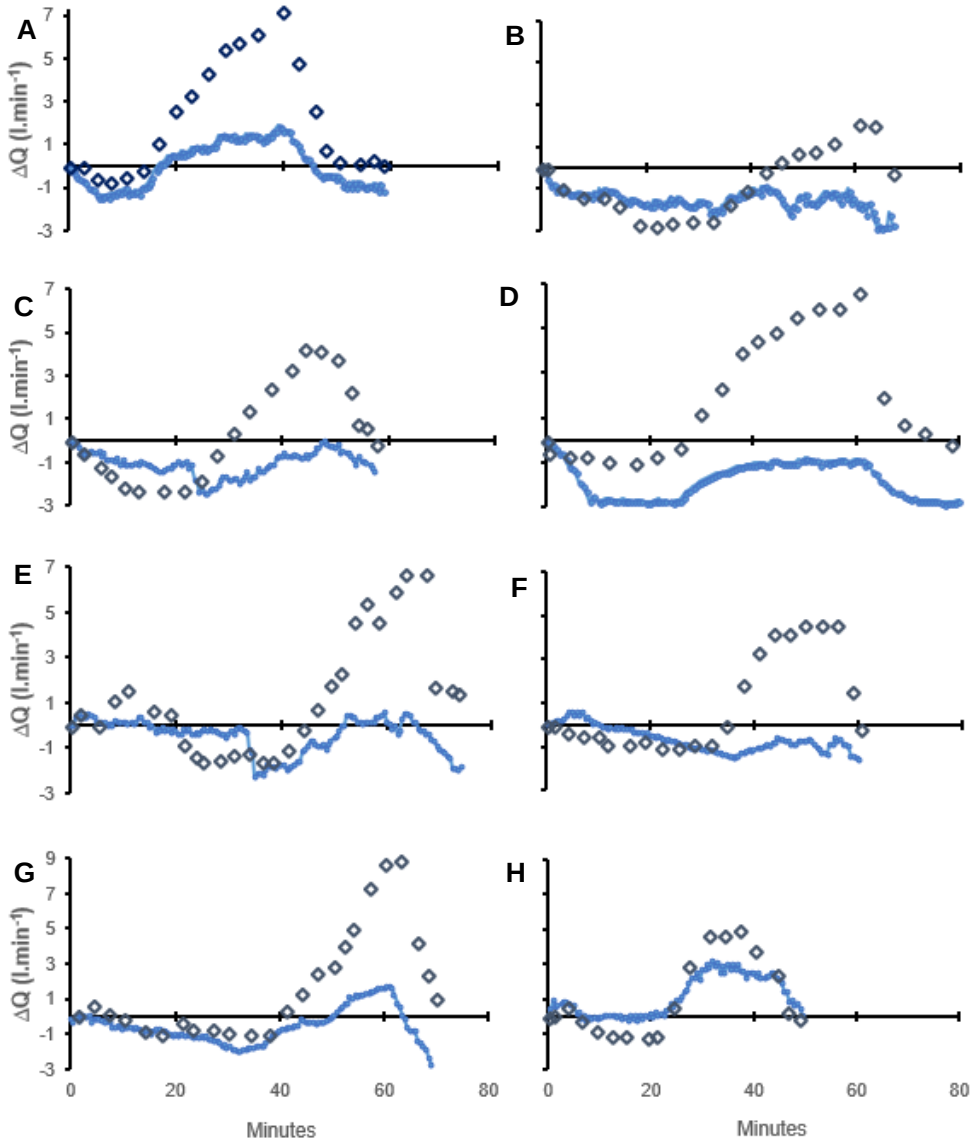


Figure 7S A-H. ΔQ̇ from baseline in all 8 animals throughout the protocol. Dark blue diamonds are $\dot{Q}_T$ measurements, and light blue dots and lines are $\dot{Q}_{IST}$ measurements.

BJA

British Journal of Anaesthesia, 124 (3): 345–353 (2020)

doi: 10.1016/j.bja.2019.11.030
Advance Access Publication Date: 14 January 2020
Respiration and the Airway

Validating the inspired sinewave technique to measure the volume of the 'baby lung' in a porcine lung-injury model

Douglas C. Crockett[1,*], Minh C. Tran[1,2], Federico Formenti[1,3,4], John N. Cronin[3], Göran Hedenstierna[5], Anders Larsson[6], Phi A. Phan[1] and Andrew D. Farmery[1]

[1]Nuffield Division of Anaesthetics, University of Oxford, Oxford, UK, [2]Department of Engineering Science, University of Oxford, Oxford, UK, [3]Centre for Human and Applied Physiological Sciences, King's College, London, UK, [4]Department of Biomechanics, University of Nebraska, Omaha, NE, USA, [5]Hedenstierna Laboratory, Department of Medical Sciences, Uppsala University, Uppsala, Sweden and [6]Department of Surgical Sciences, Uppsala University, Uppsala, Sweden

*Corresponding author. E-mail: douglas.crockett@ndcn.ox.ac.uk

Abstract

Background: Bedside lung volume measurement could personalise ventilation and reduce driving pressure in patients with acute respiratory distress syndrome (ARDS). We investigated a modified gas-dilution method, the inspired sinewave technique (IST), to measure the effective lung volume (ELV) in pigs with uninjured lungs and in an ARDS model.
Methods: Anaesthetised mechanically ventilated pigs were studied before and after surfactant depletion by saline lavage. Changes in PEEP were used to change ELV. Paired measurements of absolute ELV were taken with IST (ELV_{IST}) and compared with gold-standard measures (sulphur hexafluoride wash in/washout [ELV_{SF6}] and computed tomography (CT) [ELV_{CT}]). Measured volumes were used to calculate changes in ELV (ΔELV) between PEEP levels for each method (ΔELV_{IST}, ΔELV_{SF6}, and ΔELV_{CT}).
Results: The coefficient of variation was <5% for repeated ELV_{IST} measurements (n=13 pigs). There was a strong linear relationship between ELV_{IST} and ELV_{SF6} in uninjured lungs (r^2=0.97), and with both ELV_{SF6} and ELV_{CT} in the ARDS model (r^2=0.87 and 0.92, respectively). ELV_{IST} had a mean bias of −12 to 13% (95% limits=±17 − 25%) compared with ELV_{SF6} and ELV_{CT}. ΔELV_{IST} was concordant with ΔELV_{SF6} and ΔELV_{CT} in 98–100% of measurements, and had a mean bias of −73 to −77 ml (95% limits=±128 − 186 ml) compared with ΔELV_{SF6} and −1 ml (95% limits ±333 ml) compared with ΔELV_{CT}.
Conclusions: IST provides a repeatable measure of absolute ELV and shows minimal bias when tracking PEEP-induced changes in lung volume compared with CT in a saline-lavage model of ARDS.

Keywords: ARDS; computed tomography; inspired sinewave technique; lung volume measurement; method comparison

Editor's key points

- The development of lung volume measurements at the bedside may enable personalised ventilatory strategies that optimise respiratory function in acute lung injury.
- The authors used a modified gas-dilution method—the inspired sinewave technique—to measure effective lung volume measured by CT in mechanically ventilated pigs with uninjured lungs and acute respiratory distress syndrome (ARDS) induced by saline lavage.
- The inspired sinewave technique provided a repeatable measure of absolute effective lung volume.
- This individualised measurement approach may help reduce ventilator-induced injury during ARDS and acute lung injury.

Received: 16 September 2019; **Accepted:** 16 November 2019

© 2020 The Authors. Published by Elsevier Ltd on behalf of British Journal of Anaesthesia. This is an open access article under the CC BY-NC-ND license (http://creativecommons.org/licenses/by-nc-nd/4.0/).
For Permissions, please email: permissions@elsevier.com

The acute respiratory distress syndrome (ARDS) affects 10% of critical care patients and has an associated mortality of 40%.[1] Patients with ARDS have a smaller aerated lung volume ('baby lung') and one of the few interventions shown to reduce mortality in ARDS is ventilating patients with 6–8 ml kg^{-1} tidal volume (V_T).[2–4] More recently, driving pressure (ΔP) has been shown to be the ventilator parameter that best stratifies risk of mortality in ARDS.[5] ΔP is dependent on V_T and respiratory system compliance (C_{RS}) ($\Delta P = V_T/C_{RS}$). C_{RS} is dependent on the size of the baby lung, and therefore, so too is ΔP.[6] It is thought that reduced mortality from low V_T ventilation may be secondary to reducing the effect that ΔP has on the ARDS baby lung.[3]

Whilst it might be possible to titrate V_T to ΔP,[7] the underlying volume of the baby lung remains the fundamental parameter on which the imposed V_T exerts its effect to produce ΔP. Therefore, there would be potential benefit in measuring the volume of lung of the baby lung at the bedside of a mechanically ventilated ARDS patient. This would allow personalised titration of V_T to the underlying lung volume, with limitation of lung strain caused by ΔP. Lung volume can be measured in ventilated patients by imaging (CT), wash-in/washout techniques, or gas-dilution techniques. CT imaging puts patients at risk by necessitating a transfer to the scanner and exposure to ionising radiation. The current bedside gas-based techniques have not proved reliable in assisted ventilation, or they require equipment that is too bulky or too time-consuming for bedside clinical use.[8–13]

The inspired sinewave technique (IST) has the potential to provide bedside measurement of the lung volume, which takes part in gas exchange (effective lung volume [ELV]). IST uses a low concentration of tracer gas (<5% nitrous oxide [N_2O]) injected into the inspired airway gases in a sinusoidally oscillating concentration.[14–16] Sinewave amplitude and phase of the concentration of the tracer gas measured in the expiratory airway gases are used to recover values of ELV (ELV_{IST}) and pulmonary blood flow. IST uses commercially available components commonly used in anaesthetic/intensive care practice, and has proven efficacy in spontaneously ventilating healthy volunteers.[17,18] To date, IST's ability to measure ELV in mechanically ventilated lungs has not been tested.

The aim of the current study was to conduct a method comparison, measuring the relationship and limits of agreement between ELV measured by IST compared with SF_6 wash in/washout and CT. To do this, we compared the absolute ELV and changes in ELV (ΔELV) at and between different PEEPs in mechanically ventilated pigs both before and after induction of ARDS by saline lavage.[10,19,20]

Table 1 Baseline characteristics for n=13 animals pre- and post-lung injury. Mean (standard deviation) are shown for parametric data and median (95% confidence interval) for non-parametric data. P-values in the final column represent results of either paired Student's t-test (of parametric data) or Wilcoxon signed rank test (of non-parametric data). CO, cardiac output; DBP, diastolic BP; FIO_2, fraction of inspired O_2; Hb, haemoglobin; $PaCO_2$, arterial CO_2 partial pressure; PADP, pulmonary artery diastolic BP; PaO_2, arterial O_2 partial pressure; PASP, pulmonary artery systolic pressure; PFR, PaO_2:FIO_2 ratio; SaO_2, arterial oxygen saturation; SBP, systolic BP.

Parameter	Pre-injury	Post-injury	P-value
Weight	29 (2)	—	
HR (bpm)	86 (70–100)	85 (80–95)	0.42
SBP (mm Hg)	100 (8)	98 (14)	0.57
DBP (mm Hg)	67 (12)	54 (8)	0.0006
CO (L min^{-1})	3.4 (0.8)	3.2 (0.4)	0.26
PASP (mm Hg)	28 (25–33)	32 (29–36)	0.03
PADP (mm Hg)	16 (4)	19 (5)	0.004
Hb (g dl^{-1})	83 (5)	84 (6)	0.93
FIO_2	0.4 (0.3–0.4)	0.8 (0.7–0.9)	0.0002
SaO_2 (%)	100 (99–100)	98 (91–99)	0.001
pH	7.38 (0.07)	7.25 (0.08)	0.0004
PaO_2 (kPa)	19.2 (15.9–21.5)	12.8 (11.3–26.0)	0.39
$PaCO_2$ (kPa)	6.7 (1.1)	8.4 (2.0)	0.003
PFR	377 (304–513)	128 (101–248)	0.0002

Methods

Ethical approval

This study of 13 domestic pigs (mean weight [standard deviation {SD}]=29 [2] kg) at the Hedenstierna Laboratory, Uppsala

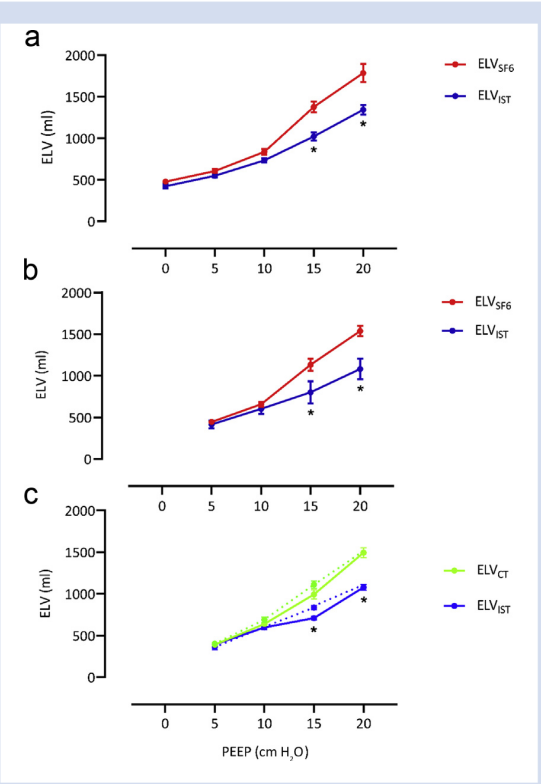


Fig 1. Effective lung volume (ELV) measurement (standard error) using ELV_{IST}, ELV_{SF6}, and ELV_{CT} at each PEEP level. (a) Paired ELV_{IST} and ELV_{SF6} measurements in the uninjured lung. (b) Paired ELV_{IST} and ELV_{SF6} measurements in the acute respiratory distress syndrome (ARDS) model. (c) Paired ELV_{IST} and ELV_{CT} measurements in the ARDS model. PEEP=0 cm H_2O was not studied post-injury; PEEP levels of 15 and 20 cm H_2O were studied in six of the total n=13 animals. Solid lines represent volumes measured during incremental PEEP titration; dashed lines represent volumes measured during decremental PEEP titration. *ELV_{IST} is significantly different to ELV_{SF6} or ELV_{CT} ($P>0.05$). Table 2 provides full details of volumes measured and probabilities of difference.

University, Uppsala, Sweden was approved by the regional animal welfare and ethics committee (Ref: C98/16). Reporting in this paper adheres to the Animal Research: Reporting of In Vivo Experiments guidelines.[21]

Animal preparation

Table 1 shows the summary baseline characteristics of the animals pre- and post-lung injury (individual values are given in Supplementary Table 1). The animals were prepared and anaesthetised using i.m. sedation and subsequent i.v. anaesthesia as described elsewhere.[22] During preparation, mechanical ventilation was delivered in volume-controlled ventilation (VCV) mode at 20–25 bpm (to maintain end-tidal CO_2 [$EtCO_2$] between 4.5 and 6 kPa), with a V_T of 10 ml kg^{-1}, PEEP of 5 cm H_2O, and an inspiratory:expiratory ratio (I:E) of 1:2 (Servo-I®; Maquet, Rastatt, Germany). Airway leaks were excluded by analysis of spirometry data. Depth of anaesthesia was confirmed by lack of spontaneous movements, absence of reaction to painful stimulation between the front hooves, and absence of cardiovascular signs of sympathetic stimulation (increases in HR or arterial BP). Subsequent muscle relaxation was achieved with a bolus of rocuronium 0.2 mg kg^{-1} followed by 0.1 mg kg^{-1} boluses when spontaneous ventilatory efforts were detected from the airway gas and pressure traces. Maintenance i.v. crystalloid fluids were administered (Ringerfundin®; B. Braun Melsungen AG, Melsungen, Germany) at a rate of 10 ml kg^{-1} h^{-1} during the preparation phase and 7 ml kg^{-1} h^{-1} for the rest of the protocol. Once anaesthetised, the right internal jugular vein was cannulated with a pulmonary artery catheter used for continuous pulmonary artery pressure, intermittent thermodilution cardiac output, and core temperature monitoring.

Data collection and processing

Cardiorespiratory variables, including peripheral oxyhaemoglobin saturation (SpO_2), ECG, invasive arterial BP (AS/3 Multi-Parameter Patient Monitor, Datex-Ohmeda, Madison, WI, USA), airway gas composition, flow, and pressure (Capnomac Ultima™; Datex-Ohmeda) were continuously monitored and acquired as analogue signals throughout the protocol. Analogue data were converted using PowerLab (ADInstruments, Dunedin, New Zealand) and displayed/recorded with LabChart version 8.1.5 (ADInstruments). Physiological data were processed using R version 3.5.1 (R Core Team (2017), Vienna, Austria).[23]

Inspired sinewave technique

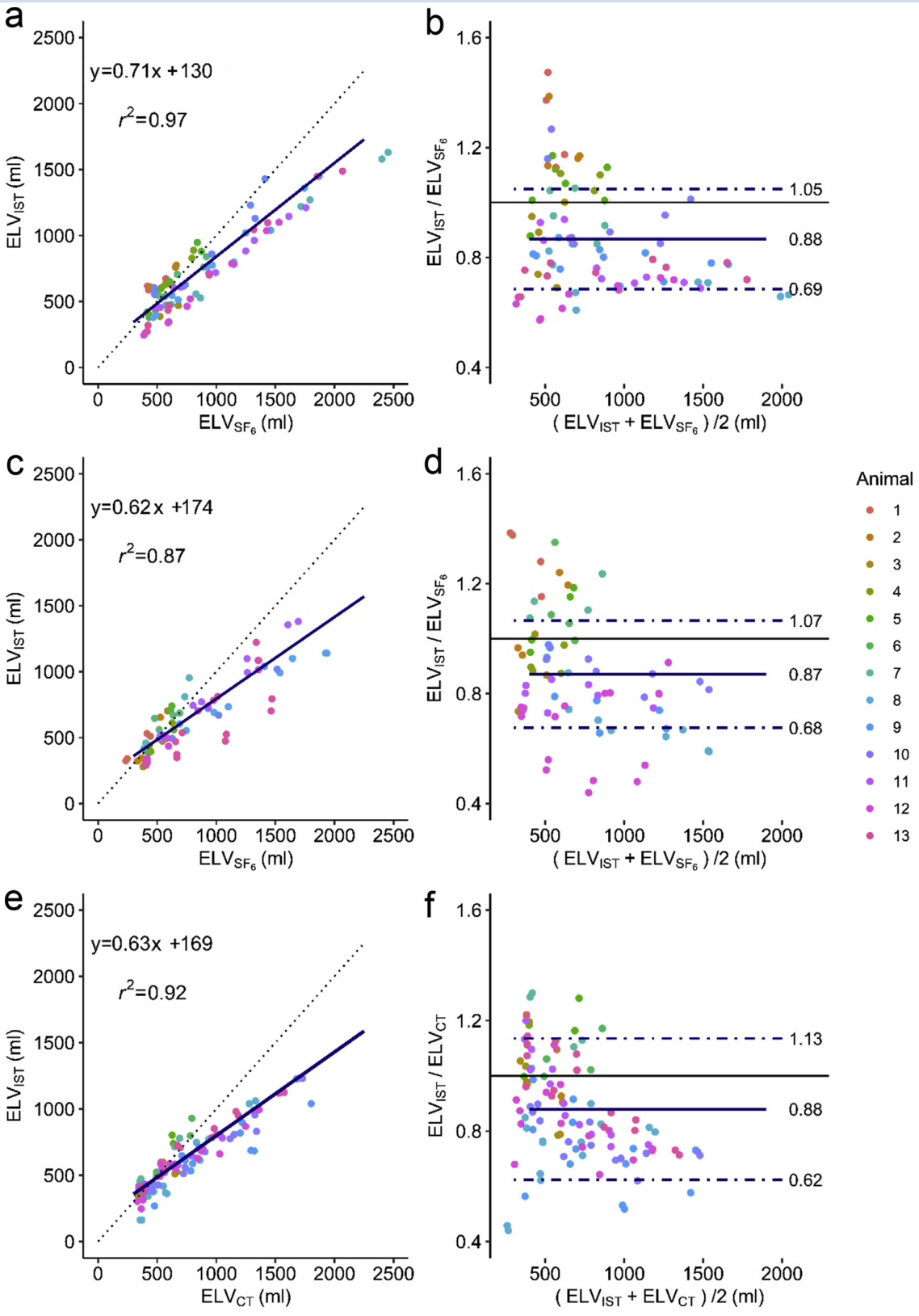
A mainstream infrared N_2O and CO_2 sensor (IRMA, Danderyd, Thor Laboratories, Budapest Sweden) and an ultrasonic flowmeter (VenThor 22/2A; Thor Laboratories, Budapest, Hungary) were placed in the breathing circuit between a patient-end heat-moisture exchange filter (Intersurgical, Wokingham, UK) and the ventilator tubing. At the start of each inspiration, a set volume of N_2O was injected into the inspired gas by a mass flow controller (Alicat Scientific, Tucson, AZ, USA). The volume of N_2O injected was proportional to the inspiratory flow and oscillated sinusoidally over consecutive breaths around a set mean concentration of 5%, with an amplitude of 4% and a period of 180 s for a duration of 270 s. The test duration of 270 s was the maximum duration that would allow repetition of each test within the permitted time frame of the protocol. By measuring the expired N_2O concentration in each consecutive breath, a set of simultaneous equations can be solved to provide estimates of ELV. Further technical details of IST are described elsewhere.[15–17,24]

SF_6 wash in/washout

The use of SF_6 as a tracer gas for wash-in/washout measurement of lung volume is detailed elsewhere.[10] The apparatus was attached between the tracheal tube and the D-lite™ spirometer attachment (GE Healthcare, Chicago, IL, USA).

Table 2 Descriptive statistics for comparisons of absolute effective lung volume (ELV) and changes in ELV (ΔELV) made in both the uninjured lung and the acute respiratory distress syndrome (ARDS) model at each PEEP level. Mean (standard deviation) volumes are shown in millilitres. n, number of observations (incomplete data sets have been excluded from the analysis; these account for 4% of total possible paired measurements). ELV_{CT}, CT measured absolute volume; ELV_{IST}, inspired sinewave technique (IST) measured absolute volume; ELV_{SF6}, SF_6 measured absolute volume; P, probability from either two-way analysis of variance or Kruskal–Wallis that mean measurements at each PEEP level are from different samples; ΔELV_{CT}, CT measured change in lung volume; ΔELV_{IST}, IST measured change in lung volume; ΔELV_{SF6}, SF_6 measured change in lung volume.

PEEP ($cm H_2O$)	Uninjured				ARDS model							
	n	ELV_{IST}	ELV_{SF6}	P-value	*n*	ELV_{IST}	ELV_{SF6}	P-value	*n*	ELV_{IST}	ELV_{CT}	P-value
0	17	422 (106)	477 (66)	0.35	—	—	—	—	—	—	—	—
5	24	548 (99)	607 (119)	0.31	25	415 (108)	444 (113)	0.84	38	381 (76)	394 (49)	0.86
10	22	734 (132)	837 (169)	0.14	26	601 (149)	657 (157)	0.26	36	598 (124)	654 (99)	0.14
15	11	1022 (159)	1377 (213)	0.002	12	801 (207)	1132 (249)	<0.0001	24	771 (107)	1051 (177)	<0.0001
20	12	1342 (194)	1785 (373)	0.01	12	1081 (197)	1535 (214)	<0.0001	12	1077 (113)	1493 (199)	<0.0001
	n	ΔELV_{IST}	ΔELV_{SF6}	P-value	*n*	ΔELV_{IST}	ΔELV_{SF6}	P-value	*n*	ΔELV_{IST}	ΔELV_{CT}	P-value
0 to >5	17	118 (60)	180 (57)	0.02	—	—	—	—	—	—	—	—
5 to >10	24	190 (87)	240 (71)	0.13	26	191 (127)	216 (91)	0.81	24	209 (105)	245 (58)	0.60
10 to >15	11	313 (90)	423 (111)	0.07	12	252 (73)	399 (91)	0.0008	12	196 (77)	371 (90)	0.0002
15 to >20	12	312 (92)	412 (233)	0.56	12	281 (102)	403 (70)	0.008	12	370 (88)	500 (75)	0.005
20 to >15	—	—	—	—	—	—	—	—	12	−243 (92)	−383 (100)	0.01
15 to >10	—	—	—	—	—	—	—	—	12	−233 (69)	−422 (67)	<0.0001
10 to >5	—	—	—	—	—	—	—	—	12	−242 (51)	−287 (64)	0.37


a
y=0.71x +130
r²=0.97
ELVIST (ml)
ELVSF6 (ml)
b
ELVIST / ELVSF6
(ELVIST + ELVSF6) /2 (ml)
1.05
0.88
0.69
c
y=0.62x +174
r²=0.87
d
1.07
0.87
0.68
Animal
1
2
3
4
5
6
7
8
9
10
11
12
13
e
y=0.63x +169
r²=0.92
ELVCT (ml)
f
ELVIST / ELVCT
(ELVIST + ELVCT) /2 (ml)
1.13
0.88
0.62

CT image acquisition and analysis

A Somatom Definition Flash (Siemens, Munich, Germany) was used to acquire images as a series of transverse sections with a reconstituted voxel size of 0.5×0.5×5 mm. Whole-lung volume scans were conducted during a 20 s end-expiratory pause without ventilator disconnection. Scans were taken using a tube voltage of 80 kV, 364 mA current, and 64×60 mm collimation. Reconstituted whole-lung scans were segmented using 3D Slicer version 4.10.2[25] (https://www.slicer.org/). The mediastinum, diaphragm, inferior vena cava, and hilar vessels were not included in segmentation. Exclusion of intrapulmonary vessels within regions of increased voxel density was not possible, as they were not distinguishable from lung tissue, and these, along with the conducting airways up to the level of the clavicles, were included in the analysis. The aerated volume of each whole-lung scan was calculated from the Hounsfield unit (HU) density of each voxel according to the formula:[26]

$$\text{Aerated volume} = \frac{-\text{mean CT density (HU)}}{1000} \times \text{segmented volume}$$

ARDS model

Lung injury was induced with a technique modified from Lachmann and colleagues.[27] Following preoxygenation, the ventilator was disconnected and the lungs lavaged by instillation of 0.9 % saline solution (at 37°C) via the tracheal tube. After 30 s, the saline was drained out of the lungs and ventilation recommenced. This process was repeated until a PaO_2:FIO_2 ratio of less than 300 mm Hg was achieved.

Study protocol

Throughout all phases of the protocol, the animals were positioned in dorsal recumbency; FIO_2 was titrated to PaO_2 >10 kPa; and the animals were mechanically ventilated with VCV, V_T 10 ml kg^{-1}, and I:E 1:2. The ventilatory frequency was adjusted to 15–20 bpm to maintain $EtCO_2$ <8 kPa. In all cases, measurements were taken after 2 min of ventilation at the studied PEEP level, and the tracheal tube was clamped during airway disconnection (e.g. to change equipment for measuring ELV_{IST} to ELV_{SF6}). Supplementary Figure S1 shows a summary timeline of each experiment.

Comparison between ELV_{IST} and ELV_{SF6} pre- and post-injury

Measurements of ELV were taken with IST (ELV_{IST}) and SF_6 wash in/washout (ELV_{SF6}). Two sets of paired measurements were taken at each PEEP level studied. Measurements were taken first with IST, and then with SF_6. After completion of experiments in the uninjured model, lung injury was induced as described previously, and a further two paired measurements of ELV_{IST} and ELV_{SF6} were repeated at each PEEP level. In all 13 animals, the studied PEEP levels were 0, 5, and 10 cm H_2O. In six of these animals, PEEP levels of 15 and 20 cm H_2O were additionally included. In all comparisons of ELV_{IST} and ELV_{SF6}, PEEP was incrementally increased from low to high. The protocol comparing ELV_{IST} and ELV_{SF6} was the same pre- and post-saline lavage, except that 0 cm H_2O PEEP was not studied post-injury because of the risk that this would not be tolerated.

Comparison between ELV_{IST} and ELV_{CT} after lung injury

Upon completion of the ELV_{IST} *vs* ELV_{SF6} comparisons, the animals were transferred to the CT scanner. Two paired measurements of ELV_{IST} and ELV estimated from CT (ELV_{CT}) were made at each PEEP level. In all 13 animals, the PEEP levels studied were 5 and 10 cm H_2O. In six of these animals, PEEP was titrated from 5 cm H_2O up to 20 cm H_2O, and then back down again. For the reason stated previously, zero PEEP was not studied post-injury. Upon completion of the study protocol, the anaesthetised pigs were euthanised with potassium chloride.

Statistical analyses

Paired measurements of ELV_{IST}, ELV_{SF6}, and ELV_{CT} at each PEEP level were tested for normality using D'Agostino–Pearson's test and QQ plots. Datasets were compared with a repeated measures, two-way analysis of variance (ANOVA) with Sidak multiple comparison test. ΔELV was calculated by subtracting one absolute ELV from its value at the preceding PEEP level. The linear relationship between measurements was tested using linear mixed effects modelling with variation caused by different animals considered a random effect. Conditional r^2 values based on the entire model are reported.[28] The agreement in measurements between techniques was assessed with Bland–Altman analysis corrected for multiple comparisons using a single-factor ANOVA with individual animal as the factor.[29–31] Non-normally distributed data were transformed (by using a ratio of measurements) to conform to the assumption of normality, and 95% limits of agreement were calculated as 1.96 SD from the mean bias. Measured changes in lung volume were compared using four quadrant plots with direction of change concordance and polar plots.[32] For polar plot analysis of trends, adequate limits of agreement are assumed to be within 30° of the horizontal. Analyses were carried out using R version 3.5.1 (R Core Development Team, Vienna, Austria),[23] GraphPad Prism version 8.1.2 (GraphPad Software, La Jolla, CA, USA; https://www.graphpad.com/), and SigmaPlot version 14.0 (Systat Software, San Jose, CA, USA).

Results

A total of n=271 paired ELV measurements in 13 pigs at five different PEEP levels were analysed. Figure 1 shows that the protocolised changes in PEEP induced changes in ELV, and

Fig 2. Scatter and Bland–Altman plots for absolute volume measurements (ELV_{IST}, ELV_{SF6}, and ELV_{CT}). (a, b) Measurements from the uninjured lung. (c–f) Experiments conducted in the acute respiratory distress syndrome model. In the left column, scatterplots show the results of mixed effects linear models, where the solid line represents the reported equation. In the right column, solid lines in the Bland–Altman plots represent the mean bias, and the dashed lines show the upper and lower limits of agreement (±1.96 standard deviation). In all plots, individual points represent a paired set of measurements, and different colours represent different animals.

that these changes were tracked by IST, SF_6, and CT. Figure 1 and Table 2 show the comparisons of paired ELV and ΔELV measurements at each PEEP level. Statistical analyses suggested that ELV_{IST} at 0, 5, and 10 cm H_2O PEEP was not different from ELV_{SF6} or ELV_{CT} in both the uninjured lung and ARDS model. At 15 and 20 cm H_2O PEEP, the measured ELV_{IST} was lower than ELV_{SF6} and ELV_{CT} in all comparisons (Table 2).

Repeatability of ELV_{IST} measurements

The mean coefficient of variation for ELV_{IST} for each subject at each PEEP level was <5% in both the uninjured lung and the ARDS model; 90% of coefficients of variation for replicate measurements were <10%.

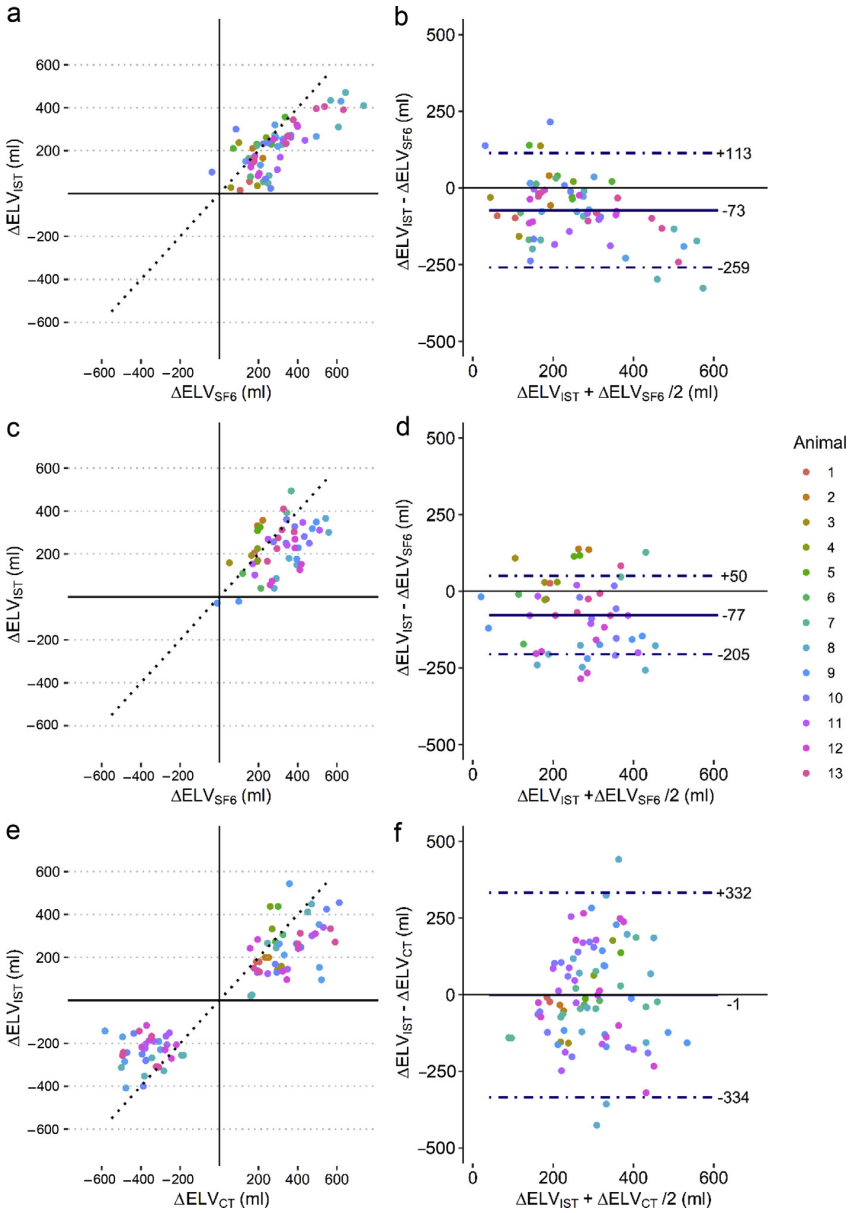


Fig 3. Scatter and Bland–Altman plots for changes in volume (ΔELV_{IST}, ΔELV_{SF6}, and ΔELV_{CT}). (a, b) Measurements from the uninjured lung. (c–f) Experiments conducted in the ARDS model. In the left column, scatterplots show changes in volume. In the right column, solid lines in the Bland–Altman plots represent the mean bias, and the dashed lines show the upper and lower limits of agreement (±1.96 standard deviation). In all plots, individual points represent a paired set of measurements, and different colours represent different animals.

Comparison between ELV_{IST}, ELV_{SF6}, and ELV_{CT}

Figure 2a, c, and e show scatterplots and linear mixed effects regression for each of the comparisons. There was a robust linear relationship between ELV_{IST} and ELV_{SF6} in both the uninjured lung (r^2=0.97) and the ARDS model (r^2=0.87). Similarly, we found a strong correlation between ELV_{IST} and ELV_{CT} in the ARDS model (r^2=0.92).

Agreement between ELV_{IST}, ELV_{SF6}, and ELV_{CT}

Figure 2b, d, and f show that in each comparison, ELV_{IST} has a mean bias of 12–13% less than the reference technique in both the uninjured lung and the ARDS model. ELV_{IST} has limits of agreement with ELV_{SF6} of ±17% in the uninjured lung and ±20% in the ARDS model. The limits of agreement between ELV_{IST} and ELV_{CT} were ±25% in the ARDS model.

Correlation between ΔELV_{IST}, ΔELV_{SF6}, and ΔELV_{CT}

Figure 3a, c, and e show four quadrant plots demonstrating the relationship of ΔELV_{IST} with ΔELV_{SF6} and ΔELV_{CT}. The linear relationship between ΔELV_{IST} and ΔELV_{SF6} in the uninjured lung yielded an r^2=0.58, and r^2=0.83 in the ARDS model. The linear relationship between ΔELV_{IST} and ΔELV_{CT} in the ARDS model had an r^2=0.16.

Agreement between ΔELV_{IST}, ΔELV_{SF6}, and ΔELV_{CT}

Direction of change concordance showed that ΔELV_{IST} has a concordance rate of 98–100% with ELV_{SF6} and ELV_{CT}. This is reflected in Figure 3a, c, and e, where 98–100% of data are in the top right and bottom left quadrants of each four-quadrant plot. Figure 3b, d, and f show the Bland–Altman plots with a mean bias (limits of agreement) of −73 (±186) ml for ΔELV_{IST} *vs* ΔELV_{SF6} in the uninjured lung, −77 (±128) ml for ΔELV_{IST} *vs* ΔELV_{SF6} in the ARDS model, and −1 (±333) ml for ΔELV_{IST} *vs* ΔELV_{CT} in the ARDS model. Figure 4 demonstrates the polar agreement in paired measurements. The mean angular bias ranged from 8 to 11°, and radial limits of agreement from ±30 to 37°.

Discussion

This study presents the ability of IST to measure absolute ELV and changes in ELV, compared with the 'gold standard' techniques of SF_6 wash in/washout (ELV_{SF6}) and CT (ELV_{CT}) in uninjured lungs and in an ARDS model of lung injury. In both the uninjured lungs and a saline-lavage model of ARDS, IST can reliably measure the absolute ELV comparably with SF_6 and CT, with acceptable measures of bias and limits of agreement. Additionally, when comparing PEEP-induced changes in lung volume, IST is >98% concordant with SF_6 and CT.

IST measurements of absolute ELV are below those measured by SF_6 and CT by 12–13% and do not fall within 5% of the reference method recommended by the European Respiratory Society/American Thoracic Society consensus statement.[33] These results are consistent with a previous study of IST, in which Bruce and colleagues[17] showed that IST underestimated functional residual capacity (FRC) by 32% (1080 ml) compared with body plethysmography in humans, where the mean FRC was 3.4 L. The underestimation was smaller in our study, with a mean bias of −12 to −13% (−129 to −161 ml), where the overall mean ELV was 809 ml. IST measures the volume of ventilated regions of the lung, and it is expected that IST will underestimate lung volume compared with CT, which estimates the entire thoracic gas volume. One reason for IST's underestimation of ELV compared with SF_6 may be that multi-breath washout techniques recover tracer gas from the slowest compartments if the washout period is long enough, whereas for IST,

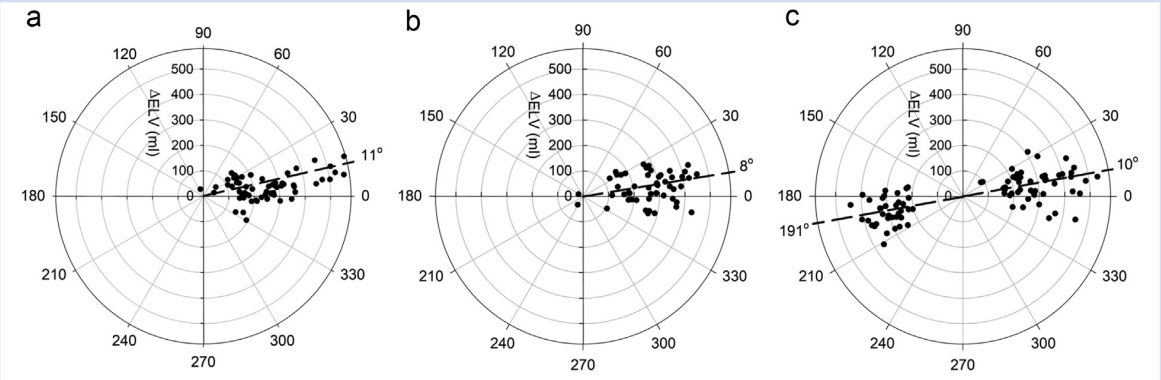


Fig 4. Polar plot analysis. The larger the mean ΔELV, the greater the distance between the point and the centre of the plot. The better the agreement between a pair of measurements, the closer the point lies to the horizontal (0°); 95% radial limits of agreement describe the angle within which 95% of the data lie. Concordance rate (%) describes the number of points that lie within the assumed limits of adequate agreement, set at ±30°. (a) Comparison of ΔELV_{IST} *vs* ΔELV_{SF6} in the uninjured lung. Mean angular bias=11°; 95% radial limits of agreement=±35°; concordance=91%. (b) Comparison of ΔELV_{IST} *vs* ΔELV_{SF6} in the acute respiratory distress syndrome (ARDS) model. Mean angular bias=8°; 95% radial limits of agreement=±37°; concordance rate 90%. (c) Comparison of ΔELV_{IST} *vs* ΔELV_{CT} in the ARDS model. Mean angular bias=10° for positive changes in volume, and 191° for negative changes in volume; 95% radial limits of agreement=±30°; concordance rate=95%.

the contribution of the slowest compartment is limited by the chosen period of the sinewave.

There is no previous study assessing the ability of IST to measure changes in lung volume. The linear relationship between ΔELV_{IST} and ΔELV_{SF6} was stronger than for ΔELV_{CT}, and the limits of agreement were narrower for ΔELV_{SF6} (±186 ml in the uninjured lung and ±128 ml in the ARDS model) compared with ΔELV_{CT} (±333 ml). One proposed explanation for the narrower limits of agreement in the ARDS model compared with the uninjured model with SF_6 was that the measured ΔELV was less in the ARDS model. Further analyses showed that the measured changes in volume (based on ΔELV_{SF6}) were no different in the uninjured and ARDS models (PEEP 5–10: $P=0.11$; PEEP 10–15: $P=0.59$; PEEP 15–20: $P=0.91$). The repeatability of IST measurements of ELV in the same subject under the same conditions was within the reported international acceptable limits of coefficient of variation (<10%)[34] and consistent with studies of IST in other circumstances.[17] IST has good repeatability and minimal bias compared with CT (mean bias=−1 ml) when measuring changes in lung volume. This provides support for the use of IST to monitor trends in lung volume, where the change (or lack of) in volume after a change in ventilator setting is potentially of most interest to the bedside clinician.

The inspired sinewave technique offers several strengths, including commercial availability of component parts and its ease of use at the bedside. As IST does not rely on a fixed inspiratory flow, it can be used in spontaneously ventilating patients. The main limitations of our study are that the use of a porcine model does not directly translate to humans, and the use of saline lavage does not necessarily comprise all the features of human ARDS. However, saline lavage does result in reduction in lung volume, which is one reason for its choice in this study. In addition, in this protocol, not all PEEP levels were studied in all experiments. This was not feasible due to time restraints because the initial seven experiments including PEEP 0, 5, and 10 cm H_2O were undertaken in parallel with data collection for another study, in keeping with the 3Rs principle.[35] Future development of IST could include assessing the feasibility of its use in mechanically ventilated human patients. IST development will enable the measurement of lung volumes when using volume-controlled and pressure-controlled ventilation modes in paralysed patients and in assisted mechanical ventilation, where less regular inspiratory flow patterns exist.

The inspired sinewave technique is a potentially translatable research tool and this study is the first to examine its use in mechanically ventilated lungs. Measuring the size of the ARDS baby lung would allow titration of ΔP to the individual patient, either directly[7] or by scaling V_T to the size of the baby lung. This has the potential to reduce mortality in patients with ARDS. We have demonstrated that IST measured lung volumes and changes in volume reliably compared to the standard techniques of SF_6 washin-washout and CT in a mechanically ventilated porcine model. Our results support further development of this technique and its translation to human medicine.

Authors' contributions

Study design: DCC, FF, PAP
Experimentation: DCC, JNC, MCT, PAP
Data analysis: DCC
Data interpretation: DCC, MCT, FF, JNC, ADF
Financial support: FF, PAP, AL, ADF
Writing manuscript: DCC
Critical revision: DCC, MCT, JNC, FF, AL, ADF

Acknowledgements

The authors are grateful to Agneta Roneus, Kerstin M. Ahlgren, Maria Swälas, Mariette Andersson, Liselotte Pihl, and Monica Segelsjö for technical support; to OxSTaR, St Peter's College, and the Nuffield Division of Anaesthetics office for their ongoing support of DCC; and to Richard Bruce and Joao Batista-Borges for their helpful advice.

Declarations of interest

ADF and PAP are named inventors on a patent application (EP3122249A1/US20170100043A1 [pending]) submitted by the University of Oxford, which may receive financial benefit when the technology is commercialised.

Funding

National Institute for Health Research (II-LA-0214-20005 and NIHR200029) to PAP and ADF; Royal Academy of Engineering Enterprise Fellowship to PAP; Swedish Heart-Lung Foundation (20170531) to AL and GH; Swedish Research Council (K2015-99X-2273101-4) to AL and GH; Medical Research Council (MC_PC_17164) to FF; The Physiological Society (Formenti 2018) to FF.

Appendix A. Supplementary data

Supplementary data to this article can be found online at https://doi.org/10.1016/j.bja.2019.11.030.

References

1. Bellani G, Laffey JG, Pham T, et al. Epidemiology, patterns of care, and mortality for patients with acute respiratory distress syndrome in intensive care units in 50 countries. *JAMA* 2016; **315**: 788–800
2. Acute Respiratory Distress Syndrome Network, Brower RG, Matthay MA, et al. Ventilation with lower tidal volumes as compared with traditional tidal volumes for acute lung injury and the acute respiratory distress syndrome. *N Engl J Med* 2000; **342**: 1301–8
3. Gattinoni L, Marini JJ, Pesenti A, Quintel M, Mancebo J, Brochard L. The "baby lung" became an adult. *Intensive Care Med* 2016; **42**: 663–73
4. Gattinoni L, Pesenti A. The concept of "baby lung". *Intensive Care Med* 2005; **31**: 776–84
5. Amato MB, Meade MO, Slutsky AS, et al. Driving pressure and survival in the acute respiratory distress syndrome. *N Engl J Med* 2015; **372**: 747–55
6. Hubmayr RD, Kallet RH. Understanding pulmonary stress-strain relationships in severe ARDS and its implications for designing a safer approach to setting the ventilator. *Respir Care* 2018; **63**: 219–26
7. Grieco DL, Chen L, Dres M, Brochard L. Should we use driving pressure to set tidal volume? *Curr Opin Crit Care* 2017; **23**: 38–44
8. Richard J-C, Pouzot C, Pinzón AM, et al. Reliability of the nitrogen washin-washout technique to assess end-

expiratory lung volume at variable PEEP and tidal volumes. *Intensive Care Med Exp* 2014; **2**: 10
9. Heinze H, Eichler W. Measurements of functional residual capacity during intensive care treatment: the technical aspects and its possible clinical applications. *Acta Anaesthesiol Scand* 2009; **53**: 1121–30
10. Larsson A, Linnarsson D, Jonmarker C, Jonson B, Larsson H, Werner O. Measurement of lung volume by sulfur hexafluoride washout during spontaneous and controlled ventilation: further development of a method. *Anesthesiology* 1987; **67**: 543–50
11. Di Marco F, Rota Sperti L, Milan B, et al. Measurement of functional residual capacity by helium dilution during partial support ventilation: in vitro accuracy and in vivo precision of the method. *Intensive Care Med* 2007; **33**: 2109–15
12. Maisch S, Boehm SH, Weismann D, et al. Determination of functional residual capacity by oxygen washin-washout: a validation study. *Intensive Care Med* 2007; **33**: 912–6
13. Patroniti N, Saini M, Zanella A, et al. Measurement of end-expiratory lung volume by oxygen washin-washout in controlled and assisted mechanically ventilated patients. *Intensive Care Med* 2008; **34**: 2235–40
14. Zwart A, Seagrave RC, Dieren AV. Ventilation-perfusion ratio obtained by a noninvasive frequency response technique. *J Appl Physiol* 1976; **41**: 419–24
15. Hahn CE. Oxygen respiratory gas analysis by sine-wave measurement: a theoretical model. *J Appl Physiol* 1996; **81**: 985–97
16. Hahn CE, Black AM, Barton SA, Scott I. Gas exchange in a three-compartment lung model analyzed by forcing sinusoids of N2O. *J Appl Physiol* 1993; **75**: 1863–76
17. Bruce RM, Phan PA, Pacpaco E, Rahman NM, Farmery AD. The inspired sine-wave technique: a novel method to measure lung volume and ventilatory heterogeneity. *Exp Physiol* 2018; **103**: 738–47
18. Phan PA, Zhang C, Geer D, Formenti F, Hahn CEW, Farmery AD. The inspired sinewave technique: a comparison study with body plethysmography in healthy volunteers. *IEEE J Transl Eng Health Med* 2017; **5**: 2700209
19. Gattinoni L, Mascheroni D, Torresin A, et al. Morphological response to positive end expiratory pressure in acute respiratory failure. Computerized tomography study. *Intensive Care Med* 1986; **12**: 137–42
20. Gattinoni L, Pesenti A, Avalli L, Rossi F, Bombino M. Pressure-volume curve of total respiratory system in acute respiratory failure. Computed tomographic scan study. *Am Rev Respir Dis* 1987; **136**: 730–6
21. Kilkenny C, Browne WJ, Cuthill IC, Emerson M, Altman DG. Improving bioscience research reporting: the ARRIVE guidelines for reporting animal research. *PLoS Biol* 2010; **8**, e1000412
22. Crockett DC, Cronin JN, Bommakanti N, et al. Tidal changes in PaO_2 and their relationship to cyclical lung recruitment/derecruitment in a porcine lung injury model. *Br J Anaesth* 2019; **122**: 277–85
23. R Development Core Team R. *A language and environment for statistical computing*. Vienna, Austria: R Foundation for Statistical Computing; 2017
24. Phan PA, Zhang C, Geer D, Hahn C, Farmery A. Inspired sinewave technique: a novel technology to measure cardiopulmonary function. In: Toi VV, Lien Phuong TH, editors. *5th international conference on biomedical engineering in vietnam*. Cham: Springer; 2015. p. 83–6
25. Fedorov A, Beichel R, Kalpathy-Cramer J, et al. 3D slicer as an image computing platform for the quantitative imaging network. *Magn Reson Imaging* 2012; **30**: 1323–41
26. Chiumello D, Cressoni M, Chierichetti M, et al. Nitrogen washout/washin, helium dilution and computed tomography in the assessment of end expiratory lung volume. *Crit Care* 2008; **12**: R150
27. Lachmann B, Robertson B, Vogel J. In vivo lung lavage as an experimental model of the respiratory distress syndrome. *Acta Anaesthesiol Scand* 1980; **24**: 231–6
28. Nakagawa S, Schielzeth H, O'Hara RB. A general and simple method for obtaining R2 from generalized linear mixed-effects models. *Methods Ecol Evol* 2013; **4**: 133–42
29. Bland JM, Altman DG. Statistical methods for assessing agreement between two methods of clinical measurement. *Lancet* 1986; **1**: 307–10
30. Bland JM, Altman DG. Measuring agreement in method comparison studies. *Stat Methods Med Res* 1999; **8**: 135–60
31. Bland JM, Altman DG. Agreement between methods of measurement with multiple observations per individual. *J Biopharm Stat* 2007; **17**: 571–82
32. Critchley LA, Lee A, Ho AM. A critical review of the ability of continuous cardiac output monitors to measure trends in cardiac output. *Anesth Analg* 2010; **111**: 1180–92
33. Robinson PD, Latzin P, Verbanck S, et al. Consensus statement for inert gas washout measurement using multiple- and single-breath tests. *Eur Respir J* 2013; **41**: 507–22
34. Wanger J, Clausen JL, Coates A, et al. Standardisation of the measurement of lung volumes. *Eur Respir J* 2005; **26**: 511–22
35. Russell WMS, Burch RL, Hume CW. *The principles of humane experimental technique*. London: Methuen; 1959

Handling editor: Gareth Ackland

Supplementary Table 1: Baseline characteristics of individual animals pre- and post- lung injury.

	Parameter	Animal Number												
		1	**2**	**3**	**4**	**5**	**6**	**7**	**8**	**9**	**10**	**11**	**12**	**13**
Pre-injury	**Weight (kg)**	31	32	30	27	27	27	27	31	32	28	28	31	31.6
	HR	68	74	76	70	90	80	63	95	103	86	106	100	99
	ABP (mmHg)	95/47	92/49	104/60	106/70	118/80	96/78	90/60	99/80	112/72	100/70	105/70	97/81	88/57
	CO (l min^{-1})	3.8	3.3	3.0	2.2	2.8	3.4	3.3	3.3	5.2	3.0	4.5	3.5	3.3
	PAP (mmHg)	25/10	28/10	26/15	44/11	44/15	30/20	33/23	29/16	30/18	27/17	20/10	25/13	21/12
	Hb (g dl^{-1})	87	80	81	83	80	86	70	83	83	88	86	87	88
	F_IO_2	0.4	0.4	0.4	0.3	0.3	0.3	0.4	0.4	0.4	0.4	0.4	0.4	0.3
	SaO_2 (%)	99	100	100	100	98	100	100	100	99	98	100	100	99
	pH	7.33	7.33	7.29	7.28	7.42	7.53	7.42	7.37	7.43	7.33	7.42	7.39	7.42
	PaO_2 (kPa)	14.2	17.8	24.0	21.5	20.5	21.0	23.5	15.9	19.2	17.2	20.1	16.2	14.9
	$PaCO_2$ (kPa)	7.6	7.6	8.9	5.6	5.6	5.2	6.5	7.3	6.2	8.0	6.2	6.6	5.4
	PFR	304	381	450	538	513	525	441	298	360	323	377	301	373
Post-injury	**HR**	79	70	88	95	85	81	80	134	80	87	81	95	120
	ABP (mmHg)	95/50	99/52	101/59	91/50	102/67	115/49	85/45	136/64	85/50	95/66	94/46	89/60	80/40
	CO (l min^{-1})	3.2	3.0	3.1	2.7	2.7	3.1	3.4	4.0	3.2	3.2	2.9	3.7	3.1
	PAP (mmHg)	32/16	36/17	32/19	29/10	42/13	34/20	34/22	39/24	32/23	30/24	28/17	30/17	25/14
	Hb (g dl^{-1})	79	87	85	78	75	77	73	90	77	88	75	89	112
	F_IO_2	0.7	0.7	0.7	0.9	0.9	0.75	0.85	0.8	0.8	0.75	0.75	0.8	0.8
	SaO_2 (%)	99	100	93.2	74	94.4	83.7	91.1	98.1	98.3	97	99.9	98.3	98.2
	pH	7.2	7.3	7.14	7.18	7.26	7.15	7.23	7.24	7.35	7.36	7.34	7.29	7.18
	PaO_2 (kPa)	10.0	26.0	11.8	12.3	11.3	12.8	11.4	28.6	26.4	15.6	23.9	10.3	20.6
	$PaCO_2$ (kPa)	10.5	8.7	13.7	7.1	8.4	8.9	9.27	8.01	7.12	6.3	6.7	7.06	7.86
	PFR	107	279	126	103	94	128	101	268	248	156	239	97	193

HR = heart rate, ABP = arterial blood pressure, CO = cardiac output, PAP = pulmonary artery pressure, Hb = haemoglobin, F_IO_2 = fraction of inspired O_2, SaO_2 = arterial oxygen saturation, PaO_2 = arterial O_2 partial pressure, $PaCO_2$ = arterial CO_2 partial pressure, PFR = PaO_2:F_IO_2 ratio

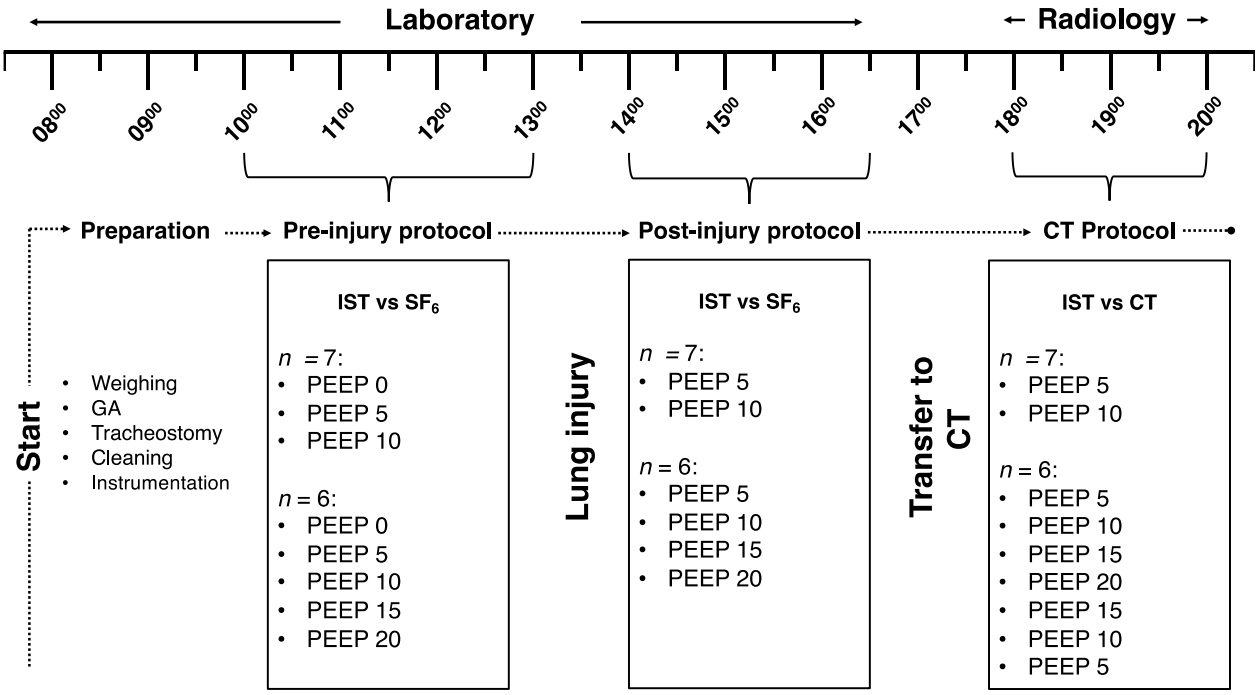


Figure S1: Timeline of experimental protocol. Paired measurements of ELV were taken with IST and either SF_6 or CT. **Pre-Injury & post-injury comparison with SF_6:** All measurements were taken using incremental steps in PEEP as shown. **Post-injured comparison with CT:** In *n* = 7 animals comparisons were made at two different lung volumes (PEEP 5 & PEEP 10), in n = 6 animals PEEP was incremented up to 20 cmH_2O and then decremented back down to 5 cmH_2O. GA = induction of general anaesthesia.

APPENDIX B

Full protocol for the validation of IST measurements of lung volume

DATE | Farmery Group – August 2018

Protocol: Uppsala experiments 21st & 22nd Aug 2018

People:

- DC + MT

Research Questions:

InspiWave Questions

- Can InspiWave measure/track changes in lung volume?

The preliminary results from the InspiWave experiments comparing it against SF_6 & CT show that it can track volume changes with good correlation to the other techniques. For the 6 experiments in June we would like to use smaller titrations in PEEP over a wider PEEP range and measure lung volume at each step before and after lung injury.

- Is InspiWave's index of homogeneity comparable to markers of inhomogeneity on CT?

A second question that we would like to answer about InspiWave is whether (or not) using different periods of sinewave and comparing them can give an estimate of homogeneity of the lung. To do this we will use the data collected from the volume experiments and compare the volumes measured by InspiWave at periods of 60s and 180s to those measurements of aeration/non-aeration on CT.

Point-of-care Ultrasound (POCUS) Questions

- Can POCUS accurately measure extra-vascular lung water? (Dr Adrian Wong, OUH ICU team collaboration)

DATE | | Farmery Group – August 2018

General Procedures:

Anaesthesia

- Induction: By the Uppsala team according to local protocol –
  - IM Zoletil®6 mg/kg (=tiletamin 3 mg/kg + zolazepam 3 mg/kg) and Xylazine 2.2 mg/kg
  - IV Fentanyl 8-10 µg/kg
- Maintenance:
  - IV Ketamine 32mg/kg/hr, Fentanyl 4 µg/kg/hr & Midazolam 120 µg/kg/hr
  - This is equivalent to 8ml/kg/hr of 1l crystalloid with
    - 4g Ketamine
    - 500 µg Fentanyl
    - 15mg Midazolam
  - Muscle Relaxation
    - Rocuronium 2.5mg/kg/hr
  - Maintenance fluid therapy:
    - Hartmann's 10ml/kg/hr

Baseline Ventilation

- Cuffed Endotracheal Tube (CETT) – usually tracheostomy
- Pressure Controlled Ventilation via GE ventilator
  - Aim Vt 6-8ml/kg , I:E 1:2, PEEP 5
- Respiratory Rate
  - As required to maintain adequate ventilation (see below for targets)
    - Pre-Injury: Target pH 7.35-7.45 & $PaCO_2$ 4.5-6kPa
    - Post-Injury: Target pH >7.2 w/ permissive hypercapnia post-injury

Instrumentation & Calibration

- Bilateral neck dissections and cannulation with insertion of O_2 Sensors
  - Vygon Arterial LeaderCath or 18G, Angiocaths for caged sensors
- Right internal jugular (IJ) cut-downs
  - Right IJ – pulmonary artery flotation catheter (PAFC)
- Bilateral Femoral Artery cut-downs
  - Vygon 8cm Arterial LeaderCath or 20G 48mm BD Angiocath ?
  - One glass and one plastic, record which type is in which artery and swap sides for the following day

Monitoring

- Cardiovascular
  - Arterial pressure via peripheral arterial cannula
  - PA pressure via PAFC
  - CO – Intermittent thermodilution & PICCO
- Respiratory
  - SpO_2, FiO_2, $EtCO_2$, airway pressure & flow
- Continuous PaO_2 sensor monitoring
- Intermittent blood gas analysis

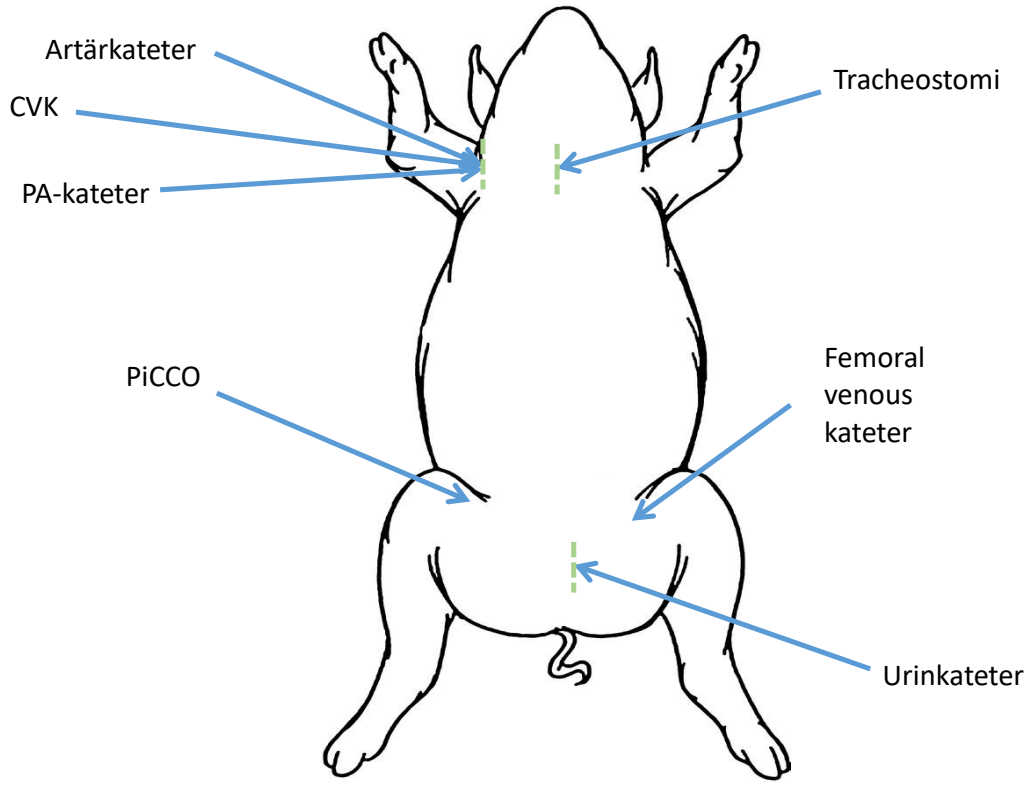
DATE | Farmery Group – August 2018

Experimental Procedures

Time	Procedure
0800 – 0930	Instrumentation and set-up - Pulse oximeter, ECG, airway gas sampler, airway flow/pressure transducers (set analogue outputs) - PiCCO line in right femoral artery - Check all signals are recorded fine (ECG, SpO_2, arterial blood pressure, PA pressure, central venous pressure, airway pressure, airway flow, airway O_2, airway CO_2, all 3 PaO_2 sensors). - acqIS – set to record ART, CVP, HR, ECG, PAP, SpO2, Tblood, CO2 %, Flow, Press and save as a preset - Calibrate PiCCO - Create new acqIS examination – surname 'Federico', first name date code e.g. 20171106 - Ensure ventilator has 0% rise time, 0% inspiratory pause and trigger turned down to -20 cmH_20
0900 - 0910	Baseline measurements: - Paired central venous, arterial and peripheral venous blood gases - Thermodilution cardiac output
0900 - 1230	InspiWave vs SF_6 - PEEP titrations as per monitoring Table 1
1230 - 1330	Induction of lung injury - FiO_2 1.0, RR 30, PCV, V_T 6 mL/kg, PEEP 5. - 30 mL/kg saline (typically 900-1000 mL) - Gently agitate chest to ensure even distribution of warmed saline. Reconnect ventilator if PaO_2 hits 50 mmHg. - Multiple saline lavages aiming for PaO_2:FiO_2 ratio of 200 mmHg at an FiO_2 of 0.7 (i.e. PaO_2 of 140 mmHg)
1330 - 1340	Baseline measurements - Paired central venous, arterial and peripheral venous blood gases - Thermodilution cardiac output
1330 - 1630	InspiWave vs SF_6 - PEEP titrations as per monitoring Table 2
1530 - 1630	Prepare for transfer to CT scanner Baseline measurements - Paired central venous and arterial blood gases - Thermodilution cardiac output
1630 – 1700	Transfer to CT
1700 – 1730	Check all signals are recorded fine (ECG, SpO_2, arterial blood pressure, PA pressure, central venous pressure, airway pressure, airway flow, airway O_2, airway CO_2. Recalibrate PiCCO and ensure recording trends (but do not resync) Baseline measurements - Paired central venous and arterial blood gases - Thermodilution cardiac output
1730 - 2000	InspiWave vs CT - PEEP titrations as pre monitoring Table 3 - All CT scans are whole lung volume scans at endexpiration
2000 – 2100	Tidy up - Export data, back up on USB and to Oxford shared hard drive

DATE

Farmery Group – August 2018



4

DATE

Farmery Group – August 2018

Equipment – Uppsala to provide

- ☐ Ventilator
- ☐ CVS monitoring
  - Arterial BP
  - Pulmonary artery pressure
  - SpO_2
  - Intermittent CO (thermodilution)
- ☐ Respiratory monitoring
  - Airway O_2, CO_2, pressure and flow
- ☐ PiCCO monitor & line
- ☐ Bettan
- ☐ Ultrasound with high frequency linear transducer and lung probe, gel and ability to export images to SD card or USB stick
- ☐ N_2O cylinder
- ☐ N_2O connection hose
- ☐ Calibration gas cylinder

DATE

Farmery Group – August 2018

Equipment – To take from Oxford

Generic

- ☐ HME x 8
- ☐ USB sticks for data backup
- ☐ Protocol print-outs
- ☐ Electric socket converters

InspiWave

- ☐ Laptop with working Labview software
- ☐ Blue gas tubing (cylinder → regulator, regulator → MFC, MFC → out)
- ☐ Grey IW box
- ☐ MFC power cable and USB cable
- ☐ Sqaure-1 sensor, power cable and USB connector

DATE

Farmery Group – August 2018

Uppsala Day Plan – August 2018

Pre-Injury	Injury	Post-Injury	Transfer	Post-Injury	Finish
Lab IW vs SF_6	Saline Lavage	Lab IW vs SF_6		CT IW vs CT	Clear-up
08.00–12.30	12.30-13.30	13.30–16.30	16.30–17.00	17.30–20.00	20.00–21.00

7

DATE

Farmery Group – August 2018

Pre-injury – Lab – IW vs SF_6

TABLE 1: Pre-Injury Lab Tests: VCV, RR12-18, V_T 10-15ml/kg, IE 1:2

Condition	Test	Start Time	Samples	Actual Start Time	FiO_2	RR	V_T	EtCO2	Pressure	SpO_2	HR	BP	PAP	CO	EVENT LOG	COMMENTS
ZEEP	ISD 60	0900	ABG													
	ISD 180															
	ISD 60															
	ISD 180															
	SF_6															
PEEP 5	SF_6	0945	ABG													
	ISD 60															
	ISD 180															
	ISD 60															
	ISD 180															
PEEP 10	ISD 60	1030	ABG													
	ISD 180															
	ISD 60															
	ISD 180															
	SF_6															
PEEP 15	SF_6	1115	ABG													
	ISD 60															
	ISD 180															
	ISD 60															
	ISD 180															
PEEP 20	ISD 60	1200	ABG													
	ISD 180															
	ISD 60															
	ISD 180															
	SF_6															

8

DATE

Lines & Sensor Codes

Vessel	Line	Device Code

Lavage Details

Lavage No	Time	Vol In	Vol Out	Δ Volume

9

DATE

Farmery Group – August 2018

Post-injury – Lab – IW vs SF_6

TABLE 2: Post-Injury Lab Tests: VCV, RR12-18, V_T 10-15ml/kg, IE 1:2[1]

Condition	Test	Start Time	Samples	Actual Start Time	FiO_2	RR	V_T	EtCO2	Pressure	SpO_2	HR	BP	PAP	CO	Event Log	Comments
PEEP 5	ISD 60	1330	ABG													
	ISD 180															
	ISD 60															
	ISD 180															
	SF_6															
PEEP 10	SF_6	1415	ABG													
	ISD 60															
	ISD 180															
	ISD 60															
	ISD 180															
PEEP 15	ISD 60	1500	ABG													
	ISD 180															
	ISD 60															
	ISD 180															
	SF_6															
PEEP 20	SF_6	1545	ABG													
	ISD 60															
	ISD 180															
	ISD 60															
	ISD 180															

[1] When getting ready for transfer, we would like to keep the InspiWave device attached for as long as possible before moving at 16.30 to get the scanner for 1700

DATE

Farmery Group – August 2018

TABLE 3: Post-Injury CT Tests: VCV, RR12-18, V_T 10-15ml/kg, IE 1:2[2]

Condition	Test	Time	Samples	Actual Start Time	FiO_2	RR	V_T	EtCO2	Pressure	SpO_2	HR	BP	PAP	CO	Event Log	Comments
PEEP 5	ISD 60	1730	ABG													
	ISD 60															
	CT 1															
	ISD 180															
	ISD 180															
	CT 2															
PEEP 10	ISD 60	1750														
	ISD 60															
	CT 3															
	ISD 180															
	ISD 180															
	CT 4															
PEEP 15	ISD 60	1810														
	ISD 60															
	CT 5															
	ISD 180															
	ISD 180															
	CT 6															
PEEP 20	ISD 60	1830														
	ISD 60															
	CT 7															
	ISD 180															
	ISD 180															
	CT 8															
PEEP 15	ISD 60	1850														
	ISD 60															
	CT 9															
	ISD 180															
	ISD 180															
	CT 10															
PEEP 10	ISD 60	1910														
	ISD 60															
	CT 11															
	ISD 180															
	ISD 180															
	CT 12															
PEEP 5	ISD 60	1930														
	ISD 60															
	CT 13															
	ISD 180															
	ISD 180															
	CT 14															

[2] We will attach and start measurements with InspiWave as soon as animal in on the table and let these continue whilst organising monitoring and lines on the CT table

DATE

Lines & Sensor Codes

Scan No.	PEEP	Scan Type	Name	Notes
1	5	Whole lung volume, end-expiratory	Exp_PEEP5_1	
2	5	Whole lung volume, end-expiratory	Exp_PEEP5_2	
3	10	Whole lung volume, end-expiratory	Exp_PEEP10_3	
4	10	Whole lung volume, end-expiratory	Exp_PEEP10_4	
5	15	Whole lung volume, end-expiratory	Exp_PEEP15_5	
6	15	Whole lung volume, end-expiratory	Exp_PEEP15_6	
7	20	Whole lung volume, end-expiratory	Exp_PEEP20_7	
8	20	Whole lung volume, end-expiratory	Exp_PEEP20_8	
9	15	Whole lung volume, end-expiratory	Exp_PEEP15_9	
10	15	Whole lung volume, end-expiratory	Exp_PEEP15_10	
11	10	Whole lung volume, end-expiratory	Exp_PEEP10_11	
12	10	Whole lung volume, end-expiratory	Exp_PEEP10_12	
13	5	Whole lung volume, end-expiratory	Exp_PEEP5_13	
14	5	Whole lung volume, end-expiratory	Exp_PEEP5_14	

DATE

ARTERIAL BLOOD GASES

13

DATE

APPENDIX C

Protocol for validation of IST measurements of cardiac output

DATE:

Farmery Group – Mar 2017

Protocol: Langford Experiments March 2017

Dates:

- 29th, 30th, 31st Mar 2017

People:

- AF, FF, PP, HMcP, DC

Research Questions:

InspiWave Questions

- Can InspiWave measure/track changes in blood flow (Qp) and lung volume?
    - Can Inspiwave track these PaO_2/FiO_2 Ratios (PFR's) equivalent to mild/moderate and severe ARDS?
    - What effect does the extra PEEP used to restore PaO_2 have on the measured lung volumes?
        - Recruitment or overdistension?
- Is there a high frequency PaO_2 signal detectable in a central vein?

PaO_2 Sensor Questions

- Does the PaO_2 sensor demonstrate the intra-breath oscillations anticipated?
    - Are they "in phase" pre-injury?
    - Are the "out of phase" post-injury?
- When does the PaO_2 oscillation phase shift?
    - Under what conditions does the oscillation shift occur?
    - Is this related to a specific PFR?
    - Is this related to a specific cardiac output (CO)?

PaO_2 Sensor Development

- Does the polymer sensor have equivalent accuracy to the glass sensor?
- Does a peripherally sited polymer sensor produce comparable results to a centrally sited glass sensor?
- Is polymer sensor is easy to use?
- Does polymer sensor fracture/break on insertion – is it safe to use?

DATE: | Farmery Group – Mar 2017

General Procedures:

Anaesthesia

- Induction: By the MRCVS – Uppsala protocol is
  - IM Zoletil®6 mg/kg (=tiletamin 3 mg/kg + zolazepam 3 mg/kg) and Xylazine 2.2 mg/kg
  - IV Fentanyl 8-10 µg/kg
- Maintenance:
  - IV Ketamine 32mg/kg/hr, Fentanyl 4 µg/kg/hr & Midazolam 120 µg/kg/hr
  - This is equivalent to 8ml/kg/hr of 1l crystalloid with
    - 4g Ketamine
    - 500 µg Fentanyl
    - 15mg Midazolam
  - Muscle Relaxation
    - Rocuronium 2.5mg/kg/hr
  - Maintenance fluid therapy:
    - Hartmann's 10ml/kg/hr

Baseline Ventilation

- Cuffed Oral Endotracheal Tube (COETT)
- Pressure Controlled Ventilation via GE ventilator
  - Aim Vt 6-8ml/kg (45kg = 270ml-360ml)
  - I:E 1:2
- Respiratory Rate
  - As required to maintain adequate ventilation (see below for targets)
  - Including 1min sections of RR6/min during each condition for PaO_2
- Pre-Injury:
  - Target pH 7.35-7.45 & $PaCO_2$ 4.5-6kPa
- Post-Injury:
  - Target pH >7.2 w/ permissive hypercapnia post-injury

Instrumentation & Calibration

- Bilateral carotid cut-downs and cannulation with insertion of O_2 Sensors
  - Vygon Arterial LeaderCath or 20G, 48mm Angiocaths?
  - One glass and one plastic, record which one is in which side and swap sides for following day
- Bilateral internal jugular (IJ) cut-downs
  - Right IJ – pulmonary artery flotation catheter (PAFC)
  - Left IJ – 20G Angiocath & PaO_2 sensor
- Bilateral Femoral Artery cannulation and insertion of O_2 sensors
  - Vygon 8cm Arterial LeaderCath or 20G 48mm BD Angiocath ?
  - One glass and one plastic, record which type is in which artery and swap sides for the following day
- Peripheral arterial cannulation (e.g. Ear)
  - Arterial pressure transduction – 22G/20G BD Angiocath or Vygon Aterial Leadercath
- Calibration – blood gases from all lines will be taken to assess calibration.

DATE:

Farmery Group – Mar 2017

Monitoring & Continuous Recording

- Cardiovascular
  - Arterial pressure via peripheral arterial cannula
  - PA pressure via PAFC
  - CO – Intermittent thermodilution & Qp by InspiWave
- Respiratory
  - FiO2, EtCO2
  - Airway pressures & flow
  - FRC Inview (intermittently)
- Continuous InspiWave monitoring
- Continuous PaO2 Sensor monitoring
- Intermittent Blood gas analysis

DATE:

Farmery Group – Mar 2017

Experimental Procedures

Throughout the experimental procedures, airway, breathing and circulatory data will be recorded continuously with analogue signals from monitors to allow post-hoc investigations of the dynamic relationships between ventilation and haemodynamics. The procedures will fall into two main categories and be repeated pre- and post- lung injury:

1. Measurement of EELV
2. Measurement of Qp

Pre-Injury EELV Measurements

With standard ventilation ongoing, InspiWave will take measurements of EELV under each PEEP condition with forcing periods of 60s and 180s. These will be repeated 6 times for each condition and compared with a single FRC INview measurement taken from the GE Engstrom ventilator. A 2 min period of RR 6/min is included under each condition to allow measurements to be taken with the PaO_2 sensors. Arterial blood gas measurements will be taken after 10 minutes of ventilation with each condition.

Table 1: Approximate Timings of EELV Measurement Pre-Injury

	Measurement Type (time/min)					
EEP	ISD 60s	ISD 180s	FRC INview	RR6	Stabilisation time	Time/condition
ZEEP					10	10
	6	6	15	2		29
5cmH_2O					10	10
	6	6	15	2		29
10cmH_2O					10	10
	6	6	15	2		29
					TOTAL TIME	117

ISD: Inspired Sinewave Device/InspiWave

Pre-Injury Qp Measurements

To assess whether InspiWave can reliably track changes in CO & compare it to the gold standard of intermittent PAFC thermodilution (TD) we will pharmacologically decrease and increase the CO using a β-blocker (Esmolol) and a β1-agonist (Dobutamine). Each phase (Low CO & High CO) will be repeated twice and measurements of Qp taken with InpsiWave. During this time:

- TD CO assessments will be made every 2 mins.
- RR6/min to allow PaO2 sensor oscillation detection will be undertaken 10mins into each CO phase
- Paired Arterial and Mixed Venous Gases will be taken.

DATE:

Table 2: Sequence of Pre-Injury CO Measurements			
	Drug	**Target**	**Time/min**
Baseline	-	-	10
Low CO 1	Esmolol	CO <50% baseline	20
Recovery	-	-	5
High CO 1	Dobutamine	CO >50% baseline	20
Recovery	-	-	5
Low CO 2	Esmolol	CO <50% baseline	20
Recovery	-	-	5
High CO 2	Dobutamine	CO >50% baseline	20
		TOTAL TIME	105

Saline Lavage (≈1hr)

This will be undertaken as per the PPL to achieve PFR's equivalent to mild, moderate and severe ARDS (PFR 200-300mmHg, 100-200mmHg & <100mmHg). When the PFR reaches the required level a 1-2min period of RR6/min will be instigated to allow PaO2 sensor measurements at PFR's equivalent to differing clinical severity of ARDS.

Once a severe lung injury has been induced, the EELV and Qp Measurement Protocols will be undertaken as follows.

Post-Injury EELV Measurements

With ventilation titrated to pH>7.2 and PaO_2 >75mmHg, InspiWave will take measurements of EELV under each PEEP condition with forcing periods of 60s and 180s. These will be repeated 6 times for each condition and compared with a single FRC INview measurement taken from the GE Engstrom ventilator. Arterial blood gas measurements will be taken after 10 minutes of ventilation with each condition.

Table 3: Approximate Timings of EELV Measurement Post-Injury						
	Measurement Type (time/min)					
EEP	ISD 60s	ISD 180s	FRC INview	RR6	Stabilisation time	Time/condition
5cmH_2O					10	10
	6	6	15	2		29
10cmH_2O					10	10
	6	6	15	2		29
					TOTAL TIME	78
ISD: Inspired Sinewave Device/InspiWave						

Post-Injury Qp Measurements (≈1.5hrs)

Again, each phase (Low CO & High CO) will be repeated twice and measurements of Qp taken with InpsiWave. Post-Injury, the High CO state will be induced first to avoid premature deterioration of the subject. The final Low CO state will include Esmolol and then humane euthanasia with Pentobarbitone. During this time:

DATE:

- TD CO assessments will be made every 2 mins.
- RR6/min to allow PaO2 sensor oscillation detection will be undertaken 10mins into each CO phase
- Paired Arterial and Mixed Venous Gases will be taken.

Table 4: Sequence of Post-Injury CO Measurements

	Drug	**Target**	**Time/min**
Baseline	-	-	10
High CO 3	Dobutamine	CO <50% baseline	20
Recovery	-	-	10
Low CO 3	Esmolol	CO >50% baseline	20
Recovery	-	-	10
High CO 4	Dobutamine	CO <50% baseline	20
Recovery	-	-	10
Low CO 4	Esmolol & Pentobarbitone	CO >50% baseline	20
		TOTAL TIME	120

DATE:

Farmery Group – Mar 2017

Day Plans

Weds 29th Mar

14:00–18:00 Set up

Thurs 30th Mar - Plastic sensors on one side, glass on the other

08:00–09:30 Clock synchronisation, anaesthesia, instrumentation and set-up

09:30–11.30 EELV Measurement Pre-Injury

11.30-13:30 Qp Measurement Pre-Injury

13.30-14.30 Saline Lavage and PaO_2 Sensor Readings

14.30-16.00 EELV Measurement Post-Injury

16.00-18.00 Qp Measurement Post-Injury

18.00-19.00 Clear up

Fri 31st Mar – Sensors on opposite sides to Thurs

08:00–09:30 Clock synchronisation, anaesthesia, instrumentation and set-up

09:30–11.30 EELV Measurement Pre-Injury

11.30-13:30 Qp Measurement Pre-Injury

13.30-14.30 Saline Lavage and PaO_2 Sensor Readings

14.30-16.00 EELV Measurement Post-Injury

16.00-18.00 Qp Measurement Post-Injury

18.00-19.00 Clear up

Other things to do:

- Visit a lovely pub in Churchill called the Crown https://www.the-crown-inn.co.uk/ and have a pint of Mendip Magic cider
- Walk up Burrington Combe: https://en.wikipedia.org/wiki/Burrington_Combe
- Have dinner at the Plume of Feathers: http://theplumeoffeathers.com/

DATE:

Farmery Group – Mar 2017

Equipment Checklist

Generic

- ☐ GE Engstrom Carestation Ventilator
- ☐ GE Engstrom Carestation Ventilator power cable
- ☐ GE Engstrom Carestation Ventilator gas sampling module, tubing and water trap
- ☐ Vascular ultrasound machine
- ☐ Ventilator breathing circuit x 2
- ☐ HME x 2
- ☐ Artery forceps (tube clamp)
- ☐ USB sticks for data backup
- ☐ Monitoring tables
- ☐ Day schedules
- ☐ Electric socket multiplug extensions
- ☐ Calculator
- ☐ Sharps bin
- ☐ Sheets of sticky labels

Monitoring

- ☐ Extra respiratory monitor (?Capnomac ultra)
- ☐ Capnomac cables
- ☐ Capnomac power cord
- ☐ Respiratory monitor output cable
- ☐ CVS Monitor cables ?
- ☐ Blood gas syringes - requested 50 from TBRC
- ☐ Blood gas cassettes
- ☐ Do we need to bring blood gas machine reagents?

Procedures

- ☐ Surgical equipment for cutdowns
  - Blades, swabs, forceps
  - Suture material
- ☐ Dobutamine – TBRC providing
- ☐ Esmolol- TBRC providing
- ☐ 50ml syringes - TVRC
- ☐ 0.9% NaCl 1000ml bags (flush/drug mixing)
- ☐ Lavage kit – funnel/tubing/measuring cylinder

PaO2 Sensor:

- ☐ 1x box (20 pieces), 8cm Vygon Arterial Leadercath (Ref 115.090)
- ☐ 1x box (20 pieces) 8cm Vygon ArterioSel (Ref 115.0901)
- ☐ 1x box BD Angiocath 20G 48mmx1.1mm (Catalogue Number 381137)
- ☐ 1x box BD Angiocath 22G 25mm x 0.9mm (Catalogue Number 381123)

8

DATE:

Farmery Group – Mar 2017

- ☐ 8 x Polymer PaO2 sensors
- ☐ 8 x Glass PaO2 sensors
- ☐ 2x Oxylite boxes
- ☐ 2 x Oxylite power cables
- ☐ 2x Analogue out Oxylite → data acquisition module cables
- ☐ AD Instruments data acquisition module
- ☐ AD Instruments module → laptop cable
- ☐ AD Instruments data acquisition power cable
- ☐ Laptop, with up to date software and Labchart
- ☐ Laptop power cable

InspiWave

- ☐ InspiWave device (PP will bring all the component parts)
- ☐ N2O Cylinders (should be in Langford) x 1 Size E
- ☐ O2 Cylinders (should be in Langford) x2 Size E
- ☐ PAFC x4 (one per pig and one spare each day)
- ☐ Swan Introducer x2
- ☐ Thermodilution 10ml sealed syringe x2

DATE:

Farmery Group – Mar 2017

Blood Gas Recording Table

Date: _____

Gas No.	A/V	Time	Condition/Experiment	Site	Comments

DATE:

Farmery Group – Mar 2017

Approximate running order of the day

Injury	Condition	Test	Scheduled Time	Samples
Pre Injury	ZEEP	Pre-test	0930 – 0940	ABG 1
		ISD 60	0940 – 0946	
		ISD 180	0946 – 0952	
		FRC INview	0952 – 1007	
		RR 6/min	1007 – 1009	ABG 2
	PEEP 5	Pre-test	1009 – 1019	ABG 3
		ISD 60	1019 – 1025	
		ISD 180	1025 – 1031	
		FRC INview	1031 – 1046	
		RR 6/min	1046 – 1048	ABG 4
	PEEP 10	Pre-Test	1048 – 1058	ABG 5
		ISD 60	1058 – 1104	
		ISD 180	1104 – 1110	
		FRC INview	1110 – 1125	
		RR 6/min	1125 – 1127	ABG 6
	Preparation Time		1127 – 1140	
	Baseline	-	1140 - -1150	ABG 7 & VBG 1
	Low CO 1	Esmolol	1150 – 1210	ABG 8 & VBG2
	Recovery	-	1210 – 1215	ABG 9 & VBG3
	High CO 1	Dobutamine	1215 – 1235	ABG 10 & VBG4
	Recovery	-	1235 – 1240	ABG 11 & VBG 5
	Low CO 2	Esmolol	1240 – 1300	ABG 12 & VBG 6
	Recovery	-	1300 – 1305	ABG 13 & VBG 7
	High CO 2	Dobutamine	1305 – 1325	ABG 14 & VBG 8
	Preparation Time		1325 – 1340	
Injury	PFR 200-300		1340	ABG 15
	PFR 100-200			ABG 16
	PFR <100		1430	ABG 17
Post-Injury	PEEP 5	Pre-test	1430 – 1440	ABG 18
		ISD 60	1440 – 1446	
		ISD 180	1446 – 1452	
		FRC INview	1452 – 1507	
		RR 6/min	1507 – 1509	ABG 19
	PEEP 10	Pre-test	1509 – 1519	ABG 20
		ISD 60	1519 – 1525	
		ISD 180	1525 – 1531	
		FRC INview	1531 – 1546	
		RR 6/min	1546 - 1548	ABG 21
	Preparation Time		1548 – 1600	
	Baseline	-	1600 – 1610	ABG 22 & VBG 9
	High CO 3	Dobutamine	1610 – 1630	ABG 23 & VBG 10
	Recovery	-	1630 – 1640	ABG24 & VBG 11
	Low CO 3	Esmolol	1640 – 1700	ABG 25 & VBG 12
	Recovery	-	1700 – 1710	ABG 26 & VBG 13
	High CO 4	Dobutamine	1710 – 1730	ABG 27 & VBG 14
	Recovery	-	1730 – 1740	ABG 28 & VBG 15
	Low CO 4	Esmolol & Pentobarb	1740 – 1800	ABG 29 & VBG 16

DATE:

Farmery Group – Mar 2017

Langford Day Plan – Mar 2017

Pre-Injury	Pre-Injury	Injury	Post-Injury	Post-Injury
ZEEP/PEEP	Cardiac Output	Saline Lavage	PEEP	Cardiac Output
09.30-11.30	11.30-13.30	13.30-14.30	14.30-16.00	16.00-18.00

12

DATE:

Monitoring Chart						RESPIRATORY						CVS				GASES		EVENT LOG	COMMENTS
Injury	Condition	Test	Scheduled Time	Samples	Actual Time	FiO_2	RR	Vt	EtCO2	Airway Pressure	SpO_2	HR	BP	PAP	CO	PaO_2	$PaCO_2$		
Pre	ZEEP	Pre-test	0930 – 0940	ABG 1															
		ISD 60	0940 – 0946																
		ISD 180	0946 – 0952																
		FRC INview	0952 – 1007																
		RR 6/min	1007 – 1009	ABG 2															
	PEEP 5	Pre-test	1009 – 1019	ABG 3															
		ISD 60	1019 – 1025																
		ISD 180	1025 – 1031																
		FRC INview	1031 – 1046																
		RR 6/min	1046 – 1048	ABG 4															
	PEEP 10	Pre-Test	1048 – 1058	ABG 5															
		ISD 60	1058 – 1104																
		ISD 180	1104 – 1110																
		FRC INview	1110 – 1125																
		RR 6/min	1125 – 1127	ABG 6															
	Preparation Time		1127 – 1140																
	Baseline	-	1140 - -1150	ABG 7 & VBG 1															
	Low CO 1	Esmolol	1150 – 1210	ABG 8 & VBG2															
	Recovery	-	1210 – 1215	ABG 9 & VBG3															
	High CO 1	Dobutamine	1215 – 1235	ABG 10 & VBG4															
	Recovery	-	1235 – 1240	ABG 11 & VBG 5															
	Low CO 2	Esmolol	1240 – 1300	ABG 12 & VBG 6															
	Recovery	-	1300 – 1305	ABG 13 & VBG 7															
	High CO 2	Dobutamine	1305 – 1325	ABG 14 & VBG 8															
	Preparation Time		1325 – 1340																
Injury	PFR 200-300		1340	ABG 15															
	PFR 100-200			ABG 16															
	PFR <100		1430	ABG 17															
Post	PEEP 5	Pre-test	1430 – 1440	ABG 18															
		ISD 60	1440 – 1446																
		ISD 180	1446 – 1452																
		FRC INview	1452 – 1507																
		RR 6/min	1507 – 1509	ABG 19															
	PEEP 10	Pre-test	1509 – 1519	ABG 20															
		ISD 60	1519 – 1525																
		ISD 180	1525 – 1531																
		FRC INview	1531 – 1546																
		RR 6/min	1546 - 1548	ABG 21															
	Preparation Time		1548 – 1600																
	Baseline	-	1600 – 1610	ABG 22 & VBG 9															
	High CO 3	Dobutamine	1610 – 1630	ABG 23 & VBG 10															
	Recovery	-	1630 – 1640	ABG24 & VBG 11															
	Low CO 3	Esmolol	1640 – 1700	ABG 25 & VBG 12															
	Recovery	-	1700 – 1710	ABG 26 & VBG 13															
	High CO 4	Dobutamine	1710 – 1730	ABG 27 & VBG 14															
	Recovery	-	1730 – 1740	ABG 28 & VBG 15															
	Low CO 4	Esmolol/Pent	1740 – 1800	ABG 29 & VBG 16															

DATE:

Lines & Sensor Codes

Vessel	Line	Device Code

OTHER NOTES